Linear AB and ABC Amphiphilic Block Copolymers: From Synthesis to Complex Self-Assembled Structures

---

Inauguraldissertation

zur

Erlangung der Würde eines Doktors der Philosophie

vorgelegt der

Philosophisch-Naturwissenschaftlichen Fakultät

der Universität Basel

von

Evgeniia Konishcheva

aus

Russland

Basel, 2018

Genehmigt von der Philosophisch-Naturwissenschaftlichen Fakultät
auf Antrag von

Prof. Dr. Wolfgang P. Meier

Prof. Dr. Richard Hoogenboom

Basel, 23.05.2017

Prof. Dr. Martin Spiess
The Dean of Faculty

Abstract

Every living organism depends on functional macromolecules assembled in aqueous solution via noncovalent interactions. Hydrophobic forces are particularly stable among other noncovalent interactions, which led to the development of amphiphilic synthetic (macro)molecules able to self-assemble into various structures for diverse applications ranging from nanotechnology to medicine. Amphiphilic block copolymers are especially advantageous due to the control over their properties achieved via tuning the chemical composition and superior stability of the self-assembled structures compared to the ones formed by low molecular weight surfactants and lipids. Particularly, structures formed by biocompatible and/or biodegradable amphiphilic block copolymers possess required properties for drug delivery applications.

Self-assembly of various AB (A – hydrophilic, B – hydrophobic) copolymers has been explicitly investigated with respect to the packing geometry of individual polymer molecules and conditions of self-assembly. Introduction of the third C block increases the level of complexity of self-assembly behavior of ABC copolymers. ABC copolymers provide possibility for developing programmable materials based on asymmetric structures with spatially separated domains possessing different chemical and physical properties. For example, multicompartment morphologies, i.e. assemblies bearing domains in the core, can be obtained in a solvent which selectively solubilizes A block, whereas B and C blocks undergo phase separation in the core. ABC copolymers with A and C soluble blocks are advantageous for creating structures with surface bearing domains in the corona, but the principles of self-assembly of such systems still lack deep understanding.

The ultimate goal of this thesis is to shed light on the complex morphological behavior of linear amphiphilic ABC copolymers with A and C water-soluble blocks targeting for biomedical applications. To approach this goal, synthesis of ABC copolymers bearing biocompatible blocks (poly(ethylene oxide) PEO, poly(2-methyl-2-oxazoline) PMOXA), biodegradable blocks (polycaprolactone PCL, poly(γ-methyl-ε-caprolactone) PMCL), and cationic block for complexation of nucleic acids (poly*(N,N*-dimethylaminoethyl methacrylate) PDMAEMA) is developed. Then, the complex self-assembly behavior of synthesized copolymers is investigated. Details of the synthesis and self-assembly behavior are summarized in three publications and one section of this thesis.

The first publication presents an optimization of the seemingly well-known synthesis of PEO-*b*-PCL. The optimization was a necessary step for the development of the toxic-free synthesis of PEO-*b*-PCL-*b*-PMOXA copolymers. The procedure for obtaining PEO-*b*-PCL with narrow dispersity ($Đ_M < 1.1$), its ω-tosylation, and the effect of aging of the catalyst, $SnOct_2$, on this polymerization is described. In addition, we have shown that lowering the dispersity of PEO-*b*-PCL results in more uniform self-assembled structures.

The second publication describes the synthesis of PEO-*b*-PCL-*b*-PMOXA with fixed PEO and different PCL and PMOXA lengths. The self-assembly of these polymers was tested in aqueous solution using film rehydration method. PEO-*b*-PCL-*b*-PMOXA self-assembled into various structures, including polymersomes. The polymersomes possessed asymmetric membrane: a longer PEO block formed the outer corona, a shorter PMOXA block formed the inner corona. The asymmetry of the membrane was proven by two independent methods.

The third publication aims to elucidate the general principles of aqueous self-assembly of bis-hydrophilic PEO-*b*-PCL-*b*-PMOXA copolymers. Self-assembly was investigated with respect to different PCL and PMOXA lengths using three different preparation methods: film rehydration, solvent evaporation, and co-solvent. The diversity of the formed structures is discussed in terms of the packing geometry and thermodynamic/kinetic control.

Finally, the fourth section describes synthesis and self-assembly of PEO-*b*-PRCL-*b*-PDMAEMA copolymers, where R is methyl (M) or phenyl (Ph). The self-assembly regarding the hydrophobicity of the middle block was investigated. Different hydrophobicity did not affect the morphology of the assemblies, but led to the increased size of the structures formed by more hydrophobic PEO-*b*-PPhCL-*b*-PDMAEMA compared to PEO-*b*-PMCL-*b*-PDMAEMA. These polymers are of particular interest for gene delivery applications due to the presence of cationic PDMAEMA block.

Acronyms

DNA	deoxyribonucleic acid
PEO-*b*-PPO-*b*-PEO	poly(ethylene oxide)-*block*-poly(propylene oxide)-*block*-poly(ethylene oxide)
LROP	living ring opening polymerization
EO	ethylene oxide
PEO	poly(ethylene oxide)
PEO-*b*-PCL	poly(ethylene oxide)-*block*-polycaprolactone
PEO-*b*-PB	poly(ethylene oxide)-*block*-polybutadiene
PEO-*b*-PS	poly(ethylene oxide)-*block*-polystyrene
PEO-*b*-PCL-*b*-PAA	poly(ethylene oxide)-*block*-polycaprolactone-*block*-poly(acrylic acid)
PO	1,2-propylene oxide
NCA	*N*-carboxyanhydride
PDMS	polydimethylsiloxane
PMOXA	poly(2-methyl-2-oxazoline)
PCL	polycaprolactone
PLA	poly(L,L-lactide)
$SnOct_2$	tin(II) 2-ethylhexanoate
FDA	Food and Drug Administration
PEO-*b*-PLA	poly(ethylene oxide)-*block*-poly(L,L-lactide)
PCL-*graft(SS)*-PMOXA	polycaprolactone-*graft(SS)*-poly(2-methyl-2-oxazoline)
THF	tetrahydrofuran
POXs	polyoxazolines
PMOXA-*b*-PEtOXA-*b*-PPhOXA	poly(2-methyl-2-oxazoline)-*block*-poly(2-ethyl-2-oxazoline)-*block*-poly(2-phenyl-2-oxazoline)
PEtOXA-*b*-PNonOXA	poly(2-ethyl-2-oxazoline)-*block*-poly(2-nonyl-2-oxazoline)
LCST	lower critical solution temperature
P*i*PrOXA	poly(2-*i*-propyl-2-oxazoline)

PMOXA-*b*-PDMS	poly(2-methyl-2-oxazoline)-*block*-polydimethylsiloxane-*block*-poly(2-phenyl-2-oxazoline
PMOXA-*b*-PDMS-*b*-PMOXA	poly(2-methyl-2-oxazoline)-*block*-polydimethylsiloxane-*block*-poly(2-methyl-2-oxazoline)
MWD	molecular weight distribution
ε-CL	epsilon-caprolactone
MOXA	2-methyl-2-oxazoline
CRP	controlled/living radical polymerization
PRE	persistent radical effect
NMP	nitroxide mediated polymerization
ATRP	atom transfer radical polymerization
TEMPO	(2,2,6,6-tetramethylpiperidin-1-yl)oxidanyl
DEPN	*N*-(2-methylpropyl)-*N*-(1-diethylphosphophono-2,2-dimethylpropyl)aminoxyl
RAFT	reversible addition-fragmentation chain transfer
DLS	dynamic light scattering
SLS	static light scattering
TEM	transmission electron microscopy
cryoTEM	cryogenic transmission electron microscopy
SEM	scanning electron microscopy
SANS	small-angle neutron scattering
SAXS	small-angle X-ray scattering
NMR	nuclear magnetic resonance spectroscopy
2D-NOESY	two-dimensional nuclear Overhauser effect spectroscopy
CLSM	confocal laser scanning microscopy
AFM	atomic force microscopy
F(C)CS	fluorescence (cross)-correlation spectroscopy
p	packing parameter
v	volume of hydrophobic chains
l_c	length of hydrophobic chains
a_0	optimal area of hydrophilic chains

f	hydrophilic weight fraction
S	spherical micelles
E	elongated micelles
P	polymersomes
PAA-*b*-PS	poly(acrylic acid)-*block*-polystyrene
T_m	melting temperature
I	irregularly shaped particles
N_{agg}	aggregation number
C	concentration
CMC	critical micellization concentration
DMF	*N*,*N*-dimethylformamide
CWC	critical water content
PMPC-*b*-PDPA	poly(methacryl phosphoryl choline)-*block*-poly(diisopropylaminoethyl methacrylate)
(PEO/PMPC)-*b*-PDPA	(poly(ethylene oxide)/poly(methacryl phosphoryl choline)-*block*-poly(diisopropylaminoethyl methacrylate)
PS-*b*-PB-*b*-PT	polysterene-*block*-polybutadiene-*block*-poly(*tert*-butyl methacrylate)
PEO-*b*-PRCL-*b*-PDMAEMA	poly(ethylene oxide)-*block*-poly(γ-R-ε-caprolactone)-*block*-poly*(N,N*-dimethylaminoethyl methacrylate)
PMCL	poly(γ-methyl-ε-caprolactone)
PPhCL	poly(γ-phenyl-ε-caprolactone)
MCL	γ-methyl-ε-caprolactone
$Đ_M$	molecular weight dispersity
D_h	hydrodynamic diameter
ζ	zeta-potential
GPC	gel permeation chromatography
PBS	phosphate buffered saline

Contents

Introduction 9
1. Polymerization techniques for synthesis of amphiphilic block copolymers 10
1.1. Living ring opening polymerization (LROP) 10
1.2. Controlled radical polymerization (CRP) 14
2. Self-assembly of amphiphilic block copolymers in solution 16
2.1. Methods of characterization of self-assembled structures 16
2.2. Self-assembly of linear AB copolymers 17
2.3. Self-assembly of linear ABC copolymers 19
3. Scope of this thesis 22
References 23
Publication 1 33
Publication 2 53
Publication 3 74
4. Effect of the hydrophobicity on self-assembly: the case of linear ABC copolymers 101
Experimental part 108
Conclusions and Outlook 113
Acknowledgments 114

Introduction

Aqueous self-assembly based on noncovalent interactions is essential for all living organisms, and water is a unique[1] medium for this process. Noncovalent interactions include hydrophobic, hydrophilic, electrostatic, H-bond, van der Waals, and π-π interactions. In nature, noncovalent interactions play a predominant role in the complex organization of functional macromolecules. For instance, H-bonds are responsible for the formation of DNA duplexes; hydrophobic interactions govern the formation of cell lipid membrane; electrostatic and hydrophobic interactions are among the driving forces for the folding of proteins. Inspired by nature, researchers have developed various synthetic amphiphilic (macro)molecules that self-assemble in water into different structures relevant for applications in technology and medicine. In particular, self-assembly of amphiphilic block copolymers, i.e. polymers consisting of spatially separated hydrophilic and hydrophobic blocks, is driven by hydrophobic interactions. Amphiphilic block copolymers are advantageous over low molecular weight surfactants and lipids due to the facile design of a copolymer molecule and high stability of the self-assembled structures,[2] and therefore structures assembled from amphiphilic block copolymers serve as a promising platform for drug delivery applications.[3-7]

Poly(ethylene oxide)-*block*-poly(propylene oxide)-*block*-poly(ethylene oxide) (PEO-*b*-PPO-*b*-PEO), also known as Pluronics, are the first reported amphiphilic block copolymers and are among the most studied block copolymers.[8-9] Pluronics are still used in various technological processes, including pharmaceutical formulations.[10] Together with the development of polymerization techniques, the number of different structures of the composing blocks increased dramatically. Nowadays, the block copolymer architectures include linear, graft, star, dendritic, and cyclic molecules.[11] Modern polymerization techniques offer a powerful strategy for the controlled synthesis of complex polymer architectures thanks to the vast variety of monomers and functional groups. Depending on the block composition, amphiphilic block copolymers and assemblies thereof can possess desired functions: biocompatibility, biodegradability, stimuli responsiveness, surface charge, etc.

In the next sections, the main polymerization techniques used for the synthesis of amphiphilic block copolymers and principles of their self-assembly are reviewed.

1. Polymerization techniques for synthesis of amphiphilic block copolymers

Discovery of living anionic polymerization by Szwarc[12-13] in 1956 and subsequent development of living cationic,[14] coordination,[15] metathesis,[16-17] ring opening,[18] and controlled radical[19] polymerizations led to the enormous progress in polymer chemistry. Living polymerization is defined as "a chain polymerization from which irreversible chain transfer and irreversible chain termination (deactivation) are absent".[20] In this chapter, I review living ring opening and controlled radical polymerizations as the most relevant polymerization techniques applied for the synthesis of amphiphilic block copolymers.

1.1. Living ring opening polymerization (LROP)

Ring opening polymerization is "a polymerization in which cyclic monomer yields a monomeric unit that is acyclic or contains fewer cycles than the monomer".[20] LROP can be anionic (i.e. kinetic chain carriers are anions), coordination (i.e. kinetic chain carriers coordinate a monomer), and cationic (i.e. kinetic chain carriers are cations) polymerizations.

Anionic LROP of ethylene oxide resulting in PEO (also abbreviated as PEG) is one of the most studied polymerizations. Elementary act of the chain growth proceeds via S_N2 nucleophilic substitution at the carbon atom (Scheme 1). Already Flory[21] pointed out that the molecular weight of the resulting polymer is determined by the ratio of the consumed monomer to initiator and exhibits Poisson distribution.

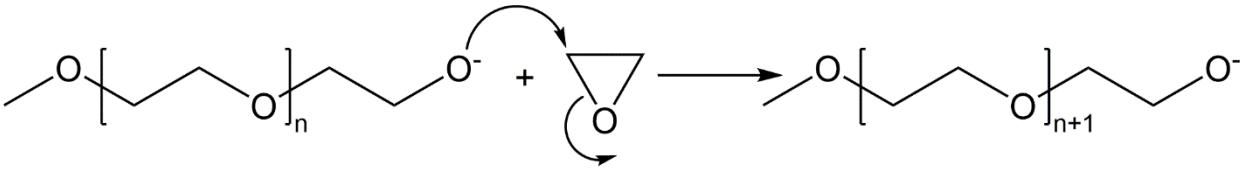

Scheme 1. Polymerization of ethylene oxide (counterion omitted).

Nowadays PEO is produced in large quantities for use in cosmetics, pharmaceutics, and food industry. For laboratory purposes, various narrowly dispersed mono- and (homo/hetero)bifunctional PEOs are commercially available. PEO is one of the most abundantly used hydrophilic building blocks for amphiphilic block copolymers due to its high solubility in water, biocompatibility, and protein-repellent properties. Examples of PEO-based amphiphilic block copolymers include PEO-*b*-polycaprolactone (PEO-*b*-PCL),[22-23] PEO-*b*-polybutadiene

(PEO-*b*-PB),[24] PEO-*b*-polystyrene (PEO-*b*-PS),[25] PEO-*b*-PCL-*b*-poly(acrylic acid) (PEO-*b*-PCL-*b*-PAA),[26] and many others.

Other examples of anionic LROP include polymerization of 1,2-propylene oxide (PO),[18] cyclic siloxanes,[27] lactams,[28] *N*-carboxyanhydrides (NCAs),[29] and cyclic esters of phosphorous acids.[30-31] PO polymerization is employed to obtain PEO-*b*-PPO-*b*-PEO. Cyclic siloxanes are utilized to produce hydrophobic polydimethylsiloxanes (PDMS), highly flexible materials with applications ranging from medical devices to food additives. PDMS is also used as a building block in amphiphilic block copolymers, e.g. PDMS-*b*-poly(2-methyl-2-oxazoline) (PDMS-*b*-PMOXA).[32] NCA polymerization results in polymers resembling natural proteins, and received considerable attention in synthesis of amphiphilic block copolymers, for example PS-*b*-poly(Z-L-lysine).[33]

Cyclic esters undergo coordination LROP resulting in biodegradable polyesters like PCL and PLA. Such polymerization can be catalyzed by metal alkoxides and carboxylates, organic species, and enzymes. Organocatalytic and enzyme-catalyzed ROP have major limitations in yielding narrowly dispersed polymers with high molecular weights. Therefore, polymerization of cyclic esters is usually performed in the presence of metal atoms. Homopolymerization of cyclic esters was studied using metal alkoxides, e.g. $R_nAl(OR')_{3-n}$, $R_nAl(OR')_{3-n}$, $Zr(OR)_4$, $Ti(OR)_4$, which initiate and catalyze ROP.[34-35] To polymerize cyclic esters on macroinitiators, e.g. PEO, polymerization is usually performed in the presence of triethylaluminum, $AlEt_3$, or tin(II) 2-ethylhexanoate, $SnOct_2$. $SnOct_2$ is FDA approved and the most frequently applied catalysts for ROP of ε-CL and L,L-lactide on various initiators, including macroinitiators bearing hydroxyl group(s). The group of Prof. Penczek in Poland has extensively studied ROP of cyclic esters and proposed the mechanism of polymerization of cyclic esters co-initiated by alcohols and $SnOct_2$ (Scheme 2).[36-40] The polymerization is initiated by reversible exchange between $SnOct_2$ and ROH resulting in Oct-Sn-OR, which further catalyze the ring opening of the cyclic ester. PLA and PCL possess biodegradability[41-42] which makes them one of the most frequently applied polymers for drug delivery applications. Examples of the amphiphilic block copolymers synthesized with the help of coordination ROP include already mentioned PEO-*b*-PCL[22, 43-45] and PEO-*b*-PLA,[46] and PCL-*graft*(SS)-PMOXA[47].

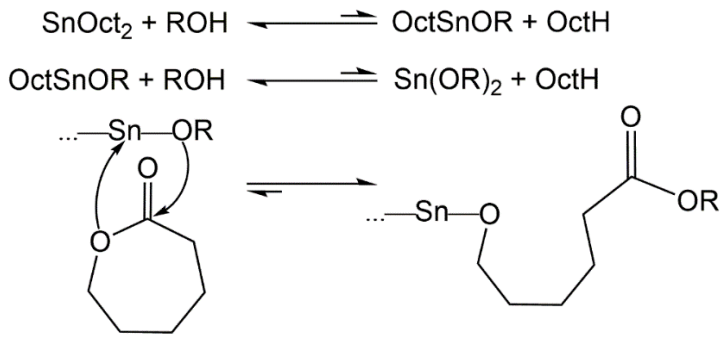

Scheme 2. Polymerization of ε-CL co-initiated by $SnOct_2$.

Polymerization of THF and 2-oxazolines are examples of cationic LROP. Polymerization of THF is usually initiated by triflic acid or its esters, and the key feature of this polymerization is similar reactivity of ions and ion pairs in the propagation step.[48]

Polymerization of various 2-oxazolines was first reported in 1960s independently by four groups.[49-52] This polymerization was investigated by different groups in Japan,[53-58] and the group of Prof. Hoogenboom in Belgium is currently developing it further by applying microwave-assisted synthesis.[59-70] Polyoxazolines (POXs) have received significant interest in the past few decades as they are considered to be an alternative to PEO which possess side effects partially caused by its non-biodegradability.[71-72]

Polymerization of 2-oxazolines can be initiated by a wide range of electrophiles and proceeds via covalent or ionic propagation.[53] Ionic polymerization is more preferable over covalent polymerization, since the latter possesses lower initiation and propagation rate constants. The typical initiators which result in ionic polymerization are tosylates and triflates. Tosylates are much more stable than triflates, but result in slower initiation. Recently a novel initiator, nosylate, was proposed for polymerization of 2-oxazolines.[65] Due to the presence of electrophilic nitro group at the *para*-position, nosylates result in faster polymerization compared to tosylates, but at the same time nosylates possess higher stability than triflates.

Ionic polymerization of 2-oxazolines is initiated by electrophilic attack of the initiator to 3-position leading to the formation of oxazolinium cation (Scheme 3). The positive charge is delocalized and partially present at the 5-position. This leads to the nucleophilic attack of another monomer resulting in the ring opening involving isomerization of the imino group to the *N*-acyl group. Typically this polymerization is performed in acetonitrile, but recently sulfolane has been shown to accelerate drastically polymerization of different 2-oxazolines.[66]

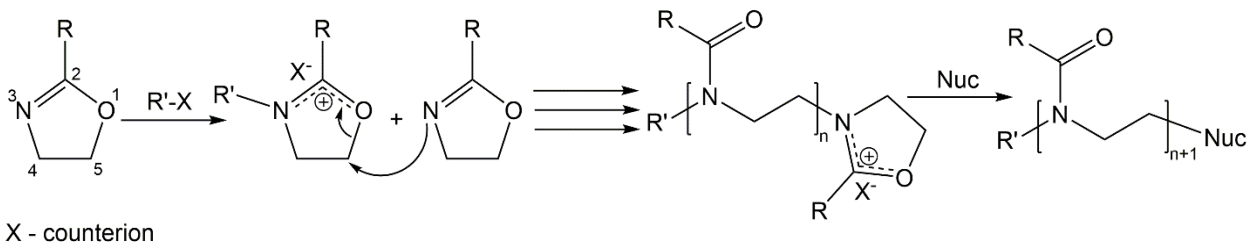

Scheme 3. Polymerization of 2-oxazolines.

The backbone of POXs resembles peptide bond, and therefore POXs are often called "pseudopeptides". Depending on the nature of the side chain *R*, the corresponding POX can be hydrophilic (methyl, ethyl) or hydrophobic (isopropyl, nonyl, phenyl). Therefore, amphiphilic block copolymers can be composed of various POXs, for instance PMOXA-*b*-PEtOXA-*b*-PPhOXA,[62] PEtOXA-*b*-PNonOXA.[59, 73] POXs possess an excellent α- and ω-group fidelity, as well as the ability to obtain functional groups at the polymer backbone.[72] In addition, the lower critical solution temperature (LCST) of P*i*PrOXA is 38 ºC, which is advantageous for its biomedical applications as thermoresponsive (co)polymer.[74] Meier and co-workers has published a large number of works exploiting PDMS-*b*-PMOXA and PMOXA-*b*-PDMS-*b*-PMOXA as artificial membranes able to host membrane proteins.[4, 75-85]

LROP is used to produce various polymers on industrial scale[18, 86] and highly relevant for the development of polymeric platforms for biomedical applications, since the resulting polymers are free of toxic compounds, possess narrow molecular weight distribution (MWD), and biodegradable polymers (e.g. polyesters, polypeptoids) can be obtained. However, all three types of LROP described above, i.e. anionic, coordination, and cationic, are very sensitive to impurities, especially moisture, and are limited in achieving narrowly dispersed high molecular weight (co)polymers due to the intra- and intermolecular chain transfer reactions.[18, 87] These issues become especially challenging when polymerization proceeds on macroinitiators. Nevertheless, (co)polymers with the desired architecture can be obtained under kinetically controlled conditions when the proper (macro)initiator is chosen, as has been outlined for ε-CL and MOXA polymerizations described in the two publications in this thesis (Publication 1 and 2).

1.2. Controlled radical polymerization (CRP)

Conventional radical polymerization (i.e. kinetic chain carriers are radicals) is used to produce various polymers on industrial scale, but the architectural control is very limited in this case.[88] Development of the controlled radical polymerization, where "a certain kinetic feature of polymerization or of a structural aspect of the polymer molecules formed, or both, is subject to control",[20] opened new routes to various polymers with controlled molecular architecture.

The key property of all CRP systems is the establishment of dynamic equilibrium between propagating radicals and dormant species which can be accomplished in two ways.[89-90] Radicals can be reversibly trapped in a deactivation/activation process (Scheme 4A), or they can be involved in a reversible degenerative exchange process (Scheme 4B). The first approach is based on persistent radical effect (PRE):[90-93] propagating species $P_n^{\bullet}$ are trapped in the deactivation process (k_{deact}) by persistent radicals X. The dormant species can be activated (k_{act}) spontaneously by light or catalyst and can propagate (k_p) and undergo termination (k_t), but persistent radicals X cannot terminate with each other. Every act of irreversible radical-radical termination is followed by accumulation of X leading to the decrease of the probability of the radical recombination. The most studied examples of polymerizations obeying the PRE are nitroxide mediated polymerization (NMP) and atom transfer radical polymerization (ATRP).[19, 88, 94] NMP can be mediated by various stable nitroxides, e.g. TEMPO, DEPN, etc.[94] ATRP employs catalyst which is a complex of transition metal (Mt^n) with ligand (L). Mt^n-L cleaves alkyl-halogen bond $R{-}X$ which results in higher oxidation state of transition metal Mt^{n+1}-X/L and organic radical $R^{\bullet}$. ATRP has been catalyzed by various metals, including Ti,[95] Mo,[96] Re,[97] Fe,[98-99] Ru,[100] Os,[101] Rh,[102] Co,[103] Ni,[104] Pd,[105] but Cu complexes have been found to be the most efficient.[19, 88] The group of Prof. Matyjaszewski made a great contribution into investigation of ATRP and published a number of comprehensive reviews and books.[106-111] ATRP is one of the most powerful synthetic techniques due to its numerous advantages: variety of monomers can be polymerized (except unprotected acids); ATRP reagents are commercially available; no Trommsdorf (autoacceleration) effect; large range of temperatures can be employed; facile end-functionalization. The main disadvantage of ATRP is the presence of toxic Cu catalyst which is hard to remove completely from the resulting polymer. NMP, on the other hand, is purely organic system and can be employed for polymerization of acidic monomers. However, it is

difficult to control the polymerization of disubstituted alkenes and introduce functional end-group, and typically high temperatures are required for this polymerization.[19]

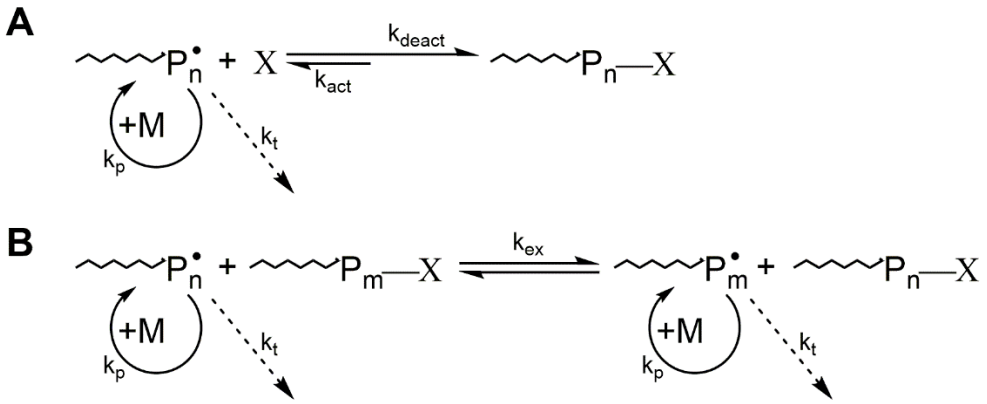

Scheme 4. Dynamic equilibrium in CRP: A: radicals are trapped in a deactivation/activation process; B: radicals are involved in exchange process.

The second approach in CRP (Scheme 4B) is not based on PRE. A steady state concentration of radicals is determined by initiation and termination steps like in conventional RP. Radicals undergo degenerative exchange with dormant species, and the exchange can proceed via atom/group transfer or addition-fragmentation process. Reversible addition-fragmentation chain transfer (RAFT) polymerization is one of the most successful examples of such type of CRP due to the high number of available monomers and control over MW and MWD of the resulting polymers.[19, 112-115] RAFT polymerization is mediated by organic reagents. However, the crucial limitations include poor stability of many transfer agents, incompatibility of some functional groups with some chain transfer agents, and difficulty with end-group functionalization.[19]

Development of CRP gives access to a virtually unlimited number of polymeric materials with designed architecture, composition, and functionality. The key advantages of CRP over LROP are a wide range of polymerizable monomers, moderate sensitivity to impurities, and ability to proceed in aqueous media. However, CRP often requires utilization of toxic reagents, control over MWD is limited, and polymers with biodegradable backbone cannot be synthesized via CRP. The latter limitation can be overcome by radical ring opening polymerization, but this technique lacks control and systematic investigation.[116]

2. Self-assembly of amphiphilic block copolymers in solution

Structures assembled from amphiphilic block copolymers are particularly advantageous for biomedical applications, such as drug delivery and tissue engineering, due to the facile design of block copolymers allowing for the fine tuning of the morphology and properties of the assemblies. In the next chapters the most important characterization techniques of the assemblies and principles of self-assembly are reviewed.

2.1. Methods of characterization of self-assembled structures

The morphology and size of nanoscale (< 1 μm) self-assembled structures are characterized in most cases by dynamic/static light scattering technique (DLS/SLS) and (cryogenic) transmission/scanning electron microscopy ((cryo)TEM, SEM). DLS provides information about hydrodynamic radius. Angular-dependent SLS allows determination of radius of gyration, weight-average molecular weight, and particles shape. By combining DLS and SLS it is possible to determine the structure of assemblies.[117] Other scattering techniques, like small angle neutron/X-ray scattering (SANS/SAXS), are used to study structure and interactions of self-assembled structures.[118] TEM and cryoTEM are the most frequently applied techniques to determine the morphology of self-assembled structures due to the high resolution (1 nm) allowing for visualization of fine details.[119] In some particular cases, NMR techniques are also suitable for the characterization of assemblies. For example, Schlaad et al.[120] used 2D-NOESY NMR to prove the asymmetry of the polymersome membrane.

Microscale (> 1 μm) structures can be characterized via optical microscopy. Fluorescence microscopy is the method of choice due to its high sensitivity and ability to visualize different morphologies labeled with fluorescent dyes. For example, confocal laser scanning microscopy (CLSM) enables visualization of the membrane and inner compartment of polymersomes when different dyes used for encapsulation and labeling of the membrane.[43, 121]

Finally, techniques like atomic force microscopy (AFM) and fluorescence (cross-)correlation spectroscopy (F(C)CS) are employed for additional characterization of self-assembled structures. AFM can be used for investigation of assemblies immobilized on surfaces. F(C)CS is a powerful method for studying both steady-state structures and monitoring dynamic processes of fluorescently labeled structures.[122-123] This technique allows exploring diffusion, binding events, and enzymatic reactions in time-resolved measurements.

2.2. Self-assembly of linear AB copolymers

Self-assembly of linear AB (A – hydrophilic, B – hydrophobic) diblock copolymers in dilute aqueous solution depending on the block ratio and method of self-assembly has been investigated for various systems. Packing parameter p, which depends on the volume v and length l_c of the hydrophobic chains and optimal area of the hydrophilic tail a_0, is inversely proportional to the hydrophilic weight fraction f.[124] As a general rule, the morphology formed by AB polymers changes in the row spherical micelles – elongated micelles – polymersomes (S–E–P) with the increase of p (or decrease of f) (Scheme 5). Such tendency was reported for PAA-*b*-PS,[125] PEO-*b*-PS,[126] PEO-*b*-PB,[24, 127] PEO-*b*-PMCL,[128] and PMOXA-*b*-PDMS[32] copolymers. PEO-*b*-PCL copolymers, however, do not fully obey this rule and self-assemble into microscale structures, whereas other copolymers form nanoscale morphologies. Unique self-assembly behavior of PEO-*b*-PCL is associated with semicrystalline nature of the PCL block. Self-assembly requires temperatures above the melting point of PCL ($T_m \approx 60$ ºC) or the presence of organic solvent. With the decrease of f the morphology changes in the row spherical particles – polymersomes – irregularly shaped particles/precipitate (S–P–I), and for some PEO-*b*-PCL the transition follows S–I pattern.[22] Perhaps such self-assembly behavior can be associated with formation of spherulites by PCL block in the bulk phase.[129]

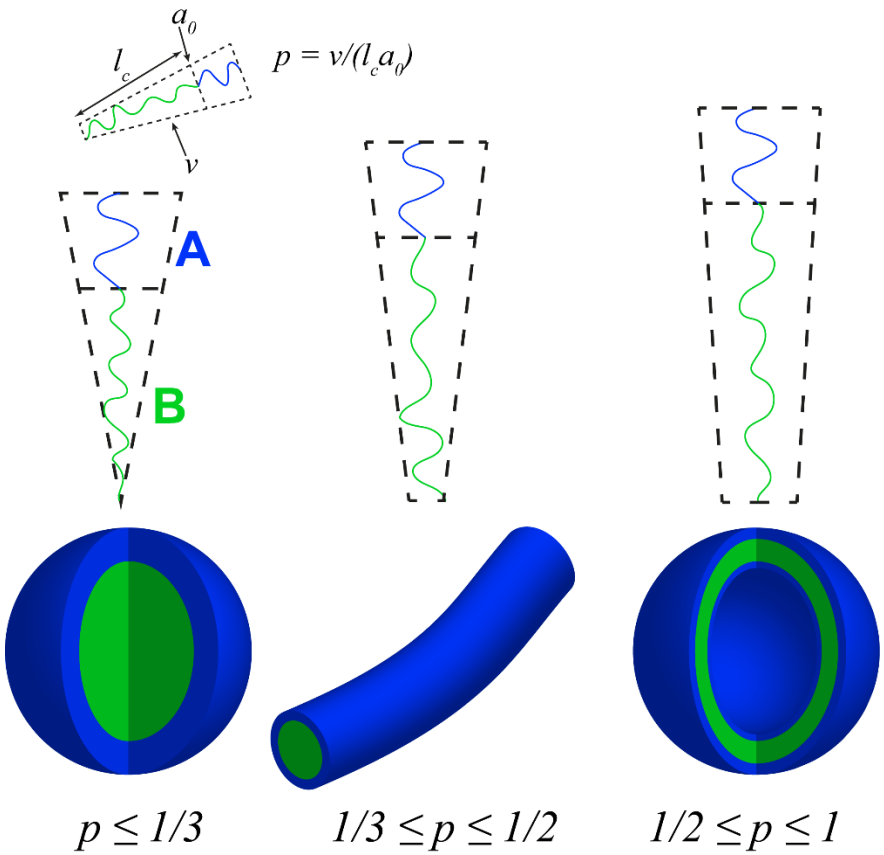

Scheme 5. Morphology of the self-assembled structures formed by AB copolymers in A-selective solvent depending on the *p*. Adapted from ref.[130]

Apart from the length of the corresponding blocks, self-assembly of AB copolymers depends on the method of self-assembly.[131] Copolymer concentration has a dramatic effect on the self-assembly: increase of the concentration has a similar effect as decrease of the corona length A.[132-133] It can be explained by increase in the aggregation number $N_{agg} = 2(C/CMC)^{1/2}$, where C is a copolymer concentration and CMC is critical micellization concentration.[124] Increase of N_{agg} leads to an increase of the sizes of micelle cores, which is accompanied by an increase of the degree of stretching of the hydrophobic chains. The higher degree of stretching of the hydrophobic block means an increase in its length l_c, which is similar to a decrease in corona length A.

Eisenberg and co-workers has extensively studied major factors influencing self-assembly of PAA-*b*-PS copolymers. They applied a co-solvent method due to a glassy nature of the PS block at room temperature ($T_g \approx 100$ ºC); in this method a polymer was dissolved first in a common solvent, e.g. DMF, THF, dioxane, and then the selective solvent, water, was slowly

added.[132] In such mixtures water content[134-135] and the rate of water addition[136] influenced the morphology. The effect of water content is ascribed to the change of N_{agg} and critical water content (*CWC*) at which the micellization starts. The rate of water addition has a strong impact on the ability of a system to reach the equilibrium state.[136] At low water content, the mobility of polymer chains is high, and the morphological transition can be faster than increase of the water content. On the other hand, at high water content the assemblies become kinetically frozen, and the thermodynamic equilibrium cannot be reached on the experimental timescale. For systems prepared using other self-assembly techniques it practically means that in the case of equilibrium morphologies the size and structure of the assemblies should not depend on the details in preparation procedure.[132] However, it is believed that global equilibrium is not achieved on experimental time scales due to slow kinetics of high molecular weight polymers which hinders structural evolution of the self-assembled morfologies.[137]

Nature of the common solvent has an effect on the morphology mainly because of the two parameters: solubility of the PS block (δ) and ionization of the PAA block which is determined by dielectric constant (ε) of the solvent.[138] Since the common solvent is present in the hydrophobic domains during water addition, δ determines the degree of swelling and mobility of the PS chains. THF and dioxane result in higher PS mobility than DMF. Therefore, the presence of THF and dioxane facilitates the growth of micelles and increases the range of water contents in which the assemblies are still labile. The repulsive forces in the corona strongly depend on the ionization of PAA, which is higher in a common solvent with a higher ε, like DMF, than in THF or dioxane. Stronger repulsion leads to an increase in the interfacial area a_0 occupied by hydrophilic chains, which is similar to an increase in the corona length A. The presence of ions and pH also contribute to the ionization and repulsion between the corona chains, possessing a significant effect on the morphology.[25, 139]

2.3. Self-assembly of linear ABC copolymers

ABC copolymers offer unique opportunities for development of sophisticated structures which cannot be accessed with conventional AB copolymers. The presence of an additional C block introduces a higher degree of complexity in self-assembly behavior. For example, ABC copolymers are predicted to form a wide range of ordered structures in bulk phase.[140-142] Battaglia and co-workers[143] have recently shown formation of stable patchy (i.e. domains in the

corona) polymersomes which were obtained by mixing poly(methacryl phosphoryl choline)-*block*-poly(diisopropylaminoethyl methacrylate) (PMPC-*b*-PDPA) diblock copolymer with (PEO/PMPC)-*b*-PDPA miktoarm star triblock copolymer. Müller and co-workers reported about various structures formed by linear ABC copolymers. For example, undulated rods were obtained via self-assembly of ABC copolymers in (A, C)-selective solvents into patchy micelles which further aggregated into rods due to the collapse of the C block by decreasing its solubility.[144-145] Using similar self-assembly approach, different multicompartment (i.e. domains in the core) nanostructures can be formed by linear ABC terpolymers in organic C-selective solvent with phase separation of A/B blocks in the core.[146-147] The rational design of such self-assembled structures was described based on polysterene-*block*-polybutadiene-*block*-poly(*tert*-butyl methacrylate) (PS-*b*-PB-*b*-PT) model system in acetone/isopropanol mixtures, where PT is always soluble, PB is insoluble, and the collapse of PS is controlled by the solvent composition (Fig. 1). The corona length (N_T) determines micelle geometry, whereas length of PB (N_B) is responsible for the morphology of PB domains in the PS core. Such multicompartment structures may serve as templates for nanooptics and nanoelectronics, and their analogues assembled in aqueous solution can be used as smart drug delivery systems with controlled pharmacokinetic release profiles.

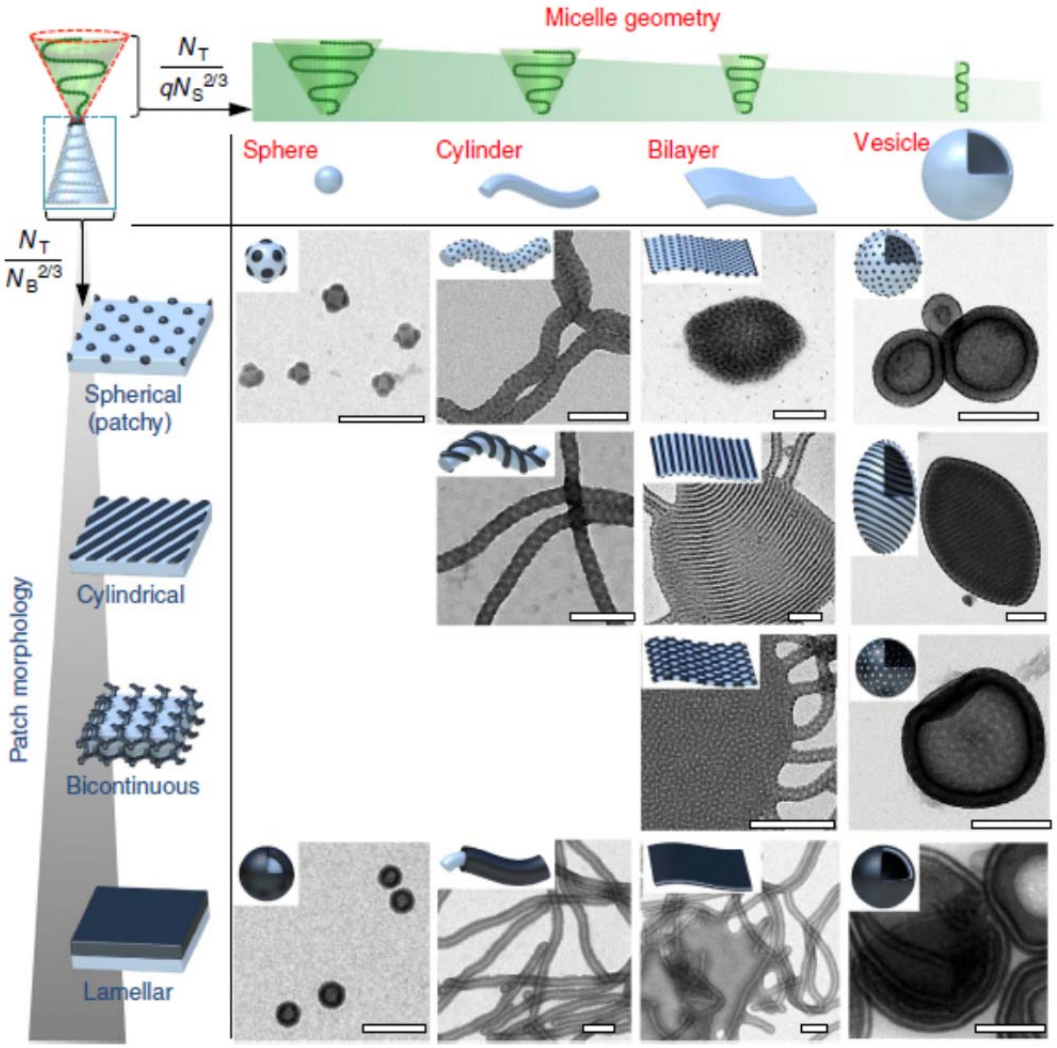

Figure 1 from ref.[147] Classification of micelle geometry by compartment morphology: spheres-on-spheres, spheres-on-cylinders, spheres-on-bilayer sheets and polymersomes; cylinders-on-cylinders (double-helix compartment), cylinders-on-bilayer sheets and polymersomes; sheets and polymersomes with bicontinuous membrane morphology; core–shell micelles, core-shell cylinders, lamellar sheets and vesicles. Scale bars are 200 nm.

Linear ABC copolymers with soluble A and C blocks can form structures with mixed, patchy, and Janus corona[144-145, 148-154] with diverse potential applications ranging from materials science to biomedicine.[155-156] Depending on the nature of A and C blocks, the domains on the surface can possess different chemical and physical properties for selective catalysis, responsiveness to certain stimuli, immobilization of specific molecules, etc. Bis-hydrophilic ABC copolymers, where A and C are water soluble blocks, self-assemble into polymersomes with asymmetric membrane.[26, 121, 157-160] The shorter block forms the inner corona due to the

preferred lower curvature, and the outer corona is composed by a longer block. Such polymersomes may have inner and outer surfaces with different properties, for example different affinity to protein absorption as was shown for PEO-*b*-PCL-*b*-PAA system.[26] Müller and co-workers[151] studied aqueous self-assembly of some bis-hydrophilic ABC copolymers depending on the preparation procedure and hydrophilic-to-hydrophobic balance, but there is still lack of systematic investigation and mechanistic understanding of self-assembly of such systems in both aqueous and organic (A, C)-selective medium.

3. Scope of this thesis

The emerging field of the complex aqueous self-assembly of linear AB and ABC (A, C – hydrophilic, B – hydrophobic) copolymers has inspired and motivated the work presented in this thesis. The following copolymers were chosen as model systems: poly(ethylene oxide)-*block*-polycaprolactone (PEO-*b*-PCL), poly(ethylene oxide)-*block*-polycaprolactone-*block*-poly(2-methyl-2-oxazoline) (PEO-*b*-PCL-*b*-PMOXA), and poly(ethylene oxide)-*block*-poly(γ-R-ε-caprolactone)-*block*-poly*(N,N*-dimethylaminoethyl methacrylate) (PEO-*b*-P(R)CL-*b*-PDMAEMA, where R = methyl (M) or phenyl (Ph)). These copolymers are highly relevant for potential biomedical applications due to biocompatible protein-repellent nature of hydrophilic PEO and PMOXA, biodegradability of hydrophobic polyesters, and ability of cationic PDMAEMA to complex nucleic acids. The synthesis has been achieved via a combination of coordination LROP of ε-CL/MCL/PhCL and microwave-assisted cationic LROP of MOXA or ATRP of DMAEMA. Self-assembled structures were investigated via laser scanning microscopy, transmission electron microscopy (TEM), and cryogenic TEM. Self-assembly was tested under different conditions and explained in terms of packing geometry of individual polymer molecules.

The main goals of this thesis have been approached via:

(i) optimization of the synthesis of PEO-*b*-PCL (Publication 1);

(ii) development of the synthetic strategy for PEO-*b*-PCL-*b*-PMOXA (Publication 2);

(iii) investigation of the aqueous self-assembly of PEO-*b*-PCL and PEO-*b*-PCL-*b*-PMOXA under different conditions (Publication 1 and 3);

(iv) investigation of the effect of hydrophobicity of the middle block of PEO-*b*-PRCL-*b*-PDMAEMA copolymers on their aqueous self-assembly (Section 4).

References

1. Ball, P., H2O. A Biography of Water. Phoenix. Orion Books Ltd, London: 2000.
2. Discher, D. E.; Ahmed, F., POLYMERSOMES. *Annual Review of Biomedical Engineering* **2006,** *8* (1), 323-341.
3. Adams, M. L.; Lavasanifar, A.; Kwon, G. S., Amphiphilic block copolymers for drug delivery. *Journal of Pharmaceutical Sciences* **2003,** *92* (7), 1343-1355.
4. Palivan, C. G.; Goers, R.; Najer, A.; Zhang, X.; Car, A.; Meier, W., Bioinspired polymer vesicles and membranes for biological and medical applications. *Chemical Society Reviews* **2016,** *45* (2), 377-411.
5. Gunkel-Grabole, G.; Sigg, S.; Lomora, M.; Lorcher, S.; Palivan, C. G.; Meier, W. P., Polymeric 3D nano-architectures for transport and delivery of therapeutically relevant biomacromolecules. *Biomaterials Science* **2015,** *3* (1), 25-40.
6. Pack, D. W.; Hoffman, A. S.; Pun, S.; Stayton, P. S., Design and development of polymers for gene delivery. *Nat Rev Drug Discov* **2005,** *4* (7), 581-593.
7. Najer, A.; Wu, D.; Vasquez, D.; Palivan, C. G.; Meier, W., Polymer nanocompartments in broad-spectrum medical applications. *Nanomedicine* **2013,** *8* (3), 425-447.
8. Vaughn, T. H.; Suter, H. R.; Lundsted, L. G.; Kramer, M. G., Properties of some newly developed nonionic detergents. *Journal of the American Oil Chemists' Society* **1951,** *28* (7), 294-299.
9. Mankowich, A. M., Micellar Molecular Weights of Selected Surface Active Agents. *The Journal of Physical Chemistry* **1954,** *58* (11), 1027-1030.
10. Alexandridis, P.; Alan Hatton, T., Poly(ethylene oxide)□poly(propylene oxide)□poly(ethylene oxide) block copolymer surfactants in aqueous solutions and at interfaces: thermodynamics, structure, dynamics, and modeling. *Colloids and Surfaces A: Physicochemical and Engineering Aspects* **1995,** *96* (1), 1-46.
11. Bates, C. M.; Bates, F. S., 50th Anniversary Perspective: Block Polymers—Pure Potential. *Macromolecules* **2017,** *50* (1), 3-22.
12. Szwarc, M.; Levy, M.; Milkovich, R., POLYMERIZATION INITIATED BY ELECTRON TRANSFER TO MONOMER. A NEW METHOD OF FORMATION OF BLOCK POLYMERS1. *Journal of the American Chemical Society* **1956,** *78* (11), 2656-2657.
13. Szwarc, M., /`Living/' Polymers. *Nature* **1956,** *178* (4543), 1168-1169.
14. Matyjaszewski, K., *Cationic Polymerizations: Mechanisms, Synthesis & Applications*. CRC Press: 1996.
15. Doi, Y.; Keii, T., Synthesis of "living" polyolefins with soluble Ziegler-Natta catalysts and application to block copolymerization. In *Chromatography/Foams/Copolymers*, Springer: 1986; pp 201-248.
16. Grubbs, R. H., Olefin-Metathesis Catalysts for the Preparation of Molecules and Materials (Nobel Lecture). *Angewandte Chemie International Edition* **2006,** *45* (23), 3760-3765.
17. Bielawski, C. W.; Grubbs, R. H., Living ring-opening metathesis polymerization. *Progress in Polymer Science* **2007,** *32* (1), 1-29.
18. Penczek, S.; Cypryk, M.; Duda, A.; Kubisa, P.; Słomkowski, S., Living ring-opening polymerizations of heterocyclic monomers. *Progress in Polymer Science* **2007,** *32* (2), 247-282.
19. Braunecker, W. A.; Matyjaszewski, K., Controlled/living radical polymerization: Features, developments, and perspectives. *Progress in Polymer Science* **2007,** *32* (1), 93-146.

20. Penczek, S., Terminology of kinetics, thermodynamics, and mechanisms of polymerization. *Journal of Polymer Science Part A: Polymer Chemistry* **2002,** *40* (11), 1665-1676.
21. Flory, P. J., Molecular Size Distribution in Ethylene Oxide Polymers. *Journal of the American Chemical Society* **1940,** *62* (6), 1561-1565.
22. Qi, W.; Ghoroghchian, P. P.; Li, G.; Hammer, D. A.; Therien, M. J., Aqueous self-assembly of poly(ethylene oxide)-block-poly(?-caprolactone) (PEO-b-PCL) copolymers: disparate diblock copolymer compositions give rise to nano- and meso-scale bilayered vesicles. *Nanoscale* **2013,** *5* (22), 10908-10915.
23. Gong, C.; Shi, S.; Dong, P.; Kan, B.; Gou, M.; Wang, X.; Li, X.; Luo, F.; Zhao, X.; Wei, Y.; Qian, Z., Synthesis and characterization of PEG-PCL-PEG thermosensitive hydrogel. *International Journal of Pharmaceutics* **2009,** *365* (1–2), 89-99.
24. Jain, S.; Bates, F. S., On the Origins of Morphological Complexity in Block Copolymer Surfactants. *Science* **2003,** *300* (5618), 460-464.
25. Zhang, L.; Yu, K.; Eisenberg, A., Ion-Induced Morphological Changes in "Crew-Cut" Aggregates of Amphiphilic Block Copolymers. *Science* **1996,** *272* (5269), 1777-1779.
26. Wittemann, A.; Azzam, T.; Eisenberg, A., Biocompatible Polymer Vesicles from Biamphiphilic Triblock Copolymers and Their Interaction with Bovine Serum Albumin. *Langmuir* **2007,** *23* (4), 2224-2230.
27. Jones, R. G.; Ando, W.; Chojnowski, J., *Silicon-containing polymers: the science and technology of their synthesis and applications*. Springer Science & Business Media: 2013.
28. Hashimoto, K., Ring-opening polymerization of lactams. Living anionic polymerization and its applications. *Progress in Polymer Science* **2000,** *25* (10), 1411-1462.
29. Deming, T. J., Polypeptide and polypeptide hybrid copolymer synthesis via NCA polymerization. In *Peptide hybrid polymers*, Springer: 2006; pp 1-18.
30. Penczek, S.; Duda, A.; Kaluzynski, K.; Lapienis, G.; Nyk, A.; Szymanski, R., Thermodynamics and kinetics of ring-opening polymerization of cyclic alkylene phosphates. *Makromolekulare Chemie. Macromolecular Symposia* **1993,** *73* (1), 91-101.
31. Penczek, S.; Biela, T.; Klosinski, P.; Lapienis, G., Polymerization of phosphorus containing cyclic monomers: Synthesis of polymers related to biopolymers. *Makromolekulare Chemie. Macromolecular Symposia* **1986,** *6* (1), 123-153.
32. Wu, D.; Spulber, M.; Itel, F.; Chami, M.; Pfohl, T.; Palivan, C. G.; Meier, W., Effect of Molecular Parameters on the Architecture and Membrane Properties of 3D Assemblies of Amphiphilic Copolymers. *Macromolecules* **2014,** *47* (15), 5060-5069.
33. Dimitrov, I.; Schlaad, H., Synthesis of nearly monodisperse polystyrene-polypeptide block copolymers via polymerisation of N-carboxyanhydrides. *Chemical Communications* **2003,** (23), 2944-2945.
34. Kricheldorf, H. R.; Lee, S.-R.; Bush, S., Polylactones 36. Macrocyclic Polymerization of Lactides with Cyclic Bu2Sn Initiators Derived from 1,2-Ethanediol, 2-Mercaptoethanol, and 1,2-Dimercaptoethane. *Macromolecules* **1996,** *29* (5), 1375-1381.
35. Kricheldorf, H. R.; Berl, M.; Scharnagl, N., Poly (lactones). 9. Polymerization mechanism of metal alkoxide initiated polymerizations of lactide and various lactones. *Macromolecules* **1988,** *21* (2), 286-293.
36. Kowalski, A.; Duda, A.; Penczek, S., Kinetics and mechanism of cyclic esters polymerization initiated with tin(II) octoate, 1. Polymerization of ε-caprolactone. *Macromolecular Rapid Communications* **1998,** *19* (11), 567-572.

37. Majerska, K.; Duda, A.; Penczek, S., Kinetics and mechanism of cyclic esters polymerisation initiated with tin(II) octoate, 4. Influence of proton trapping agents on the kinetics of ε-caprolactone and L,L-dilactide polymerisation. *Macromolecular Rapid Communications* **2000,** *21* (18), 1327-1332.
38. Libiszowski, J.; Kowalski, A.; Duda, A.; Penczek, S., Kinetics and mechanism of cyclic esters polymerization initiated with covalent metal carboxylates, 5. End-group studies in the model ε-caprolactone and L,L-dilactide/Tin(II) and zinc octoate/butyl alcohol systems. *Macromolecular Chemistry and Physics* **2002,** *203* (10-11), 1694-1701.
39. Kowalski, A.; Duda, A.; Penczek, S., Mechanism of Cyclic Ester Polymerization Initiated with Tin(II) Octoate. 2.† Macromolecules Fitted with Tin(II) Alkoxide Species Observed Directly in MALDI−TOF Spectra. *Macromolecules* **2000,** *33* (3), 689-695.
40. Kowalski, A.; Libiszowski, J.; Biela, T.; Cypryk, M.; Duda, A.; Penczek, S., Kinetics and Mechanism of Cyclic Esters Polymerization Initiated with Tin(II) Octoate. Polymerization of ε-Caprolactone and l,l-Lactide Co-initiated with Primary Amines. *Macromolecules* **2005,** *38* (20), 8170-8176.
41. Goldberg, D., A review of the biodegradability and utility of poly(caprolactone). *Journal of environmental polymer degradation* **1995,** *3* (2), 61-67.
42. Tokiwa, Y.; Calabia, B. P., Biodegradability and Biodegradation of Polyesters. *Journal of Polymers and the Environment* **2007,** *15* (4), 259-267.
43. Ghoroghchian, P. P.; Li, G.; Levine, D. H.; Davis, K. P.; Bates, F. S.; Hammer, D. A.; Therien, M. J., Bioresorbable Vesicles Formed through Spontaneous Self-Assembly of Amphiphilic Poly(ethylene oxide)-block-polycaprolactone. *Macromolecules* **2006,** *39* (5), 1673-1675.
44. Rajagopal, K.; Mahmud, A.; Christian, D. A.; Pajerowski, J. D.; Brown, A. E. X.; Loverde, S. M.; Discher, D. E., Curvature-Coupled Hydration of Semicrystalline Polymer Amphiphiles Yields flexible Worm Micelles but Favors Rigid Vesicles: Polycaprolactone-Based Block Copolymers. *Macromolecules* **2010,** *43* (23), 9736-9746.
45. Geng, Y.; Dalhaimer, P.; Cai, S.; Tsai, R.; Tewari, M.; Minko, T.; Discher, D. E., Shape effects of filaments versus spherical particles in flow and drug delivery. *Nat Nano* **2007,** *2* (4), 249-255.
46. Cohn, D.; Younes, H., Biodegradable PEO/PLA block copolymers. *Journal of Biomedical Materials Research* **1988,** *22* (11), 993-1009.
47. Najer, A.; Wu, D.; Nussbaumer, M. G.; Schwertz, G.; Schwab, A.; Witschel, M. C.; Schafer, A.; Diederich, F.; Rottmann, M.; Palivan, C. G.; Beck, H.-P.; Meier, W., An amphiphilic graft copolymer-based nanoparticle platform for reduction-responsive anticancer and antimalarial drug delivery. *Nanoscale* **2016,** *8* (31), 14858-14869.
48. Penczek, S., Cationic ring-opening polymerization (CROP) major mechanistic phenomena. *Journal of Polymer Science Part A: Polymer Chemistry* **2000,** *38* (11), 1919-1933.
49. Kagiya, T.; Narisawa, S.; Maeda, T.; Fukui, K., Ring-opening polymerization of 2-substituted 2-oxazolines. *Journal of Polymer Science Part B: Polymer Letters* **1966,** *4* (7), 441-445.
50. Tomalia, D. A.; Sheetz, D. P., Homopolymerization of 2-alkyl- and 2-aryl-2-oxazolines. *Journal of Polymer Science Part A-1: Polymer Chemistry* **1966,** *4* (9), 2253-2265.
51. Bassiri, T. G.; Levy, A.; Litt, M., Polymerization of cyclic imino ethers. I. Oxazolines. *Journal of Polymer Science Part B: Polymer Letters* **1967,** *5* (9), 871-879.

52. Seeliger, W.; Aufderhaar, E.; Diepers, W.; Feinauer, R.; Nehring, R.; Thier, W.; Hellmann, H., Recent Syntheses and Reactions of Cyclic Imidic Esters. *Angewandte Chemie International Edition in English* **1966,** *5* (10), 875-888.
53. Aoi, K.; Okada, M., Polymerization of oxazolines. *Progress in Polymer Science* **1996,** *21* (1), 151-208.
54. Saegusa, T.; Ikeda, H.; Fujii, H., Isomerization Polymerization of 2-Oxazoline. IV. Kinetic Study of 2-Methyl-2-oxazoline Polymerization. *Macromolecules* **1972,** *5* (4), 359-362.
55. Kobayashi, S.; Saegusa, T., Block and graft copolymers of 2-oxazolines. *Macromolecular Chemistry and Physics* **1985,** *12* (S19851), 11-24.
56. Kobayashi, S., Ethylenimine polymers. *Progress in Polymer Science* **1990,** *15* (5), 751-823.
57. Kobayashi, S.; Uyama, H., Polymerization of cyclic imino ethers: From its discovery to the present state of the art. *Journal of Polymer Science Part A: Polymer Chemistry* **2002,** *40* (2), 192-209.
58. Makino, A.; Kobayashi, S., Chemistry of 2-oxazolines: A crossing of cationic ring-opening polymerization and enzymatic ring-opening polyaddition. *Journal of Polymer Science Part A: Polymer Chemistry* **2010,** *48* (6), 1251-1270.
59. Hoogenboom, R., Poly(2-oxazoline)s: A Polymer Class with Numerous Potential Applications. *Angewandte Chemie International Edition* **2009,** *48* (43), 7978-7994.
60. Hoogenboom, R.; Fijten, M. W. M.; Schubert, U. S., Parallel kinetic investigation of 2-oxazoline polymerizations with different initiators as basis for designed copolymer synthesis. *Journal of Polymer Science Part A: Polymer Chemistry* **2004,** *42* (8), 1830-1840.
61. Hoogenboom, R.; Fijten, M. W. M.; Thijs, H. M. L.; van Lankvelt, B. M.; Schubert, U. S., Microwave-assisted synthesis and properties of a series of poly(2-alkyl-2-oxazoline)s. *Designed Monomers and Polymers* **2005,** *8* (6), 659-671.
62. Hoogenboom, R.; Wiesbrock, F.; Huang, H.; Leenen, M. A. M.; Thijs, H. M. L.; van Nispen, S. F. G. M.; van der Loop, M.; Fustin, C.-A.; Jonas, A. M.; Gohy, J.-F.; Schubert, U. S., Microwave-Assisted Cationic Ring-Opening Polymerization of 2-Oxazolines: A Powerful Method for the Synthesis of Amphiphilic Triblock Copolymers. *Macromolecules* **2006,** *39* (14), 4719-4725.
63. Wiesbrock, F.; Hoogenboom, R.; Leenen, M.; van Nispen, S. F. G. M.; van der Loop, M.; Abeln, C. H.; van den Berg, A. M. J.; Schubert, U. S., Microwave-Assisted Synthesis of a 42-Membered Library of Diblock Copoly(2-oxazoline)s and Chain-Extended Homo Poly(2-oxazoline)s and Their Thermal Characterization. *Macromolecules* **2005,** *38* (19), 7957-7966.
64. Wiesbrock, F.; Hoogenboom, R.; Leenen, M. A. M.; Meier, M. A. R.; Schubert, U. S., Investigation of the Living Cationic Ring-Opening Polymerization of 2-Methyl-, 2-Ethyl-, 2-Nonyl-, and 2-Phenyl-2-oxazoline in a Single-Mode Microwave Reactor†. *Macromolecules* **2005,** *38* (12), 5025-5034.
65. Glassner, M.; D'hooge, D. R.; Young Park, J.; Van Steenberge, P. H. M.; Monnery, B. D.; Reyniers, M.-F.; Hoogenboom, R., Systematic investigation of alkyl sulfonate initiators for the cationic ring-opening polymerization of 2-oxazolines revealing optimal combinations of monomers and initiators. *European Polymer Journal* **2015,** *65*, 298-304.
66. Vergaelen, M.; Verbraeken, B.; Monnery, B. D.; Hoogenboom, R., Sulfolane as Common Rate Accelerating Solvent for the Cationic Ring-Opening Polymerization of 2-Oxazolines. *ACS Macro Letters* **2015,** *4* (8), 825-828.

67. de la Rosa, V. R.; Tempelaar, S.; Dubois, P.; Hoogenboom, R.; Mespouille, L., Poly(2-ethyl-2-oxazoline)-block-polycarbonate block copolymers: from improved end-group control in poly(2-oxazoline)s to chain extension with aliphatic polycarbonate through a fully metal-free ring-opening polymerisation process. *Polymer Chemistry* **2016,** *7* (8), 1559-1568.
68. Bouten, P. J. M.; Hertsen, D.; Vergaelen, M.; Monnery, B. D.; Boerman, M. A.; Goossens, H.; Catak, S.; van Hest, J. C. M.; Van Speybroeck, V.; Hoogenboom, R., Accelerated living cationic ring-opening polymerization of a methyl ester functionalized 2-oxazoline monomer. *Polymer Chemistry* **2015,** *6* (4), 514-518.
69. Baeten, E.; Verbraeken, B.; Hoogenboom, R.; Junkers, T., Continuous poly(2-oxazoline) triblock copolymer synthesis in a microfluidic reactor cascade. *Chemical Communications* **2015,** *51* (58), 11701-11704.
70. Lava, K.; Verbraeken, B.; Hoogenboom, R., Poly(2-oxazoline)s and click chemistry: A versatile toolbox toward multi-functional polymers. *European Polymer Journal* **2015,** *65*, 98-111.
71. Knop, K.; Hoogenboom, R.; Fischer, D.; Schubert, U. S., Poly(ethylene glycol) in Drug Delivery: Pros and Cons as Well as Potential Alternatives. *Angewandte Chemie International Edition* **2010,** *49* (36), 6288-6308.
72. Sedlacek, O.; Monnery, B. D.; Filippov, S. K.; Hoogenboom, R.; Hruby, M., Poly(2-Oxazoline)s – Are They More Advantageous for Biomedical Applications Than Other Polymers? *Macromolecular Rapid Communications* **2012,** *33* (19), 1648-1662.
73. Lambermont-Thijs, H. M. L.; Hoogenboom, R.; Fustin, C.-A.; Bomal-D'Haese, C.; Gohy, J.-F.; Schubert, U. S., Solubility behavior of amphiphilic block and random copolymers based on 2-ethyl-2-oxazoline and 2-nonyl-2-oxazoline in binary water–ethanol mixtures. *Journal of Polymer Science Part A: Polymer Chemistry* **2009,** *47* (2), 515-522.
74. Diab, C.; Akiyama, Y.; Kataoka, K.; Winnik, F. M., Microcalorimetric Study of the Temperature-Induced Phase Separation in Aqueous Solutions of Poly(2-isopropyl-2-oxazolines). *Macromolecules* **2004,** *37* (7), 2556-2562.
75. Nardin, C.; Thoeni, S.; Widmer, J.; Winterhalter, M.; Meier, W., Nanoreactors based on (polymerized) ABA-triblock copolymer vesicles. *Chemical Communications* **2000,** (15), 1433-1434.
76. Baumann, P.; Spulber, M.; Fischer, O.; Car, A.; Meier, W., Investigation of Horseradish Peroxidase Kinetics in an "Organelle-Like" Environment. *Small* **2017**, 1603943-n/a.
77. Zhang, X.; Lomora, M.; Einfalt, T.; Meier, W.; Klein, N.; Schneider, D.; Palivan, C. G., Active surfaces engineered by immobilizing protein-polymer nanoreactors for selectively detecting sugar alcohols. *Biomaterials* **2016,** *89*, 79-88.
78. Kowal, J.; Wu, D.; Mikhalevich, V.; Palivan, C. G.; Meier, W., Hybrid Polymer–Lipid Films as Platforms for Directed Membrane Protein Insertion. *Langmuir* **2015,** *31* (17), 4868-4877.
79. Itel, F.; Najer, A.; Palivan, C. G.; Meier, W., Dynamics of Membrane Proteins within Synthetic Polymer Membranes with Large Hydrophobic Mismatch. *Nano Letters* **2015,** *15* (6), 3871-3878.
80. Kowal, J. Ł.; Kowal, J. K.; Wu, D.; Stahlberg, H.; Palivan, C. G.; Meier, W. P., Functional surface engineering by nucleotide-modulated potassium channel insertion into polymer membranes attached to solid supports. *Biomaterials* **2014,** *35* (26), 7286-7294.
81. Langowska, K.; Palivan, C. G.; Meier, W., Polymer nanoreactors shown to produce and release antibiotics locally. *Chemical Communications* **2013,** *49* (2), 128-130.

82. Wang, H.; Chung, T.-S.; Tong, Y. W.; Jeyaseelan, K.; Armugam, A.; Chen, Z.; Hong, M.; Meier, W., Highly Permeable and Selective Pore-Spanning Biomimetic Membrane Embedded with Aquaporin Z. *Small* **2012,** *8* (8), 1185-1190.
83. Thoma, J.; Belegrinou, S.; Rossbach, P.; Grzelakowski, M.; Kita-Tokarczyk, K.; Meier, W., Membrane protein distribution in composite polymer-lipid thin films. *Chemical Communications* **2012,** *48* (70), 8811-8813.
84. Tanner, P.; Onaca, O.; Balasubramanian, V.; Meier, W.; Palivan, C. G., Enzymatic Cascade Reactions inside Polymeric Nanocontainers: A Means to Combat Oxidative Stress. *Chemistry – A European Journal* **2011,** *17* (16), 4552-4560.
85. Graff, A.; Fraysse-Ailhas, C.; Palivan, C. G.; Grzelakowski, M.; Friedrich, T.; Vebert, C.; Gescheidt, G.; Meier, W., Amphiphilic Copolymer Membranes Promote NADH:Ubiquinone Oxidoreductase Activity: Towards an Electron-Transfer Nanodevice. *Macromolecular Chemistry and Physics* **2010,** *211* (2), 229-238.
86. Kamber, N. E.; Jeong, W.; Waymouth, R. M.; Pratt, R. C.; Lohmeijer, B. G. G.; Hedrick, J. L., Organocatalytic Ring-Opening Polymerization. *Chemical Reviews* **2007,** *107* (12), 5813-5840.
87. Litt, M.; Levy, A.; Herz, J., Polymerization of Cyclic Imino Ethers. X. Kinetics, Chain Transfer, and Repolymerization. *Journal of Macromolecular Science: Part A - Chemistry* **1975,** *9* (5), 703-727.
88. Matyjaszewski, K., Atom Transfer Radical Polymerization (ATRP): Current Status and Future Perspectives. *Macromolecules* **2012,** *45* (10), 4015-4039.
89. Greszta, D.; Mardare, D.; Matyjaszewski, K., "Living" radical polymerization. 1. Possibilities and limitations. *Macromolecules* **1994,** *27* (3), 638-644.
90. Goto, A.; Fukuda, T., Kinetics of living radical polymerization. *Progress in Polymer Science* **2004,** *29* (4), 329-385.
91. Fischer, H., The Persistent Radical Effect: A Principle for Selective Radical Reactions and Living Radical Polymerizations. *Chemical Reviews* **2001,** *101* (12), 3581-3610.
92. Tang, W.; Tsarevsky, N. V.; Matyjaszewski, K., Determination of Equilibrium Constants for Atom Transfer Radical Polymerization. *Journal of the American Chemical Society* **2006,** *128* (5), 1598-1604.
93. Tang, W.; Fukuda, T.; Matyjaszewski, K., Reevaluation of Persistent Radical Effect in NMP. *Macromolecules* **2006,** *39* (13), 4332-4337.
94. Hawker, C. J.; Bosman, A. W.; Harth, E., New Polymer Synthesis by Nitroxide Mediated Living Radical Polymerizations. *Chemical Reviews* **2001,** *101* (12), 3661-3688.
95. Kabachii, Y. A.; Kochev, S. Y.; Bronstein, L. M.; Blagodatskikh, I. B.; Valetsky, P. M., Atom Transfer Radical Polymerization with Ti(III) Halides and Alkoxides. *Polymer Bulletin* **2003,** *50* (4), 271-278.
96. Maria, S.; Stoffelbach, F.; Mata, J.; Daran, J.-C.; Richard, P.; Poli, R., The Radical Trap in Atom Transfer Radical Polymerization Need Not Be Thermodynamically Stable. A Study of the MoX3(PMe3)3 Catalysts. *Journal of the American Chemical Society* **2005,** *127* (16), 5946-5956.
97. Kotani, Y.; Kamigaito, M.; Sawamoto, M., Re(V)-Mediated Living Radical Polymerization of Styrene: ReO2I(PPh3)2/R−I Initiating Systems. *Macromolecules* **1999,** *32* (8), 2420-2424.

98. Matyjaszewski, K.; Wei, M.; Xia, J.; McDermott, N. E., Controlled/“Living” Radical Polymerization of Styrene and Methyl Methacrylate Catalyzed by Iron Complexes. *Macromolecules* **1997,** *30* (26), 8161-8164.
99. Silva, T. B.; Spulber, M.; Kocik, M. K.; Seidi, F.; Charan, H.; Rother, M.; Sigg, S. J.; Renggli, K.; Kali, G.; Bruns, N., Hemoglobin and Red Blood Cells Catalyze Atom Transfer Radical Polymerization. *Biomacromolecules* **2013,** *14* (8), 2703-2712.
100. Simal, F.; Demonceau, A.; Noels, A. F., Highly Efficient Ruthenium-Based Catalytic Systems for the Controlled Free-Radical Polymerization of Vinyl Monomers. *Angewandte Chemie International Edition* **1999,** *38* (4), 538-540.
101. Braunecker, W. A.; Itami, Y.; Matyjaszewski, K., Osmium-mediated radical polymerization. *Macromolecules* **2005,** *38* (23), 9402-9404.
102. Percec, V.; Barboiu, B.; Neumann, A.; Ronda, J. C.; Zhao, M., Metal-Catalyzed “Living” Radical Polymerization of Styrene Initiated with Arenesulfonyl Chlorides. From Heterogeneous to Homogeneous Catalysis. *Macromolecules* **1996,** *29* (10), 3665-3668.
103. Wang, B.; Zhuang, Y.; Luo, X.; Xu, S.; Zhou, X., Controlled/“Living” Radical Polymerization of MMA Catalyzed by Cobaltocene. *Macromolecules* **2003,** *36* (26), 9684-9686.
104. Granel, C.; Dubois, P.; Jérôme, R.; Teyssié, P., Controlled Radical Polymerization of Methacrylic Monomers in the Presence of a Bis(ortho-chelated) Arylnickel(II) Complex and Different Activated Alkyl Halides. *Macromolecules* **1996,** *29* (27), 8576-8582.
105. Lecomte, P.; Drapier, I.; Dubois, P.; Teyssié, P.; Jérôme, R., Controlled Radical Polymerization of Methyl Methacrylate in the Presence of Palladium Acetate, Triphenylphosphine, and Carbon Tetrachloride. *Macromolecules* **1997,** *30* (24), 7631-7633.
106. Wang, J.-S.; Matyjaszewski, K., Controlled/"living" radical polymerization. atom transfer radical polymerization in the presence of transition-metal complexes. *Journal of the American Chemical Society* **1995,** *117* (20), 5614-5615.
107. Matyjaszewski, K.; Xia, J., Atom Transfer Radical Polymerization. *Chemical Reviews* **2001,** *101* (9), 2921-2990.
108. Matyjaszewski, K.; Davis, T. P., *Handbook of radical polymerization*. John Wiley & Sons: 2003.
109. Matyjaszewski, K.; Tsarevsky, N. V., Nanostructured functional materials prepared by atom transfer radical polymerization. *Nat Chem* **2009,** *1* (4), 276-288.
110. Pyun, J.; Matyjaszewski, K., Synthesis of Nanocomposite Organic/Inorganic Hybrid Materials Using Controlled/“Living” Radical Polymerization. *Chemistry of Materials* **2001,** *13* (10), 3436-3448.
111. Qiu, J.; Charleux, B.; Matyjaszewski, K., Controlled/living radical polymerization in aqueous media: homogeneous and heterogeneous systems. *Progress in Polymer Science* **2001,** *26* (10), 2083-2134.
112. Moad, G.; Rizzardo, E.; Thang, S. H., Living Radical Polymerization by the RAFT Process A Second Update. *Australian Journal of Chemistry* **2009,** *62* (11), 1402-1472.
113. Chiefari, J.; Chong, Y. K.; Ercole, F.; Krstina, J.; Jeffery, J.; Le, T. P. T.; Mayadunne, R. T. A.; Meijs, G. F.; Moad, C. L.; Moad, G.; Rizzardo, E.; Thang, S. H., Living Free-Radical Polymerization by Reversible Addition−Fragmentation Chain Transfer: The RAFT Process. *Macromolecules* **1998,** *31* (16), 5559-5562.
114. Moad, G.; Rizzardo, E.; Thang, S. H., Living Radical Polymerization by the RAFT Process. *Australian Journal of Chemistry* **2005,** *58* (6), 379-410.

115. Moad, G.; Rizzardo, E.; Thang, S. H., Living Radical Polymerization by the RAFT ProcessA First Update. *Australian Journal of Chemistry* **2006,** *59* (10), 669-692.
116. Agarwal, S., Chemistry, chances and limitations of the radical ring-opening polymerization of cyclic ketene acetals for the synthesis of degradable polyesters. *Polymer Chemistry* **2010,** *1* (7), 953-964.
117. Burchard, W., Static and dynamic light scattering from branched polymers and biopolymers. In *Light Scattering from Polymers*, Springer Berlin Heidelberg: Berlin, Heidelberg, 1983; pp 1-124.
118. Pedersen, J. S.; Svaneborg, C., Scattering from block copolymer micelles. *Current Opinion in Colloid & Interface Science* **2002,** *7* (3–4), 158-166.
119. Kita-Tokarczyk, K.; Grumelard, J.; Haefele, T.; Meier, W., Block copolymer vesicles—using concepts from polymer chemistry to mimic biomembranes. *Polymer* **2005,** *46* (11), 3540-3563.
120. Schlaad, H.; You, L.; Sigel, R.; Smarsly, B.; Heydenreich, M.; Mantion, A.; Masic, A., Glycopolymer vesicles with an asymmetric membrane. *Chemical Communications* **2009,** (12), 1478-1480.
121. Konishcheva, E. V.; Zhumaev, U. E.; Meier, W. P., PEO-b-PCL-b-PMOXA Triblock Copolymers: From Synthesis to Microscale Polymersomes with Asymmetric Membrane. *Macromolecules* **2017,** *50* (4), 1512-1520.
122. Zhang, X.; Tanner, P.; Graff, A.; Palivan, C. G.; Meier, W., Mimicking the cell membrane with block copolymer membranes. *Journal of Polymer Science Part A: Polymer Chemistry* **2012,** *50* (12), 2293-2318.
123. Bacia, K.; Kim, S. A.; Schwille, P., Fluorescence cross-correlation spectroscopy in living cells. *Nat Meth* **2006,** *3* (2), 83-89.
124. Israelachvili, J. N., *Intermolecular and surface forces*. Academic press: 2011.
125. Cameron, N. S.; Corbierre, M. K.; Eisenberg, A., 1998 EWR Steacie Award Lecture Asymmetric amphiphilic block copolymers in solution: a morphological wonderland. *Canadian journal of chemistry* **1999,** *77* (8), 1311-1326.
126. Yu, K.; Eisenberg, A., Multiple Morphologies in Aqueous Solutions of Aggregates of Polystyrene-block-poly(ethylene oxide) Diblock Copolymers. *Macromolecules* **1996,** *29* (19), 6359-6361.
127. Jain, S.; Bates, F. S., Consequences of Nonergodicity in Aqueous Binary PEO−PB Micellar Dispersions. *Macromolecules* **2004,** *37* (4), 1511-1523.
128. Zupancich, J. A.; Bates, F. S.; Hillmyer, M. A., Aqueous Dispersions of Poly(ethylene oxide)-b-poly(γ-methyl-ε-caprolactone) Block Copolymers. *Macromolecules* **2006,** *39* (13), 4286-4288.
129. He, C.; Sun, J.; Deng, C.; Zhao, T.; Deng, M.; Chen, X.; Jing, X., Study of the Synthesis, Crystallization, and Morphology of Poly(ethylene glycol)−Poly(ε-caprolactone) Diblock Copolymers. *Biomacromolecules* **2004,** *5* (5), 2042-2047.
130. Blanazs, A.; Armes, S. P.; Ryan, A. J., Self-Assembled Block Copolymer Aggregates: From Micelles to Vesicles and their Biological Applications. *Macromolecular Rapid Communications* **2009,** *30* (4-5), 267-277.
131. Dionzou, M.; Morere, A.; Roux, C.; Lonetti, B.; Marty, J. D.; Mingotaud, C.; Joseph, P.; Goudouneche, D.; Payre, B.; Leonetti, M.; Mingotaud, A. F., Comparison of methods for the fabrication and the characterization of polymer self-assemblies: what are the important parameters? *Soft Matter* **2016,** *12* (7), 2166-2176.

132. Mai, Y.; Eisenberg, A., Self-assembly of block copolymers. *Chemical Society Reviews* **2012,** *41* (18), 5969-5985.
133. Battaglia, G.; Ryan, A. J., Effect of Amphiphile Size on the Transformation from a Lyotropic Gel to a Vesicular Dispersion. *Macromolecules* **2006,** *39* (2), 798-805.
134. Discher, D. E.; Eisenberg, A., Polymer Vesicles. *Science* **2002,** *297* (5583), 967-973.
135. Shen, H.; Eisenberg, A., Morphological Phase Diagram for a Ternary System of Block Copolymer PS310-b-PAA52/Dioxane/H2O. *The Journal of Physical Chemistry B* **1999,** *103* (44), 9473-9487.
136. Zhang, L.; Eisenberg, A., Thermodynamic vs Kinetic Aspects in the Formation and Morphological Transitions of Crew-Cut Aggregates Produced by Self-Assembly of Polystyrene-b-poly(acrylic acid) Block Copolymers in Dilute Solution. *Macromolecules* **1999,** *32* (7), 2239-2249.
137. Won, Y.-Y.; Brannan, A. K.; Davis, H. T.; Bates, F. S., Cryogenic Transmission Electron Microscopy (Cryo-TEM) of Micelles and Vesicles Formed in Water by Poly(ethylene oxide)-Based Block Copolymers. *The Journal of Physical Chemistry B* **2002,** *106* (13), 3354-3364.
138. Yu, Y.; Zhang, L.; Eisenberg, A., Morphogenic Effect of Solvent on Crew-Cut Aggregates of Apmphiphilic Diblock Copolymers. *Macromolecules* **1998,** *31* (4), 1144-1154.
139. Zhang, L.; Eisenberg, A., Morphogenic Effect of Added Ions on Crew-Cut Aggregates of Polystyrene-b-poly(acrylic acid) Block Copolymers in Solutions. *Macromolecules* **1996,** *29* (27), 8805-8815.
140. Wei, Z.; Wang, Z.-G., Morphology of ABC triblock copolymers. *Macromolecules* **1995,** *28* (21), 7215-7223.
141. Guo, Z.; Zhang, G.; Qiu, F.; Zhang, H.; Yang, Y.; Shi, A.-C., Discovering Ordered Phases of Block Copolymers: New Results from a Generic Fourier-Space Approach. *Physical Review Letters* **2008,** *101* (2), 028301.
142. Bates, F. S.; Hillmyer, M. A.; Lodge, T. P.; Bates, C. M.; Delaney, K. T.; Fredrickson, G. H., Multiblock Polymers: Panacea or Pandora's Box? *Science* **2012,** *336* (6080), 434-440.
143. Gaitzsch, J.; Chudasama, V.; Morecroft, E.; Messager, L.; Battaglia, G., Synthesis of an Amphiphilic Miktoarm Star Terpolymer for Self-Assembly into Patchy Polymersomes. *ACS Macro Letters* **2016,** *5* (3), 351-354.
144. Fang, B.; Walther, A.; Wolf, A.; Xu, Y.; Yuan, J.; Müller, A. H. E., Undulated Multicompartment Cylinders by the Controlled and Directed Stacking of Polymer Micelles with a Compartmentalized Corona. *Angewandte Chemie International Edition* **2009,** *48* (16), 2877-2880.
145. Walther, A.; Barner-Kowollik, C.; Müller, A. H. E., Mixed, Multicompartment, or Janus Micelles? A Systematic Study of Thermoresponsive Bis-Hydrophilic Block Terpolymers. *Langmuir* **2010,** *26* (14), 12237-12246.
146. Gröschel, A. H.; Schacher, F. H.; Schmalz, H.; Borisov, O. V.; Zhulina, E. B.; Walther, A.; Müller, A. H. E., Precise hierarchical self-assembly of multicompartment micelles. *Nature Communications* **2012,** *3*, 710.
147. Löbling, T. I.; Borisov, O.; Haataja, J. S.; Ikkala, O.; Gröschel, A. H.; Müller, A. H. E., Rational design of ABC triblock terpolymer solution nanostructures with controlled patch morphology. *Nature Communications* **2016,** *7*, 12097.
148. Njikang, G.; Han, D.; Wang, J.; Liu, G., ABC Triblock Copolymer Micelle-Like Aggregates in Selective Solvents for A and C. *Macromolecules* **2008,** *41* (24), 9727-9735.

149. Du, J.; Armes, S. P., Patchy multi-compartment micelles are formed by direct dissolution of an ABC triblock copolymer in water. *Soft Matter* **2010,** *6* (19), 4851-4857.
150. Schmalz, H.; Schmelz, J.; Drechsler, M.; Yuan, J.; Walther, A.; Schweimer, K.; Mihut, A. M., Thermo-Reversible Formation of Wormlike Micelles with a Microphase-Separated Corona from a Semicrystalline Triblock Terpolymer. *Macromolecules* **2008,** *41* (9), 3235-3242.
151. Walther, A.; Millard, P.-E.; Goldmann, A. S.; Lovestead, T. M.; Schacher, F.; Barner-Kowollik, C.; Müller, A. H. E., Bis-Hydrophilic Block Terpolymers via RAFT Polymerization: Toward Dynamic Micelles with Tunable Corona Properties. *Macromolecules* **2008,** *41* (22), 8608-8619.
152. Erhardt, R.; Böker, A.; Zettl, H.; Kaya, H.; Pyckhout-Hintzen, W.; Krausch, G.; Abetz, V.; Müller, A. H. E., Janus Micelles. *Macromolecules* **2001,** *34* (4), 1069-1075.
153. Saito, R.; Fujita, A.; Ichimura, A.; Ishizu, K., Synthesis of microspheres with microphase-separated shells. *Journal of Polymer Science Part A: Polymer Chemistry* **2000,** *38* (11), 2091-2097.
154. Hoppenbrouwers, E.; Li, Z.; Liu, G., Triblock Nanospheres with Amphiphilic Coronal Chains. *Macromolecules* **2003,** *36* (3), 876-881.
155. Walther, A.; Müller, A. H. E., Janus Particles: Synthesis, Self-Assembly, Physical Properties, and Applications. *Chemical Reviews* **2013,** *113* (7), 5194-5261.
156. Du, J.; O'Reilly, R. K., Anisotropic particles with patchy, multicompartment and Janus architectures: preparation and application. *Chemical Society Reviews* **2011,** *40* (5), 2402-2416.
157. Stoenescu, R.; Meier, W., Vesicles with asymmetric membranes from amphiphilic ABC triblock copolymers. *Chemical communications (Cambridge, England)* **2002,** (24), 3016-7.
158. Liu, F.; Eisenberg, A., Preparation and pH Triggered Inversion of Vesicles from Poly(acrylic Acid)-block-Polystyrene-block-Poly(4-vinyl Pyridine). *Journal of the American Chemical Society* **2003,** *125* (49), 15059-15064.
159. Mason, A. F.; Thordarson, P., Polymersomes with Asymmetric Membranes Based on Readily Accessible Di- and Triblock Copolymers Synthesized via SET-LRP. *ACS Macro Letters* **2016,** *5* (10), 1172-1175.
160. Liu, Q.; Chen, J.; Du, J., Asymmetrical Polymer Vesicles with a “Stealthy” Outer Corona and an Endosomal-Escape-Accelerating Inner Corona for Efficient Intracellular Anticancer Drug Delivery. *Biomacromolecules* **2014,** *15* (8), 3072-3082.

Publication 1

Key aspects to yield low dispersity of PEO-*b*-PCL diblock copolymers and their mesoscale self-assembly

Evgeniia Konishcheva, Daniel Häussinger, Samuel Lörcher, Wolfgang Meier

Published in *European Polymer Journal*, 2016, 83: p. 300-310

Contribution of Evgeniia Konishcheva:

- Synthesized and characterized the polymers
- Investigated kinetics of ε-CL polymerization on PEO macroinitiator
- Prepared and characterized the self-assembled structures
- Wrote the manuscript

European Polymer Journal 83 (2016) 300–310

Contents lists available at ScienceDirect

European Polymer Journal

journal homepage: www.elsevier.com/locate/europolj

Macromolecular Nanotechnology

Key aspects to yield low dispersity of PEO-*b*-PCL diblock copolymers and their mesoscale self-assembly

Evgeniia Konishcheva, Daniel Häussinger, Samuel Lörcher, Wolfgang Meier *

Department of Chemistry, University of Basel, Klingelbergstrasse 80, 4056 Basel, Switzerland

ARTICLE INFO

Article history:
Received 2 June 2016
Received in revised form 5 August 2016
Accepted 12 August 2016
Available online 18 August 2016

Keywords:
PEO-*b*-PCL
$SnOct_2$ catalyst
Dispersity
Self-assembly
Polymersomes

ABSTRACT

Poly(ethylene oxide)-*block*-polycaprolactone (PEO-*b*-PCL) is one of the widely used biocompatible amphiphilic block copolymers which is able to self-assemble into a variety of 3D structures, including polymersomes. Controlled self-assembly into a 3D structure with a certain size and morphology might require uniform PEO-*b*-PCL ($Đ_M < 1.1$), which has not been possible to synthesize so far. In this work, we optimized the well-known synthesis of PEO-*b*-PCL, catalyzed by $SnOct_2$, leading to a low molecular-weight dispersity (< 1.1), and discussed the aging effects of $SnOct_2$ on the overall kinetics of the synthesis. To understand the effect of the dispersity of PEO-*b*-PCL on its self-assembly, we compared self-assembled structures formed by uniform PEO-*b*-PCL ($Đ_M < 1.1$) with the ones formed by non-uniform analogues ($Đ_M > 1.1$). Furthermore, we demonstrated the benefits of uniform PEO-*b*-PCL when a high degree of end-group activation is required through ω-tosylation.

1. Introduction

Micelles and vesicles are a few examples from the large variety of 3D structures which can be formed by molecular self-assembly. Among them, vesicles are of special interest due to the protected hydrophilic core where encapsulated drugs or enzymes are shielded from the external media [1–3]. For this purpose, vesicles are typically formed from natural lipids or amphiphilic synthetic block copolymers. Vesicles based on block copolymers, or polymersomes, exhibit higher mechanical stability and more advanced functionalization capability, and thus are increasingly more preferred to lipid-based vesicles [4–8]. The type of 3D structure strongly depends on the nature of the composing blocks and the hydrophilic weight fraction [9]. A prominent example of a biocompatible block copolymer forming polymersomes is poly(ethylene oxide)-*block*-polycaprolactone (PEO-*b*-PCL), where PEO is a hydrophilic, biocompatible, protein repellent polyether which prolongs blood circulation time of self-assembled structures [10], and PCL a hydrophobic, biodegradable polyester often used in drug delivery systems [11–14]. PEO-*b*-PCL self-assembles into a variety of meso- and nanoscale structures depending on the hydrophilic weight fraction, block lengths, and the method of preparation [15–19]. In general, an increase of a copolymer molecular-weight dispersity leads to the formation of a mixture of different self-assembled structures [20–23] and broadening of the size distribution of the corresponding aggregates [23,24]. Consequently, the self-assembly of distinct and uniform 3D structures might require PEO-*b*-PCL with a certain block length and rather narrow molecular-weight dispersity. For example, PEO (2K)-*b*-PCL(9.5K) with a dispersity of 1.14 forms predominantly mesoscale polymersomes [16], whereas the comparable copolymer PEO(2K)-*b*-PCL(9K) with a higher dispersity of 1.42 forms mostly mesoscale worms [17] by film rehydration.

* Corresponding author.
E-mail address: wolfgang.meier@unibas.ch (W. Meier).

http://dx.doi.org/10.1016/j.eurpolymj.2016.08.011
0014-3057/

The synthesis of PEO-*b*-PCL diblock copolymers is usually performed using PEO as a macroinitiator for the polymerization of ε-caprolactone (ε-CL) with either tin(II) 2-ethylhexanoate ($SnOct_2$) as a catalyst [15–17,25–28] or triethylaluminium as a precursor [29,30]. ε-CL polymerization performed with triethylaluminium requires an excess of the precursor (~ 1.1 eq. with respect to PEO). For biomedical and food applications the residual aluminum has to be removed [31], which is usually done by quenching the polymerization with hydrochloric acid, which might lead to the degradation of the polyester backbone. To avoid intensive acidic purification, $SnOct_2$, an FDA approved catalyst [31] can be used, since PEO-*b*-PCL synthesis in this case requires only trace amount of the catalyst. Unfortunately, $Đ_M$ values scatter in a wide range (1.1–1.6) for PEO-*b*-PCL copolymers when the synthesis is catalyzed by $SnOct_2$. It is known that at short polymerization times during the homopolymerization of ε-CL the obtained polymers exhibit a rather narrow dispersity (< 1.1). After long polymerization times, however, side processes result in a broadening of the polymer molecular weight distribution [32]. In this work, we investigated the kinetics of a PEO-*b*-PCL synthesis catalyzed by $SnOct_2$ in order to clarify the rise of the PEO-*b*-PCL dispersity, and consequently optimized the synthesis towards uniform PEO-*b*-PCL block copolymers. We compared mesoscale self-assembled structures of synthesized uniform PEO-*b*-PCL ($Đ_M < 1.1$) with the ones assembled from its non-uniform analogues ($Đ_M > 1.1$), to gain insight into the effect of dispersity on the self-assembly process. Furthermore, we showed how to tosylate the PCL end of PEO-*b*-PCL for further modifications, and thus to expand the functionalization capability of PEO-*b*-PCL copolymers and their self-assembled structures.

2. Experimental section

2.1. Materials

All glassware was dried overnight at 120 °C prior to use. All chemicals were obtained from Sigma-Aldrich and used as received unless otherwise mentioned. Milli-Q water with a resistivity of 15 MΩ cm was used from a Purelab Option-R 7/15 system (ELGA). Poly(ethylene oxide) monomethyl ether (PEO) with a molar mass of 2000 g mol^{-1} was dissolved in water and then lyophilized to obtain the polymer in a form of a dry powder. ε-Caprolactone (ε-CL) was dried under reduced pressure over CaH_2 for at least 12 h. ε-CL was purified by vacuum distillation and stored under argon atmosphere (not longer than 2 days). Toluene was dried over CaH_2 and distilled under argon atmosphere prior to use. Just before use tin(II) 2-ethylhexanoate ($SnOct_2$) was purified by vacuum distillation. Bodipy 630/650 NHS ester was purchased from Thermo Fisher Scientific Inc.

2.2. Nuclear magnetic resonance spectroscopy

^1H NMR spectra were recorded at 295 K in $CDCl_3$ on a Bruker Avance III NMR spectrometer operating at 400.13 MHz proton frequency. The instrument was equipped with a direct observe 5-mm BBFO smart probe. Chemical shifts are reported in ppm relative to tetramethylsilane. ^{119}Sn NMR, diffusion-ordered NMR spectroscopy (DOSY), and ^{119}Sn-HMBC (heteronuclear multiple bond correlation) experiments were performed in CD_2Cl_2 on a Bruker Avance III NMR spectrometer operating at 600.13 MHz proton frequency. The instrument was equipped with a direct observe 5-mm BBFO smart probe. The experiments were performed at 298 K and the temperature was calibrated using a methanol standard showing accuracy within ±0.2 K. The external reference for ^{119}Sn was tetramethyl tin at 0 ppm. NMR spectra were processed with MestReNova software, DOSY NMR experiments were processed with TopSpin software.

2.3. Gel permeation chromatography

GPC traces were analyzed and recorded in WinGPC (v 8.20 build 4815, PSS systems). The chloroform GPC system was equipped with 2 PSS SDV columns (1000 Å and 100,000 Å, each 30 cm long, 5 μm particles, 0.8 cm diameter) and a refractive index (RI), UV–vis, and viscosity detectors ran at 35 °C and 1 ml min^{-1}. The system was calibrated against narrow distributed polystyrene standards.

2.4. Matrix-assisted laser desorption/ionization time-of-flight mass spectrometry (MALDI-TOF MS)

Molecular weight and end groups of PEO starting material were determined by MALDI-TOF. The data was acquired on a Bruker microflex LT instrument equipped with a 337 nm pulsed nitrogen laser in linear mode. The samples were prepared using multiple-layer spotting approach [33]. First, the matrix (0.5 μl of saturated dithranol in $CHCl_3$) was spotted on the MALDI target. Then 0.5 μl of NaI saturated in acetone was applied followed by 0.5 μl of 25 mg ml^{-1} of a polymer. The data analysis and predictions were performed using the Bruker DataAnalysis software.

2.5. Laser scanning microscopy

LSM images were recorded on an inverted Zeiss LSM510 META/ConfoCor 2 FCS microscope using a Zeiss Plan-Apochromat 100x/1.4 Oil DIC objective. Bodipy 630/650 and calcein disodium salt were excited by the 633 nm He—Ne laser line (10 %

output) and by the 488 nm Argon laser line (11 % output), respectively. The excitation light was passed through a HFT UV 488/543/633 beam splitter. The emission light was passed through a NFT 545 beam splitter and a BP 474–525 band pass filter for the signal from calcein disodium salt, and through a LP 650 long pass filter for the signal from Bodipy 630/650. The fluorescence signals were recorded on the LSM photomultiplier tubes (PMT). The transmittance signal was recorded simultaneously on a T-PMT detector. Twelve bit images of 1024 × 1024 pixels were acquired at a scan speed of 51.20 μs per pixel. The pinholes for the respective laser lines were > 10 μm to record maximum signal intensities. 5 μl of a stained sample were placed onto a glass cover slip (22 mm × 50 mm), covered with a round (Ø 12 mm) cover slip. To prevent sample evaporation, the samples were sealed with nail polish. The images were processed with ImageJ (ver. 1.50B) and its LSM toolbox plug-in (ver. 4.1.1). The average diameter of polymersomes was determined as an average Feret's diameter based on at least three different images (∼ 600 objects in total).

2.6. Transmission electron microscopy

5 μl of a sample were adsorbed on a glow discharged copper grid (formvar coated, 200 mesh) and blotted off after 1 min. Two times 5 μl of H_2O were applied to the grid and blotted off right away to remove residual salts. This was repeated with 5 μl of 2 % aqueous uranyl acetate where the sample was stained for 10 s in the last step. The prepared grids were air dried for at least 10 min before imaging on a Philips CM100 transmission electron microscope at an acceleration voltage of 80 kV.

2.7. Synthesis of PEO-b-PCL diblock copolymers

PEO-*b*-PCL was synthetized via $SnOct_2$ catalyzed coordination-insertion ring-opening polymerization of ε-CL using PEO as a macroinitiator. In a representative experiment, PEO (1 eq., 1.0 g, 0.5 mmol) was mixed with ε-CL (500 eq., 28.5 g, 0.25 mol) and toluene (33.5 ml) in a three-neck flask equipped with a Teflon-coated stir bar. One of the necks was covered with a septum to allow sample aspiration for ^{1}H NMR and GPC analysis; the second neck was equipped with a condenser, the third was covered with a valve allowing exchange of atmosphere in the flask. The mixture was degassed with three freeze-pump-thaw cycles and backfilled with argon. Freshly distilled $SnOct_2$ (0.1 eq., 0.5 ml (0.1 M solution in toluene)) was added to the reaction mixture followed by three freeze-pump-thaw cycles. The polymerization was carried out at 110 °C. The reaction time varied depending on the targeted length of the PCL block. When the desired degree of polymerization was reached, the flask with a clear viscous liquid was cooled to room temperature and precipitated 3 times in cold diethyl ether to remove residual monomers. The white precipitate was collected by filtration and dried under vacuum. PEO(2K)-*b*-PCL(16.0K) ($Đ_M$ = 1.23) was obtained in similar conditions, but in the presence of 150 eq. of ε-CL, the reaction was carried out for 24 h. PEO(2K)-*b*-PCL (16.3K) ($Đ_M$ = 1.55) was synthesized like PEO(2K)-*b*-PCL(16.0K), but in the presence of 0.6 eq. of $SnOct_2$. The block ratio was determined by integrating the peak from the terminal methyl group of PEO at 3.36 ppm and the peaks of the PCL backbone at 2.31 and 4.06 ppm. The polymers were also characterized by $CHCl_3$ GPC. ^{1}H NMR (400.13 MHz, δ, $CDCl_3$): 1.38 ppm (m, O═C—CH_2—CH_2—C***H₂***—CH_2—CH_2—O—), 1.65 ppm (m, O═C—CH_2—C***H₂***—CH_2—C***H₂***—CH_2—O—), 2.31 ppm (t, *J* = 7.1 Hz, O═C—C***H₂***—CH_2—CH_2—CH_2—CH_2—O—), 3.38 ppm (s, C***H₃***—O—), 3.65 ppm (s, —O—C***H₂***—C***H₂***—O—), 4.06 ppm (t, *J* = 6.5 Hz, O═C—CH_2—CH_2—CH_2—CH_2—C***H₂***—O—).

2.8. Synthesis of PEO-b-PCL-OTs

PEO-*b*-PCL was ω-functionalized with *p*-toluenesulfonyl chloride (TsCl). In a typical experiment, PEO-*b*-PCL (1 eq., 2 g, 0.15 mmol) and TsCl (100 eq., 2.81 g, 15 mmol) were added into a two-neck flask equipped with a Teflon-coated stir bar. The mixture was dissolved in anhydrous CH_2Cl_2 (28.6 ml). The solution was degassed by three freeze-pump-thaw cycles, backfilled with argon and allowed to stir for 15 min at room temperature. Anhydrous pyridine (10 eq., 0.12 ml, 1.5 mmol) was added and the reaction was left stirring overnight at room temperature. The mixture was precipitated 3 times in cold diethyl ether to remove the excess of TsCl. The precipitate was dissolved in CH_2Cl_2 (30 ml) and washed with Milli-Q water (3 × 10 ml) to remove residual pyridine and pyridinium salts. The polymer containing organic phase was dried over $MgSO_4$ overnight. The solution was filtered and the filtrate was dried under vacuum to give PEO-*b*-PCL-OTs as white solid. The percentage of ω-modification was determined by integrating the peak from the terminal methyl group of PEO at 3.36 ppm and the aromatic doublets at 7.35 and 7.79 ppm originating from the covalently attached tosyl group. ^{1}H NMR (400.13 MHz, δ, $CDCl_3$): 1.38 ppm (m, O═C—CH_2—CH_2—C***H₂***—CH_2—CH_2—O—), 1.65 ppm (m, O═C—CH_2—C***H₂***—CH_2—C***H₂***—CH_2—O—), 2.31 ppm (t, *J* = 7.1 Hz, O═C—C***H₂***—CH_2—CH_2—CH_2—CH_2—O—), 2.45 ppm (s, C***H₃***—Ph), 3.38 ppm (s, C***H₃***—O—), 3.65 ppm (s, —O—C***H₂***—C***H₂***—O—), 4.02 ppm (t, *J* = 6.5 Hz, —C***H₂***—OTs), 4.06 ppm (t, *J* = 6.5 Hz, O═C—CH_2—CH_2—CH_2—CH_2—C***H₂***—O—), 7.35 ppm (d, *J* = 8.1 Hz, Ph), 7.79 ppm (d, *J* = 8.3 Hz, Ph).

2.9. Self-assembly

Four methods of self-assembly have been employed to obtain mesoscale structures of PEO-*b*-PCL copolymers: co-solvent, film rehydration, solvent switch, and solvent evaporation.

For the co-solvent method, 2 mg of polymer were dissolved in 200 μl THF and added dropwise (∼200 μl min^{-1}) into a stirred solution of 800 μl Milli-Q water. The mixture was stirred at 350 rpm overnight at 25 °C.

Film rehydration method was performed using two different substrates: a non-roughened glass and a roughened Teflon surface. 2 mg of polymer were dissolved in 200 μl of CH_2Cl_2 and placed in the glass round-bottom flask or onto the round Teflon plate (Ø ~ 12 mm). In the case of the glass flask, the organic solvent was removed by rotary evaporation followed by vacuum evaporation for 12 h to get a dry polymer film. The Teflon plate with a polymer film was placed into a round-bottom flask and connected to the vacuum line for 12 h. After the addition of 1 ml of Milli-Q water the samples were stirred (350 rpm) for 24 h at 60 °C.

For the solvent-switch method, 2 mg of polymer were dissolved in 1 ml of THF, the solution was transferred into a regenerated cellulose dialysis tube (MWCO 3.5–5 kDa, SpectraPor) and dialyzed for 2 days against 1 L of Milli-Q water at 25 °C (water was exchanged 4 times).

The solvent evaporation method was performed at 25 and 60 °C. 2 mg of polymer were dissolved in 200 μl of CH_2Cl_2 and added in one shot to 1 ml of a solution of Milli-Q water stirred at 350 rpm. The organic solvent was left to evaporate while stirring at 350 rpm for 12 h at 25 °C, or for 0.5 h at 60 °C.

For the encapsulation experiments a 10 mM aqueous solution of calcein sodium salt was used during the assembly. After the self-assembly the samples were dialyzed for three days against Milli-Q water (water was exchanged 7 times). Solutions of the mesoscale structures (50 μl) were stained with 0.5 μl of 0.72 μM Bodipy 630/650 dye and visualized by LSM.

3. Results and discussion

3.1. End-group modifiable PEO-b-PCL diblock copolymers

Due to its low price and easy handling $SnOct_2$ is the most commonly used catalyst for the production of polyesters. This catalyst is also frequently applied for the polymerization of ε-CL, using PEO as a macroinitiator to produce amphiphilic PEO-*b*-PCL diblock copolymers. Polymerization of PEO-*b*-PCL is typically performed in two ways: (1) without any solvent (bulk polymerization) or (2) in a solvent, typically toluene. In both ways, the polymerization is often performed until 100 % conversion of ε-CL is reached. In our experiments, during bulk polymerization, the colorless polymerization mixture often turned yellow or brown depending on both the amount of catalyst and the reaction time, whereas polymerizations in toluene always proceeded colorlessly. ^{1}H NMR and GPC analysis did not reveal any significant differences between these brown (bulk synthesized) and white (solvent synthesized) PEO-*b*-PCL copolymers. The observed change in color during bulk polymerization most likely corresponded to the formation of SnO species [34]. The color could not be removed or reduced neither by precipitation in ether or hexanes, nor by filtration over silica, celite, or aluminum oxide. The brown color disappeared and returned to white only after incubation with 0.025 M HCl, but simultaneously led to an increase of dispersity of the polymer from 1.20 to 2.03 due to the acidic degradation of the polyester backbone (Fig. S1). Since we do not know the effect of the color on further experiments, the polymerization was always performed in toluene to obtain white copolymers.

The increase of the dispersity of polymers typically occurs due to terminating reactions during polymerization, which is often caused by impurities. Since the purity of PEO (see Fig. S2 for MALDI-TOF MS) and ε-CL was assessed carefully before each polymerization, we concluded, that the source of contamination was in the catalyst, as in most cases reported in literature and initially in this work, commercial $SnOct_2$ has been used for the polymerizations as received [15–17,25–28]. Polymerizations performed with distilled $SnOct_2$ resulted in polymers exhibiting lower $Đ_M$ (< 1.2) compared to the polymerization with as-received $SnOct_2$ ($Đ_M$ > 1.2) (Fig. 1). In addition, PEO-*b*-PCL copolymers obtained using distilled catalyst exhibited a pronounced high molecular weight shoulder (Fig. 1, red curve). ^{1}H NMR spectra of these polymers were

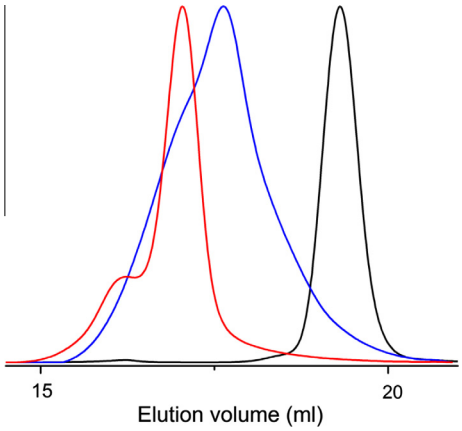

Fig. 1. GPC ($CHCl_3$) traces of PEO (black curve, $Đ_M$ = 1.08), PEO-*b*-PCL (blue curve, $Đ_M$ = 1.42) obtained by polymerization using as-received $SnOct_2$, and PEO-*b*-PCL (red curve, $Đ_M$ = 1.19) obtained by polymerization using freshly distilled $SnOct_2$. (For interpretation of the references to color in this figure legend, the reader is referred to the web version of this article.)

identical to those obtained with non-distilled catalyst and showed all of the typical features of a PEO-*b*-PCL copolymer. We believe that these high molecular weight species are also present in diblock copolymers, obtained in the presence of as-received catalyst, but due to the rather large width of the GPC peaks they have not been distinguished in the corresponding elugrams reported previously in the literature (see e.g., Fig. 1, blue curve). Although the catalyst is typically used in very small amounts, its purification seems to drastically affect the PEO-*b*-PCL molecular weight distribution. For the details about impurities in $SnOct_2$ see subsection 3.3.

Tosylation is a frequently utilized ω-modification in polymer chemistry, since it allows further substitution of the tosyl group to an azide, allowing fast and convenient click reactions. In addition, tosylated PEO-*b*-PCL copolymers may serve as a platform for subsequent 2-alkyl-2-oxazoline polymerization [35] resulting in triblock copolymers. We observed that PEO-*b*-PCL copolymers obtained after 100 % conversion in the presence of distilled or as-received catalyst were quite passive against modifications at the PCL terminus, at least using *p*-toluenesulfonyl chloride. The percentage of tosylation of PEO-*b*-PCL diblock copolymers was determined by integrating the aromatic doublets at 7.35 ppm and 7.79 ppm on ^{1}H NMR spectra, which correspond to the covalently attached tosyl group (Fig. S3A). The triplet at 4.02 ppm can also serve as an indication of tosylation, since it corresponds to the terminal —CH_2— group of the PCL block attached to the tosyl group. ω-Modification using 0.55 M *p*-toluenesulfonyl chloride resulted in < 50 % tosylation after 24 h. Perhaps an esterification of the end —OH groups by impurities and the catalyst is responsible for such passivation of PEO-*b*-PCL copolymers [36–38]. Interestingly, the relative amount of high molecular weight species in a PEO-*b*-PCL copolymer (shoulder area in the corresponding elugram) is inversely proportional to the level of PEO-*b*-PCL tosylation. The degree of polymer tosylation with a relative shoulder species concentration of 26 % reached about 50 % after 24 h, whereas tosylation of polymers with a relative shoulder species concentration of 4 % reached 100 % already after 12 h (Fig. S3B). Such a correlation encouraged us to reveal the possible origin of the high molecular weight shoulder in order to find ways to minimize its formation during polymerization and consequently, to enable the end-group modification of PEO-*b*-PCL diblock copolymers.

3.2. High molecular weight shoulder: origin and suppression

To investigate how the high molecular weight shoulder changes over the reaction time, we took samples during the polymerization of ε-CL using PEO macroinitiator and analyzed them by means of ^{1}H NMR and GPC. As can be seen from Fig. 2A, this high molecular weight shoulder increases over the reaction time, and at 100 % of conversion the relative amount of these species reach about 26 % (Fig. 2D, blue curve). DOSY NMR experiments also confirmed the presence of high molecular weight species. The data for 5 different peaks with the highest intensities were fitted with one and two component fits (equations and representative fitting curves are in Fig. S4). The one component fit for PEO-*b*-PCL with a big shoulder (Fig. 2D, blue curve) gives the diffusion coefficient $(6.81 \pm 0.15)\cdot10^{-11}$ m·s^{-2}, whereas the two component fit gives the diffusion coefficients $(9.14 \pm 0.71)\cdot10^{-11}$ m·s^{-2} and $(5.46 \pm 0.29)\cdot10^{-11}$ m·s^{-2} confirming the presence of two distinctly different species. In the case of the polymer with a small shoulder (Fig. 2D, red curve) both one and two component fits give similar values of the diffusion coefficient: $(9.83 \pm 0.13)\cdot10^{-11}$ m·s^{-2} and $(10.02 \pm 0.28)\cdot10^{-11}$ m·s^{-2}, respectively. In the latter case the intensity of the second component was negligible or even negative, and therefore the second diffusion coefficient was poorly reproducible for 3 different peaks (relative error about 50 %), or did not have a meaningful value (Table S1).

The formation of high molecular weight species can be explained by side transesterification reactions [39,40] and/or by the polymerization of ε-CL on coupled PEO-O-Sn-O-PEO or PEO-*b*-PCL-O-Sn-O-PCL-*b*-PEO species [41]. However, the latter mechanism seems to be unlikely, as our ^{119}Sn-HMBC experiments did not detect any tin bound to the polymer chains. Therefore, we assume that intra- and intermolecular transesterification reactions are responsible for the formation of the high molecular weight shoulder. Depending on the type of the molecules which undergo this process, transesterification side reactions can result in the formation of PCL homopolymer, PEO-*b*-PCL with shorter and longer PCL chain lengths, PEO-*b*-PCL-*b*-PEO, and cyclic molecules. However, as determined by GPC, the molecular weight of the shoulder species is double the molecular weight of the main peak, at least during the first 5 h (Fig. 2B). Therefore, we assume that the shoulder mainly consists of PEO-*b*-PCL-*b*-PEO species. MALDI-TOF MS analysis is generally a very advantageous method for the end-group characterization and helpful for the investigation of the mechanism of a polymerization [37]. However, we were not able to record reliable MS spectra for the end-group analysis of PEO-*b*-PCL using multiple-layer spotting approach [33]. This issue was also pointed out by Meier et al. [26].

Two different reaction mechanisms are responsible for the formation of the PEO-*b*-PCL copolymer and the shoulder species. According to Fig. 2A, the rate constant of these reactions seems to differ significantly. Therefore, by changing the reaction conditions one could change the relative rate of these reactions to minimize the growth of the shoulder.

The molecular weight increase of the diblock copolymer for different monomer concentrations is shown in Fig. 2C. The polymerization was investigated in the presence of 100, 300, and 500 equivalents of ε-CL. As can be seen, the increase in the monomer concentration boosts the formation of PEO-*b*-PCL copolymer. The concentration of the shoulder increases over the reaction time, and the rate of its accumulation is proportional to the monomer concentration (Fig. 2C). The concentration of the high molecular weight shoulder was determined as a ratio between the area under the shoulder of the Gauss fitted peak to the total area. Note that the point at 0 h, which corresponds to PEO, does not follow the trend, since the shoulder present in the initiator has a different origin. Obviously, the earlier the polymerization is terminated, the less side products are generated. Therefore, to minimize the formation of the shoulder species an excess of ε-CL can be used for the synthesis of PEO-*b*-PCL diblock copolymers with a targeted number of PCL units. For instance, if the targeted length of the PCL block is

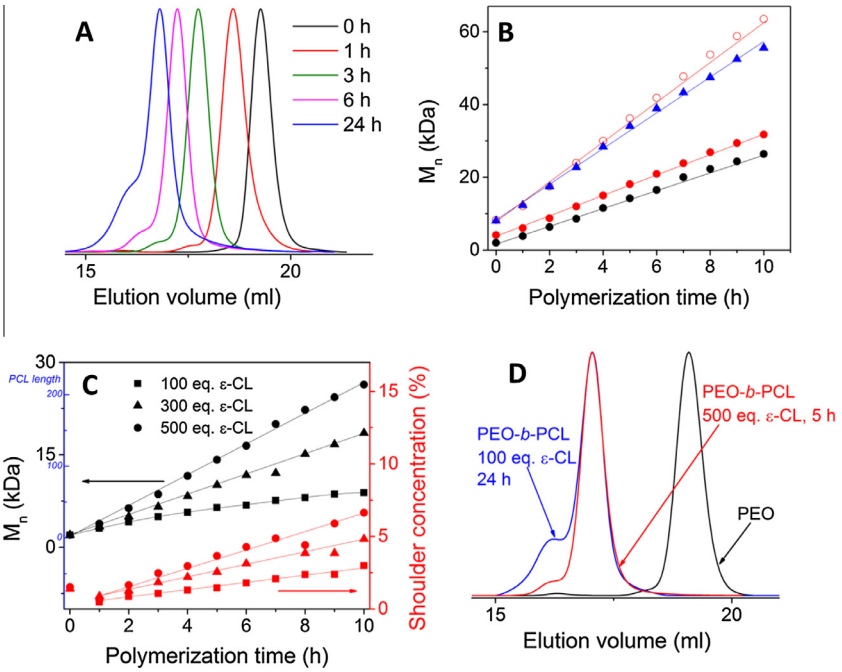

Fig. 2. (A) GPC ($CHCl_3$) traces at various time points during the polymerization of 100 equivalents of ε-CL with respect to PEO; (B) M_n versus polymerization time (500 eq. of ε-CL) determined by ^1H NMR ($CDCl_3$) spectroscopy (●), GPC ($CHCl_3$) (●); M_n of the high molecular weight shoulder determined by GPC (▲); M_n of the diblock copolymer determined by GPC and multiplied by a factor of 2 (○); (C) M_n and relative area of high molecular weight shoulder versus polymerization time for 100, 300, and 500 equivalents of ε-CL; D: GPC ($CHCl_3$) traces of PEO, two PEO-*b*-PCL diblock copolymers with similar molecular weights (~ 13.4 kDa) obtained by running the reaction until 100 % of conversion (24 h, blue curve) and by terminating the reaction at 20 % of conversion (5 h, red curve). (For interpretation of the references to color in this figure legend, the reader is referred to the web version of this article.)

100 units, which corresponds to the molecular weight of the diblock copolymer being 13.4 kDa, the polymerization should be stopped after 24, 7, or 5 h when 100, 300, or 500 equivalents of ε-CL are used, respectively. Moreover, the dispersity of the main peak without the high molecular weight shoulder remains constant during the polymerization (Fig. S5). Elugrams of two copolymers with similar molecular weights (~ 13.4 kDa), determined by ^1H NMR spectroscopy, are illustrated in Fig. 2D. As can be seen, a significant decrease (from 26 to 4 %) of the shoulder products can be achieved by using the excess (500 equivalents) of ε-CL for the polymerization. The dispersity of PEO-*b*-PCL copolymer synthesized under these conditions is similar to that of the starting material, PEO, and does not exceed the value of 1.1. A low dispersity of PEO-*b*-PCL diblock copolymer, which often serve as a platform for amphiphilic triblock copolymers [42–48], is very advantageous for obtaining well-defined triblock copolymers, since the subsequent polymerization or coupling may result in the increase of the dispersity.

Therefore, to obtain a PEO-*b*-PCL diblock copolymer with the targeted number of PCL units and with a low dispersity (< 1.1), the polymerization should be carried out in the presence of an excess of monomer (depending on the targeted number of PCL units) and terminated at a certain time point. However, sometimes we observed different behavior of polymerization, e.g., slower non-linear increase of the molecular weight during polymerization (Fig. S6A). Since the purity of PEO and ε-CL was confirmed by means of ^1H NMR (ε-CL, PEO), GPC (PEO), and MALDI-TOF MS (PEO), we assumed the cause of these observations was $SnOct_2$. From the one hand, if the catalyst was used just after its distillation, the growth of polymer chain was linear and reproducible. From the other hand, if distilled $SnOct_2$ (stored under vacuum at room temperature) was used more than 5 days after its distillation, the polymerization proceeded differently. In addition, the formation of species with a molecular weight lower than the one of the PEO initiator was observed (Fig. S6B). This fact can be attributed to the hydrolysis of $SnOct_2$ to Oct—Sn—OH or of Sn(IV) to Sn(IV)—OH [49,50], which can initiate the polymerization of ε-CL by itself. These observations encouraged us to investigate the changes of $SnOct_2$ catalyst under different storage conditions.

3.3. $SnOct_2$ catalyst: transformation during storage

Commercial $SnOct_2$ contains some 2-ethylhexanoic acid which can act as a terminating agent [51], and can contribute to an increase in $Đ_M$ of the respective polymer. This acid can be partially removed by distillation (Fig. S7). Commercial $SnOct_2$ also contains an organic impurity completely removable by distillation. This impurity is presumably toluene (Fig. S7), since the chemical shifts are identical to the ones reported for toluene in CD_2Cl_2 [52]. We also hypothesized that the catalyst contains some amount of stabilizer (antioxidant) preventing oxidation of Sn(II) to Sn(IV), since ^{119}Sn NMR spectra of $SnOct_2$

stored under different conditions showed different features (Fig. 3). If the impurities contain hydroxyl or amino groups (typical for antioxidants), they can also, apart from PEO, initiate the polymerization of ε-CL and increase the $Đ_M$ of the product. Besides, as can be seen from the ^{119}Sn NMR spectra (Fig. 3A), non-purified catalyst contains some tin species at −704 ppm and −708 ppm, which can be associated with hydrolyzed Sn(II) and Sn(IV) species [49]. These compounds may also contribute to the increase of $Đ_M$, since the Sn(II/IV)—OH species can initiate homopolymerization of ε-CL.

Even when stored under vacuum, the distilled catalyst undergoes some changes, causing different polymerization behavior over time (Fig. S6). ^{1}H NMR spectra of the catalyst during its storage showed no significant difference. To investigate the changes of the catalyst after its purification and during its storage, ^{119}Sn NMR spectra were recorded. On the basis of ^{119}Sn, ^{13}C NMR and ^{119}Sn Mössbauer spectroscopies Labouriau et al. [49] have associated the peak at −528 ppm with $SnOct_2$. However, we observed peaks at −539 ppm (commercial, non-distilled catalyst, Fig. 3A) and −519 ppm (freshly distilled catalyst, Fig. 3B). These differences can mainly be explained by different concentrations of the samples. In addition, impurities (e.g., H_2O, alcohols, amines, etc.) can result in different coordination of Sn(II), since Sn(II) is known to have a tricoordinate pyramidal structure [53]. Furthermore, the peak at −708 ppm (Fig. 3A) can be associated with Sn(IV) [49], and tin carboxylates with mixed oxidation states Sn(II) and Sn(IV) are known to form compounds with carboxylate ligand bridging Sn(II) and Sn (IV) atoms [54]. Thus, after distillation of the catalyst coordination of Sn(II) atoms can be strongly influenced. Distilled catalyst, stored 2 months under argon, has only one peak at −522 ppm (Fig. 3C), whereas freshly distilled catalyst, stored one day in air, exhibits peaks only at −704 ppm and −708 ppm (Fig. 3D), which are associated with hydrolyzed Sn(II) and Sn(IV) species [49]. Moreover, commercial catalyst, stored one year under ambient conditions, also showed these peaks (Fig. 3E). Distilled catalyst, stored one year in air, showed completely different features (Fig. 3F).

Hence, ^{119}Sn NMR spectra of $SnOct_2$ confirmed transformation of the catalyst during its storage under different conditions. These data support our hypothesis that the catalyst contains some additive which inhibits the changes of the commercial catalyst. However, the additive does not prevent the catalyst completely from its transformation (Fig. 3E). Therefore, for reproducible polymerization kinetics the commercial $SnOct_2$ must be stored under inert conditions and distilled just before use, or verified by ^{119}Sn NMR spectroscopy prior to use.

3.4. Effect of the dispersity of PEO-b-PCL on size and morphology of the self-assembled structures

Amphiphilic PEO-*b*-PCL diblock copolymers have received considerable interest due to their ability to form nano- and mesoscale objects depending on the hydrophilic weight fraction, the length of PEO and PCL blocks, and the method of preparation used for self-assembly [15,16]. To investigate how the method of preparation influences the self-assembly process, we have employed four techniques: co-solvent, film rehydration on glass or Teflon surface, solvent evaporation at 25 °C or 60 °C, and solvent switch. We have particularly focused on two model polymers for self-assembly: PEO(2K)-*b*-PCL(17.4K) ($Đ_M$ = 1.08) and PEO(2K)-*b*-PCL(11.6K) ($Đ_M$ = 1.08) (elugrams Fig. S8). The representative LSM images of the self-assembled structures of PEO(2K)-*b*-PCL(17.4K) are presented in Fig. 4, and the images of PEO(2K)-*b*-PCL(11.6K) structures are depicted in Fig. S9. For both polymers the co-solvent method yielded small structures which could not be visualized by optical microscopy. Therefore, self-assembled structures were visualized via TEM. As can be seen from Figs. 4A and S9A, the samples mainly consist of a continuous polymeric phase with some rods and particles. Therefore, the co-solvent method results in partial dissolution of the polymers. In all the other methods, both polymers formed mesoscale structures, which were stained with hydrophobic Bodipy 630/650 dye. In the case of PEO(2K)-*b*-PCL(11.6K) all methods resulted mostly in the formation of spherical particles with diameter < 2 μm (Fig. S9B–F). TEM image of particles prepared by solvent evaporation technique at 60 °C showed the presence of rods and solid particles composed of separate domains (Fig. S10A). Inter-

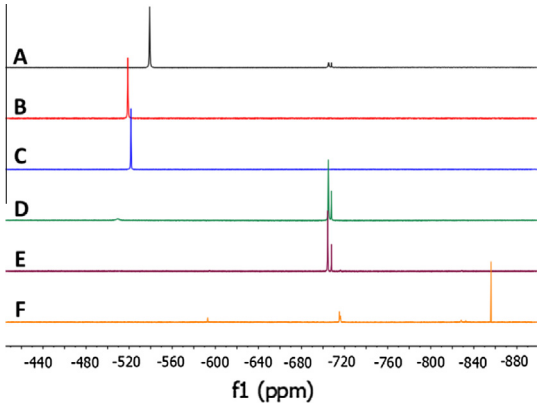

Fig. 3. ^{119}Sn NMR (CD_2Cl_2) spectra of $SnOct_2$ stored under different conditions: (A) just bought as-received; (B) just bought, distilled and stored one day under argon; (C) just bought, distilled and stored two months under argon; (D) just bought, distilled and stored one day exposed to air; (E) 1-year old (after purchase) non-distilled; (F) stored 1 year in air after distillation.

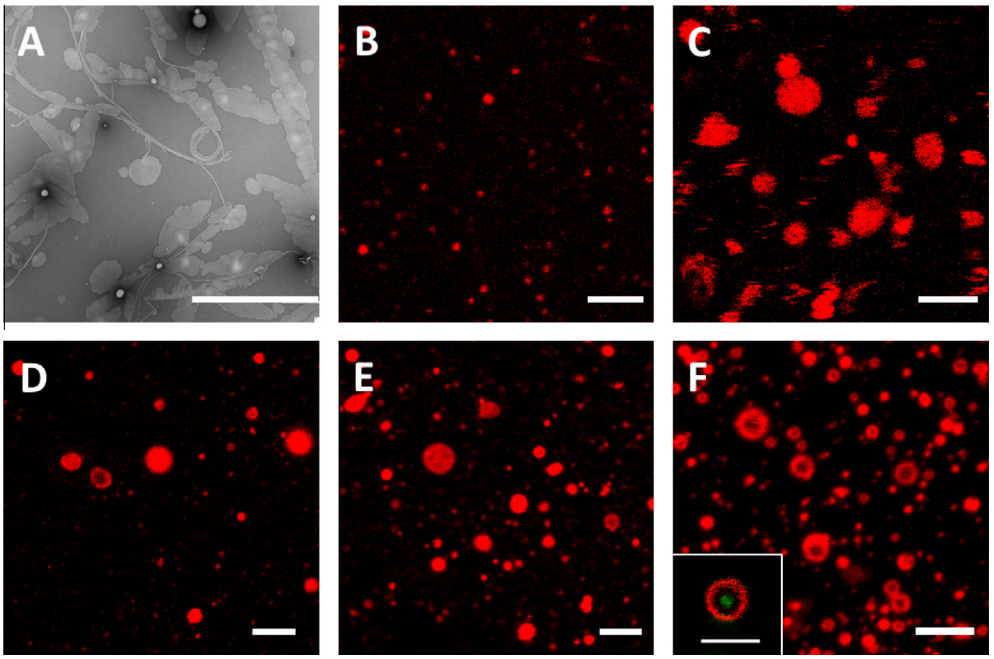

Fig. 4. Self-assembled structures formed by PEO(2K)-*b*-PCL(17.4K) ($Đ_M$ = 1.08) polymer using different preparation methods: TEM image (A) co-solvent method, scale bar is 2 μm; LSM images (B) solvent switch method; (C) solvent evaporation at 25 °C; (D) solvent evaporation at 60 °C; (E) film rehydration on Teflon surface at 60 °C; (F) film rehydration on glass surface at 60 °C. Inset in the left lower corner represents a vesicle with encapsulated hydrophilic dye calcein. Microscale structures were stained with Bodipy 630/650 dye. Scale bars for LSM images are 5 μm.

estingly, these particles are able to encapsulate the hydrophilic dye calcein, which stayed entrapped even after 3 days of dialysis (Fig. S10B). In the case of a polymer with a longer PCL block, PEO(2K)-*b*-PCL(17.4K), most of the preparation methods resulted in the formation of solid particles and some polymersomes (Fig. 4B–E). However, film rehydration method on glass surface yielded small uniform polymersomes, which are also able to entrap the hydrophilic dye calcein (Fig. 4F). Therefore, we applied this technique for further investigation of self-assembly properties of PEO-*b*-PCL polymers.

We have shown that the film rehydration method, in the case of PEO(2K)-*b*-PCL(17.4K), results in the formation of polymersomes with diameters ranging from 1 to 2.5 μm. Our results, however, are not in complete agreement with those obtained by film rehydration method [15–17]. This could be explained by differences in the calculation of PEO-*b*-PCL block ratios used in our work: we took the peak at 3.36 ppm (terminal methyl group of PEO) as a reference, whereas the authors [15–17] used the methylene protons of PEO backbone as a reference (3.65 ppm). We believe that the reference peak at 3.36 ppm gives more precise and reproducible integrals of the other peaks, because PEO synthesis is initiated by CH_3OK, and, therefore, all molecules contain a terminal methyl group (Fig. S2). The disagreement could also be explained by some differences in the preparation procedures of the self-assembled structures. However, we hypothesize the main reason to be the dispersity of PEO-*b*-PCL, as the polymers reported here exhibited rather low $Đ_M$ (1.08), whereas the ones with similar molecular weights and block ratios reported by Therien et al. [15,16] have dispersity around 1.2, and reported by Discher et al. [17] around 1.6. The influence of the dispersity of the diblock copolymers on the morphology [20–23] and size distribution [23,24] of nanoscale self-assemblies was shown for different systems and supported by computer simulations [55,56].

To test the hypothesis of the influence of the dispersity on the self-assembly of PEO-*b*-PCL diblock copolymers, we took three different PEO-*b*-PCL polymers with similar molecular weights, block ratios, and identical chemical structures as determined by ^{1}H NMR spectroscopy (Fig. S11): PEO(2K)-*b*-PCL(17.4K), PEO(2K)-*b*-PCL(16.0K), PEO(2K)-*b*-PCL(16.3K), but with different $Đ_M$, and studied their self-assembly using film rehydration method at 60 °C on glass surfaces. The $Đ_M$ in this case represents the dispersity of the hydrophobic block, since side transesterification reactions affect only polyester backbone as discussed earlier.

All three polymers self-assemble into mesoscale structures. The morphology and size of the self-assembled structures differ dramatically for polymers with different $Đ_M$ (Fig. 5). The polymer with the lowest $Đ_M$ gives the most uniform self-assembly. The polymersomes have diameter 1.6 ± 0.5 μm. Interestingly, the polymer with a $Đ_M$ of 1.23 gives mostly polymersomes which are very similar to those obtained by Therien et al. [15,16]. The obtained polymersomes are much bigger and less uniform (4.1 ± 2.5 μm) compared to those formed by the polymer with a $Đ_M$ = 1.08. The polymer with the highest $Đ_M$ = 1.55 forms two types of morphologies: polymersomes and aggregates. The polymersomes in this case exhibit a variety of shapes, including elongated polymersomes, multicompartment polymersomes with a few polymersomes inside, etc. (Fig. S12).

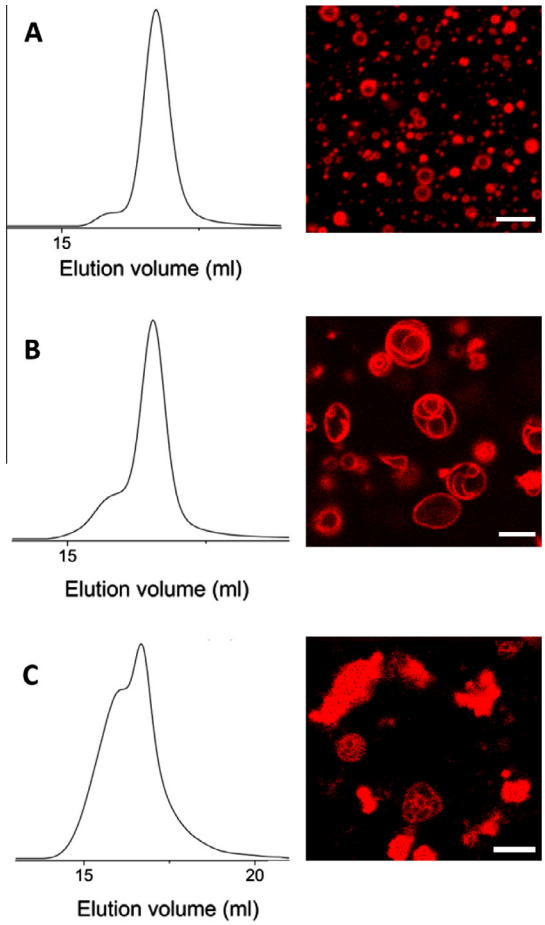

Fig. 5. Elugrams of PEO-*b*-PCL polymers and LSM images of the corresponding self-assembled structures formed using film rehydration on a glass surface: (A) PEO(2K)-*b*-PCL(17.4K), $Đ_M$ = 1.08; (B) PEO(2K)-*b*-PCL(16.0K), $Đ_M$ = 1.23; (C) PEO(2K)-*b*-PCL(16.3K), $Đ_M$ = 1.55. Self-assembled structures were stained with Bodipy 630/650 dye. Scale bars are 5 μm.

To investigate the effect of PEO-*b*-PCL dispersity on its nanoscale self-assemblies, we applied the method described in [16]. However, the polymers discussed here mostly precipitated under the tested self-assembly conditions. This fact is not very surprising, since phase diagrams for meso- and nanoscale structures formed by PEO-*b*-PCL do not entirely match [16]. Nevertheless, the data discussed in this article support the hypothesis that the lower the PEO-*b*-PCL dispersity is, the more uniform are the mesoscale self-assembled structures in size and shape. This conclusion is based on 3–4 self-assembly experiments which resulted in the formation of similar structures. Generalization of the hypothesis would require additional studies investigating the effect of the copolymer dispersity on nanoassemblies of PEO-*b*-PCL and self-assembled structures of other amphiphilic block copolymers.

4. Conclusions

The optimization of the synthesis of PEO-*b*-PCL diblock copolymers catalyzed by $SnOct_2$ yielded a robust and reproducible strategy to obtain block copolymers with tunable length of the PCL block while maintaining a low dispersity ($Đ_M$ < 1.1). We demonstrated the importance of $SnOct_2$ purification prior to the polymerization, and investigated its degradation during storage under different conditions. Furthermore, the tosylation of PCL end of PEO-*b*-PCL copolymers was discussed and outlined. The application of PEO-*b*-PCL-OTs as a macroinitiator for the polymerization of 2-alkyl-2-oxazolines will be addressed elsewhere.

The comparison of the mesoscale self-assembled structures formed by PEO-*b*-PCL diblock copolymers suggests that uniform polymers are beneficial for the self-assembly of distinct and uniform 3D structures. However, further experimental and theoretical studies are required to make this conclusion more solid.

The obtained copolymers and the assemblies thereof might serve as platform to study the effect of the dispersity on different processes, for example, on the insertion of membrane proteins into thick polymeric membranes. Such a system is dou-

bly beneficial, since it is believed that two factors are responsible for the successful incorporation of a protein: polymer chain flexibility and contraction around the membrane protein, and/or arrangement of shorter polymer chains around the protein [57,58]. If the latter hypothesis plays a predominant role, then the dispersity of a polymer can drastically affect the incorporation of a functional membrane protein into such polymeric membrane.

Acknowledgments

The Swiss National Science Foundation and the University of Basel are acknowledged for financial support. E. K. acknowledges Dr. Ulmas Zhumaev (MPIP, Mainz, Germany) for fruitful discussions and editing the manuscript. We acknowledge Dr. Jason Duskey and Dr. Jens Gaitzsch for useful comments. We thank Pascal Richard for helping with the MALDI-TOF MS experiments.

Appendix A. Supplementary material

Supplementary data associated with this article can be found, in the online version, at http://dx.doi.org/10.1016/j.eurpolymj.2016.08.011.

References

[1] G. Gunkel-Grabole, S. Sigg, M. Lomora, S. Lorcher, C.G. Palivan, W.P. Meier, Polymeric 3D nano-architectures for transport and delivery of therapeutically relevant biomacromolecules, Biomater. Sci. 3 (1) (2015) 25–40.
[2] C. Nardin, T. Hirt, J. Leukel, W. Meier, Polymerized ABA triblock copolymer vesicles, Langmuir 16 (3) (2000) 1035–1041.
[3] C.G. Palivan, R. Goers, A. Najer, X. Zhang, A. Car, W. Meier, Bioinspired polymer vesicles and membranes for biological and medical applications, Chem. Soc. Rev. 45 (2) (2016) 377–411.
[4] H. Bermudez, A.K. Brannan, D.A. Hammer, F.S. Bates, D.E. Discher, Molecular weight dependence of polymersome membrane structure, elasticity, and stability, Macromolecules 35 (21) (2002) 8203–8208.
[5] D.E. Discher, A. Eisenberg, Science (Washington, DC) 297 (5583) (2002) 967.
[6] B.M. Discher, Y.Y. Won, D.S. Ege, J.C.M. Lee, F.S. Bates, D.E. Discher, D.A. Hammer, Science (Washington, DC) 284 (5417) (1999) 1143.
[7] J.C.M. Lee, H. Bermudez, B.M. Discher, M.A. Sheehan, Y.-Y. Won, F.S. Bates, D.E. Discher, Preparation, stability, and in vitro performance of vesicles made with diblock copolymers, Biotechnol. Bioeng. 73 (2) (2001) 135–145.
[8] P.P. Ghoroghchian, P.R. Frail, K. Susumu, D. Blessington, A.K. Brannan, F.S. Bates, B. Chance, D.A. Hammer, M.J. Therien, Near-infrared-emissive polymersomes: self-assembled soft matter for in vivo optical imaging, Proc. Natl. Acad. Sci. U. S. A. 102 (8) (2005) 2922–2927.
[9] D.E. Discher, F. Ahmed, Polymersomes, Annu. Rev. Biomed. Eng. 8 (1) (2006) 323–341.
[10] P.J. Photos, L. Bacakova, B. Discher, F.S. Bates, D.E. Discher, Polymer vesicles in vivo: correlations with PEG molecular weight, J. Control Release 90 (3) (2003) 323–334.
[11] A.S. Hoffman, Hydrogels for biomedical applications, Adv. Drug Deliv. Rev. 64 (Supplement) (2012) 18–23.
[12] K. Letchford, R. Liggins, K.M. Wasan, H. Burt, In vitro human plasma distribution of nanoparticulate paclitaxel is dependent on the physicochemical properties of poly(ethylene glycol)-block-poly(caprolactone) nanoparticles, Eur. J. Pharm. Biopharm. 71 (2) (2009) 196–206.
[13] C.E. Mora-Huertas, H. Fessi, A. Elaissari, Polymer-based nanocapsules for drug delivery, Int. J. Pharm. 385 (1–2) (2010) 113–142.
[14] P. Lim Soo, J. Lovric, P. Davidson, D. Maysinger, A. Eisenberg, Polycaprolactone-block-poly(ethylene oxide) micelles: a nanodelivery system for 17β-estradiol, Mol. Pharm. 2 (6) (2005) 519–527.
[15] P.P. Ghoroghchian, G. Li, D.H. Levine, K.P. Davis, F.S. Bates, D.A. Hammer, M.J. Therien, Bioresorbable vesicles formed through spontaneous self-assembly of amphiphilic poly(ethylene oxide)-block-polycaprolactone, Macromolecules 39 (5) (2006) 1673–1675.
[16] W. Qi, P.P. Ghoroghchian, G. Li, D.A. Hammer, M.J. Therien, Aqueous self-assembly of poly(ethylene oxide)-block-poly(?-caprolactone) (PEO-b-PCL) copolymers: disparate diblock copolymer compositions give rise to nano- and meso-scale bilayered vesicles, Nanoscale 5 (22) (2013) 10908–10915.
[17] K. Rajagopal, A. Mahmud, D.A. Christian, J.D. Pajerowski, A.E.X. Brown, S.M. Loverde, D.E. Discher, Curvature-coupled hydration of semicrystalline polymer amphiphiles yields flexible worm micelles but favors rigid vesicles: polycaprolactone-based block copolymers, Macromolecules 43 (23) (2010) 9736–9746.
[18] D.J. Adams, C. Kitchen, S. Adams, S. Furzeland, D. Atkins, P. Schuetz, C.M. Fernyhough, N. Tzokova, A.J. Ryan, M.F. Butler, On the mechanism of formation of vesicles from poly(ethylene oxide)-block-poly(caprolactone) copolymers, Soft Matter 5 (16) (2009) 3086–3096.
[19] M. Dionzou, A. Morere, C. Roux, B. Lonetti, J.D. Marty, C. Mingotaud, P. Joseph, D. Goudouneche, B. Payre, M. Leonetti, A.F. Mingotaud, Comparison of methods for the fabrication and the characterization of polymer self-assemblies: what are the important parameters?, Soft Matter 12 (7) (2016) 2166–2176
[20] O. Terreau, L. Luo, A. Eisenberg, Effect of poly(acrylic acid) block length distribution on polystyrene-b-poly(acrylic acid) aggregates in solution. 1. Vesicles, Langmuir 19 (14) (2003) 5601–5607.
[21] O. Terreau, C. Bartels, A. Eisenberg, Effect of poly(acrylic acid) block length distribution on polystyrene-b-poly(acrylic acid) block copolymer aggregates in solution. 2. A partial phase diagram, Langmuir 20 (3) (2004) 637–645.
[22] P. Schuetz, M.J. Greenall, J. Bent, S. Furzeland, D. Atkins, M.F. Butler, T.C.B. McLeish, D.M.A. Buzza, Controlling the micellar morphology of binary PEO-PCL block copolymers in water-THF through controlled blending, Soft Matter 7 (2) (2011) 749–759.
[23] S. Jain, F.S. Bates, Consequences of nonergodicity in aqueous binary PEO−PB micellar dispersions, Macromolecules 37 (4) (2004) 1511–1523.
[24] S. George, R. Champagne-Hartley, G. Deeter, D. Campbell, B. Reck, D. Urban, M. Cunningham, Amphiphilic block copolymers as stabilizers in emulsion polymerization: effects of the stabilizing block molecular weight dispersity on stabilization performance, Macromolecules 48 (24) (2015) 8913–8920.
[25] C. Choi, S.Y. Chae, T.-H. Kim, J.K. Kweon, C.S. Cho, M.-K. Jang, J.-W. Nah, Synthesis and physicochemical characterization of amphiphilic block copolymer self-aggregates formed by poly(ethylene glycol)-block-poly(∈-caprolactone), J. Appl. Polym. Sci. 99 (6) (2006) 3520–3527.
[26] M.A.R. Meier, S.N.H. Aerts, B.B.P. Staal, M. Rasa, U.S. Schubert, PEO-b-PCL block copolymers: synthesis, detailed characterization, and selected micellar drug encapsulation behavior, Macromol. Rapid Commun. 26 (24) (2005) 1918–1924.
[27] R. Savić, T. Azzam, A. Eisenberg, D. Maysinger, Assessment of the integrity of poly(caprolactone)-b-poly(ethylene oxide) micelles under biological conditions: a fluorogenic-based approach, Langmuir 22 (8) (2006) 3570–3578.
[28] H.M. Aliabadi, A. Mahmud, A.D. Sharifabadi, A. Lavasanifar, Micelles of methoxy poly(ethylene oxide)-b-poly(ε-caprolactone) as vehicles for the solubilization and controlled delivery of cyclosporine A, J. Control Release 104 (2) (2005) 301–311.
[29] P. Vangeyte, R. Jérôme, Amphiphilic block copolymers of high-molecular-weight poly(ethylene oxide) and either ε-caprolactone or γ-methyl-ε-caprolactone: synthesis and characterization, J. Polym. Sci., Part A: Polym. Chem. 42 (5) (2004) 1132–1142.
[30] J.A. Zupancich, F.S. Bates, M.A. Hillmyer, Macromolecules 39 (13) (2006) 4286.

[31] C. Jérôme, P. Lecomte, Recent advances in the synthesis of aliphatic polyesters by ring-opening polymerization, Adv. Drug Deliv. Rev. 60 (9) (2008) 1056–1076.
[32] A.L. Korich, A.R. Walker, C. Hincke, C. Stevens, P.M. Iovine, Synthesis, characterization, and star polymer assembly of boronic acid end-functionalized polycaprolactone, J. Polym. Sci., Part A: Polym. Chem. 48 (24) (2010) 5767–5774.
[33] M.A.R. Meier, U.S. Schubert, Evaluation of a new multiple-layer spotting technique for matrix-assisted laser desorption/ionization time-of-flight mass spectrometry of synthetic polymers, Rapid Commun. Mass Spectrom. 17 (7) (2003) 713–716.
[34] H.R. Kricheldorf, I. Kreiser-Saunders, A. Stricker, Polylactones 48. SnOct2-initiated polymerizations of lactide: a mechanistic study, Macromolecules 33 (3) (2000) 702–709.
[35] F. Wiesbrock, R. Hoogenboom, M.A.M. Leenen, M.A.R. Meier, U.S. Schubert, Investigation of the living cationic ring-opening polymerization of 2-methyl-, 2-ethyl-, 2-nonyl-, and 2-phenyl-2-oxazoline in a single-mode microwave reactor, Macromolecules 38 (12) (2005) 5025–5034.
[36] J. Libiszowski, A. Kowalski, A. Duda, S. Penczek, Kinetics and mechanism of cyclic esters polymerization initiated with covalent metal carboxylates, 5. End-group studies in the model ε-caprolactone and L, L-dilactide/Tin(II) and zinc octoate/butyl alcohol systems, Macromol. Chem. Phys. 203 (10–11) (2002) 1694–1701.
[37] A. Kowalski, A. Duda, S. Penczek, Mechanism of cyclic ester polymerization initiated with tin(II) octoate. 2.† macromolecules fitted with tin(II) alkoxide species observed directly in MALDI−TOF spectra, Macromolecules 33 (3) (2000) 689–695.
[38] A. Kowalski, A. Duda, S. Penczek, Kinetics and mechanism of cyclic esters polymerization initiated with tin(II) octoate. 3.† polymerization of l, l-dilactide, Macromolecules 33 (20) (2000) 7359–7370.
[39] J. Baran, A. Duda, A. Kowalski, R. Szymanski, S. Penczek, Quantitative comparison of selectivities in the polymerization of cyclic esters, Macromol. Symp. 123 (1) (1997) 93–101.
[40] S. Penczek, A. Duda, R. Szymanski, Intra- and intermolecular chain transfer to macromolecules with chain scission. The case of cyclic esters, Macromol. Symp. 132 (1) (1998) 441–449.
[41] K. Majerska, A. Duda, S. Penczek, Kinetics and mechanism of cyclic esters polymerisation initiated with tin(II) octoate, 4. Influence of proton trapping agents on the kinetics of ε-caprolactone and L, L-dilactide polymerisation, Macromol. Rapid Commun. 21 (18) (2000) 1327–1332.
[42] T.K. Endres, M. Beck-Broichsitter, O. Samsonova, T. Renette, T.H. Kissel, Self-assembled biodegradable amphiphilic PEG–PCL–lPEI triblock copolymers at the borderline between micelles and nanoparticles designed for drug and gene delivery, Biomaterials 32 (30) (2011) 7721–7731.
[43] G. Liu, S. Ma, S. Li, R. Cheng, F. Meng, H. Liu, Z. Zhong, The highly efficient delivery of exogenous proteins into cells mediated by biodegradable chimaeric polymersomes, Biomaterials 31 (29) (2010) 7575–7585.
[44] Q. Liu, J. Chen, J. Du, Asymmetrical polymer vesicles with a "stealthy" outer corona and an endosomal-escape-accelerating inner corona for efficient intracellular anticancer drug delivery, Biomacromolecules 15 (8) (2014) 3072–3082.
[45] C.-Q. Mao, J.-Z. Du, T.-M. Sun, Y.-D. Yao, P.-Z. Zhang, E.-W. Song, J. Wang, A biodegradable amphiphilic and cationic triblock copolymer for the delivery of siRNA targeting the acid ceramidase gene for cancer therapy, Biomaterials 32 (11) (2011) 3124–3133.
[46] T.-M. Sun, J.-Z. Du, L.-F. Yan, H.-Q. Mao, J. Wang, Self-assembled biodegradable micellar nanoparticles of amphiphilic and cationic block copolymer for siRNA delivery, Biomaterials 29 (32) (2008) 4348–4355.
[47] A. Wittemann, T. Azzam, A. Eisenberg, Biocompatible polymer vesicles from biamphiphilic triblock copolymers and their interaction with bovine serum albumin, Langmuir 23 (4) (2007) 2224–2230.
[48] W. Zhang, J. He, Z. Liu, P. Ni, X. Zhu, Biocompatible and pH-responsive triblock copolymer mPEG-b-PCL-b-PDMAEMA: synthesis, self-assembly, and application, J. Polym. Sci., Part A: Polym. Chem. 48 (5) (2010) 1079–1091.
[49] A. Labouriau, D. Taylor, T.S. Stephens, M. Pasternak, Mössbauer and NMR characterization of tin octoate: neat and residues in RTV foams, Polym. Degrad. Stab. 91 (8) (2006) 1896–1902.
[50] F.W. van Der Weij, The action of tin compounds in condensation-type RTV silicone rubbers, Die Makromolekulare Chemie 181 (12) (1980) 2541–2548.
[51] A. Kowalski, A. Duda, S. Penczek, Kinetics and mechanism of cyclic esters polymerization initiated with tin(II) octoate, 1. Polymerization of ε-caprolactone, Macromol. Rapid Commun. 19 (11) (1998) 567–572.
[52] G.R. Fulmer, A.J.M. Miller, N.H. Sherden, H.E. Gottlieb, A. Nudelman, B.M. Stoltz, J.E. Bercaw, K.I. Goldberg, NMR chemical shifts of trace impurities: common laboratory solvents, organics, and gases in deuterated solvents relevant to the organometallic chemist, Organometallics 29 (9) (2010) 2176–2179.
[53] J.D. Donaldson, A. Jelen, The Mossbauer effect in tin(II) compounds. Part IV. The spectra of some tin(II) carboxylates and tricarboxylatostannates(II), J. Chem. Soc. A: Inorg., Phys., Theor. (1968) 1448–1450.
[54] T. Birchall, J.P. Johnson, Preparation and characterization of mixed-oxidation-state tin carboxylates and related tin(IV) carboxylates, Inorg. Chem. 21 (10) (1982) 3724–3731.
[55] Y. Han, J. Cui, W. Jiang, Effect of polydispersity on the self-assembly structure of diblock copolymers under various confined states: a Monte Carlo study, Macromolecules 41 (16) (2008) 6239–6245.
[56] Y. Jiang, T. Chen, F. Ye, H. Liang, A.-C. Shi, Effect of polydispersity on the formation of vesicles from amphiphilic diblock copolymers, Macromolecules 38 (15) (2005) 6710–6717.
[57] F. Itel, A. Najer, C.G. Palivan, W. Meier, Dynamics of membrane proteins within synthetic polymer membranes with large hydrophobic mismatch, Nano Lett. 15 (6) (2015) 3871–3878.
[58] G. Srinivas, D.E. Discher, M.L. Klein, Key roles for chain flexibility in block copolymer membranes that contain pores or make tubes, Nano Lett. 5 (12) (2005) 2343–2349.

Supporting information

Key aspects to yield low dispersity of PEO-*b*-PCL diblock copolymers and their mesoscale self-assembly

*Evgeniia Konishcheva, Daniel Häussinger, Samuel Lörcher, Wolfgang Meier**

Department of Chemistry, University of Basel, Klingelbergstrasse 80, 4056 Basel, Switzerland

*Corresponding author: wolfgang.meier@unibas.ch

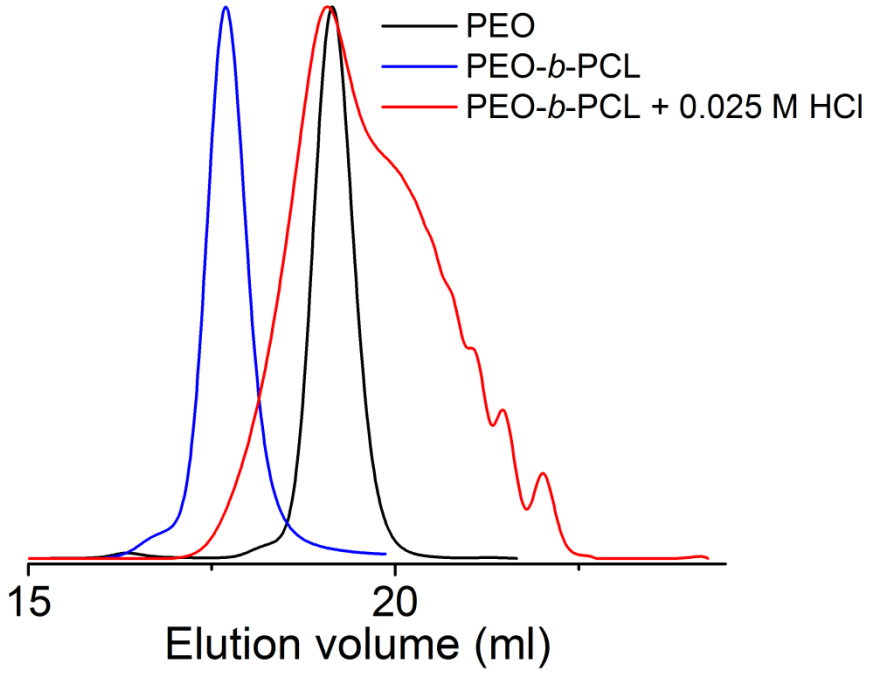

Figure S1. GPC ($CHCl_3$) traces of PEO (black curve), PEO-*b*-PCL diblock copolymers (M_n = 12.4 kDa, blue curve) and the same polymer treated with 0.025 M HCl for 1 h at room temperature (red curve).

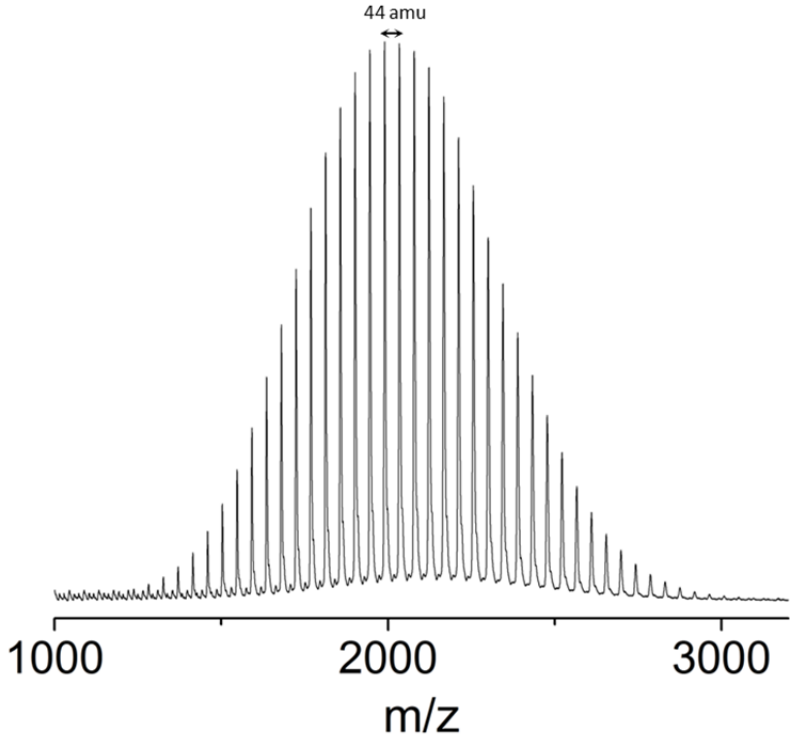

Figure S2. MALDI-TOF MS spectrum of PEO. $[M + Na^+]$ calculated 2036.39, observed 2034.57.

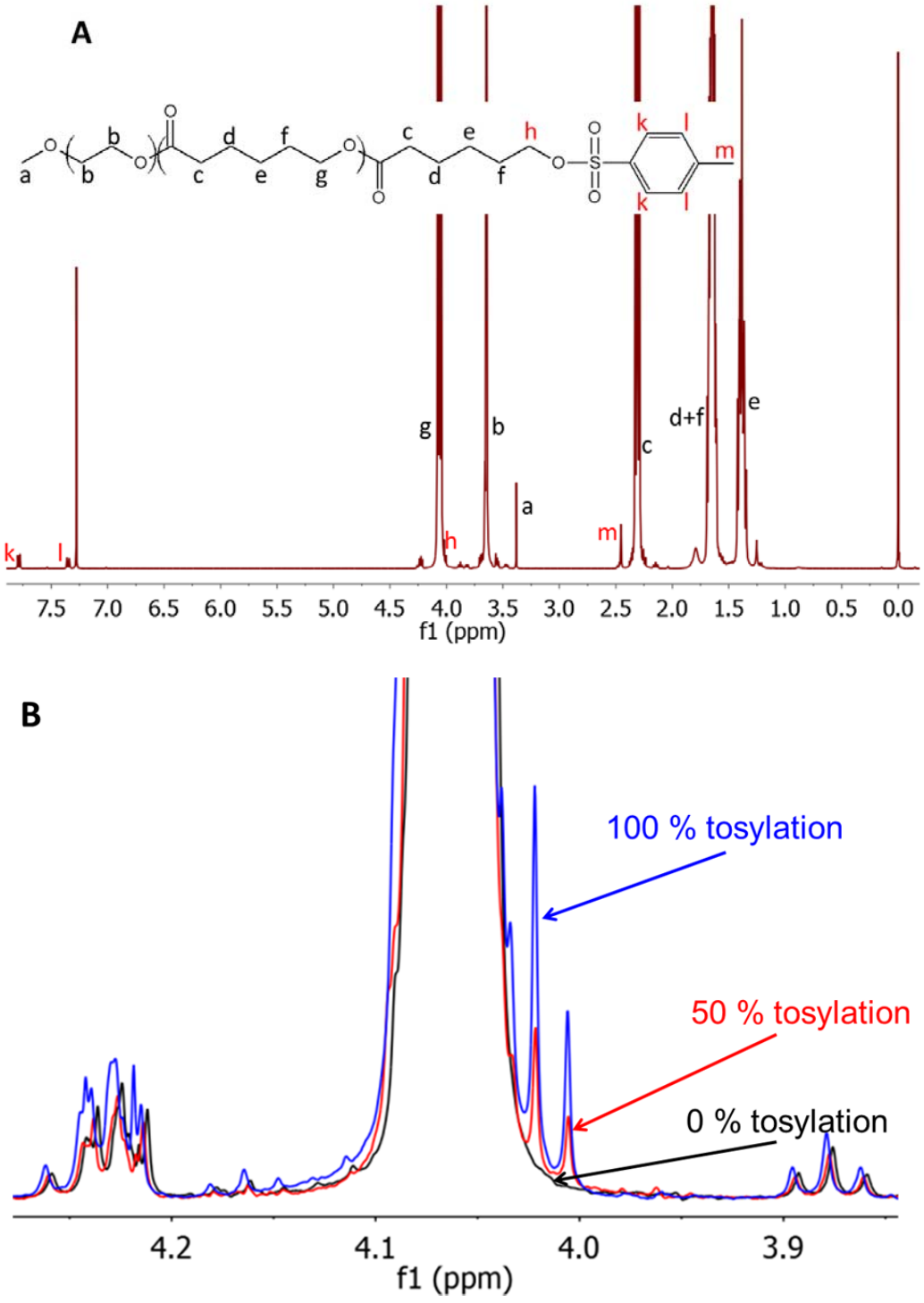

Figure S3. A: representative ^{1}H NMR ($CDCl_3$) spectrum of a tosylated PEO-*b*-PCL diblock copolymer; B: comparison of ^{1}H NMR ($CDCl_3$) spectra of PEO-*b*-PCL diblock copolymers with different percentage of tosylation.

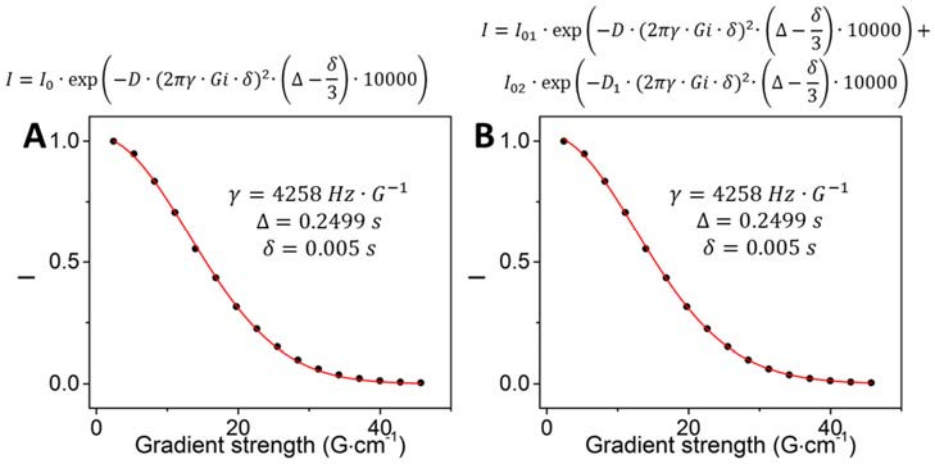

Figure S4. Representative one (A) and two (B) component fits for a peak at 2.28 ppm for the polymer with a big shoulder.

Table S1. Diffusion coefficients for two PEO-*b*-PCL polymers ($M_n \approx 13.4$ kDa) with big and small shoulders.

	Chemical shift, ppm	One component fit		Two component fit			
		D, m·s^{-2}	I_0	D, m·s^{-2}	I_{01}	D_1, m·s^{-2}	I_{02}
PEO-*b*-PCL big shoulder	1.36	$6.76 \cdot 10^{-11}$	1.017	$9.90 \cdot 10^{-11}$	0.36	$5.69 \cdot 10^{-11}$	0.67
	1.62	$6.81 \cdot 10^{-11}$	1.014	$9.57 \cdot 10^{-11}$	0.41	$5.59 \cdot 10^{-11}$	0.61
	2.28	$6.72 \cdot 10^{-11}$	1.019	$8.76 \cdot 10^{-11}$	0.51	$5.32 \cdot 10^{-11}$	0.51
	3.59	$7.06 \cdot 10^{-11}$	1.026	$9.34 \cdot 10^{-11}$	0.49	$5.66 \cdot 10^{-11}$	0.54
	4.02	$6.68 \cdot 10^{-11}$	1.023	$8.12 \cdot 10^{-11}$	0.64	$5.02 \cdot 10^{-11}$	0.39
	average	$(6.81 \pm 0.15) \cdot 10^{-11}$	1.020±0.005	$(9.14 \pm 0.71) \cdot 10^{-11}$	0.48±0.11	$(5.46 \pm 0.29) \cdot 10^{-11}$	0.54±0.11
PEO-*b*-PCL small shoulder	1.36	$9.80 \cdot 10^{-11}$	1.031	$9.99 \cdot 10^{-11}$	1.02	$3.11 \cdot 10^{-11}$	0.01
	1.62	$9.91 \cdot 10^{-11}$	1.026	$1.05 \cdot 10^{-10}$	0.94	$5.66 \cdot 10^{-11}$	0.08
	2.28	$9.76 \cdot 10^{-11}$	1.032	$9.88 \cdot 10^{-11}$	1.03	$2.41 \cdot 10^{-11}$	0.01
	3.59	$1.00 \cdot 10^{-10}$	1.041	$1.00 \cdot 10^{-10}$	1.04	$1.42 \cdot 10^{-7}$	-0.04
	4.02	$9.69 \cdot 10^{-11}$	1.035	$9.74 \cdot 10^{-11}$	1.03	$1.41 \cdot 10^{-8}$	-0.72
	average	$(9.83 \pm 0.13) \cdot 10^{-11}$	1.033±0.006	$(10.02 \pm 0.28) \cdot 10^{-11}$	1.01±0.04		

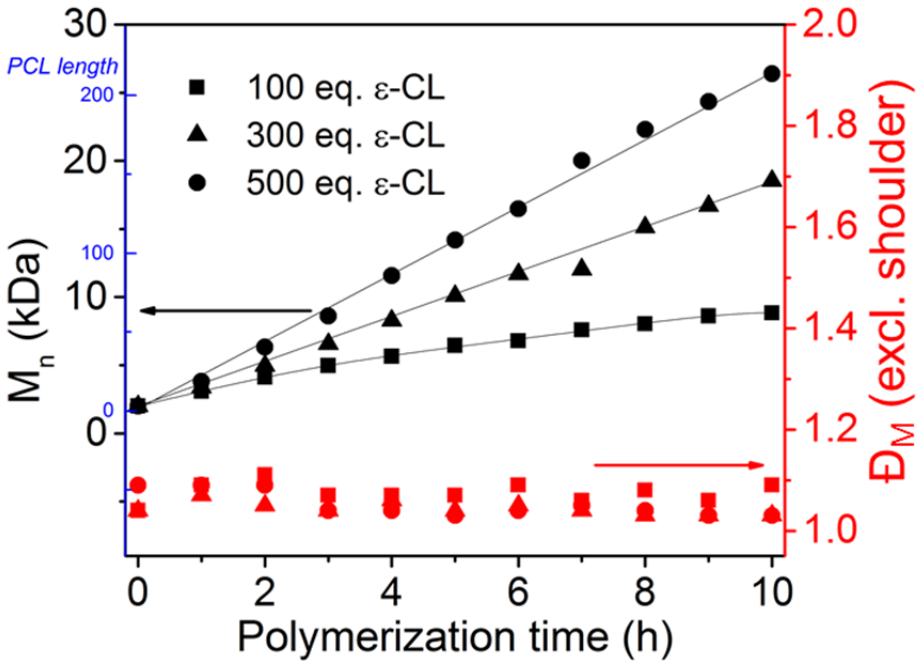

Figure S5. M_n and $Đ_M$ (excluding shoulder) versus polymerization time for 100, 300, and 500 equivalents of ε-CL.

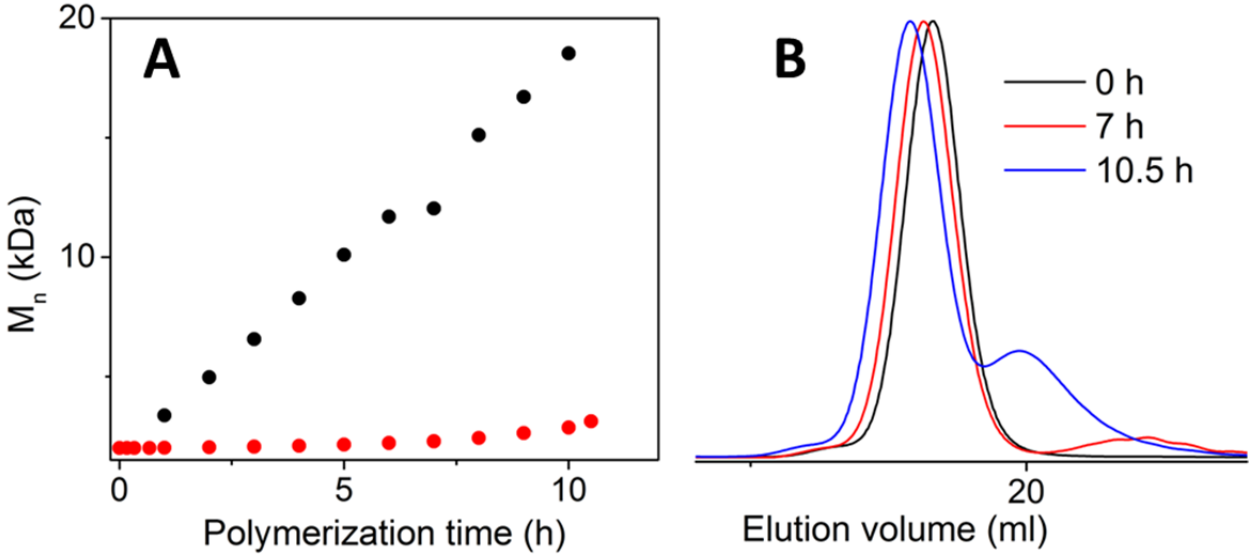

Figure S6. A: Kinetic plot of M_n (PEO-*b*-PCL) versus polymerization time when freshly distilled $SnOct_2$ was used (●), and the same catalyst stored for 5 days under vacuum at room temperature (●); B: distinct GPC ($CHCl_3$) traces at various time points corresponding to A (●).

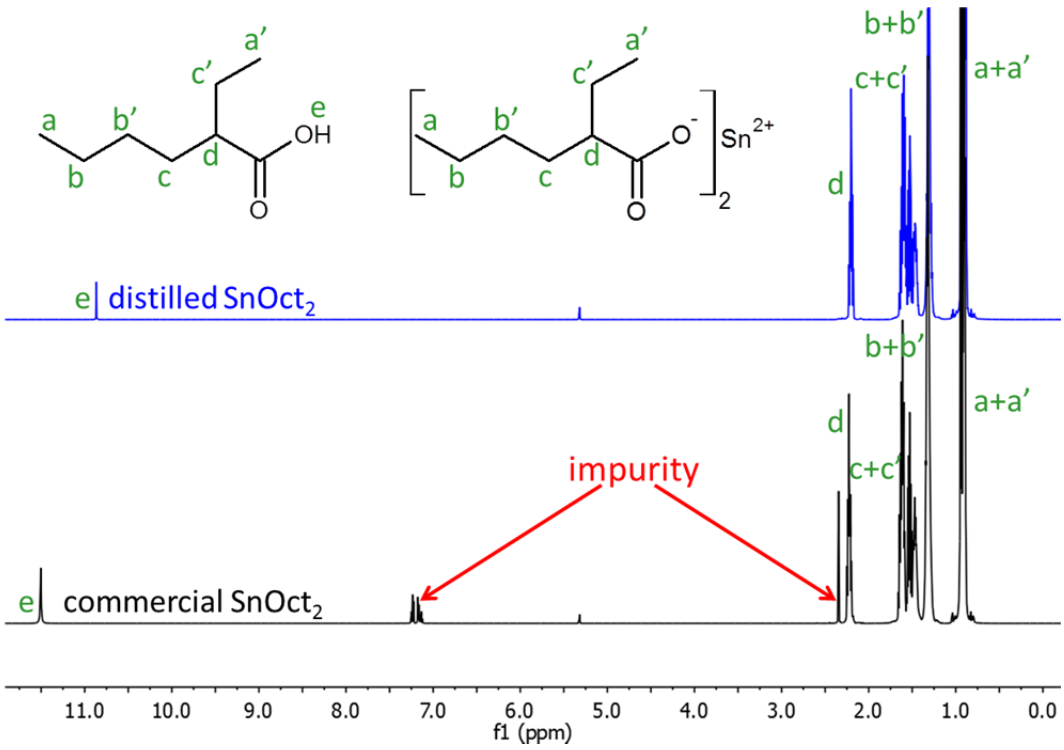

Figure S7. ^{1}H NMR (CD_2Cl_2) spectra of commercial (lower) and distilled (upper) $SnOct_2$. ^{1}H NMR of the impurity (600.13 MHz, δ, CD_2Cl_2): 2.35 ppm (s), 7.15 ppm (m), 7.24 ppm (m).

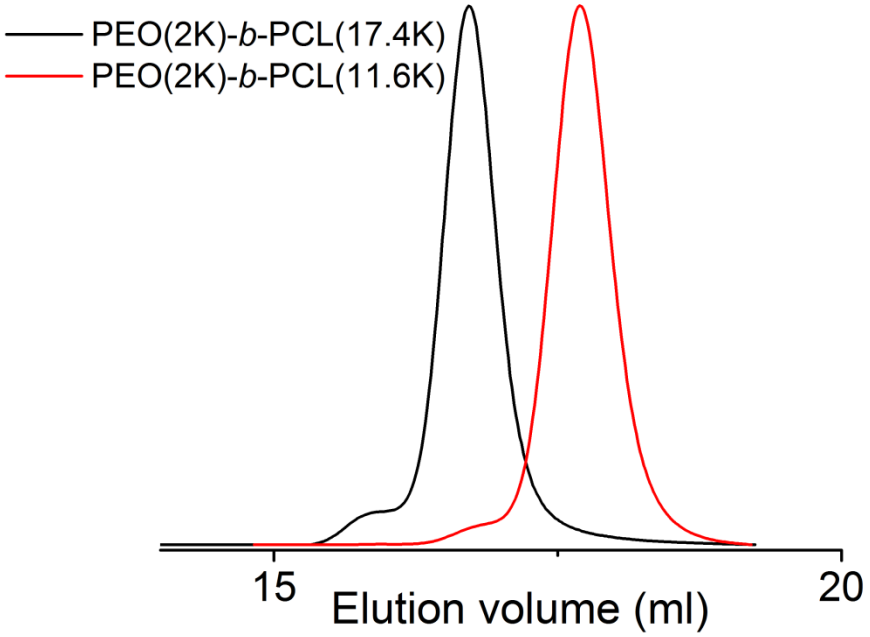

Figure S8. GPC ($CHCl_3$) traces of two PEO-*b*-PCL diblock copolymers.

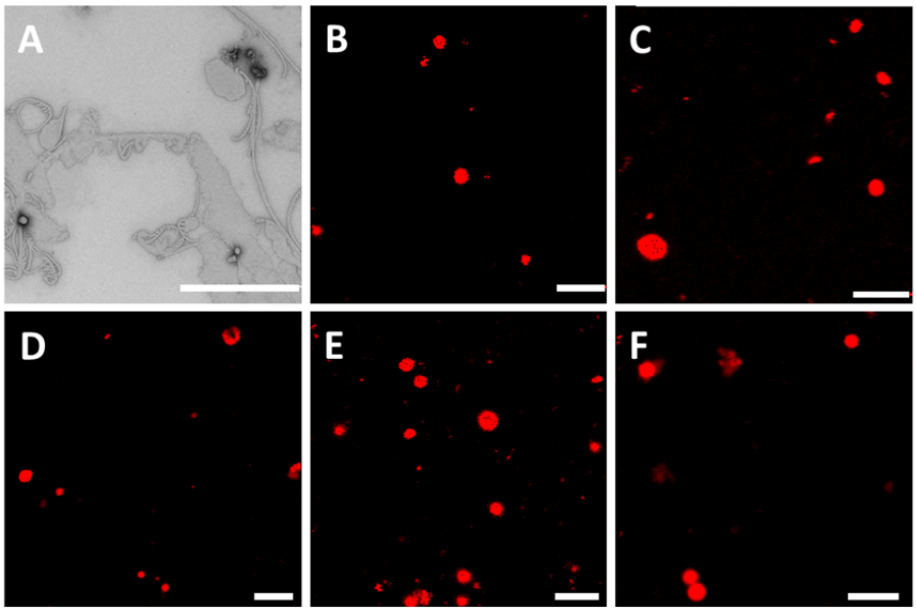

Figure S9. Self-assembled structures formed by PEO(2K)-*b*-PCL(11.6K) ($Đ_M$ = 1.08) polymer using different preparation methods: TEM image A: co-solvent method, scale bar 2 μm; LSM images B: solvent switch method; C: solvent evaporation at 25 °C; D: solvent evaporation at 60 °C; E: film rehydration on Teflon surface; F: film rehydration on glass surface. Scale bars for LSM images are 5 μm.

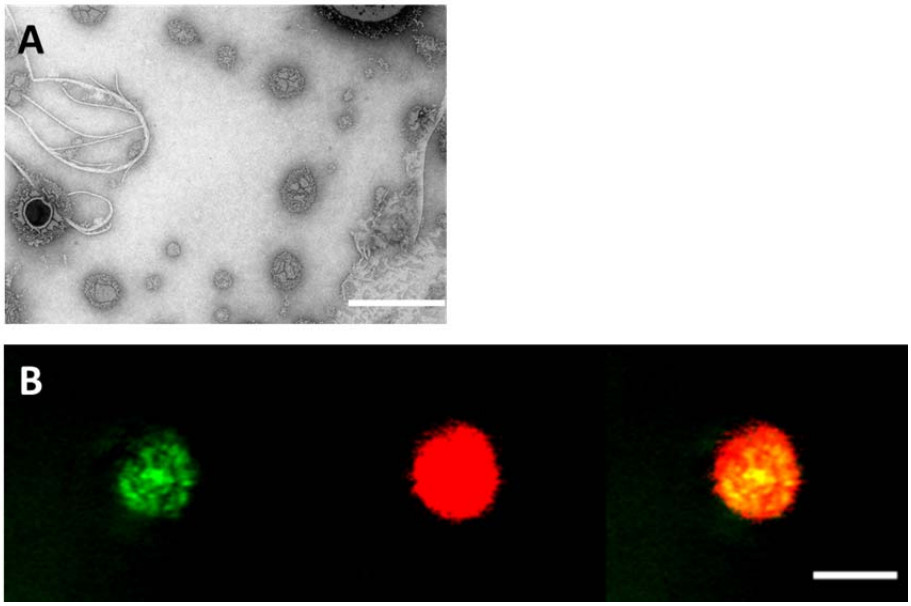

Figure S10. Self-assembled structures formed by PEO(2K)-*b*-PCL(11.6K) ($Đ_M$ = 1.08) polymer using solvent evaporation method at 60 °C: TEM image A, scale bar is 1 μm; LSM images B (from the left to the right) of entrapped calcein, particles stained with Bodipy 630/650 dye, and their overlay. Scale bar is 3 μm.

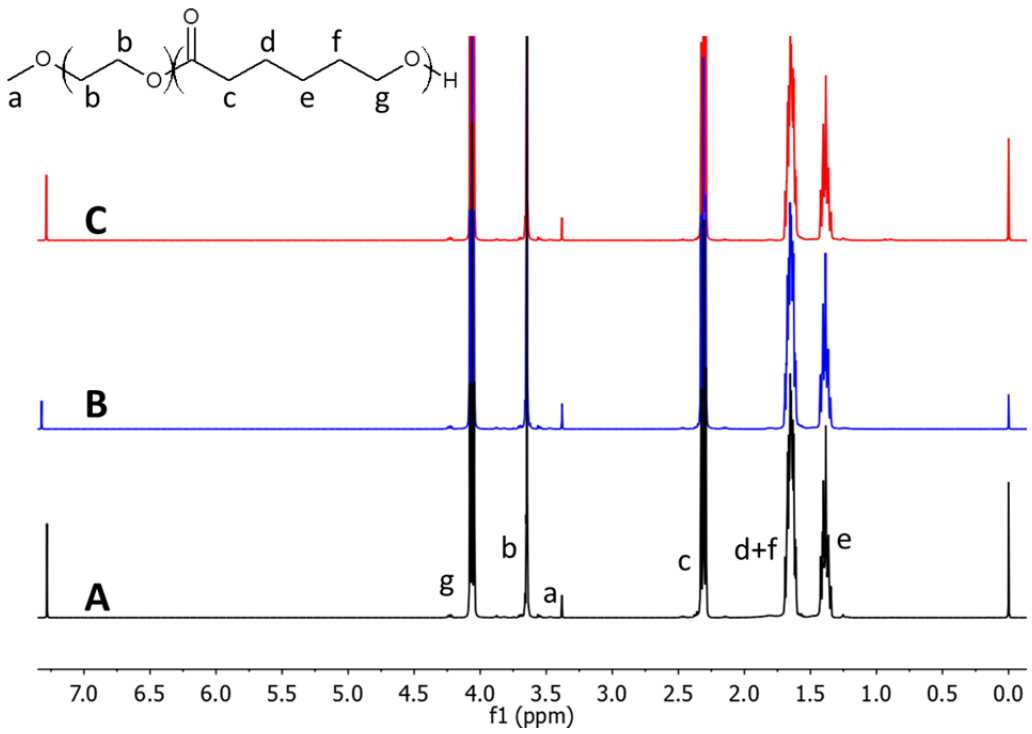

Figure S11. ^{1}H NMR ($CDCl_3$) spectra of: A: PEO(2K)-*b*-PCL(17.4K), $Đ_M$ = 1.08; B: PEO(2K)-*b*-PCL(16.0K), $Đ_M$ = 1.23; C: PEO(2K)-*b*-PCL(16.3K), $Đ_M$ = 1.55.

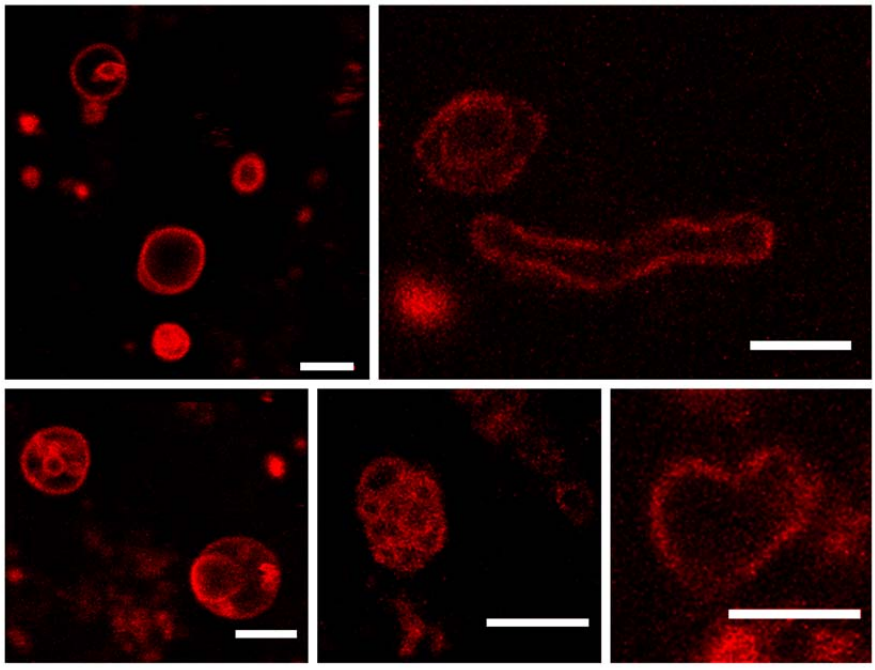

Figure S12. Different self-assembled polymersomes formed by PEO(2K)-*b*-PCL(16.3K) ($Đ_M$ = 1.55) polymer using film rehydration method. Scale bars are 5 μm.

Publication 2

PEO-*b*-PCL-*b*-PMOXA triblock copolymers: From synthesis to microscale polymersomes with asymmetric membrane

Evgeniia V. Konishcheva, Ulmas E. Zhumaev, Wolfgang P. Meier

Reprinted with permission from *Macromolecules*, 2017, 50(4): p. 1512-1520.

Contribution of Evgeniia Konishcheva:

- Synthesized and characterized the polymers
- Prepared and characterized the self-assembled structures
- Investigated the asymmetry of the polymersome membrane
- Wrote the manuscript

Macromolecules

Article

pubs.acs.org/Macromolecules

PEO-*b*-PCL-*b*-PMOXA Triblock Copolymers: From Synthesis to Microscale Polymersomes with Asymmetric Membrane

Evgeniia V. Konishcheva,[†] Ulmas E. Zhumaev,[‡] and Wolfgang P. Meier*[,†]

[†]Department of Chemistry, University of Basel, Klingelbergstrasse 80, 4056 Basel, Switzerland

[‡]Max Planck Institute for Polymer Research, Ackermannweg 10, 55128 Mainz, Germany

Supporting Information

ABSTRACT: We report a new family of amphiphilic ABC triblock copolymers: poly(ethylene oxide)-*block*-polycaprolactone-*block*-poly(2-methyl-2-oxazoline) (PEO-*b*-PCL-*b*-PMOXA). The synthesis is free of toxic reagents, well-controlled and results in polymers with $Đ_M$ < 1.25 and PMOXA length up to 25 units (2 kDa). We compare the self-assembly of PEO-*b*-PCL-*b*-PMOXA with PEO-*b*-PCL depending on PCL length and hydrophilic weight fraction (f) using the film rehydration method. Polymers self-assemble into different microscale structures, including polymersomes, which were studied by laser scanning microscopy. We proved the asymmetry of polymersome membrane by two independent methods, which confirmed the presence of a longer PEO block and the absence of a shorter PMOXA block on the outer surface of polymersomes.

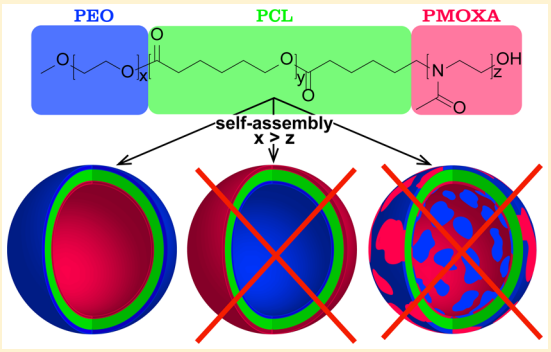

INTRODUCTION

Nature provides a vast variety of fascinating complex structures assembled from different macromolecules. Structures of such assemblies determine their function. A prominent example is a lipid bilayer, which functions as a membrane confining biochemical reactions within a living cell. Artificial membranes assembled from amphiphilic block copolymers exhibit higher chemical and mechanical stability,[1] opening new routes for various bioapplications like drug delivery and nanoreactors.[2−7] Most of the investigated copolymers have AB or ABA structures, where A = hydrophilic and B = hydrophobic blocks, which self-assemble into symmetric membranes. Recently developed ABC triblock copolymers consisting of two different hydrophilic (A, C) blocks can self-assemble into asymmetric membranes that increases the functionality and flexibility in the design of membranes for bioapplications. For example, ABC membrane induces the directed insertion of membrane proteins[8] and enhances the delivery of some drugs.[9−11] Only few studies report the synthesis of ABC asymmetric copolymers.[11−17] Most of them are obtained via atom transfer radical polymerization[11,13−17] requiring toxic copper catalyst that may limit bioapplications of such polymers.

In this work, we present a novel asymmetric triblock copolymer consisting of biocompatible blocks: poly(ethylene oxide)-*block*-polycaprolactone-*block*-poly(2-methyl-2-oxazoline) (PEO-*b*-PCL-*b*-PMOXA). The synthesis is free of toxic agents and well-controlled, yielding polymers with $Đ_M$ < 1.25 and PMOXA length up to 25 units (2 kDa). Furthermore, we present the self-assembly of the synthesized polymers depending on both PCL length and hydrophilic weight fraction (f) using the film rehydration method. The polymers form microscale structures, including polymersomes, which were characterized by laser scanning microscopy. We confirm, for the first time, the complete membrane asymmetry of ABC polymersomes. We show by two independent methods that only the PEO block, which is longer than PMOXA, composes mainly the outer surface of the polymersome membrane.

EXPERIMENTAL SECTION

Materials. Glassware for polymerization was dried overnight at 120 °C prior to use. Chemicals were obtained from Sigma-Aldrich and used as received unless otherwise mentioned. Milli-Q water (15 MΩ·cm) was used from ELGA Purelab Option-R 7/15 system. Poly(ethylene oxide) monomethyl ether (PEO, 2000 g mol^{-1}) and bifunctional HC≡C-CH_2-O-PEO-OH (Alkyne-PEO, 2000 g mol^{-1}, Laysan Bio) were dissolved in water and then lyophilized. ε-Caprolactone (ε-CL) was dried over CaH_2 and distilled under reduced pressure. Toluene was dried over CaH_2 and distilled under an argon atmosphere prior to use. Tin(II) 2-ethylhexanoate ($SnOct_2$) was distilled under reduced pressure. 2-Methyl-2-oxazoline (MOXA) was dried under an argon atmosphere over CaH_2 for at least 12 h and distilled prior to use. Sulfolane was dried over CaH_2 for 24 h under reduced pressure at 35 °C, distilled, and stored in the glovebox. 2-Methyl p-toluenesulfonate (MeOTs) was dried under vacuum over CaH_2 for at least 12 h and distilled prior to use. Bodipy 630/650 NHS ester was purchased from Thermo Fisher Scientific Inc. Sulfo-Cyanine3 azide and Sulfo-Cyanine3 alkyne were purchased from Lumiprobe.

Microwave-Assisted Synthesis. Microwave polymerization was performed on a Biotage Initiator System equipped with Robot Eight.

Received: December 20, 2016
Revised: January 19, 2017
Published: February 8, 2017

DOI: 10.1021/acs.macromol.6b02743
Macromolecules 2017, 50, 1512−1520

The microwave synthesizer operated at a constant set temperature monitored by the IR sensor.

Nuclear Magnetic Resonance Spectroscopy (NMR). ^{1}H NMR spectra were recorded in $CDCl_3$ (0.05% tetramethylsilane) on a Bruker Avance III NMR spectrometer (400.13 MHz). Spectra were processed with MestReNova software, and chemical shifts are reported in ppm.

Gel Permeation Chromatography (GPC). GPC traces were analyzed and recorded in WinGPC (v 8.20 build 4815, PSS systems). The DMF (20 mM LiBr) GPC system was equipped with three PSS GRAM columns (one 30 Å, two 1000 Å, each 30 cm long, 10 μm particles, 0.8 cm diameter) and a Viscotek TDA 305 detector system including refractive index (RI), triple UV−vis operating at different wavelengths (189−506 nm), light scattering at 90° (LS 90°, 670 nm), and viscosity (DP) detectors. The samples were measured at 60 °C with the flow rate of 1 mL min^{-1}. The system was calibrated against narrowly distributed poly(methyl methacrylate) (PMMA) standards.

Laser Scanning Microscopy (LSM). LSM images were recorded on a Zeiss LSM510 META/ConfoCor 2 FCS microscope using a Zeiss Plan-Apochromat 100×/1.4 Oil DIC objective lens. Bodipy 630/650 was excited by the 633 nm He−Ne laser line (10% output). Sulfo-Cy3 was excited by the 514 nm argon laser line (10% output). Calcein was excited by the 488 nm argon laser line (10% output). The excitation light was passed through a HFT UV 488/543/633 or HFT 405/514 beam splitter. The emission light from Bodipy 630/650 was passed through a LP 650 long pass filter. The emission light from Sulfo-Cy3 was passed through a LP 560 long pass filter. The emission light from calcein was passed through a NFT 545 beam splitter and a BP 474-525 band-pass filter. The fluorescence signals were recorded on the photomultiplier tubes. 12-bit images with the resolution of 1024 × 1024 pixels were acquired at a scan speed of 51.20 μs per pixel. The pinholes were adjusted accordingly to record maximum signal intensity. 5 μL of a sample was placed onto a glass coverslip (22 mm × 50 mm) and covered with a round coverslip (ϕ 13 mm) which was sealed with nail polish. The images were processed with ImageJ (ver. 1.50B) software.

Synthesis of PEO-*b*-PCL Diblock Copolymers. PEO-*b*-PCL was synthesized using an optimized procedure described in our previous work.[18] Briefly, PEO (1 equiv, 1.0 g, 0.5 mmol) was mixed with ε-CL (500 equiv, 28.5 g, 0.25 mol) and toluene (33.5 mL) in a three-neck flask. Freshly distilled $SnOct_2$ (0.1 equiv, 0.5 mL (0.1 M solution in toluene)) was added to the reaction mixture, and the mixture was degassed by three freeze−pump−thaw cycles. The polymerization was carried out at 110 °C, and the reaction time varied depending on the targeted length of the PCL block. PEO-*b*-PCL copolymer was precipitated three times in cold diethyl ether, and the precipitate was collected by filtration and dried under vacuum. The block ratio was determined by integrating the peak from the terminal methyl group of PEO at 3.38 ppm and the peaks of the PCL backbone at 2.31 and 4.06 ppm. The polymers were also characterized by DMF GPC. ^{1}H NMR (400.13 MHz, δ, $CDCl_3$): 1.38 ppm (m, (O)C-CH_2-CH_2-CH_2-CH_2-CH_2-O-), 1.65 ppm (m, (O)C-CH_2-CH_2-CH_2-CH_2-CH_2-O-), 2.31 ppm (t, J = 7.1 Hz, (O)C-CH_2-CH_2-CH_2-CH_2-CH_2-O-), 3.38 ppm (s, CH_3-O-), 3.65 ppm (s, -O-CH_2-CH_2-O-), 4.06 ppm (t, J = 6.5 Hz, (O)C-CH_2-CH_2-CH_2-CH_2-CH_2-O-).

Synthesis of PEO-*b*-PCL-OTs Macroinitiator. PEO-*b*-PCL-OTs was synthesized using an optimized procedure described in our previous work.[18] In a representative experiment, PEO-*b*-PCL (1 equiv, 2 g, 0.15 mmol) and *p*-toluenesulfonyl chloride (TsCl) (100 equiv, 2.81 g, 15 mmol) were added into a two-neck flask, and the mixture was dissolved in anhydrous CH_2Cl_2 (28.6 mL). The solution was degassed with three freeze−pump−thaw cycles and backfilled with argon. Then anhydrous pyridine (10 equiv, 0.12 mL, 1.5 mmol) was added, and the reaction was carried out for 12 h at 25 °C. The mixture was precipitated three times in cold diethyl ether; the final precipitate was dissolved in CH_2Cl_2 (30 mL) and washed with Milli-Q water (3 × 10 mL). The CH_2Cl_2 phase was dried over $MgSO_4$ overnight and filtered, and the filtrate was dried under vacuum. The percentage of tosylation was determined by integrating the peak from terminal methyl group of PEO at 3.38 ppm and the aromatic doublets at 7.35 and 7.79 ppm. The polymers were also characterized by DMF GPC. ^{1}H NMR (400.13 MHz, δ, $CDCl_3$): 1.38 ppm (m, (O)C-CH_2-CH_2-CH_2-CH_2-CH_2-CH_2-O-), 1.65 ppm (m, (O)C-CH_2-CH_2-CH_2-CH_2-CH_2-CH_2-O-), 2.31 ppm (t, J = 7.1 Hz, (O)C-CH_2-CH_2-CH_2-CH_2-CH_2-O-), 2.45 ppm (s, CH_3-Ph), 3.38 ppm (s, CH_3-O-), 3.65 ppm (s, -O-CH_2-CH_2-O-), 4.02 ppm (t, J = 6.5 Hz, -CH_2-OTs), 4.06 ppm (t, J = 6.5 Hz, (O)C-CH_2-CH_2-CH_2-CH_2−CH_2-O-), 7.35 ppm (d, J = 8.1 Hz, Ph), 7.79 ppm (d, J = 8.3 Hz, Ph).

Synthesis of PEO-*b*-PCL-*b*-PMOXA Triblock Copolymers. PEO-*b*-PCL-*b*-PMOXA was synthesized using PEO-*b*-PCL-OTs macroinitiator for cationic ring-opening polymerization of MOXA by microwave-assisted synthesis. PEO-*b*-PCL-OTs (1 equiv, 0.5 g, 0.04 mmol) was dissolved in a freshly distilled MOXA (2500 equiv, 7.9 mL, 93 mmol), and sulfolane (10 g) was added in the glovebox. The desired volume of the solution was transferred into microwave vials. The vials were sealed in the glovebox under an argon atmosphere prior to the transfer to the microwave reactor. After the microwave irradiation at 100 °C the polymerization mixture was cooled down to room temperature. To get the desired PMOXA length, the reaction time was varied from 3 to 15 min. To remove sulfolane and residual monomer, the polymerization mixture was placed into a regenerated cellulose dialysis membrane (MWCO 3.5−5 kDa, SpectraPor) and dialyzed against THF:H_2O (9:1) mixture for 2 days and THF:CH_2Cl_2 (9:1) mixture for 1 day (solution was exchanged 7 times). The block ratio was determined by integrating the peak from terminal methyl group of PEO at 3.38 ppm and peaks of PMOXA backbone at 2.12 and 3.46 ppm. The polymers were also characterized by DMF GPC. ^{1}H NMR (400.13 MHz, δ, $CDCl_3$): 1.38 ppm (m, (O)C-CH_2-CH_2-CH_2-CH_2-CH_2-CH_2-O-), 1.65 ppm (m, (O)C-CH_2-CH_2-CH_2-CH_2-CH_2-CH_2-O-), 2.12 ppm (m, (-N(C(O)CH_3)-), 2.31 ppm (t, J = 7.1 Hz, (O)C-CH_2-CH_2-CH_2-CH_2-CH_2-O-), 3.38 ppm (s, CH_3-O-), 3.46 ppm (m, -N(C(O)CH_3)-CH_2-CH_2-), 3.65 ppm (s, -O-CH_2-CH_2-O-), 4.06 ppm (t, J = 6.5 Hz, (O)C-CH_2-CH_2-CH_2-CH_2-CH_2-O-).

Synthesis of Alkyne-PEO-*b*-PCL-*b*-PMOXA and PEO-*b*-PCL-*b*-PMOXA-Azide Triblock Copolymers. Alkyne-PEO-*b*-PCL-*b*-PMOXA was synthesized using the same procedure as for PEO-*b*-PCL-*b*-PMOXA, except Alkyne-PEO was used as a macroinitiator. To obtain PEO-*b*-PCL-*b*-PMOXA-Azide, 0.1 g of NaN_3 in 1 mL of DMF was added to the 10 mL solution of polymerization mixture after microwave-assisted synthesis, and the mixture was incubated for 12 h at room temperature and dialyzed as described above. ^{1}H NMR Alkyne-PEO-*b*-PCL-*b*-PMOXA (400.13 MHz, δ, $CDCl_3$): 1.38 ppm (m, (O)C-CH_2-CH_2-CH_2-CH_2-CH_2-O-), 1.65 ppm (m, (O)C-CH_2-CH_2-CH_2-CH_2-CH_2-O-), 2.12 ppm (m, (-N(C(O)CH_3)-), 2.31 ppm (t, J = 7.1 Hz, (O)C-CH_2-CH_2-CH_2-CH_2-CH_2-O-), 3.46 ppm (m, -N(C(O)CH_3)-CH_2-CH_2-), 3.65 ppm (s, -O-CH_2-CH_2-O−), 4.06 ppm (t, J = 6.5 Hz, (O)C-CH_2-CH_2-CH_2-CH_2-CH_2-O-), 4.21 ppm (d, J = 2.4 Hz, HC≡C-CH_2-O-). ^{1}H NMR PEO-*b*-PCL-*b*-PMOXA-Azide (400.13 MHz, δ, $CDCl_3$): 1.38 ppm (m, (O)C-CH_2-CH_2-CH_2-CH_2-CH_2-O-), 1.65 ppm (m, (O)C-CH_2-CH_2-CH_2-CH_2-CH_2-O-), 2.12 ppm (m, (-N(C(O)CH_3)-), 2.31 ppm (t, J = 7.1 Hz, (O)C-CH_2-CH_2-CH_2-CH_2-CH_2-O-), 3.28 ppm (t, J = 6.9 Hz, -N(C(O)CH_3)-CH_2-CH_2-N_3), 3.38 ppm (s, CH_3-O-), 3.46 ppm (m, -N(C(O)CH_3)-CH_2-CH_2-), 3.65 ppm (s, -O-CH_2-CH_2-O-), 4.06 ppm (t, J = 6.5 Hz, (O)C-CH_2-CH_2-CH_2-CH_2-CH_2-O-).

Reaction between Alkyne-PEO-*b*-PCL-*b*-PMOXA/PEO-*b*-PCL-*b*-PMOXA-Azide Containing Polymersomes and Sulfo-Cyanine3 Azide/Sulfo-Cyanine3 Alkyne. Polymersomes were prepared by mixing in a round-bottom flask 0.2 mL of 17 mg mL^{-1} PEO(2.0K)-*b*-PCL(12.5K)-*b*-PMOXA(0.3K) dissolved in CH_2Cl_2 with 0.1 mL of 2 mg mL^{-1} Alkyne-PEO(2.0K)-*b*-PCL(11.4K)-*b*-PMOXA(0.3K) or PEO(2.0K)-*b*-PCL(11.7K)-*b*-PMOXA(0.3K)-Azide dissolved in CH_2Cl_2 to yield a final concentration of a modified polymer 15%. CH_2Cl_2 solvent was removed by rotary evaporation. After addition of 1 mL of Milli-Q water the samples were stirred at 350 rpm for 24 h at 60 °C. After cooling the mixture to 25 °C, 30 μL of 7 mM aqueous solution of Sulfo-Cy3-Alkyne or Sulfo-Cy3-Azide was added to Azide- or Alkyne-containing polymersomes, respectively. Then 50 μL of aqueous solution of 10 mM Cu(II)−bathocuproine-disulfonic acid and 100 μL of freshly prepared aqueous solution of 5

DOI: 10.1021/acs.macromol.6b02743
Macromolecules 2017, 50, 1512−1520

mM sodium ascorbate were added, followed by three freeze–pump–thaw cycles and backfilling with argon. The reaction was carried out for 48 h at 25 °C. After 48 h approximately 300 μL of a reaction mixture was placed into a round-bottom flask, water was removed by rotary evaporation, and the sample was dissolved in DMF (20 mM LiBr) to a final concentration of 2 mg mL^{-1}, filtered using 0.2 μm PTFE filter, and analyzed by DMF GPC.

Synthesis of PMOXA Homopolymers. MeOTs (1 equiv, 0.1 mL, 0.66 mmol), the desired amount of freshly distilled MOXA (5 or 45 equiv), and sulfolane (10 g) were mixed in the glovebox. The desired volume of the solution was transferred into microwave vials. The vials were sealed in the glovebox under an argon atmosphere prior to the transfer to the microwave reactor. After the microwave irradiation at 80 °C for 10 min ($PMOXA_5$) or 30 min ($PMOXA_{45}$) the polymerization mixture was cooled down to room temperature, and the polymers were precipitated twice in cold diethyl ether. The block ratio was determined by integrating the peak from terminal methyl group at 2.35 ppm and peaks of PMOXA backbone at 2.12 and 3.46 ppm. The polymers were also characterized by DMF GPC: $Đ(PMOXA_5)$ = 1.13, $Đ(PMOXA_{45})$ = 1.21. ^1H NMR (400.13 MHz, δ, $CDCl_3$): 2.12 ppm (m, (-N(C(O)CH_3)-), 2.35 ppm (s, CH_3-N(C(O)CH_3)-CH_2-CH_2-), 3.46 ppm (m, -N(C(O)CH_3)-CH_2-CH_2-).

Self-Assembly. Microscale structures of PEO-*b*-PCL and PEO-*b*-PCL-*b*-PMOXA copolymers were obtained using film rehydration method. 2 mg of a polymer was dissolved in 200 μL of CH_2Cl_2 and placed in the glass round-bottom flask. CH_2Cl_2 was removed by rotary evaporation, and then 1 mL of Milli-Q water was added. The samples were stirred at 350 rpm for 24 h at 60 °C. For the encapsulation experiments we used 10 mM aqueous solution of calcein disodium salt. After self-assembly in the presence of calcein the solution was dialyzed (cellulose ester membrane, MWCO 100 kDa, SpectraPor) for 3 days against Milli-Q water (solution was exchanged 9 times). Solutions of the structures (50 μL) were stained with 0.5 μL of 0.72 μM Bodipy 630/650 dye and characterized by LSM.

Bicinhoninic Acid Assay (BCA). 50 μL of 15 mg mL^{-1} (1 mM) polymer samples was incubated with 400 μL of BCA solution in a 2.5 mL vial at 25 °C (500 rpm). After incubating for 2 or 8 h the samples containing polymers were centrifuged at 13000*g* for 10 min. Then 300 μL of a supernatant was transferred into 96-well plate, and the absorbance at 562 nm was measured. Each series consisted of 10 samples.

RESULTS AND DISCUSSION

Synthesis of PEO-*b*-PCL-*b*-PMOXA Triblock Copolymers. PEO-*b*-PCL-*b*-PMOXA represents a new family of asymmetric triblock copolymers consisting of well-known biocompatible (PEO, PCL, PMOXA) and biodegradable (PCL) blocks, and its synthesis is free of toxic reagents. PEO-*b*-PCL and PEO-*b*-PCL-OTs were synthesized using an optimized procedure described in our previous work.[18] We chose PEO-*b*-PCL-OTs as a macroinitiator for polymerization of MOXA (Scheme 1), since tosylates are stable, initiate ionic type of polymerization, and result in polymers with a narrow size distribution.[19−21] Tosylation was performed for 12 h at 25 °C using 100-fold excess of TsCl, since 10-fold excess resulted only in ∼10% of ω-modification. Interestingly, the order of mixing of the compounds played a dramatic role: when we dissolved the polymer first and then added the solution of TsCl, tosylation reached only 50%, whereas when we mixed the polymer and TsCl first and then added the solvent, tosylation reached 100%. Utilization of triethylamine as a base did not result in the tosylated diblock copolymer and led to an increase of high molecular weight shoulder on GPC elugram which was also observed in the case of PCL.[22] Utilization of pyridine resulted in tosylation, but the solution often turned yellow after addition of pyridine, presumably due to the formation of unstable pyridine radical anion[23] formed because of the residual tin(II) left after polymerization of ε-CL. After ∼30 min the color always disappeared.

We performed MOXA polymerization in a microwave reactor. According to Hoogenboom and co-workers, the microwave-assisted synthesis is advantageous over conventional heating for the polymerization of 2-alkyl-2-oxazolines initiated by alkyl tosylates.[21,24−27] The formation of PMOXA backbone was confirmed by appearance of the peaks at 2.12 and 3.46 ppm in the ^1H NMR spectra (Figure 1A). We optimized the reaction varying the solvent, temperature, reaction time, and MOXA concentration. Sulfolane was more preferable over acetonitrile, a commonly used solvent for MOXA polymerization, since the latter resulted in the slower initiation: the ^1H NMR spectrum exhibited the presence of both covalently attached tosyl group

Scheme 1. Synthetic Strategy for PEO-*b*-PCL-*b*-PMOXA Copolymers

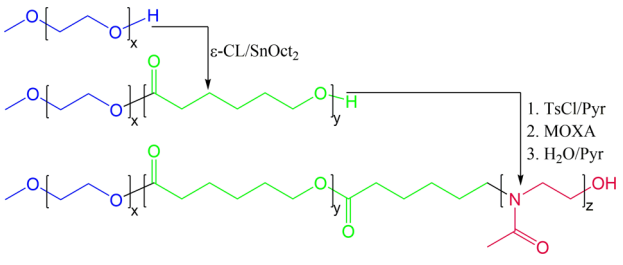

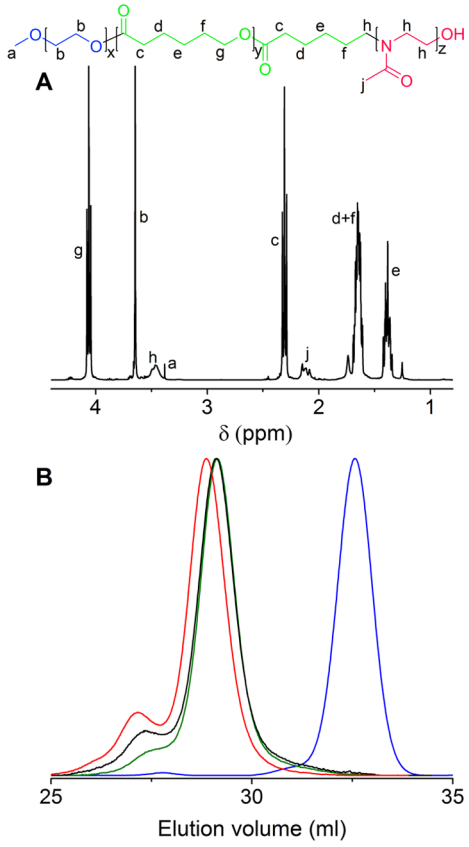

Figure 1. (A) Representative ^1H NMR ($CDCl_3$) spectrum of PEO-*b*-PCL-*b*-PMOXA triblock copolymer. (B) Representative GPC (DMF) traces of PEO (blue, $Đ_M$ = 1.08), PEO-*b*-PCL (green, $Đ_M$ = 1.08), PEO-*b*-PCL-OTs (black, $Đ_M$ = 1.11), and PEO-*b*-PCL-*b*-PMOXA (red, $Đ_M$ = 1.14).

DOI: 10.1021/acs.macromol.6b02743
Macromolecules 2017, 50, 1512−1520

and tosyl anion (Figure S1). Furthermore, sulfolane accelerates the polymerization of 2-alkyl-2-oxazolines.[28]

High temperatures (140, 160, and 180 °C) at short reaction times (5−60 s) resulted in the broadening of the corresponding peak on the elugram (Figure S2). This tendency was observed for all tested MOXA concentrations (0.092, 0.46, 0.92, 2.3, 11.5, and 11.8 M (pure MOXA)). The broadening was a result of two side processes: tailing from low molecular weight side (formation of PMOXA homopolymer) and shouldering from high molecular weight side due to the chain transfer reactions.[29] The high molecular weight shoulder mainly consists of PEO-*b*-PCL-*b*-PEO formed during polymerization of ε-CL, as we have shown earlier.[18] It also might contain some amounts of PEO-*b*-PCL-*b*-PMOXA-*b*-PCL-*b*-PEO because analogues coupling species were observed in polymerization of 2-alkyl-2-oxazolines.[21] At 120 and 100 °C side reactions were also observed (Figure S3), but after longer reaction times (>15 min). At 120 °C side products accumulated faster compared to 100 °C (data not shown). Low temperatures (60 and 80 °C) did not result in the polymerization even after 2−6 h, but induced the growth of high molecular weight shoulder. Consequently, 100 °C and reaction time up to 15 min were found to be an optimal temperature and time for the synthesis of PMOXA block due to a relatively low amount of the side products (Figure 1B).

The concentration and storage of MOXA had a big influence on the polymerization kinetics and accumulation of side products. The reaction was much slower when MOXA was stored over CaH_2 for ∼6 months prior to distillation compared to 12 h storage (Figure S4). The effect of MOXA storage on overall kinetics of the polymerization is not clear for us, especially since ^{1}H NMR spectra of MOXA did not reveal any difference (data not shown). Therefore, we used only freshly distilled MOXA stored <24 h over CaH_2. Increase of MOXA concentration in the polymerization mixture up to 11.5 M (2500 equiv) led to the decrease of the amount of high molecular weight shoulder and homopolymer. With further increase of MOXA concentration (11.8 M, pure MOXA) polymerization rate approached zero presumably due to the low solubility of PMOXA block.[28] Therefore, all triblock copolymers were obtained by microwave-assisted synthesis in sulfolane using 11.5 M MOXA at 100 °C with reaction times up to 15 min.

The discussed above synthesis has a limitation for obtaining triblock copolymers with PMOXA block length longer than 25 units (2 kDa) while maintaining relatively narrow dispersity ($Đ_M$ < 1.25). The synthesis could be improved by using an alternative to tosylated diblock copolymer−nosylated (Nos) macroinitiator, as nosylates result in faster initiation.[30] However, we were not able to purify PEO-*b*-PCL-ONos while maintaining attached the active end group.

Combining the previously optimized synthesis of PEO-*b*-PCL-OTs[18] and newly developed polymerization of MOXA on this macroinitiator, we synthesized a library of narrowly dispersed ($Đ_M$ = 1.10−1.24, Table 1) PEO-*b*-PCL-*b*-PMOXA copolymers with different PCL and PMOXA lengths to further investigate their self-assembly in aqueous solution.

Microscale Self-Assembled Structures of PEO-*b*-PCL-*b*-PMOXA Triblock Copolymers in Aqueous Solution. Amphiphilic AB diblock copolymers self-assemble into various structures depending on the length of the hydrophobic B block and hydrophilic weight fraction (f).[31−36] However, very little is known about self-assembly of ABC triblock copolymers. To investigate how self-assembly of ABC copolymers depends on B length and f, we synthesized polymers with one PEO (2 kDa) and different PCL (5.5−17.4 kDa) and PMOXA (0.2−2.1 kDa) block lengths and tested their self-assembly in aqueous solution using the film rehydration method. We also compared the structures formed by di- and triblock copolymers to study how addition of the hydrophilic PMOXA block influences self-assembly of the corresponding PEO-*b*-PCL precursors (Figure 2A, Figure S5, and Table 1). The polymers self-assembled into microscale structures which were visualized using LSM. Self-assembly in this case requires high temperatures (∼60 °C) due to the semicrystalline nature of the PCL block. Film rehydration at 25 °C did not result in self-assembly even after a week of incubation.

As discussed in the section *Synthesis of PEO-b-PCL-b-PMOXA Triblock Copolymers*, polymers contain high molecular weight side species which might affect self-assembly process. However, the amount of these species is rather low (∼15%),

Table 1. Characterization of PEO-*b*-PCL and PEO-*b*-PCL-*b*-PMOXA Copolymers and Their Microscale Self-Assembled Structures

copolymer[a]	$Đ_M$[b]	f[c] (%)	morphology[d]
PEO(2.0K)-*b*-PCL(5.5K)	1.19	27	S, D
PEO(2.0K)-*b*-PCL(5.5K)-*b*-PMOXA(0.2K)	1.16	29	S, D
PEO(2.0K)-*b*-PCL(5.5K)-*b*-PMOXA(0.6K)	1.21	32	S, D
PEO(2.0K)-*b*-PCL(7.5K)	1.15	21	S
PEO(2.0K)-*b*-PCL(7.5K)-*b*-PMOXA(0.4K)	1.11	24	P, S
PEO(2.0K)-*b*-PCL(11.7K)	1.05	15	S
PEO(2.0K)-*b*-PCL(11.7K)-*b*-PMOXA(0.3K)	1.14	16	P, S
PEO(2.0K)-*b*-PCL(11.7K)-*b*-PMOXA(1.0K)	1.12	20	P, S, A
PEO(2.0K)-*b*-PCL(11.7K)-*b*-PMOXA(1.4K)	1.13	23	A
PEO(2.0K)-*b*-PCL(12.5K)	1.06	14	S
PEO(2.0K)-*b*-PCL(12.5K)-*b*-PMOXA(0.3K)	1.12	16	P
PEO(2.0K)-*b*-PCL(15.4K)	1.15	11	S
PEO(2.0K)-*b*-PCL(15.4K)-*b*-PMOXA(0.3K)	1.22	13	P, S
PEO(2.0K)-*b*-PCL(15.4K)-*b*-PMOXA(0.8K)	1.22	15	S, P
PEO(2.0K)-*b*-PCL(15.4K)-*b*-PMOXA(1.7K)	1.23	19	A, P, S
PEO(2.0K)-*b*-PCL(15.4K)-*b*-PMOXA(2.1K)	1.24	21	A, P, S
PEO(2.0K)-*b*-PCL(16.8K)	1.09	11	S, P
PEO(2.0K)-*b*-PCL(16.8K)-*b*-PMOXA(0.3K)	1.10	12	S, P, I
PEO(2.0K)-*b*-PCL(16.8K)-*b*-PMOXA(0.8K)	1.12	14	I, S, P
PEO(2.0K)-*b*-PCL(16.8K)-*b*-PMOXA(1.5K)	1.11	17	I, S, P
PEO(2.0K)-*b*-PCL(17.4K)	1.08	10	P
PEO(2.0K)-*b*-PCL(17.4K)-*b*-PMOXA(0.3K)	1.13	12	I, S, P
PEO(2.0K)-*b*-PCL(17.4K)-*b*-PMOXA(0.9K)	1.15	14	S, E

[a]Number-average molecular weight of copolymers was determined by ^{1}H NMR spectroscopy. [b]Dispersity was determined from RI data of samples analyzed by DMF GPC using PMMA calibration. [c]Hydrophilic weight fraction of PEO (diblocks) and PEO + PMOXA (triblocks) was calculated from ^{1}H NMR data. [d]S = spherical particles, P = polymersomes, I = irregularly shaped particles, E = elongated particles, A = loosely packed aggregates, and D = partial dissolution.

DOI: 10.1021/acs.macromol.6b02743
Macromolecules 2017, 50, 1512−1520

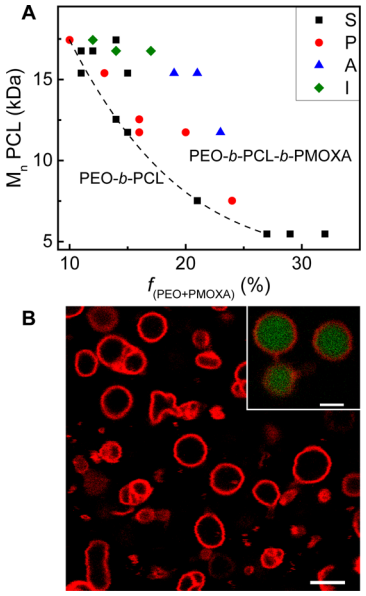

Figure 2. (A) Phase diagram of microscale self-assembled structures formed by PEO-*b*-PCL (points on the dashed line) and PEO-*b*-PCL-*b*-PMOXA (points above the dashed line) copolymers using film rehydration method at 60 °C. S = spherical particles, P = polymersomes, A = aggregates, and I = irregularly shaped particles. Morphologies were determined qualitatively from LSM images. Most of the systems exhibited mixed morphologies, but to simplify the scheme, only the major component is reported. For more detailed information see Table 1. (B) LSM image of polymersomes formed by PEO(2.0K)-*b*-PCL(12.5K)-*b*-PMOXA(0.3K). Polymersomes were stained with Bodipy 630/650 dye; scale bar is 5 μm. Inset in the right upper corner represents polymersomes with encapsulated hydrophilic dye calcein; scale bar is 2 μm.

and they are present in each triblock copolymer. We assume that the effect of these species on self-assembly, if present, is not prevalent over change in PMOXA block length.

The majority of PEO-*b*-PCL copolymers self-assembled into solid spherical particles. Most of PEO-*b*-PCL-*b*-PMOXA copolymers formed a mixture of different structures, and the major morphology depends on *f*, suggesting a strong effect of the PMOXA block length on self-assembly. PEO-*b*-PCL-*b*-PMOXA copolymers with the shortest PCL (5.5 kDa) formed predominantly solid spherical particles. The triblock copolymers with PCL ranging from 7.5 to 15.4 kDa self-assembled mainly into polymersomes (Figure 2B and Figure S5A−F). However, with the increase of PMOXA block length, and therefore *f*, the triblock copolymers formed loosely packed aggregates, suggesting the tendency of a polymer to dissolve (Figure S5C). The triblock copolymers with the largest PCL (16.8−17.4 kDa) formed predominantly spherical and irregularly shaped particles and some polymersomes (Figure S5G,J). Only one of the diblock copolymers, PEO(2.0K)-*b*-PCL(17.4K), formed polymersomes (Figure S5H), but they were much smaller (ϕ < 2 μm) compared to the ones formed by the triblock copolymers (ϕ ∼ 5 μm). We assume that this fact can be explained by different membrane structure of polymersomes: the diblock copolymer formed a bilayer membrane, whereas the triblock copolymers assembled into a monolayer. This could be proven by difference in the membrane thickness determined from cryoTEM, but in this case assemblies could not be visualized due to the problems with sample preparation caused by the large size of polymersomes.

Among the obtained self-assembled structures, polymersomes are of a particular interest due to the ability of their membrane to confine aqueous media. As has been shown for symmetric AB- and ABA-based membranes, microscale polymersomes are advantageous for studying the properties of such membranes.[37] ABC microscale polymersomes are especially intriguing due to the possibility to have an asymmetric membrane. To test the asymmetry in the case of PEO-*b*-PCL-*b*-PMOXA polymersomes, we took PEO(2.0K)-*b*-PCL(12.5K)-*b*-PMOXA(0.3K) as it yielded the most robust formation of polymersomes (Figure 2B and Figure S5D), which were stable after 6 months of storage at room temperature.

Orientation of PEO-*b*-PCL-*b*-PMOXA Chains in the Membrane of Polymersomes. Polymersomes formed by ABC copolymers with two different hydrophilic blocks (A, C) can potentially have three different orientations of hydrophilic blocks: A outside, C outside, and mixed A and C (Scheme 2).

Scheme 2. Possible Composition of the Membrane of Polymersomes Formed by ABC Copolymer: (a) A Outside; (b) C Outside; (c) A and C Form a Mixed Membrane

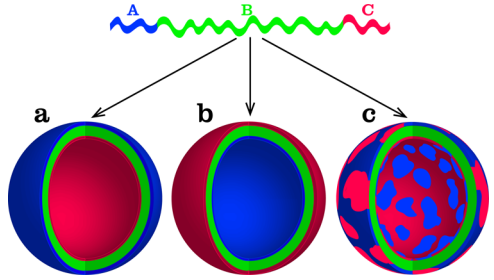

When A and C blocks have different lengths, the longer one should prefer to segregate on the outer surface of the membrane due to a larger radius of curvature, and the shorter one should be inside. Such orientation of A and C blocks leads to an asymmetric membrane. There were few methods reported for testing the asymmetry of a polymersome membrane. Measurement of ζ potential at different pH can be a suitable method when one of the blocks, A or C, is charged.[9,11,13−15] However, this method does not exclude the possibility to have a membrane with a mixture of both hydrophilic blocks inside and outside (Scheme 2c). ^{1}H NOESY NMR was used to determine 3D spatial correlations and hydrogen bonding interactions between two hydrophilic blocks in the case of nanoscale polymersomes,[10,38] but for our system the latter method did not give a reliable signal presumably because of the micrometer size of polymersomes. To show the presence of a longer PMOXA block on the surface of PEO-*b*-PDMS-*b*-PMOXA polymersomes, the polymer was modified before its self-assembly with a fluorescent dye on PMOXA end, and the quencher of the fluorescent dye was added to the solution of aggregates after self-assembly.[12] However, this approach did not exclude the presence of PEO outside and the possibility of the inversion of PMOXA block by a bulky dye. To avoid these issues and prove the asymmetry of PEO-*b*-PCL-*b*-PMOXA microscale polymersomes, we used a reaction between polymersomes with functional end-groups on PEO or PMOXA sides and a fluorescent dye. We chose Cu-catalyzed alkyne−azide coupling reaction, as it proceeds under ambient conditions. To get the alkyne group on the PEO side, we used

DOI: 10.1021/acs.macromol.6b02743
Macromolecules 2017, 50, 1512−1520

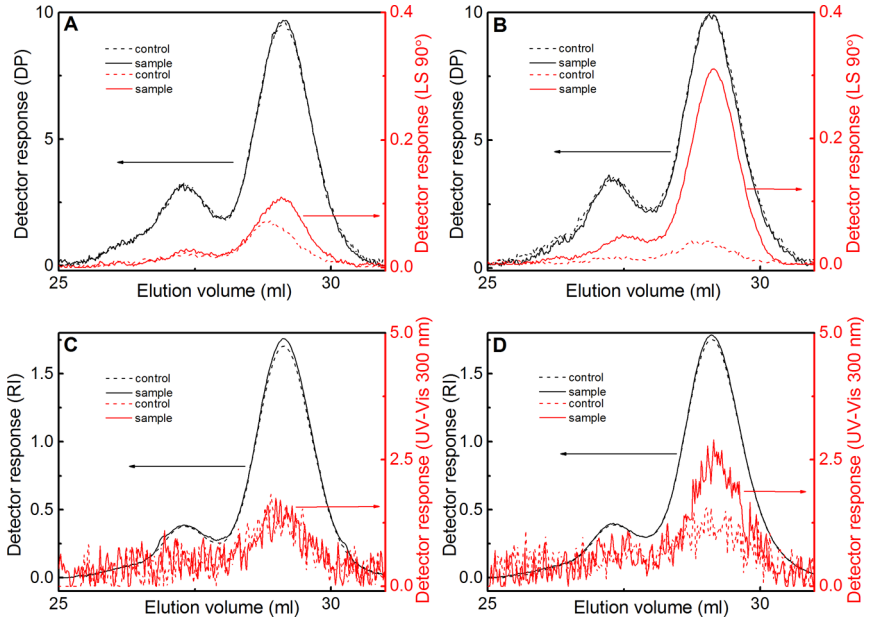

Figure 3. GPC (DMF) traces recorded on DP/LS 90° (A, B) and RI/UV−vis (300 nm) (C, D) detectors of a mixture after reaction between alkyne/azide containing polymersomes and azide/alkyne-dye: (A, C) 85% PEO(2.0K)-*b*-PCL(12.5K)-*b*-PMOXA(0.3K) + 15% PEO(2.0K)-*b*-PCL(11.7K)-*b*-PMOXA(0.3K)-Azide + Sulfo-Cy3-Alkyne; (B, D) 85% PEO(2.0K)-*b*-PCL(12.5K)-*b*-PMOXA(0.3K) + 15% Alkyne-PEO(2.0K)-*b*-PCL(11.4K)-*b*-PMOXA(0.3K) + Sulfo-Cy3-Azide. "Controls" were obtained from the reaction mixture which did not contain Cu(II) complex and sodium ascorbate. "Samples" corresponded to the reaction mixture which contained Cu(II) complex and sodium ascorbate. The samples for GPC analysis were prepared by removing water from the reaction mixture and dissolving them in DMF (20 mM LiBr) to a final concentration of 2 mg mL^{-1} followed by filtration.

bifunctional Alkyne-PEO as a precursor for triblock copolymer, since alkyne group was inert in the subsequent steps of the synthesis. The Azide functionality on PMOXA terminus was obtained by quenching the polymerization of MOXA with NaN_3. The end-group modifications did not affect the dispersity of polymers (Figure S6), and alkyne/azide groups were stable under self-assembly conditions (Figure S7). As a reactive fluorescent dye, we chose Sulfo-Cy3-Alkyne/Azide as it is highly soluble in water and does not pass through a semicrystalline hydrophobic polymersome membrane due to the presence of charged sulfo groups (Figure S8).

PEO(2.0K)-*b*-PCL(12.5K)-*b*-PMOXA(0.3K) was chosen to test the orientation of polymer molecules in the membrane of polymersomes as it yielded the most robust formation of polymersomes (Figure 2B and Figure S5D). The polymer was mixed with 15% of Alkyne-PEO(2.0K)-*b*-PCL(11.4K)-*b*-PMOXA(0.3K) or PEO(2.0K)-*b*-PCL(11.7K)-*b*-PMOXA-(0.3K)-Azide, which by itself formed a mixture of polymersomes and spherical particles. The final mixtures yielded polymersomes, suggesting that the addition of the alkyne/azide-modified polymers did not disturb the self-assembly (Figure S9). After the reaction between polymersomes and a dye, we were not able to remove the free dye completely by dialysis, SEC on sepharose column, or centrifugal filtration. To check whether the polymersomes reacted with a dye, water was removed by rotary evaporation and the mixture was dissolved in DMF (20 mM LiBr) solvent for GPC analysis. The elugrams were analyzed using different detectors. RI and DP detectors were chosen as reference detectors, since they should not be sensitive to such a low concentration of the attached dye. On the contrary, LS 90° and UV−vis detectors should give an increased response in the case of the covalently attached dye. Figure 3A,C corresponds to the ABC-Azide containing polymersomes and Figure 3B,D to the Alkyne-ABC containing polymersomes. In the case of ABC-Azide containing polymer both sample (reaction mixture) and control (reaction mixture without a catalyst) showed similar detector responses (Figure 3A,C and Figure S10A), which indicates that PMOXA forms the inner side of polymersomes (Scheme 2a). The Alkyne-ABC sample showed major differences between the sample and the control on LS 90° detector (Figure 3B), UV−vis 300 nm (Figure 3D), and UV−vis 506 nm (Figure S10B), suggesting the presence of PEO on the outer surface of polymersomes (Scheme 2a). The increase in the LS 90° signal is caused by the fluorescence of the covalently attached dye. Note that LS 90° signal fluctuates from injection to injection even for the same sample, and the difference between sample and control is not significant in the case of Figure 3A. On the contrary, UV−vis detector gives a reproducible signal, and the difference between samples is significant. The reaction was performed the second time, and the results were identical (Figure S11). Since no increase in the detector response was observed for the ABC-Azide containing polymersomes after reaction with the dye as compared to the increase in signal for the Alkyne-ABC containing polymersomes, the PEO block shows to be preferentially oriented on the outer surface of the polymersomes.

To check whether this reaction can be more favorable in the case of Alkyne-ABC compared to ABC-Azide containing polymersomes, we prepared mixtures containing 50% of Alkyne-ABC or ABC-Azide and incubated them at 60 °C for 24 h before the reaction with a dye. The reaction in both cases yielded the polymer with a covalently attached dye (Figure S12), thus excluding the assumption of a more favorable reaction conditions for alkyne-containing polymersomes.

In addition to the approach discussed above, we tested the asymmetry using a difference in the chemical structures of PEO and PMOXA. We chose bicinhoninic acid assay (BCA) used for

DOI: 10.1021/acs.macromol.6b02743
Macromolecules 2017, 50, 1512−1520

measuring peptide concentration[39] to detect PMOXA, since PMOXA, like peptides, contains amide bonds. This assay is based on the reduction of Cu^{2+} to Cu^{1+} by a peptide bond in alkaline medium and its further complexation with bicinhoninic acid yielding a purple complex with a maximum of absorbance at 562 nm. Incubation of PEO and PMOXA containing similar number of repeating units (~45) with BCA solution for 24 h at 25 °C resulted in much higher signal of $PMOXA_{45}$ samples compared to PEO_{45} (Figure S13A). The response of $PMOXA_5$ (which corresponds to the length of PMOXA block in the triblock copolymer) is much lower compared to $PMOXA_{45}$ (Figure S13B), which can be explained by the necessity of the presence of a few amide bonds to coordinate Cu ions. At the low concentrations (0.1−5 mM) of $PMOXA_5$ and PEO_{45} (which corresponds to the length of PEO block in the triblock copolymer), $PMOXA_5$ yielded higher signal compared to PEO_{45}, whereas at higher concentrations (>25 mM) PEO_{45} resulted in higher absorbance values. Therefore, 1 mM (15 mg mL^{-1}) ABC concentration was chosen to determine if PMOXA block formed inner or outer part of the membrane of polymersomes. We incubated AB suspension, ABC polymersomes, and ABC suspension with BCA solution for 2 h at 25 °C, since polymersomes were not stable already after 8 h (Figure 4D), and the absorbance of 1 mM $PMOXA_5$ sample

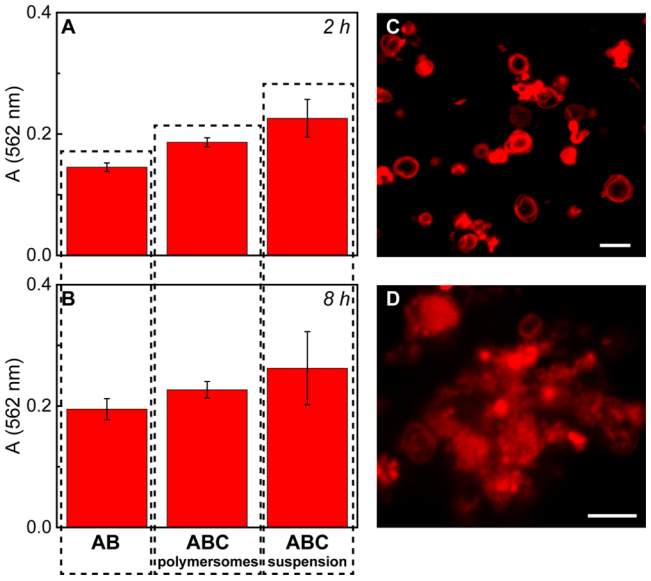

Figure 4. Absorbance (562 nm) of the supernatant after incubation of 50 μL of 15 mg mL^{-1} (1 mM) samples with 400 μL of BCA solution at 25 °C. AB: suspension of PEO(2.0K)-*b*-PCL(12.5K); ABC polymersomes: polymersomes formed by PEO(2.0K)-*b*-PCL(12.5K)-*b*-PMOXA(0.3K); ABC suspension: suspension of PEO(2.0K)-*b*-PCL(12.5K)-*b*-PMOXA(0.3K). Incubation time: (A) 2 h; (B) 8 h. LSM images of the aggregates after incubation with BCA solution for (C) 2 h and (D) 8 h. Scale bars are 5 μm.

(0.123 ± 0.002) was still higher than that of 1 mM PEO_{45} (0.115 ± 0.004) under these conditions. We compared the absorbance of the supernatant of the samples without the background subtraction, since our aim was to determine only a difference between the samples. The sample with ABC suspension after 2 h exhibited higher absorbance value (0.226 ± 0.031) than $PMOXA_5$ (0.123 ± 0.002), which can be explained by more efficient coordination of Cu ions by "concentrated" PMOXA chains in the case of nonsoluble ABC suspension. The sample with ABC polymersomes had higher absorbance than AB suspension but lower than ABC suspension. The latter can be explained by two possible reasons: either some of the PMOXA chains are located on the outer surface of the polymersomes, or the polymersomes get partially permeabilized under these conditions. The latter hypothesis seemed to play a predominant role, since polymersomes might be destabilized due to the osmotic pressure, and polymer (presumably PCL block) is slightly hydrolyzed under these conditions (Figure S14). Based on the Student's *t* test, the mean values of the samples with ABC polymersomes and ABC suspension after 2 h were significantly different, whereas after 8 h the mean absorbance was comparable (Table S1).

Based on two independent methods, the data support that PEO-*b*-PCL-*b*-PMOXA with a longer PEO block forms microscale polymersomes with asymmetric membrane containing a shorter PMOXA block inside. Asymmetry might be affected by the presence of high molecular weight species in the polymer, but since their concentration is rather low (~15%), we do not expect a significant impact on the orientation of the polymer molecules in the membrane of polymersomes. The reactions between polymersomes with reactive groups and fluorescent dyes showed not only the presence of PEO block on the outer surface of polymersomes but also the absence of PMOXA block outside. The data were also confirmed by BCA assay, which was based on the difference in the chemical composition of PEO and PMOXA blocks.

CONCLUSIONS

A series of novel amphiphilic asymmetric PEO-*b*-PCL-*b*-PMOXA triblock copolymers with different PCL and PMOXA block lengths were synthesized by the combination of coordination−insertion ring-opening polymerization of ε-CL followed by cationic ring-opening polymerization of MOXA. The synthesis is free of toxic agents and well-controlled, yielding narrowly dispersed ($Đ_M$ < 1.25) polymers with PMOXA block length up to 25 units (2 kDa). We demonstrated the difference in self-assembly behavior of di- and triblock copolymers and showed that PEO-*b*-PCL-*b*-PMOXA copolymers self-assembled into different microscale structures, including polymersomes, depending on both PCL length and *f*. Self-assembly required 60 °C due to a semicrystalline nature of the PCL block, which limits the compatibility of the self-assembly process with biomolecules. To overcome this drawback, PCL can be replaced with its amorphous analogue, poly(γ-methyl-ε-caprolactone) (PMCL), since self-assembly in the case of PEO-*b*-PMCL proceeds under ambient conditions.[40,41] In addition, PEO-*b*-PMCL-*b*-PMOXA should presumably form nanoscale structures, since the aggregates assembled from PEO-*b*-PMCL have nanometer size range.[40] Preparation of the nanoscale structures from PEO-*b*-PCL-*b*-PMOXA using the method described for PEO-*b*-PCL[31] resulted only in the precipitation of the polymers.

Microscale polymersomes assembled from PEO-*b*-PCL-*b*-PMOXA exhibited an asymmetric orientation of the membrane, which was proven by two independent methods. This creates the possibility to have different functional groups from both sides of the membrane, opening new opportunities toward targeted localization of the desired molecules on the specific side of the polymersome.

DOI: 10.1021/acs.macromol.6b02743
Macromolecules 2017, 50, 1512−1520

■ ASSOCIATED CONTENT

Supporting Information

The Supporting Information is available free of charge on the ACS Publications website at DOI: 10.1021/acs.macromol.6b02743.

Figures S1−S14 and Table S1 (PDF)

■ AUTHOR INFORMATION

Corresponding Author

*E-mail: wolfgang.meier@unibas.ch (W.M.).

ORCID

Wolfgang P. Meier: 0000-0002-7551-8272

Notes

The authors declare no competing financial interest.

■ ACKNOWLEDGMENTS

We acknowledge SNSF, NCCR Molecular Systems Engineering, and the University of Basel for financial support. E.K. acknowledges Samuel Lörcher for fruitful discussions.

■ REFERENCES

(1) Discher, D. E.; Eisenberg, A. *Science (Washington, DC, U. S.)* **2002**, *297* (5583), 967.

(2) Palivan, C. G.; Goers, R.; Najer, A.; Zhang, X.; Car, A.; Meier, W. Bioinspired polymer vesicles and membranes for biological and medical applications. *Chem. Soc. Rev.* **2016**, *45* (2), 377−411.

(3) Nardin, C.; Thoeni, S.; Widmer, J.; Winterhalter, M.; Meier, W. Nanoreactors based on (polymerized) ABA-triblock copolymer vesicles. *Chem. Commun.* **2000**, No. 15, 1433−1434.

(4) Langowska, K.; Palivan, C. G.; Meier, W. Polymer nanoreactors shown to produce and release antibiotics locally. *Chem. Commun.* **2013**, *49* (2), 128−130.

(5) Tanner, P.; Balasubramanian, V.; Palivan, C. G. Aiding Nature's Organelles: Artificial Peroxisomes Play Their Role. *Nano Lett.* **2013**, *13* (6), 2875−2883.

(6) Lomora, M.; Garni, M.; Itel, F.; Tanner, P.; Spulber, M.; Palivan, C. G. Polymersomes with engineered ion selective permeability as stimuli-responsive nanocompartments with preserved architecture. *Biomaterials* **2015**, *53*, 406−414.

(7) Lomora, M.; Itel, F.; Dinu, I. A.; Palivan, C. G. Selective ion-permeable membranes by insertion of biopores into polymersomes. *Phys. Chem. Chem. Phys.* **2015**, *17* (24), 15538−15546.

(8) Stoenescu, R.; Graff, A.; Meier, W. Asymmetric ABC-triblock copolymer membranes induce a directed insertion of membrane proteins. *Macromol. Biosci.* **2004**, *4* (10), 930−5.

(9) Blanazs, A.; Massignani, M.; Battaglia, G.; Armes, S. P.; Ryan, A. J. Tailoring Macromolecular Expression at Polymersome Surfaces. *Adv. Funct. Mater.* **2009**, *19* (18), 2906−2914.

(10) Liu, G.; Ma, S.; Li, S.; Cheng, R.; Meng, F.; Liu, H.; Zhong, Z. The highly efficient delivery of exogenous proteins into cells mediated by biodegradable chimaeric polymersomes. *Biomaterials* **2010**, *31* (29), 7575−7585.

(11) Liu, Q.; Chen, J.; Du, J. Asymmetrical Polymer Vesicles with a "Stealthy" Outer Corona and an Endosomal-Escape-Accelerating Inner Corona for Efficient Intracellular Anticancer Drug Delivery. *Biomacromolecules* **2014**, *15* (8), 3072−3082.

(12) Stoenescu, R.; Meier, W. Vesicles with asymmetric membranes from amphiphilic ABC triblock copolymers. *Chem. Commun. (Cambridge, U. K.)* **2002**, No. 24, 3016−7.

(13) Wittemann, A.; Azzam, T.; Eisenberg, A. Biocompatible Polymer Vesicles from Biamphiphilic Triblock Copolymers and Their Interaction with Bovine Serum Albumin. *Langmuir* **2007**, *23* (4), 2224−2230.

(14) Du, J.; Fan, L.; Liu, Q. pH-Sensitive Block Copolymer Vesicles with Variable Trigger Points for Drug Delivery. *Macromolecules* **2012**, *45* (20), 8275−8283.

(15) Mason, A. F.; Thordarson, P. Polymersomes with Asymmetric Membranes Based on Readily Accessible Di- and Triblock Copolymers Synthesized via SET-LRP. *ACS Macro Lett.* **2016**, *5* (10), 1172−1175.

(16) Matter, Y.; Enea, R.; Casse, O.; Lee, C. C.; Baryza, J.; Meier, W. Amphiphilic PEG-b-PMCL-b-PDMAEMA Triblock Copolymers: From Synthesis to Physico-Chemistry of Self-Assembled Structures. *Macromol. Chem. Phys.* **2011**, *212* (9), 937−949.

(17) Zhang, W.; He, J.; Liu, Z.; Ni, P.; Zhu, X. Biocompatible and pH-responsive triblock copolymer mPEG-b-PCL-b-PDMAEMA: Synthesis, self-assembly, and application. *J. Polym. Sci., Part A: Polym. Chem.* **2010**, *48* (5), 1079−1091.

(18) Konishcheva, E.; Häussinger, D.; Lörcher, S.; Meier, W. Key aspects to yield low dispersity of PEO-b-PCL diblock copolymers and their mesoscale self-assembly. *Eur. Polym. J.* **2016**, *83*, 300−310.

(19) Aoi, K.; Okada, M. Polymerization of oxazolines. *Prog. Polym. Sci.* **1996**, *21* (1), 151−208.

(20) Saegusa, T.; Ikeda, H.; Fujii, H. Isomerization Polymerization of 2-Oxazoline. IV. Kinetic Study of 2-Methyl-2-oxazoline Polymerization. *Macromolecules* **1972**, *5* (4), 359−362.

(21) Wiesbrock, F.; Hoogenboom, R.; Leenen, M. A. M.; Meier, M. A. R.; Schubert, U. S. Investigation of the Living Cationic Ring-Opening Polymerization of 2-Methyl-, 2-Ethyl-, 2-Nonyl-, and 2-Phenyl-2-oxazoline in a Single-Mode Microwave Reactor†. *Macromolecules* **2005**, *38* (12), 5025−5034.

(22) Korich, A. L.; Walker, A. R.; Hincke, C.; Stevens, C.; Iovine, P. M. Synthesis, characterization, and star polymer assembly of boronic acid end-functionalized polycaprolactone. *J. Polym. Sci., Part A: Polym. Chem.* **2010**, *48* (24), 5767−5774.

(23) Schmulbach, C. D.; Hinckley, C. C.; Wasmund, D. Solutions of alkali metals in anhydrous pyridine. *J. Am. Chem. Soc.* **1968**, *90* (24), 6600−6602.

(24) Hoogenboom, R.; Fijten, M. W. M.; Schubert, U. S. Parallel kinetic investigation of 2-oxazoline polymerizations with different initiators as basis for designed copolymer synthesis. *J. Polym. Sci., Part A: Polym. Chem.* **2004**, *42* (8), 1830−1840.

(25) Hoogenboom, R.; Fijten, M. W. M.; Thijs, H. M. L.; van Lankvelt, B. M.; Schubert, U. S. Microwave-assisted synthesis and properties of a series of poly(2-alkyl-2-oxazoline)s. *Des. Monomers Polym.* **2005**, *8* (6), 659−671.

(26) Hoogenboom, R.; Wiesbrock, F.; Huang, H.; Leenen, M. A. M.; Thijs, H. M. L.; van Nispen, S. F. G. M.; van der Loop, M.; Fustin, C.-A.; Jonas, A. M.; Gohy, J.-F.; Schubert, U. S. Microwave-Assisted Cationic Ring-Opening Polymerization of 2-Oxazolines: A Powerful Method for the Synthesis of Amphiphilic Triblock Copolymers. *Macromolecules* **2006**, *39* (14), 4719−4725.

(27) Wiesbrock, F.; Hoogenboom, R.; Leenen, M.; van Nispen, S. F. G. M.; van der Loop, M.; Abeln, C. H.; van den Berg, A. M. J.; Schubert, U. S. Microwave-Assisted Synthesis of a 42-Membered Library of Diblock Copoly(2-oxazoline)s and Chain-Extended Homo Poly(2-oxazoline)s and Their Thermal Characterization. *Macromolecules* **2005**, *38* (19), 7957−7966.

(28) Vergaelen, M.; Verbraeken, B.; Monnery, B. D.; Hoogenboom, R. Sulfolane as Common Rate Accelerating Solvent for the Cationic Ring-Opening Polymerization of 2-Oxazolines. *ACS Macro Lett.* **2015**, *4* (8), 825−828.

(29) Litt, M.; Levy, A.; Herz, J. Polymerization of Cyclic Imino Ethers. X. Kinetics, Chain Transfer, and Repolymerization. *J. Macromol. Sci., Chem.* **1975**, *9* (5), 703−727.

(30) Glassner, M.; D'hooge, D. R.; Young Park, J.; Van Steenberge, P. H. M.; Monnery, B. D.; Reyniers, M.-F.; Hoogenboom, R. Systematic investigation of alkyl sulfonate initiators for the cationic ring-opening polymerization of 2-oxazolines revealing optimal combinations of monomers and initiators. *Eur. Polym. J.* **2015**, *65*, 298−304.

(31) Qi, W.; Ghoroghchian, P. P.; Li, G.; Hammer, D. A.; Therien, M. J. Aqueous self-assembly of poly(ethylene oxide)-*block*-poly(?-caprolactone) (PEO-b-PCL) copolymers: disparate diblock copolymer

DOI: 10.1021/acs.macromol.6b02743
Macromolecules 2017, 50, 1512−1520

compositions give rise to nano- and meso-scale bilayered vesicles. *Nanoscale* **2013**, *5* (22), 10908−10915.
(32) Rajagopal, K.; Mahmud, A.; Christian, D. A.; Pajerowski, J. D.; Brown, A. E. X.; Loverde, S. M.; Discher, D. E. Curvature-Coupled Hydration of Semicrystalline Polymer Amphiphiles Yields flexible Worm Micelles but Favors Rigid Vesicles: Polycaprolactone-Based Block Copolymers. *Macromolecules* **2010**, *43* (23), 9736−9746.
(33) Zupancich, J. A.; Bates, F. S.; Hillmyer, M. A. Aqueous Dispersions of Poly(ethylene oxide)-b-poly(γ-methyl-ε-caprolactone) Block Copolymers. *Macromolecules* **2006**, *39* (13), 4286−4288.
(34) Jain, S.; Bates, F. S. Consequences of Nonergodicity in Aqueous Binary PEO−PB Micellar Dispersions. *Macromolecules* **2004**, *37* (4), 1511−1523.
(35) Wu, D.; Spulber, M.; Itel, F.; Chami, M.; Pfohl, T.; Palivan, C. G.; Meier, W. Effect of Molecular Parameters on the Architecture and Membrane Properties of 3D Assemblies of Amphiphilic Copolymers. *Macromolecules* **2014**, *47* (15), 5060−5069.
(36) Jain, S.; Bates, F. S. On the Origins of Morphological Complexity in Block Copolymer Surfactants. *Science* **2003**, *300* (5618), 460−464.
(37) Itel, F.; Chami, M.; Najer, A.; Lörcher, S.; Wu, D.; Dinu, I. A.; Meier, W. Molecular Organization and Dynamics in Polymersome Membranes: A Lateral Diffusion Study. *Macromolecules* **2014**, *47* (21), 7588−7596.
(38) Schlaad, H.; You, L.; Sigel, R.; Smarsly, B.; Heydenreich, M.; Mantion, A.; Masic, A. Glycopolymer vesicles with an asymmetric membrane. *Chem. Commun.* **2009**, No. 12, 1478−1480.
(39) Smith, P. K.; Krohn, R. I.; Hermanson, G. T.; Mallia, A. K.; Gartner, F. H.; Provenzano, M. D.; Fujimoto, E. K.; Goeke, N. M.; Olson, B. J.; Klenk, D. C. Measurement of protein using bicinchoninic acid. *Anal. Biochem.* **1985**, *150* (1), 76−85.
(40) Vangeyte, P.; Jérôme, R. Amphiphilic block copolymers of high-molecular-weight poly(ethylene oxide) and either ε-caprolactone or γ-methyl-ε-caprolactone: Synthesis and characterization. *J. Polym. Sci., Part A: Polym. Chem.* **2004**, *42* (5), 1132−1142.
(41) Petersen, M. A.; Yin, L.; Kokkoli, E.; Hillmyer, M. A. Synthesis and characterization of reactive PEO-PMCL polymersomes. *Polym. Chem.* **2010**, *1* (8), 1281−1290.

DOI: 10.1021/acs.macromol.6b02743
Macromolecules 2017, 50, 1512−1520

Supporting information

PEO-*b*-PCL-*b*-PMOXA Triblock Copolymers: from Synthesis to Microscale Polymersomes with Asymmetric Membrane

Evgeniia V. Konishcheva[†], *Ulmas E. Zhumaev*[‡], *Wolfgang P. Meier*[†]*

[†]Department of Chemistry, University of Basel, Klingelbergstrasse 80, 4056 Basel, Switzerland

[‡]Max Planck Institute for Polymer Research, Ackermannweg 10, 55128 Mainz, Germany

*Corresponding author: wolfgang.meier@unibas.ch

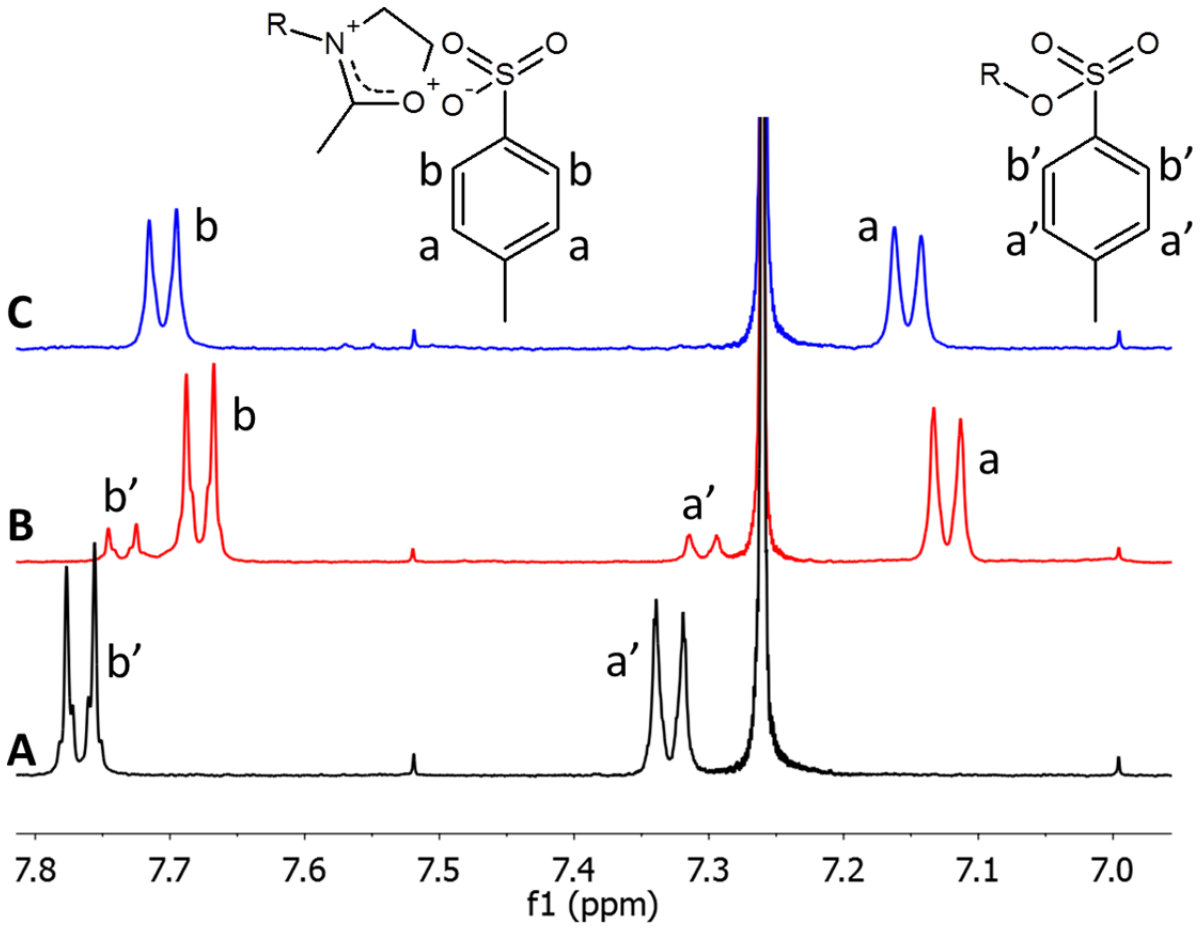

Figure S1. ^{1}H NMR ($CDCl_3$) spectra of: A: PEO(2.0K)-*b*-PCL(11.7K)-OTs; B: PEO(2.0K)-*b*-PCL(11.7K)-*b*-PMOXA(0.3K) synthesized in acetonitrile; C: PEO(2.0K)-*b*-PCL(11.7K)-*b*-PMOXA(0.3K) synthesized in sulfolane. The triblock copolymers were obtained by microwave-assisted synthesis using 0.92 M MOXA at 100 °C after 1 h.

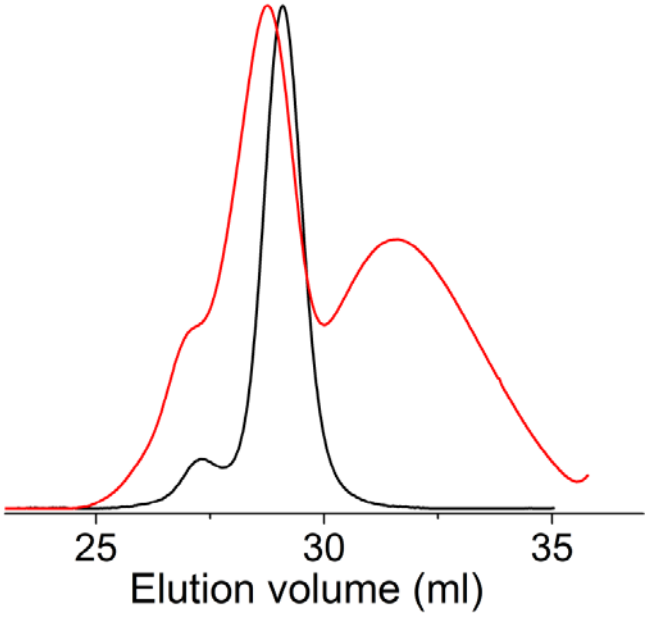

Figure S2. GPC (DMF) traces of PEO(2.0K)-*b*-PCL(12.5K)-OTs (black) and PEO(2.0K)-*b*-PCL(12.5K)-*b*-PMOXA(xK) (red) obtained by microwave-assisted synthesis using 2.3 M MOXA at 180 °C after 10 seconds.

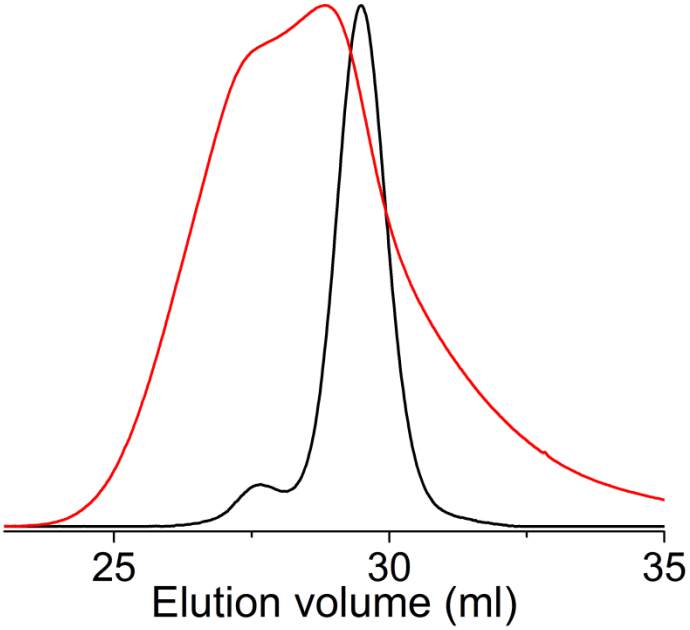

Figure S3. GPC (DMF) traces of PEO(2.0K)-*b*-PCL(11.7K)-OTs (black) and PEO(2.0K)-*b*-PCL(11.7K)-*b*-PMOXA(xK) (red) obtained by microwave-assisted synthesis using 11.5 M MOXA at 100 °C after 2 h.

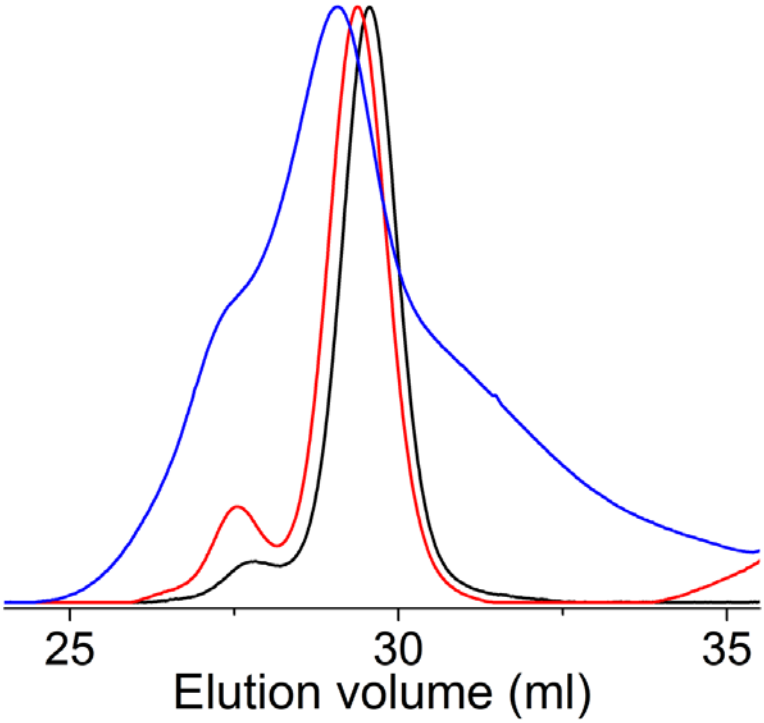

Figure S4. GPC (DMF) traces of PEO(2.0K)-*b*-PCL(11.7K)-OTs (black), PEO(2.0K)-*b*-PCL(11.7K)-*b*-PMOXA(xK) obtained after polymerization in the microwave reactor at 100 °C after 40 min using different MOXA: stored ~6 months over CaH_2 and distilled prior to use (red), stored ~12 h over CaH_2 and distilled prior to use (blue).

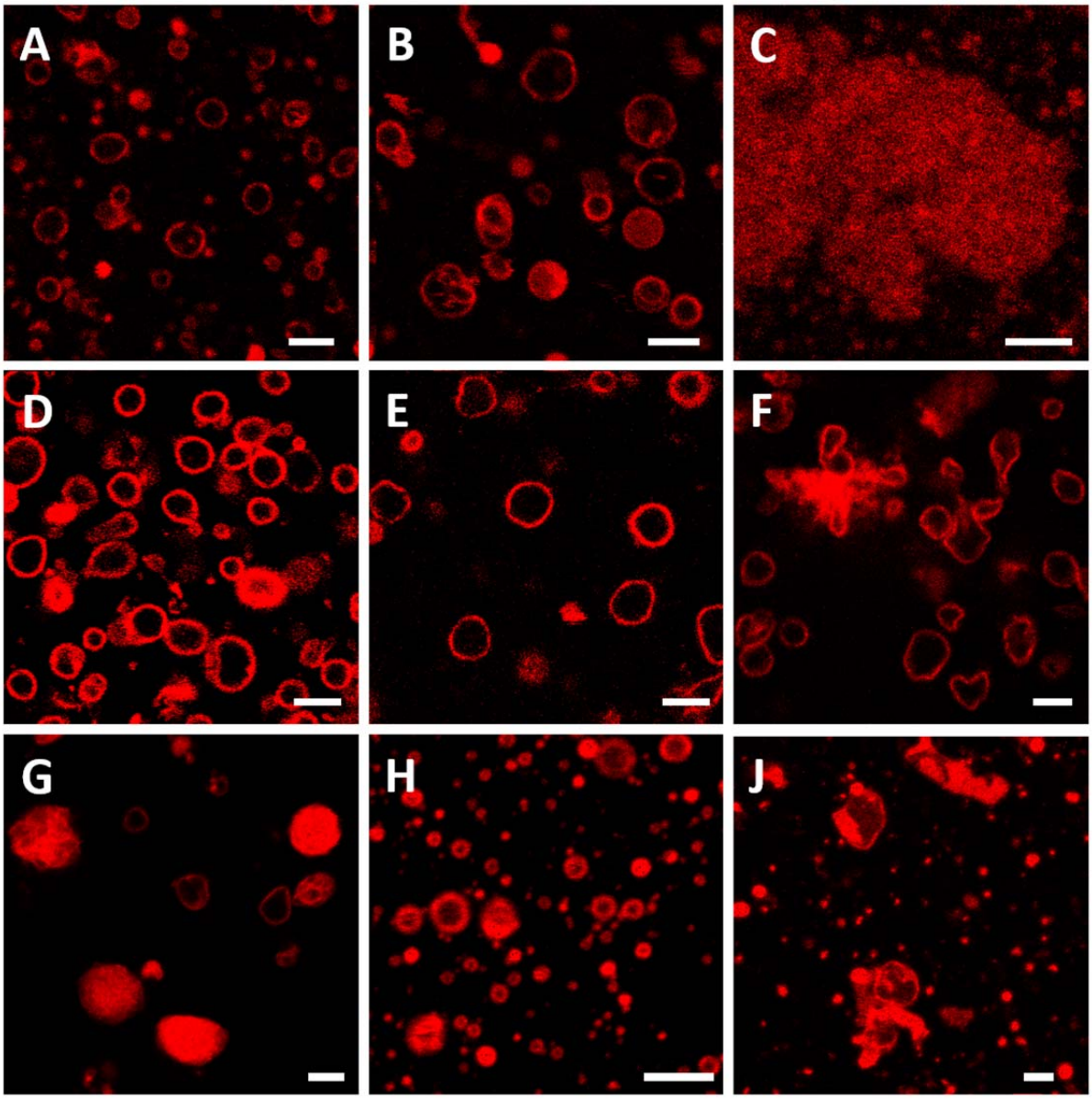

Figure S5. LSM images of the self-assembled structures formed by: A: PEO(2.0K)-*b*-PCL(7.5K)-*b*-PMOXA(0.4K); B: PEO(2.0K)-*b*-PCL(11.7K)-*b*-PMOXA(0.3K); C: PEO(2.0K)-*b*-PCL(11.7K)-*b*-PMOXA(1.4K); D: PEO(2.0K)-*b*-PCL(12.5K)-*b*-PMOXA(0.3K); E: PEO(2.0K)-*b*-PCL(15.4K)-*b*-PMOXA(0.3K); F: PEO(2.0K)-*b*-PCL(15.4K)-*b*-PMOXA(2.1K); G: PEO(2.0K)-*b*-PCL(16.8K)-*b*-PMOXA(1.5K); H: PEO(2.0K)-*b*-PCL(17.4K); J: PEO(2.0K)-*b*-PCL(17.4K)-*b*-PMOXA(0.9K). Structures were stained with Bodipy 630/650 dye. Scale bars are 5 μm.

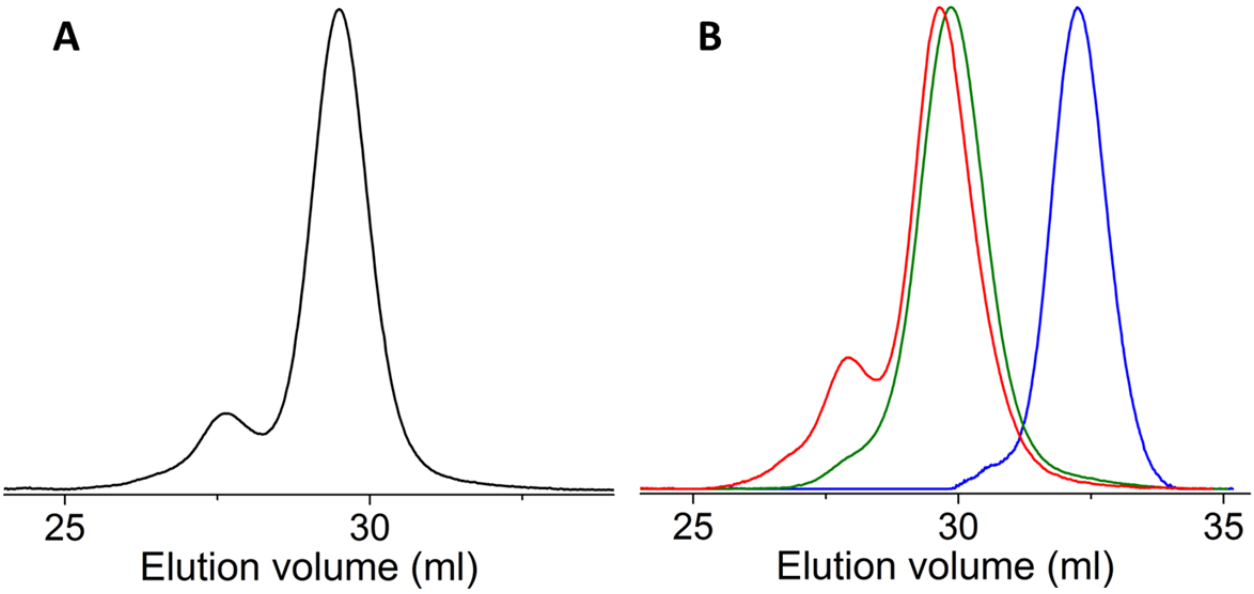

Figure S6. GPC (DMF) traces of: A: PEO(2.0K)-*b*-PCL(11.7K)-*b*-PMOXA(0.3K)-Azide; B: Alkyne-PEO(2K) (blue), Alkyne-PEO(2.0K)-*b*-PCL(11.4K) (green), Alkyne-PEO(2.0K)-*b*-PCL(11.4K)-*b*-PMOXA(0.3K) (red).

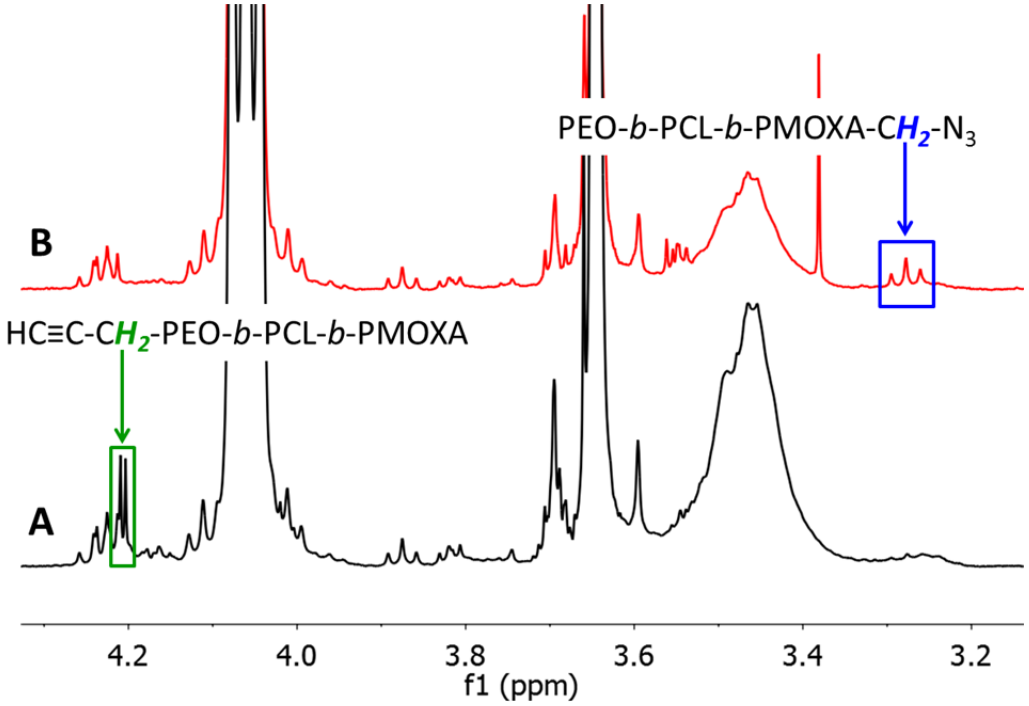

Figure S7. ^{1}H NMR ($CDCl_3$) spectra after incubation at 60 °C for 24 h in aqueous solution of: A: Alkyne-PEO(2.0K)-*b*-PCL(11.4K)-*b*-PMOXA(1.7K); B: PEO(2.0K)-*b*-PCL(11.7K)-*b*-PMOXA(0.8K)-Azide.

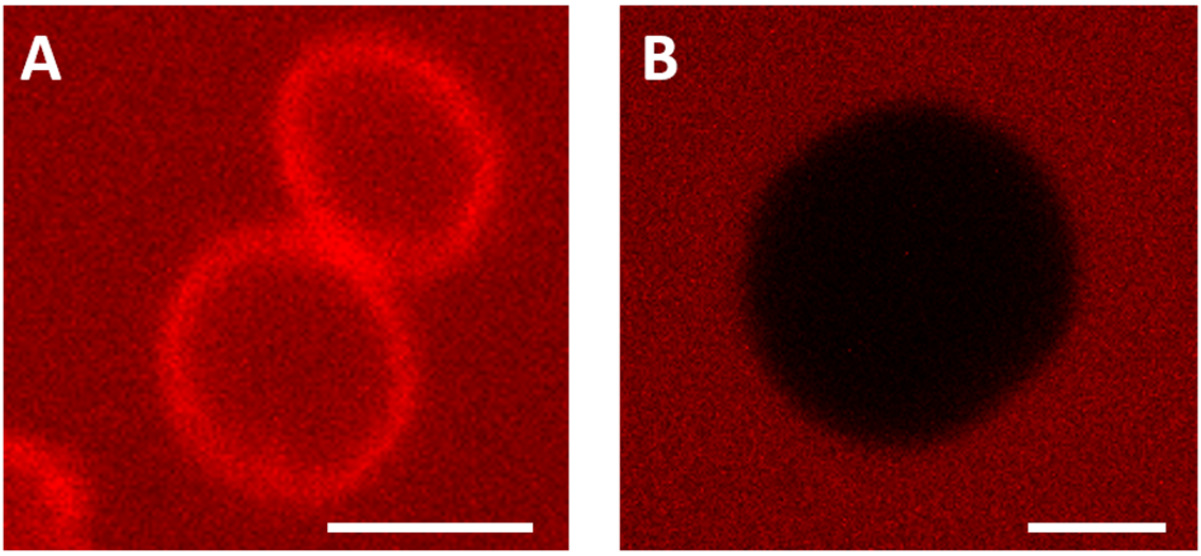

Figure S8. LSM images of polymersomes formed by PEO(2.0K)-*b*-PCL(12.5K)-*b*-PMOXA(0.3K) with Sulfo-Cy3 (final concentration 0.2 mM) added externally: A: in aqueous solution; B: after addition of 10x PBS buffer (final concentration of salts is 150 mM). Due to the high accumulation of Sulfo-Cy3 on the outer surface of polymersomes analysis was conducted in the presence of electrolyte which shields Coulomb interactions between hydrophilic corona and the dye thus preventing it from accumulation. Scale bars are 5 μm.

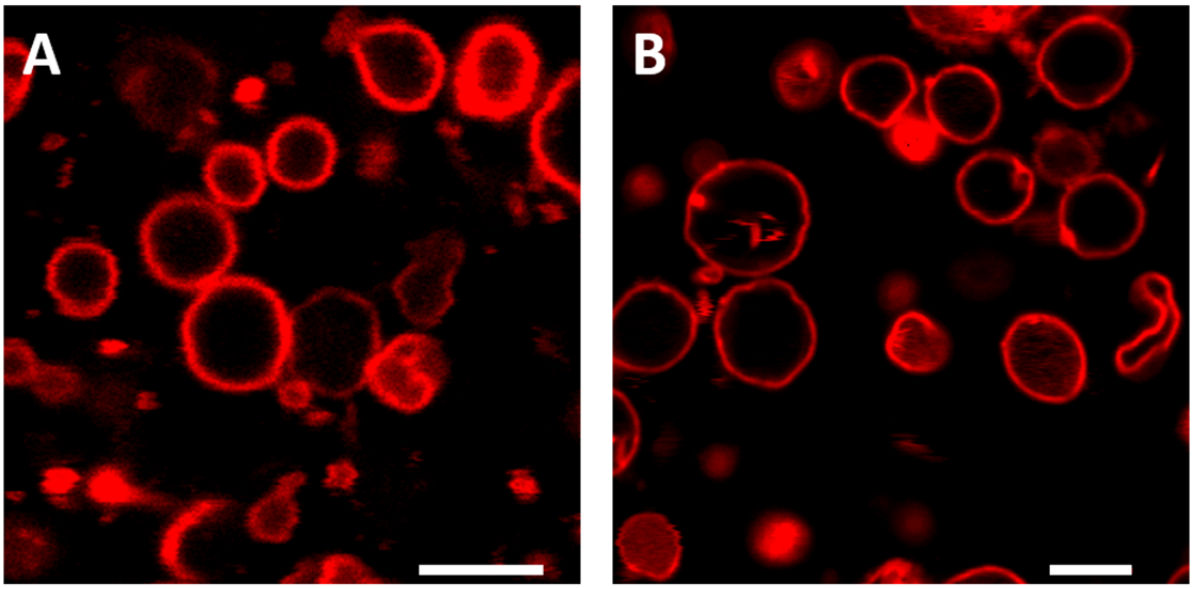

Figure S9. LSM images of the self-assembled structures formed by: A: 85 % PEO(2.0K)-*b*-PCL(12.5K)-*b*-PMOXA(0.3K) + 15 % Alkyne-PEO(2.0K)-*b*-PCL(11.4K)-*b*-PMOXA(0.3K); B: 85 % PEO(2.0K)-*b*-PCL(12.5K)-*b*-PMOXA(0.3K) + 15 % PEO(2.0K)-*b*-PCL(11.7K)-*b*-PMOXA(0.3K)-Azide. Structures were stained with Bodipy 630/650 dye. Scale bars are 5 μm.

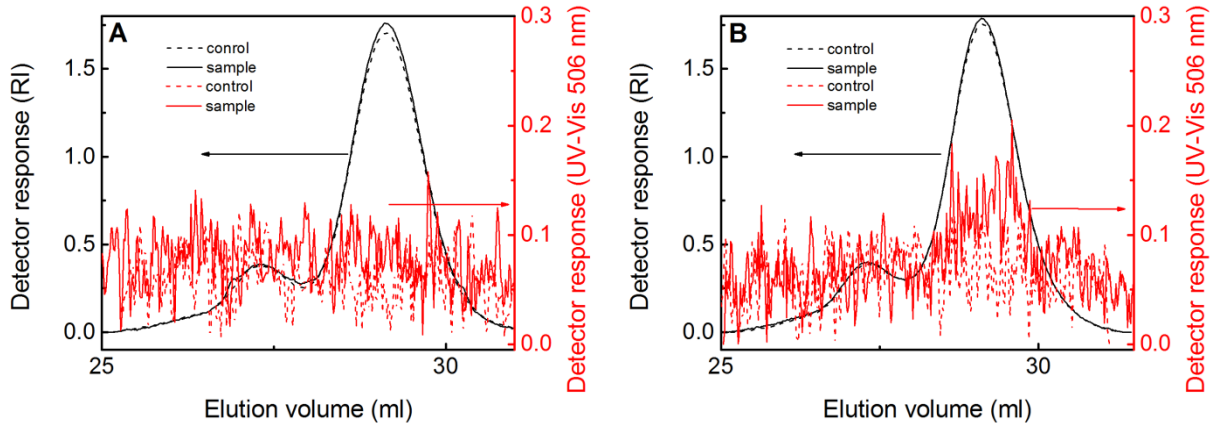

Figure S10. GPC (DMF) traces recorded on RI/UV-Vis (506 nm) detectors of a mixture after reaction between alkyne/azide containing polymersomes and azide/alkyne-dye: A: 85 % PEO(2.0K)-*b*-PCL(12.5K)-*b*-PMOXA(0.3K) + 15 % PEO(2.0K)-*b*-PCL(11.7K)-*b*-PMOXA(0.3K)-Azide + Sulfo-Cy3-Alkyne; B: 85 % PEO(2.0K)-*b*-PCL(12.5K)-*b*-PMOXA(0.3K) + 15 % Alkyne-PEO(2.0K)-*b*-PCL(11.4K)-*b*-PMOXA(0.3K) + Sulfo-Cy3-Azide. "Controls" were obtained from the reaction mixture which did not contain Cu(II) complex and sodium ascorbate. "Samples" corresponded to the reaction mixture which contained Cu(II) complex and sodium ascorbate. The samples for GPC analysis were prepared by removing water from the reaction mixture and dissolving them in DMF (20 mM LiBr) to a final concentration of 2 mg·ml^{-1} followed by filtration.

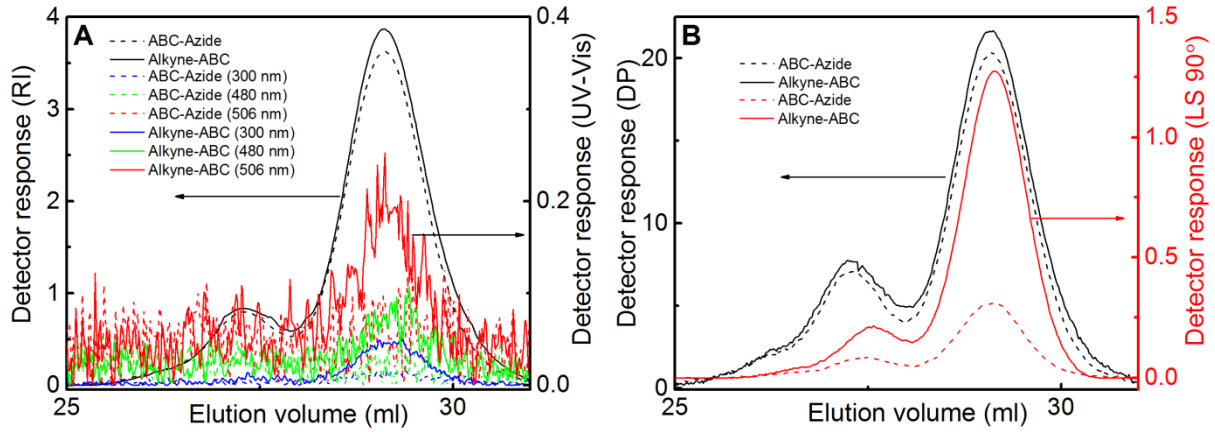

Figure S11. Repetition of the reaction between 15 % alkyne/azide containing polymersomes and Sulfo-Cy3-azide/alkyne. GPC (DMF) traces: A: RI/UV-Vis signals; B: DP-LS 90° signals. ABC-Azide: 85 % PEO(2.0K)-*b*-PCL(12.5K)-*b*-PMOXA(0.3K) + 15 % PEO(2.0K)-*b*-PCL(11.7K)-*b*-PMOXA(0.3K)-Azide; Alkyne-ABC: 85 % PEO(2.0K)-*b*-PCL(12.5K)-*b*-PMOXA(0.3K) + 15 % Alkyne-PEO(2.0K)-*b*-PCL(11.4K)-*b*-PMOXA(0.3K). The samples for GPC analysis were prepared by removing water from the reaction mixture and dissolving them in DMF (20 mM LiBr) to a final concentration of 5 mg·ml^{-1}.

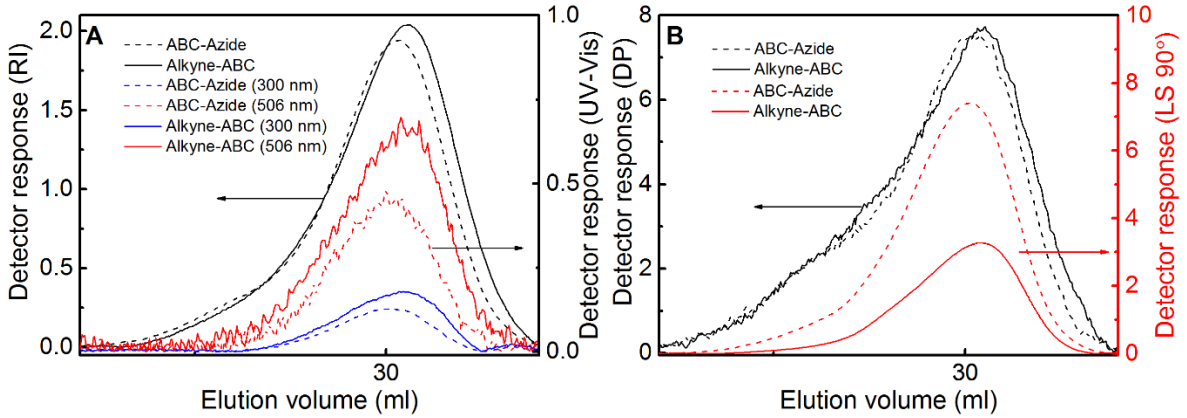

Figure S12. Reaction between 50 % alkyne/azide containing polymer and Sulfo-Cy3-azide/alkyne. Polymer aggregates were incubated at 60 °C for 24 h before the reaction. The reaction conditions were the same as for 15 % alkyne/azide containing polymersomes. GPC (DMF) traces: A: RI/UV-Vis signals; B: DP-LS 90° signals. ABC-Azide: 50 % PEO(2.0K)-*b*-PCL(12.5K)-*b*-PMOXA(0.3K) + 50 % PEO(2.0K)-*b*-PCL(11.7K)-*b*-PMOXA(0.3K)-Azide; Alkyne-ABC: 50 % PEO(2.0K)-*b*-PCL(12.5K)-*b*-PMOXA(0.3K) + 50 % Alkyne-PEO(2.0K)-*b*-PCL(11.4K)-*b*-PMOXA(0.3K). The samples for GPC analysis were prepared by dissolving 50 µl of a reaction mixture in 0.5 ml DMF (20 mM LiBr).

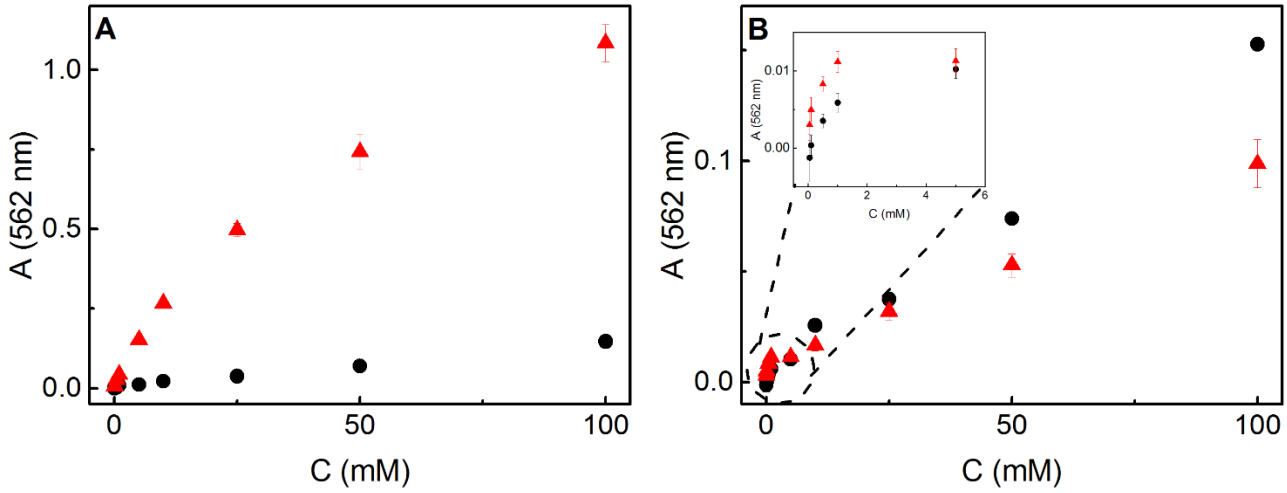

Figure S13. Absorbance (562 nm) after incubation for 24 h at 25 ºC of 33 µl of samples with 267 µl of BCA solution of: A: PEO_{45} (●), $PMOXA_{45}$ (▲); B: PEO_{45} (●), $PMOXA_5$ (▲). Each concentration consisted of 3 samples.

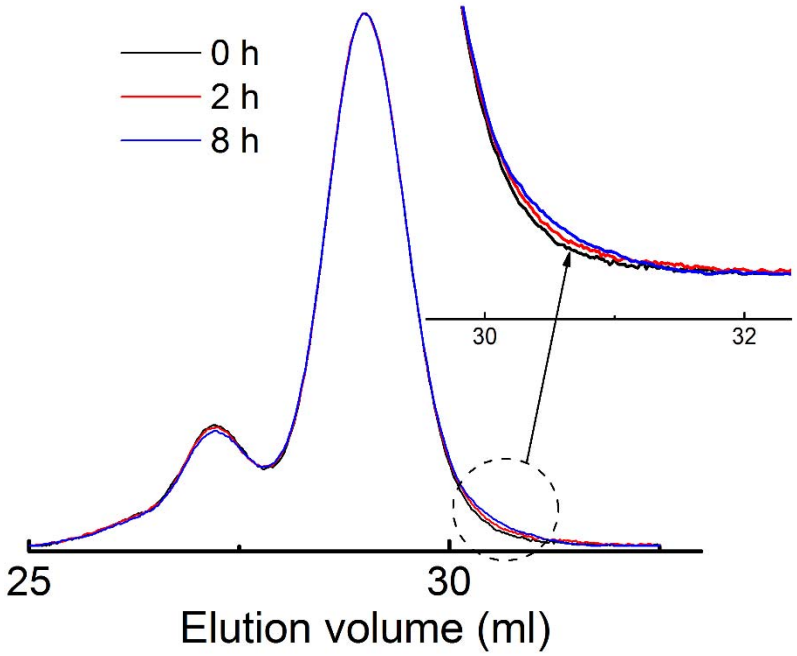

Figure S14. GPC (DMF) traces of PEO(2.0K)-*b*-PCL(12.5K)-*b*-PMOXA(0.3K) after incubation of its polymersomes with BCA solution at 25 ºC at various time points.

Table S1. Absorbance (562 nm) of the supernatant after incubation of 50 µl of 15 mg·ml^{-1} sample with 400 µl of BCA solution at 25 ºC at various time points. Each series consisted of 10 samples. The outliers were determined using Dixon's Q-test.[1]

Sample	2 h	8 h
Background	0.130±0.006	0.158±0.007
PEO(2.0K)-*b*-PCL(12.5K) suspension	0.145±0.007	0.195±0.017
PEO(2.0K)-*b*-PCL(12.5K)-*b*-PMOXA(0.3K) polymersomes	0.186±0.007	0.227±0.014
PEO(2.0K)-*b*-PCL(12.5K)-*b*-PMOXA(0.3K) suspension	0.226±0.031	0.262±0.060

To test the hypothesis if the samples with ABC polymersomes and ABC suspension have different mean values, Student's t-test was applied.

$t_{2h(16;\,0.99)} = 3.336 > t_{c(16;\,0.99)} = 2.921$. Consequently, the mean values are significantly different.

$t_{8h(18;\,0.99)} = 1.726 < t_{c(18;\,0.99)} = 2.878$. Consequently, the mean values are not significantly different.

References:

1. Dean, R. B.; Dixon, W. J., Simplified Statistics for Small Numbers of Observations. *Analytical Chemistry* **1951,** *23* (4), 636-638.

Publication 3

Complex self-assembly behavior of bis-hydrophilic PEO-*b*-PCL-*b*-PMOXA triblock copolymers in aqueous solution

Evgeniia V. Konishcheva, Ulmas E. Zhumaev, Maximilian Kratt, Valentin Oehri, Wolfgang P. Meier

Contribution of Evgeniia Konishcheva:

- Synthesized and characterized the polymers
- Prepared and characterized the self-assembled structures
- Investigated influence of the preparation procedure on the morphology of the assemblies
- Suggested the mechanism of self-assembly for different self-assembly methods
- Wrote the manuscript

Macromolecules

Article

pubs.acs.org/Macromolecules

Complex Self-Assembly Behavior of Bis-hydrophilic PEO-*b*-PCL-*b*-PMOXA Triblock Copolymers in Aqueous Solution

Evgeniia V. Konishcheva,*[,†] Ulmas E. Zhumaev,[‡] Maximilian Kratt,[†] Valentin Oehri,[†] and Wolfgang Meier*[,†]

[†]Department of Chemistry, University of Basel, Klingelbergstrasse 80, 4056 Basel, Switzerland

[‡]Molecular Spectroscopy Department, Max Planck Institute for Polymer Research, Ackermannweg 10, 55128 Mainz, Germany

Supporting Information

ABSTRACT: We report aqueous self-assembly of linear amphiphilic triblock copolymers poly(ethylene oxide)-*block*-polycaprolactone-*block*-poly(2-methyl-2-oxazoline) (PEO-*b*-PCL-*b*-PMOXA) and their PEO-*b*-PCL precursors with different PCL and PMOXA block lengths using three preparation methods: film rehydration, solvent evaporation, and cosolvent. For PEO-*b*-PCL, the self-assembled structures were ordinary spherical particles and polymersomes. For PEO-*b*-PCL-*b*-PMOXA, we observed polymersomes with asymmetric membrane, cloud-like aggregates, elongated particles, Y-shaped elongated particles, and 3D networks. All structures were of micrometer size and characterized using laser scanning microscopy (LSM). 3D networks were also characterized using *z*-stack confocal LSM, transmission electron microscopy (TEM), and cryogenic TEM. We demonstrated that film rehydration method results in pseudoequilibrium structures, whereas structures formed using solvent evaporation and cosolvent methods are under kinetic control. We showed how kinetically controlled structures can be transformed into pseudoequilibrium morphologies.

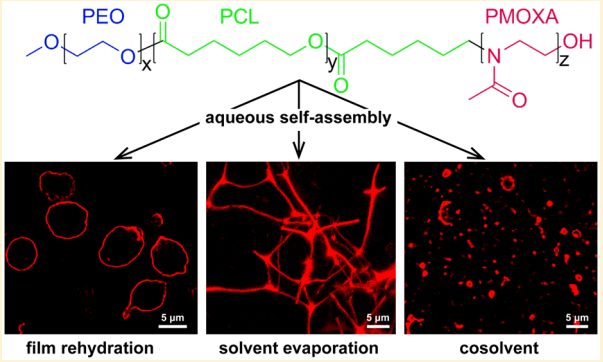

INTRODUCTION

Complex structural organization achieved through noncovalent interactions leads to unique functions (e.g., DNA, RNA) and very specific catalytic activity (e.g., enzymes) of natural macromolecules. Mimicking such complex structural organization by self-assembly of synthetic molecules is a promising approach toward the rational design of programmable functional (nano)materials. Water is a unique solvent[1] for self-assembly based on noncovalent interactions, and structures self-assembled in aqueous solution are of particular importance for biomedical applications, such as drug delivery and tissue engineering. Low molecular weight surfactants and amphiphilic block copolymers are prominent examples of synthetic molecules that self-assemble into various structures in water. Self-assembly of these synthetic molecules is driven by hydrophobic interactions. Amphiphilic block copolymers are advantageous over low molecular weight surfactants and natural lipids due to the higher stability of the self-assembled structures[2] and possibility to tune properties of the aggregates by changing composition and length of the blocks. Such a tuning procedure is becoming more and more straightforward thanks to the fast development of polymerization techniques and vast availability of different monomers.[3−5]

Linear AB diblock copolymers, where A and B stand for the hydrophilic and hydrophobic blocks, respectively, are the most explored type of amphiphilic block copolymers. It has been found that aqueous self-assembled structures of linear AB polymers can be described in terms of the packing geometry of an individual polymer molecule, and in most cases such structures formed in dilute solutions (few wt %) are limited to micelles, rods, and polymersomes.[6−13] Introduction of the third hydrophilic C block can break this limitation and facilitate access to more complex self-assembled structures that are not accessible with conventional linear AB polymers. However, there is a lack of experimental data on aqueous self-assembly of linear ABC triblock copolymers. Consequently, in contrast to linear AB polymers, in the case of linear ABC polymers, it is not known how hydrophilic weight fraction and conditions of self-assembly influence morphology of the self-assembled structures.

Only few works report about aqueous self-assembly of linear ABC polymers. Some of them do not represent more complex self-assembly behavior of ABC compared to AB polymers, since the observed structures are ordinary micelles, rods, and polymersomes.[14,15] The other works do represent more complex self-assembly behavior by reporting polymersomes with asymmetric membrane[16−24] and structures with domains in the corona and stimuli-responsive blocks.[25−28] Aqueous self-assembled structures formed by linear ABC polymers can be more diverse, as suggested by the recent studies devoted to the

Received: July 14, 2017
Revised: August 23, 2017
Published: September 8, 2017

DOI: 10.1021/acs.macromol.7b01498
Macromolecules 2017, 50, 7155−7168

self-assembly of linear triblock copolymers in organic solvents.[29,30] The structures possessed various morphologies with domains in the core, for example, spheres on spheres, spheres on rods, rods on vesicles, spheres on vesicles, etc. However, these structures were observed for linear ABC polymers in organic C-selective solvent, and the established rules are not necessarily applicable for (A and C)-selective solvent, that is, for water in the case of hydrophilic A and C blocks.

In this work, we present the first systematic investigation of self-assembly of linear bis(A, C)-hydrophilic ABC polymers in dilute aqueous solution. Our aim is to gain insight into the effect of hydrophilic weight fraction and conditions of self-assembly on the morphology of the self-assembled structures. As a first step toward the major aim, we explore the latter effects in dilute aqueous solution (0.2 wt %). As a model ABC system, we chose narrowly dispersed ($Đ_M$ < 1.25) poly(ethylene oxide)-*block*-polycaprolactone-*block*-poly(2-methyl-2-oxazoline) (PEO-*b*-PCL-*b*-PMOXA) polymers, recently developed by us.[16] Since the synthesis of PEO-*b*-PCL-*b*-PMOXA is free of toxic reagents, PEO and PMOXA are biocompatible hydrophilic blocks, and PCL is a biodegradable hydrophobic block, the reported self-assembled structures might serve as potential candidates for biomedical applications. We tune the hydrophilic weight fraction of PEO-*b*-PCL-*b*-PMOXA by changing PCL and PMOXA block lengths, while keeping PEO block length constant (45 units), and explore structures resulting from three self-assembly methods and conditions, namely, film rehydration, solvent evaporation, and cosolvent. To explain the formation of the observed structures assembled from PEO-*b*-PCL-*b*-PMOXA, we compare them with self-assembled structures formed by their precursors, PEO-*b*-PCL, under the same self-assembly conditions. Finally, to understand whether the observed structures are under thermodynamic or kinetic control, we investigate how change of details in self-assembly procedures, such as temperature, rate of the cosolvent addition, stirring rate, and self-assembly duration, affects the morphology of the self-assembled structures.

EXPERIMENTAL PROCEDURES

Experimental details on methods (NMR, GPC, DSC, TEM, cryoTEM) and synthesis of PEO-*b*-PCL[31] and PEO-*b*-PCL-*b*-PMOXA[16] can be found in related publications and Supporting Information.

Laser Scanning Microscopy (LSM). LSM images were recorded on an inverted Zeiss LSM510 META/ConfoCor 2 FCS microscope using a 100× 1.4 Oil Plan-Apochromat DIC objective lens. Bodipy 630/650 and calcein disodium salt were excited by the 633 nm He−Ne laser line (10% output) and 488 nm Argon laser line (10% output), respectively. The excitation light was passed through a HFT UV 488/543/633 beam splitter. The emission light from Bodipy 630/650 was passed through a LP 650 and the signal from calcein through a BP 474−525 filters. The transmittance signal was recorded simultaneously on a T-PMT detector. Twelve bit images of 1024 × 1024 pixels were recorded at a scan speed of 51.20 μs per pixel. *z*-Stack confocal LSM (CLSM) was performed on an inverted Zeiss LSM880 using a 63× 1.4 Oil Plan-Apochromat DIC M27 objective. Bodipy 630/650 was excited by the 633 nm He−Ne laser line. To get *z*-stacks with identical signal intensity, the laser power was increased from 0.1% to 3% output over the *z*-scan range. The excitation light was passed through a HFT UV 488/543/633 beam splitter. The emission light was passed through a LP 650 and recorded on PMT detector. The pinhole was set to 1 airy unit, and the *z*-slices were recorded with 0.5 μm step enabling 50% overlap for efficient 3D reconstruction. Sixteen bit images of 1280 × 1280 pixels were recorded at a scan speed of 13.11 μs per pixel. Five microliters of a stained sample was placed onto a 22 mm × 50 mm glass coverslip, covered with a round (Ø 13 mm) coverslip, and sealed with nail polish. The LSM images were processed with ImageJ and its LSM toolbox plug-in. The average diameter of polymersomes was calculated from area ($d = 2(s/\pi)^{1/2}$) determined for each individual particle using "Analyze Particles" option based on at least 3 different images (at least 300 objects in total). Length of elongated structures was determined as Feret's diameter based on at least 3 different images (at least 70 objects in total). *z*-Stack CLSM images were recorded in ZEN software and deconvoluted in Huygens software, and *z*-projection was performed in ImageJ software using Z Projection option.

Self-Assembly. Three methods of self-assembly were employed to obtain microscale structures of PEO-*b*-PCL and PEO-*b*-PCL-*b*-PMOXA: film rehydration, solvent evaporation, and cosolvent. In all experiments, we used 2 mm × 5 mm PTFE magnetic stir bars, and final polymer concentration was 0.2 wt %. Microscale structures (50 μL) were stained with 0.5 μL of 0.72 μM Bodipy 630/650 prior to visualization by LSM. Possible effect of Bodipy 630/650 on self-assembled structures was tested by comparing bright field images of the assemblies formed by $E_{45}C_{110}M_4$ and $E_{45}C_{153}M_{11}$ before and after dye addition. No visible differences in self-assembled structures were observed, suggesting no effect of fluorescent dye on the morphology of the self-assembled structures, at least on the experimental time scale (data not shown).

Film Rehydration. Two milligrams of a polymer was dissolved in 200 μL of CH_2Cl_2 and transferred into a 5 mL glass round-bottom flask. CH_2Cl_2 was slowly removed by rotary evaporation (110 rpm, 40 °C, 710 mbar), the polymer film was dried for 30 min (110 rpm, 40 °C, 5 mbar), and 1 mL of Milli-Q water was added for the rehydration. The samples were placed into an oil bath, which was quickly heated by a heating plate to 62 °C (3 °C·min^{-1}). The samples were stirred at 500 rpm for 24 h at 62 °C. After 24 h, the oil bath (62 °C) was removed, leading to a rapid decrease of the sample temperature to 22 °C. In the experiments where the heating rate was controlled, the temperature was increased by steps of 10 °C (1.5 °C·min^{-1}) from 22 to 62 °C, and the samples were left equilibrating at each temperature for 1 h. After incubation for 24 h (500 rpm, 62 °C), the solutions were cooled to 22 °C by removing the oil bath. In the experiments where the cooling rate was controlled, the samples were placed into an oil bath, which was quickly heated by a heating plate to 62 °C (3 °C·min^{-1}), and incubated for 24 h (500 rpm, 62 °C), the temperature was decreased by steps of 10 °C (0.6 °C·min^{-1}) from 62 to 22 °C, and the samples were left equilibrating at each temperature for 1 h.

Solvent Evaporation. Two milligrams of a polymer was dissolved in 200 μL of CH_2Cl_2 and transferred into a 2.5 mL glass vial, and then 1 mL of Milli-Q water was added in one shot. The mixtures were left open for the evaporation of CH_2Cl_2 (350 rpm, 24 h, 22 °C) and covered with a 500 mL beaker to avoid contamination of the samples. To check whether the structures formed in solvent evaporation method can undergo a morphological transition to the ones formed in film rehydration method, different structures formed by polymers with different PCL and PMOXA lengths, that is, $E_{45}C_{110}M_4$, $E_{45}C_{135}M_4$, and $E_{45}C_{135}M_{20}$, were incubated at 62 °C for 24 h at 350 rpm after evaporation of CH_2Cl_2.

Cosolvent. Two milligrams of a polymer was dissolved in 200 μL of THF and added dropwise (~200 μL·min^{-1}) into 800 μL of Milli-Q water stirring at 350 rpm in a 2.5 mL glass vial. The vials were closed, and the mixture was left stirring at 350 rpm for 24 h at 22 °C. To check the influence of the cosolvent nature on self-assembly, self-assembly of $E_{45}C_{153}M_4$ was performed using DMF/ACN/acetone as a cosolvent, since these solvents are among those able to solubilize PEO-*b*-PCL-*b*-PMOXA polymers. For the encapsulation experiments, 10 mM solution of calcein disodium salt was used instead of water. After the self-assembly, the solution was placed into a dialysis membrane (RC, MWCO 3.5−5 kDa, SpectraPor) and dialyzed against 1 L of Milli-Q water for 3 days (solution was exchanged 9 times).

DOI: 10.1021/acs.macromol.7b01498
Macromolecules 2017, 50, 7155−7168

RESULTS AND DISCUSSION

Bis-hydrophilic PEO-*b*-PCL-*b*-PMOXA triblock copolymers (Scheme 1) with fixed PEO length (45 units/2 kDa) and

Scheme 1. Structure of PEO-*b*-PCL-*b*-PMOXA Polymers

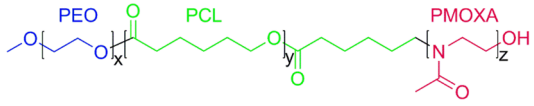

various PCL (48−153 units/5.5−17.4 kDa) and PMOXA (3−25 units/0.2−2.1 kDa) lengths were tested for the ability to self-assemble in aqueous solution using film rehydration, solvent evaporation, and cosolvent methods. In all self-assembly methods, final polymer concentration was 0.2 wt %. All polymers self-assembled into microscale structures, which were characterized by LSM. We discuss the observed structures in the following subsections devoted to each self-assembly method. Further in the text, PEO-*b*-PCL-*b*-PMOXA polymers are abbreviated as $E_xC_yM_z$, where *x*, *y*, and *z* denote the number of monomer units of PEO, PCL, and PMOXA, respectively.

Film Rehydration Method. In film rehydration method, a polymer was dissolved in CH_2Cl_2 and placed in a round-bottom glass flask. A thin polymer film was formed on the wall of the glass flask by removing CH_2Cl_2 by rotary evaporation. The film was rehydrated for 24 h after addition of water. Rehydration was performed at 62 °C due to the semicrystalline nature of the PCL block. The melting temperature of PEO-*b*-PCL-*b*-PMOXA polymers is $T_m \approx 61$ °C (DSC, Figure S1). Self-assembly did not occur at 55 °C, and the polymers remained as a precipitate.

Figure 1A depicts the predominant structures formed by PEO-*b*-PCL-*b*-PMOXA and their precursors, PEO-*b*-PCL, where each structure corresponds to the polymer with a certain molecular weight, M_n (or length), of PCL and hydrophilic weight fraction *f*:

$$f = \frac{M_{\text{hydrophilic}}}{M_{\text{hydrophilic}} + M_{\text{hydrophobic}}} = \frac{M_n(\text{PEO}) + M_n(\text{PMOXA})}{M_n(\text{PEO}) + M_n(\text{PMOXA}) + M_n(\text{PCL})} \quad (1)$$

Most PEO-*b*-PCL-*b*-PMOXA polymers formed two or three types of structures (e.g., Figure S2), but for simplicity reasons, only predominant structures are plotted in Figure 1A. More detailed information on morphology of the self-assembled structures can be found in Table S1. Here, in Figure 1A, and in the following morphology diagrams, points of the same color represent polymers with similar PMOXA lengths. For simplicity, we combined close values of PMOXA lengths in groups indicated by dashed lines, for example, the lengths of 7−12 units belong to the group PMOXA 10. Such combination is reasonable taking into account the dispersity of our triblock copolymers ($1.10 < D_M < 1.25$, Table S1). Point shapes in morphology diagrams indicate certain morphologies. The gray areas point out regions of the same morphology.

In the absence of PMOXA block, that is, in the case of PEO-*b*-PCL, morphology of the self-assembled structures changes from polymersomes to spherical particles (Figure 1B) with an increase in *f*. These spherical particles with diameters 0.2−2 μm (determined from TEM) are composed of distinct domains, and the domains have shapes ranging from spheres to rods

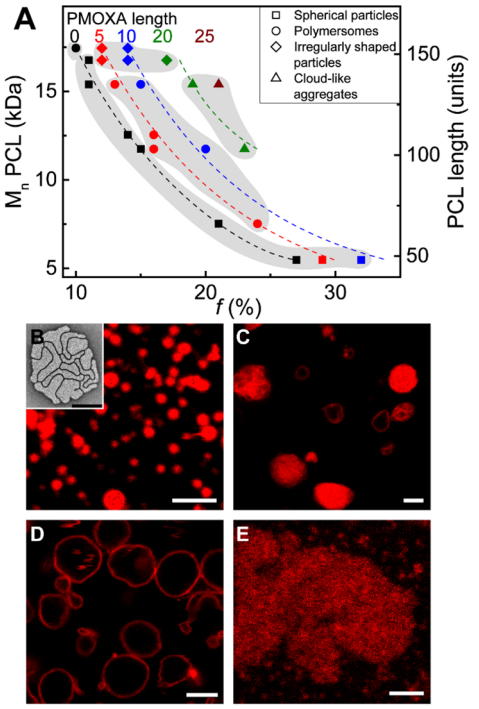

Figure 1. Self-assembled structures observed in film rehydration method. (A) Morphology diagram showing structures formed by PEO-*b*-PCL and PEO-*b*-PCL-*b*-PMOXA in aqueous solution as a function of the molecular composition. Points of each color correspond to polymers with a certain PMOXA length. Points of each shape correspond to a certain morphology: spherical particles (squares), polymersomes (circles), irregularly shaped particles (diamonds), cloud-like aggregates (triangles). The gray areas point out regions of the same morphology. Representative LSM images of the structures formed by (B) $E_{45}C_{147}$, spherical particles, (C) $E_{45}C_{147}M_{18}$, irregularly shaped particles, (D) $E_{45}C_{110}M_4$, polymersomes, (E) $E_{45}C_{135}M_{20}$, cloud-like aggregates. Structures were stained with Bodipy 630/650. Scale bars are 5 μm. Panel B inset is a representative TEM image of negatively stained spherical particles formed by $E_{45}C_{147}$; scale bar is 200 nm.

(Figure 1B, inset, and Figure S3). Perhaps such domains aggregate into spherical particles while cooling of the solution and crystallization of PCL block, but in this case one would expect formation of particles with rather irregular shape. In the case of PEO-*b*-PCL-*b*-PMOXA with PMOXA length of 5 and 10 units, morphology of the structures changes in the order irregularly shaped particles (Figure 1C) to polymersomes (Figure 1D) to spherical particles with an increase in *f*. In the case of PEO-*b*-PCL-*b*-PMOXA with PMOXA length of 20 units, morphology of the self-assembled structures changes from irregularly shaped particles to cloud-like aggregates (Figure 1E) with an increase in *f*. Revealing trends between morphology of self-assembled structures and *f* is a common practice in studies of self-assembly of diblock copolymers. For PEO-*b*-PCL in film rehydration method, the trend is known to be irregularly shaped particles, polymersomes, and spherical particles with increasing *f*.[32] Our observed trend for PEO-*b*-PCL follows this literature trend for PEO-*b*-PCL diblock copolymers (Figure 1A, black). Interestingly, our triblock copolymers, PEO-*b*-PCL-*b*-PMOXA, with PMOXA length of 5 and 10 units (Figure 1A, red and blue) also follow the literature trend for diblock copolymers. An exception is that PEO-*b*-PCL-*b*-PMOXA polymersomes have asymmetric membrane in

DOI: 10.1021/acs.macromol.7b01498
Macromolecules 2017, 50, 7155−7168

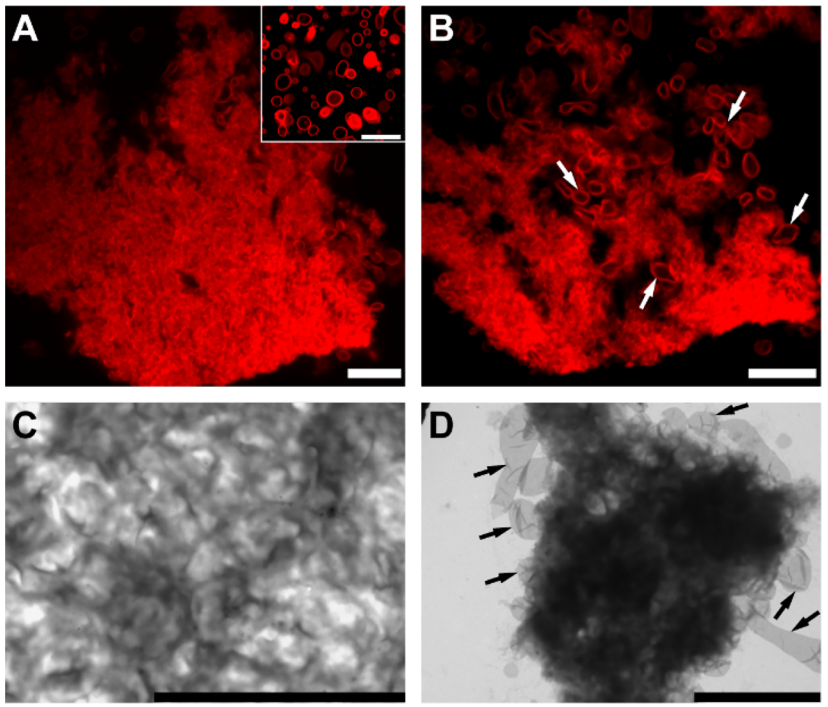

Figure 2. Characterization of cloud-like aggregates formed by $E_{45}C_{135}M_{20}$ in aqueous solution. (A, B) LSM images at different *z*-focal planes: (A) middle; (B) lower surface. Inset in image A represents polymersomes formed by this polymer ($E_{45}C_{135}M_{20}$) in PBS. Structures were stained with Bodipy 630/650. (C, D) TEM images of unstained cloud-like aggregates. Arrows on images B and D point out polymersomes, which are often found on the edges of cloud-like aggregates. Scale bars are 10 μm.

contrast to PEO-*b*-PCL polymersomes as we have shown previously.[16] We observe a part of radically different trends for PEO-*b*-PCL-*b*-PMOXA with PMOXA length of 20 and 25 units (Figure 1A, green and dark red). They consist of cloud-like aggregates (Figures 1E and 2) that have not been reported previously for any amphiphilic block copolymer. These aggregates have loosely packed branched structure without any defined pattern and with dimensions up to a few hundred micrometers (Figure 2A,C). Typically, these structures coexist with polymersomes often found on the edges of the cloud-like aggregates (indicated by arrows on Figure 2B,D). We discuss a possible reason for the formation of cloud-like aggregates further in the text.

So far, we have looked at morphology trends while increasing *f* by decreasing PCL length and keeping PMOXA length constant. However, for PEO-*b*-PCL-*b*-PMOXA, *f* can also be increased by increasing PMOXA length and keeping PCL length constant. Such flexibility in increasing *f* is, obviously, due to an additional degree of freedom brought into the system by C (PMOXA) block. Since there is lack of systematic data for ABC polymers in literature, morphology trends are not known for the case when *f* is varied through C block. We made a first attempt and revealed such (partial) morphology trends as discussed below.

In Figure 1A, we split the tested polymers into 3 groups with common morphology trends: polymers with PCL ∼50 units, polymers with PCL ∼60−130 units, and polymers with PCL ∼150 units. Polymers with the shortest PCL, ∼50 units, formed predominantly spherical particles and partially dissolved under the tested conditions. In the case of polymers with PCL ∼60−130 units, morphology of the structures changes in the order spherical particles (Figure 1B) to polymersomes (Figure 1D) to cloud-like aggregates (Figure 1E) with an increase in *f*. For polymers with PCL ∼150 units with an increase in *f* morphology of the structures changes from spherical particles/polymersomes to irregularly shaped particles (Figure 1C). Irregularly shaped particles are observed along with macroscopic precipitate and can be considered as smaller pieces of the insoluble polymer.

To explain formation of the observed self-assembled structures, we refer to packing geometry model. For AB diblock copolymers, packing geometry is defined by packing parameter *p*:[33]

$$p = \frac{\nu_B}{a_{A-B} l_B} \tag{2}$$

where a_{A-B} is the optimal area of the hydrophilic block A at the interface A−B and ν_B and l_B are the volume and critical length of the hydrophobic block B, respectively.

PEO-*b*-PCL polymers with PCL ∼150 units form polymersomes, and according to packing geometry model, individual molecules of these polymers are packed into cylinders (Scheme 2a). We speculate that addition of the PMOXA block does not influence packing geometry for the PEO−PCL interface but adds another area, a_{C-B}, and creates a new packing geometry at the C−B (PMOXA−PCL) interface (Scheme 2b). Such assumption is based on the immiscibility of PEO and PMOXA polymers in aqueous solution.[34,35] The final packing geometry of PEO-*b*-PCL-*b*-PMOXA molecules can be considered as a result of the superposition of two packing geometries for PEO−PCL and PMOXA−PCL interfaces. PEO-*b*-PCL-*b*-PMOXA with PCL ∼150 units precipitated in FR method, in contrast to the corresponding PEO-*b*-PCL polymers, which formed polymersomes and spherical particles. We attribute it to the appearance of PMOXA−PCL packing geometry, which corresponds to precipitate. The combination

DOI: 10.1021/acs.macromol.7b01498
Macromolecules 2017, 50, 7155−7168

Scheme 2. Illustration of the Packing Geometry of Polymers with ∼150 units of PCL: (a) AB and (b) ABC Resulting in Polymersomes and Irregularly Shaped Particles (Precipitate), Respectively

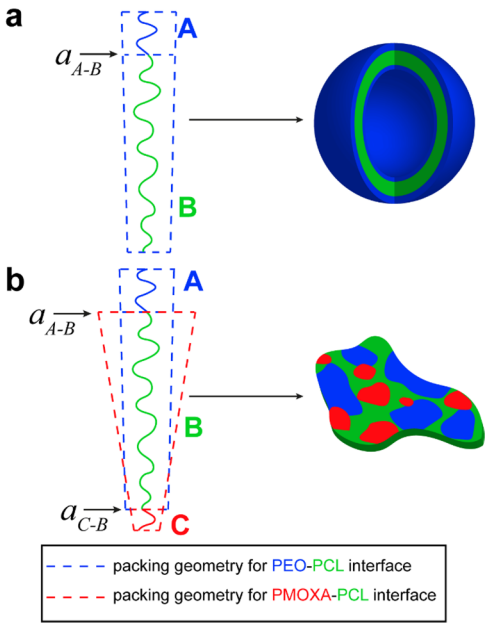

of long PCL and relatively short PMOXA results in high curvature at PMOXA−PCL interface, which prevents triblock copolymers from being dispersed, that is, hydrophobic attractive forces between PCL chains become predominant over repulsive forces between PEO and PMOXA chains, and the triblock copolymer remains as a precipitate.

Morphology of the self-assembled structures formed by polymers with PCL ∼60−130 units changes in the order spherical particles (PMOXA = 0 units) to polymersomes (PMOXA = 5−10 units, Figure 1D) to cloud-like aggregates (PMOXA = 20−25 units, Figure 1E and 2) with an increase in *f*. In this case, change of PCL length (∼60−130 units) has almost no effect on self-assembled morphology presumably due to the ability of PCL chains to compress or stretch in the fluid state (for PCL above T_m), which leads to the adjustment of a polymer molecule to a certain packing geometry.[33] PEO-*b*-PCL forms spherical particles composed of distinct domains, and such domains possess shapes ranging from spheres to rods (Figure 1B, inset, and Figure S3). Despite the mechanism of self-assembly of such particles remaining unclear, the packing geometry of PEO-*b*-PCL molecules can be attributed to a cone (spherical micelles) and truncated cylinder (rod-like micelles). For simplicity reasons, we generalize packing geometry of PEO-*b*-PCL forming spherical particles as a cone (Scheme 3a).

PEO-*b*-PCL-*b*-PMOXA polymers with PCL ∼60−130 and relatively short PMOXA (5−10 units) form polymersomes with diameters ∼3 μm (Figure 1D, Table 1). According to the Student's *t* test[36] with $p = 0.05$, the values of diameters are not significantly different. As discussed above, addition of the PMOXA block presumably introduces area a_{C-B} at the C−B (PMOXA−PCL) interface. Assuming that hydrophilic blocks are in the stretched conformation, the counter length of PEO (162.00 Å) is longer than that of PMOXA (for 5/10 units the length is 18.30/36.60 Å) (for calculations see Supporting Information). The approximate diameter of PEO chain (∼2 Å) is smaller compared to that of PMOXA (∼7 Å) due to the side

Scheme 3. Illustration of the Packing Geometry of Polymers with Fixed A and B (∼60−130 units) but Different C Block Lengths: (a) AB, (b) ABC with Short C Block, and (c) ABC with Long C Block

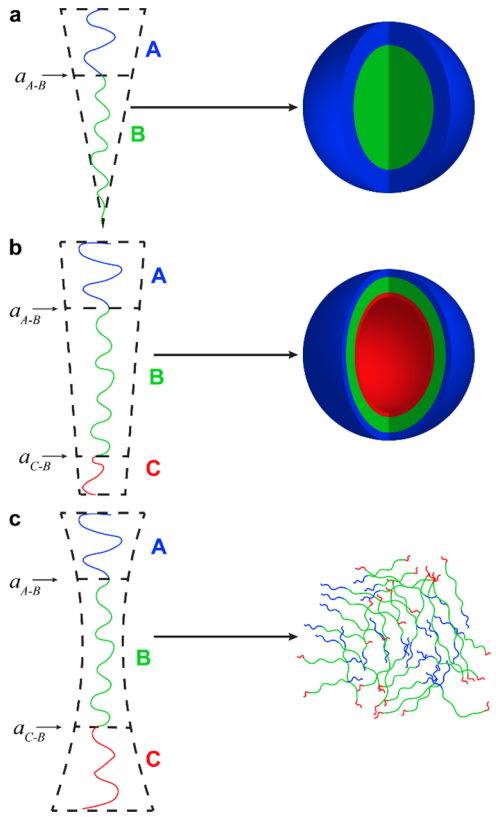

Table 1. Average Diameter of Polymersomes Formed by Different Polymers in Film Rehydration Method[a]

polymer	polymersome diameter, μm
$E_{45}C_{66}M_5$	2.4 ± 0.9
$E_{45}C_{103}M_4$	2.8 ± 1.2
$E_{45}C_{103}M_{12}$	3.1 ± 1.2
$E_{45}C_{110}M_4$	3.1 ± 1.2
$E_{45}C_{135}M_4$	3.5 ± 1.4
$E_{45}C_{135}M_{10}$	3.2 ± 1.3
$E_{45}C_{153}$	1.3 ± 0.5

[a]The diameter was determined based on at least 3 different LSM images containing at least 300 objects in total.

chain in PMOXA backbone, and this difference is likely to be larger in the hydrated state, since PEO needs 3 water molecules[37] and PMOXA 5.2 per repeating unit.[35] Nevertheless, due to much longer PEO length the resulting packing geometry of ABC molecules corresponds to a cylinder slightly truncated at the C side (Scheme 3b). Such packing geometry results in polymersomes with the inner surface formed by a shorter PMOXA block and the outer surface formed by a longer PEO block (Scheme 3b), which we indeed proved by two independent methods.[16]

PEO-*b*-PCL-*b*-PMOXA polymers with PCL ∼60−130 and relatively long PMOXA (20−25 units) self-assembled into cloud-like aggregates (Figure 1E and 2). We explain formation of such morphology by the increase of a_{C-B} interfacial area compared to PEO-*b*-PCL-*b*-PMOXA polymers with a shorter PMOXA (5−10 units) (Scheme 3c). In the case of PMOXA

DOI: 10.1021/acs.macromol.7b01498
Macromolecules 2017, 50, 7155−7168

20/25 units, its larger length (73.20/91.50 Å for 20/25 units) and diameter (~7 Å + 5.2 water molecules per repeating unit[35]) results in the increase of repulsive forces between hydrophilic chains, which compete with hydrophobic attractive forces between PCL chains. The packing geometry of ABC molecules in this case approaches the double cone shape (Scheme 3c). The aggregates have 3D-extended structure of several hundred micrometer size. Such branched structure with large size supposedly helps shield hydrophobic interactions from the aqueous environment. To support our assumption that cloud-like aggregates form due to strong hydrophilic repulsion between water-soluble chains, we tried to decrease these forces by performing self-assembly in the presence of salts. In PBS buffer such polymers form predominately polymersomes (Figure 2A, inset), suggesting that repulsion between hydrophilic chains indeed decreases in the presence of salts, and hence the packing geometry changes from double cone shape (Scheme 3c) to cylinder (Scheme 3b).

Solvent Evaporation Method. In solvent evaporation method, a polymer was dissolved in CH_2Cl_2 in a glass vial. After addition of water, the solution was stirred at 22 °C in the open vial until CH_2Cl_2 evaporated. Figure 3A summarizes the predominant structures formed by PEO-*b*-PCL-*b*-PMOXA and their precursors, PEO-*b*-PCL, in solvent evaporation method. Similar to film rehydration method, most of the polymers formed two or three types of structures, but to simplify the morphology diagram in Figure 3A, only predominant structures are plotted. More detailed information on morphology of the self-assembled structures can be found in Table S1.

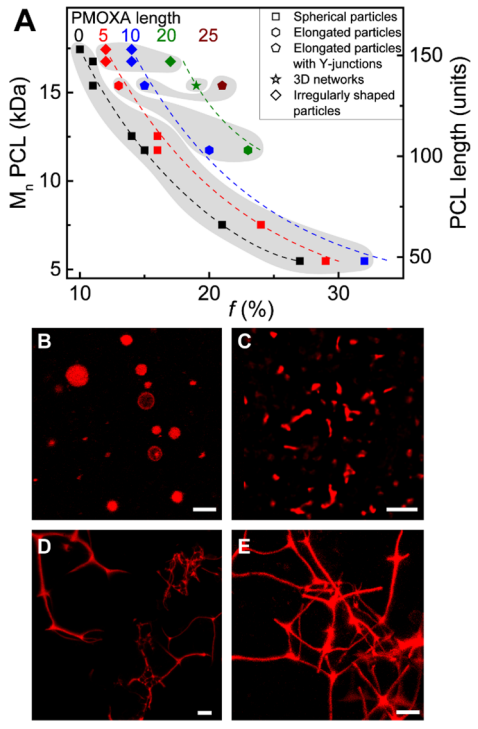

Figure 3. Self-assembled structures observed in solvent evaporation method. (A) Morphology diagram showing structures formed by PEO-*b*-PCL and PEO-*b*-PCL-*b*-PMOXA in aqueous solution as a function of the molecular composition. Points of each color correspond to polymers with a certain PMOXA length. Points of each shape correspond to a certain morphology: spherical particles (squares), elongated structures (hexagons), elongated structures with Y-junctions (pentagons), 3D networks (star), irregularly shaped particles (diamonds). The gray areas point out regions of the same morphology. Representative LSM images of the structures formed by (B) $E_{45}C_{153}$, spherical particles, (C) $E_{45}C_{103}M_{12}$, elongated particles. *z*-Projection of *z*-stack CLSM of the structures formed by (D) $E_{45}C_{135}M_{10}$, elongated particles with Y-junctions, and (E) $E_{45}C_{135}M_{20}$, 3D networks. Structures were stained with Bodipy 630/650. Scale bars are 5 μm.

In the absence of PMOXA block, that is, in the case of PEO-*b*-PCL, self-assembled structures are predominantly spherical particles with diameters 0.2−2 μm (Figure 3B; the range of diameters was determined from TEM). In the case of PEO-*b*-PCL-*b*-PMOXA with PMOXA 5, morphology of the structures changes in the order irregularly shaped particles to elongated particles to spherical particles with an increase in *f*. Morphology of the structures formed by PEO-*b*-PCL-*b*-PMOXA with PMOXA 10 undergoes transition irregularly shaped particles to elongated particles with Y-junctions (Figure 3D) to elongated particles (Figure 3C) to spherical particles with an increase in *f*. In the case of PEO-*b*-PCL-*b*-PMOXA with PMOXA length of 20 units, morphology of the self-assembled structures changes in the order irregularly shaped particles to 3D networks (Figure 3E) to elongated particles with an increase in *f*. Typical literature trend for PEO-*b*-PCL assembled under similar solvent evaporation conditions is irregularly shaped particles to polymersomes to spherical particles with increasing *f*.[38] Our morphology trends for PEO-*b*-PCL and PEO-*b*-PCL-*b*-PMOXA differ dramatically: we did not observe polymersomes as a predominant morphology. Interestingly, few PEO-*b*-PCL[38] polymers were reported to self-assemble into elongated structures, whereas our PEO-*b*-PCL with comparable molecular composition formed spherical particles.

To reveal morphology trends while *f* is varied through C block, we divide the tested polymers into 4 groups in Figure 3A: polymers with PCL ~50−70 units, polymers with PCL ~100 units, polymers with PCL ~130 units, and polymers with PCL ~150 units. Polymers with the shortest PCL, ~50−70 units, formed predominantly spherical particles. Morphology of the self-assembled structures formed by polymers with PCL ~100 units changes from spherical particles to elongated particles (Figure 3C) with increasing *f*. In the case of polymers with PCL ~130 units morphology of the structures changes in the order spherical particles to elongated particles to elongated particles with Y-junctions (Figure 3D) to 3D networks (Figure 3E) to elongated particles with Y-junctions with an increase in *f*. Morphology of the self-assembled structures formed by polymers with PCL ~150 units changes from spherical particles to irregularly shaped particles.

From the trends discussed above, one can observe some similarities between film rehydration and solvent evaporation methods: PEO-*b*-PCL form predominantly spherical particles; PEO-*b*-PCL-*b*-PMOXA with PCL ~50 units and ~150 units form spherical particles and irregularly shaped particles, respectively. These findings suggest little effect of the preparation method on the self-assembly of these particular polymers. On the other hand, PEO-*b*-PCL-*b*-PMOXA polymers with PCL ~60−130 units self-assemble into elongated rod-like structures in solvent evaporation method, while forming polymersomes and cloud-like aggregates in film rehydration method.

PEO-*b*-PCL-*b*-PMOXA polymers with PCL ~130 units form rods with Y-junctions and 3D microscale networks. Formation of such structures by amphiphilic block copolymers is rarely observed and so far was reported only for a few AB systems.[8,39]

DOI: 10.1021/acs.macromol.7b01498
Macromolecules 2017, 50, 7155−7168

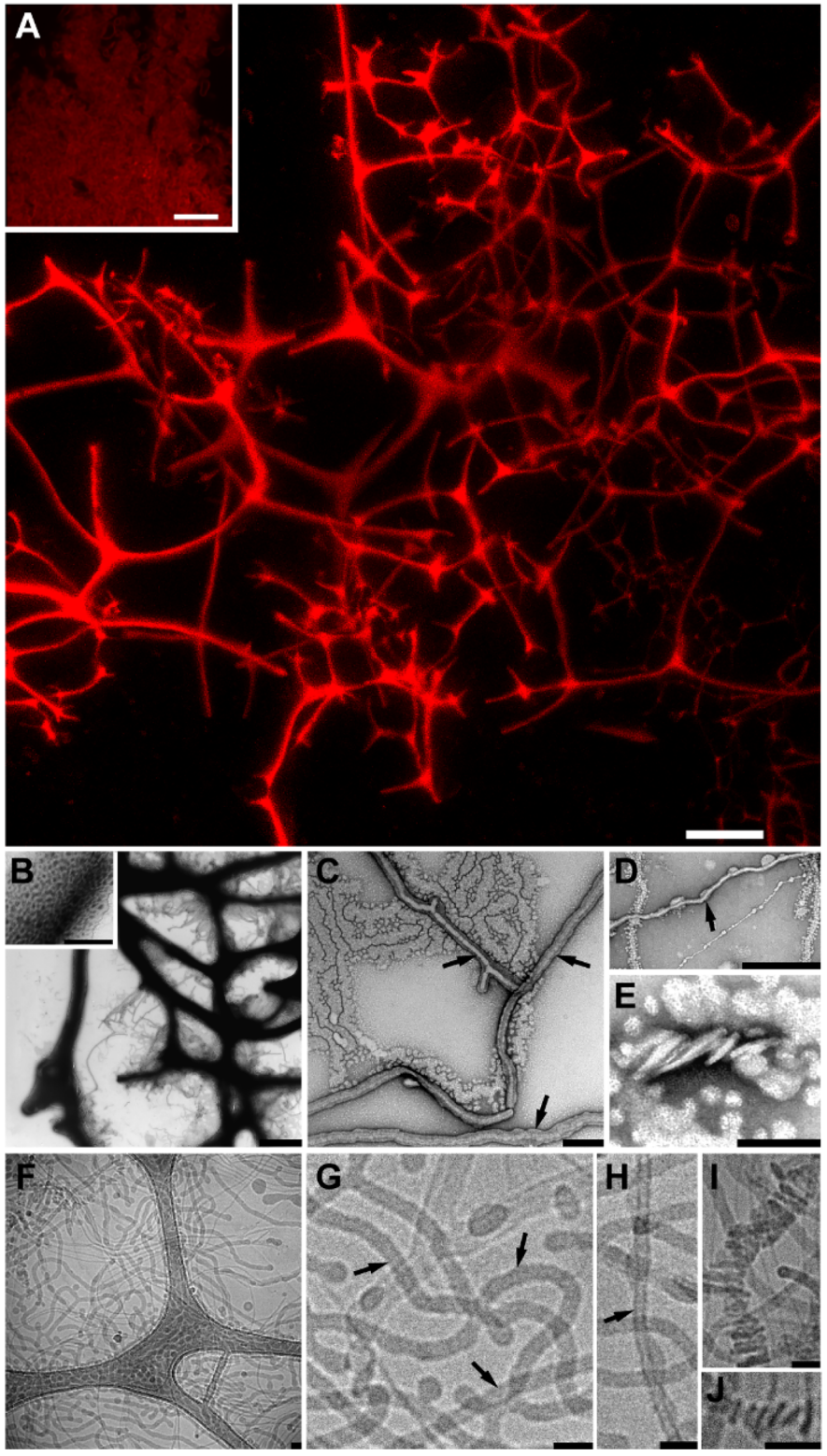

Figure 4. Characterization of 3D networks formed by $E_{45}C_{135}M_{20}$ in solvent evaporation method: (A) *z*-projection of *z*-stack CLSM; inset, cloud-like aggregates formed by the same polymer in film rehydration method (LSM); structures were stained with Bodipy 630/650; (B−E) negatively stained TEM; (F−J) cryoTEM. Scale bars: (A, A inset, B) 10 μm; (B inset, C−E) 1 μm; (F−J) 50 nm. The arrows on C, D, G, and H point out possibly hollow rods.

It is believed that such networks are formed above a critical molecular weight of the polymer.[8] Similarly to poly(ethylene oxide)-*block*-polybutadiene (PEO-*b*-PB) 3D nanoscale networks,[8] we also observed macroscopic phase separation in the case of PEO-*b*-PCL-*b*-PMOXA 3D microscale networks. To gain insight into the microscale structure of these networks, we characterized them using *z*-stack CLSM (Figure 4A). Interestingly, the polymer forming these networks,

DOI: 10.1021/acs.macromol.7b01498
Macromolecules 2017, 50, 7155−7168

$E_{45}C_{135}M_{20}$, assembles into 3D cloud-like aggregates in the film rehydration method (Figures 4A inset, 1E, and 2), suggesting the inherent tendency of this polymer to form branched 3D structures. 3D networks are composed of rods typically with a length of 5−50 μm and thickness up to 10 μm. To gain a better understanding of the structure of the networks at the nanoscale, we performed TEM (Figure 4B−E) and cryoTEM (Figure 4F−J) imaging. Since these techniques require a special sample preparation procedure, most of the microscale parts of 3D networks were blotted off. We found only one piece of networks in the negatively stained TEM sample (Figure 4B). The thickest rods of the networks might have porous structure (Figure 4B, inset). Some of the thinner rods with diameters ~20−200 nm possibly exhibit hollow structure (pointed out by arrows in Figure 4C,D,G,H), but this cannot be concluded without doubt. In some TEM and cryoTEM images, we observed rods that have helical structure or are composed of the disks stacked together (Figure 4E,I,J), and diameter of these rods ranges from ~20 up to ~500 nm.

Formation of the self-assembled structures observed in solvent evaporation method can be explained in the following way. Amphiphilic polymers dissolved in CH_2Cl_2 upon addition of water and stirring start to orient with their hydrophilic tails toward aqueous solution (Scheme 4). Diblock copolymers have only one hydrophilic tail, and therefore they form mainly I-shaped monolayers at the CH_2Cl_2−H_2O interface. Upon evaporation of the organic solvent, these monolayers transfer into aqueous solution in the form of spherical particles (Scheme 4a). Triblock copolymers have two water-soluble blocks, A and C, and both of them tend to transfer into water phase, thus resulting in U-shaped loops at the CH_2Cl_2−H_2O interface. When C block is relatively short, its attraction into water phase is weaker than that of PEO (i.e., 5.2 × 5 = 26 water molecules for PMOXA[35] 5 units vs 3 × 45 = 135 water molecules for PEO[37]). Triblock copolymers form a mixture of I-shaped monolayers and U-shaped loops, which upon evaporation of CH_2Cl_2 transfer into spherical particles and short rods (Scheme 4b). In the case of relatively long C block, its attraction into water phase becomes stronger (i.e., 52 water molecules for PMOXA 10 units vs 135 for PEO), and ABC molecules predominantly form loops at the CH_2Cl_2−H_2O interface. Upon evaporation of the organic solvent, these loops transfer into aqueous solution in the form of long rods (Scheme 4c). The microscale rods with thickness >140 nm (2 × length of triblock copolymer in U-shaped confirmation, see Supporting Information) might possess hollow morphology, but as has been shown for 3D networks (Figure 4), this cannot be concluded with certainty from LSM images due to limited resolution and from TEM or cryoTEM analysis due to sample preparation procedure leading to removal of thick rods.

Thus, spherical particles are observed for PEO-*b*-PCL polymers (Figure 2B), spherical and short elongated (<5 μm) particles are common for PEO-*b*-PCL-*b*-PMOXA polymers with short PMOXA (~5 units), and mostly long (>5 μm) elongated structures are observed for PEO-*b*-PCL-*b*-PMOXA with longer PMOXA (>5 units) (Figures 3C−E and 4, Table 2). Size values of the elongated structures scattered too much and could not be fitted with conventional functions for statistical analysis; therefore only the range of the lengths is provided in Table 2.

Scheme 4. Proposed Mechanism of Self-Assembly in Solvent Evaporation Method for (a) AB Polymers, (b) ABC with Short C, (c) ABC with Long C

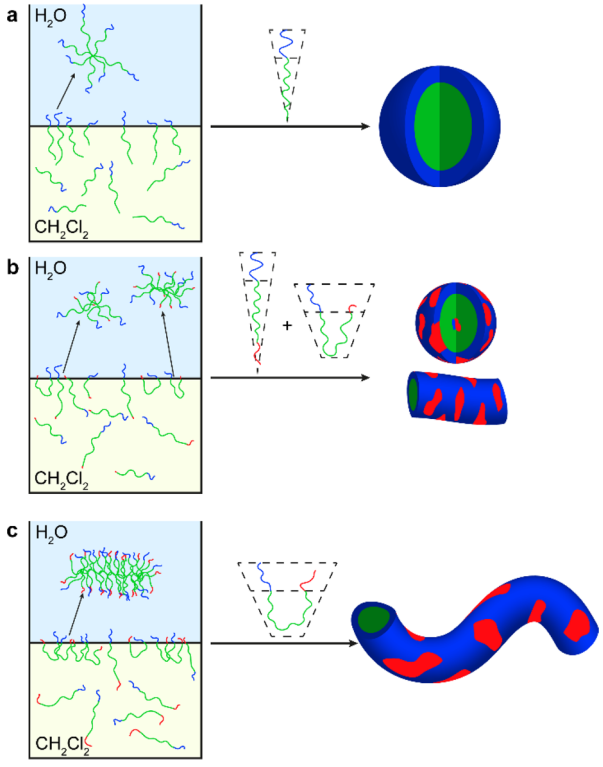

Table 2. Length of Elongated Structures Formed by Different PEO-*b*-PCL-*b*-PMOXA Polymers in Solvent Evaporation Method[a]

polymer	range of the lengths of elongated structures, μm
$E_{45}C_{48}M_3$	1.5−4.5
$E_{45}C_{66}M_5$	1.5−5
$E_{45}C_{110}M_4$	1−6
$E_{45}C_{103}M_{12}$	5−40
$E_{45}C_{135}M_{10}$	5−30
$E_{45}C_{135}M_{25}$	2−40

[a]The length was determined based on at least 3 different images containing at least 70 objects in total.

For PEO-*b*-PCL[38] and PEO-*b*-PCL-*b*-PMOXA elongated structures are uniquely accessible only via solvent evaporation method. As discussed above, we attribute formation of elongated structures to the presence of two terminal hydrophilic blocks. To prove the latter assumption, we compared self-assembly of diblock copolymer $E_{45}C_{153}$ (PEO(2.0K)-*b*-PCL(17.4K), $Đ_M$ = 1.08) and its analogue PEO(2.0K)-*b*-PCL(16.0K) ($Đ_M$ = 1.23) containing 26% of PEO-*b*-PCL-*b*-PEO species.[31] $E_{45}C_{153}$ assembled mainly into spherical particles, whereas polymer PEO(2.0K)-*b*-PCL(16.0K) formed mostly elongated and irregularly shaped structures in solvent evaporation method (Figure S4). These findings support the proposed mechanism of self-assembly of di- and triblock copolymers in solvent evaporation method and also possibly explain how PEO-*b*-PCL[38] formed elongated structures under similar conditions, since those polymers most likely contained some PEO-*b*-PCL-*b*-PEO species.[31]

Cosolvent Method. In cosolvent method, a polymer was dissolved in THF, and the resulting solution was added

DOI: 10.1021/acs.macromol.7b01498
Macromolecules 2017, 50, 7155−7168

dropwise into a glass vial with stirred aqueous solution. The mixture was stirred at 22 °C in the closed vial. In this method, we tested only polymers with PCL 110−153 units, because polymers already with PCL 110 units dissolved under these conditions.

Figure 5A depicts the predominant structures formed by PEO-*b*-PCL-*b*-PMOXA and their precursors, PEO-*b*-PCL, in

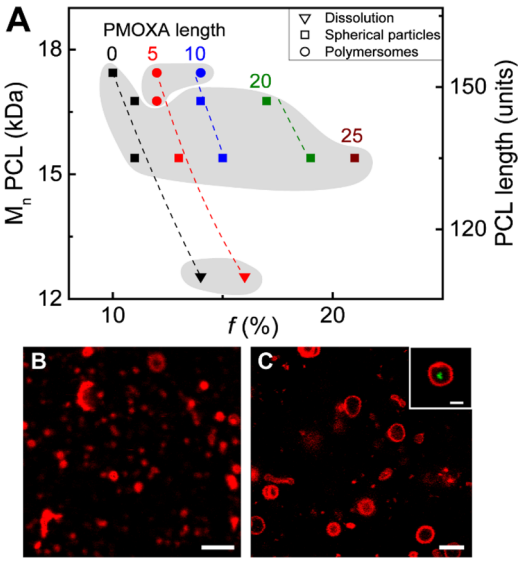

Figure 5. Self-assembled structures observed in cosolvent method. (A) Morphology diagram showing structures formed by PEO-*b*-PCL and PEO-*b*-PCL-*b*-PMOXA in aqueous solution as a function of the molecular composition. Points of each color correspond to polymers with a certain PMOXA length. Points of each shape correspond to a certain morphological state: dissolution (triangles), spherical particles (squares), polymersomes (circles). The gray areas point out regions of the same morphology. Representative LSM images of the structures formed by (B) $E_{45}C_{135}M_{10}$, spherical particles, and (C) $E_{45}C_{153}M_{11}$, polymersomes. Structures were stained with Bodipy 630/650. Scale bars are 5 μm. Inset in the image C represents polymersomes with encapsulated hydrophilic dye calcein; scale bar is 2 μm.

cosolvent method. Similar to film rehydration and solvent evaporation methods, most of the polymers formed two or three types of structures, but to simplify the morphology diagram in Figure 5A, only predominant structures are plotted. More detailed information on morphology of the self-assembled structures can be found in Table S1.

PEO-*b*-PCL, that is, where PMOXA length is 0, self-assembled predominantly into spherical particles with diameters 0.2−1.5 μm (determined from TEM). In the case of PEO-*b*-PCL-*b*-PMOXA with PMOXA 5 and 10 units, morphology of the self-assembled structures changes from polymersomes to spherical particles (Figure 5B), and the polymers then dissolve with an increase in *f*. PEO-*b*-PCL-*b*-PMOXA with PMOXA 20 and 25 units self-assembled into spherical particles.

Morphology trends when *f* is varied through C block are the following. Polymers with PCL 110 units predominantly dissolved in cosolvent method. The diblock copolymer formed some spherical particles, whereas the triblock copolymer dissolved completely and resulted in optically transparent solution. Such self-assembly behavior of the triblock copolymer can be attributed to the weakening of hydrophobic interactions between PCL chains in the presence of THF, which are not able to compensate hydrophilic repulsive forces in the corona. Polymers with PCL 135 units self-assembled into spherical particles (Figure 5B), which is analogous to the case of PCL ∼50 units in film rehydration method. Morphology of the structures formed by polymers with PCL 147 changes in the order spherical particles to polymersomes to spherical particles with increasing *f*. For polymers with PCL 153 units, with an increase in *f* morphology undergoes transition from spherical particles to polymersomes (Figure 5C), which is analogous to the trend observed for PCL ∼60−130 units in film rehydration method. The average diameter of polymersomes formed in cosolvent method is ∼3 μm (Table 3), which is similar to the ones formed in film rehydration method (Table 1).

Table 3. Average Diameter of Polymersomes Formed by PEO-*b*-PCL-*b*-PMOXA Polymers in Cosolvent Method[a]

polymer	polymersome diameter, μm
$E_{45}C_{147}M_4$	2.4 ± 0.6
$E_{45}C_{153}M_4$	2.5 ± 0.8
$E_{45}C_{153}M_{11}$	3.3 ± 0.9

[a]The diameter was determined based on at least 3 different LSM images containing at least 300 objects in total.

To the best of our knowledge, there are no studies reporting about systematic investigation of self-assembly of PEO-*b*-PCL in cosolvent method. In the case of our polymers, cosolvent method allowed us to expand the range of the self-assembled structures for polymers that precipitated in film rehydration and solvent evaporation methods. The key difference of cosolvent method is the presence of 20% THF in the self-assembly mixture. Considering the packing geometry model, we assume that this solvent composition does not change interactions between PEO chains, because this block is soluble in both water and THF. THF is a good solvent for the PCL block, and therefore THF−H_2O mixture is able to solubilize partially the PCL block. Thus, the effective v_B and l_B occupied by the PCL block changes, leading to different self-assembly behavior of PEO-*b*-PCL polymers compared to film rehydration and solvent evaporation methods (Scheme 5a). For example, while forming predominantly polymersomes in film rehydration method, $E_{45}C_{153}$ self-assembled into spherical particles and partially dissolved in cosolvent method. The presence of 20% THF has similar effect in the case of PEO-*b*-PCL-*b*-PMOXA, insoluble in film rehydration and solvent evaporation methods, but the self-assembled morphology changes from precipitate to polymersomes (Scheme 5b).

The morphological trend observed for polymers with PCL 147 (spherical particles to polymersomes to spherical particles) is not completely clear, but it might deal with partial solubility of PMOXA in THF−H_2O mixture. PMOXA homopolymer precipitates in THF. In the case of $E_{45}C_{147}M_4$ formation of polymersomes can be explained as described above (Scheme 5b). With further increase of PMOXA length, its insolubility in THF−H_2O mixture becomes more pronounced, and probably PMOXA block tends to collapse resulting in structures with only one completely soluble block, PEO.

As has been shown for some amphiphilic diblock copolymers,[11,40,41] the nature of a cosolvent (i.e., a common solvent for both blocks) has a dramatic effect on the observed morphology. To check whether the nature of the cosolvent affects self-assembly of PEO-*b*-PCL-*b*-PMOXA polymers, we tested the self-assembly of $E_{45}C_{153}M_4$ using different cosolvents: DMF, ACN, and acetone. These solvents are

DOI: 10.1021/acs.macromol.7b01498
Macromolecules 2017, 50, 7155−7168

Scheme 5. Illustration How Packing Geometry of (a) AB and (b) ABC Polymers Changes in the Presence of 20% THF

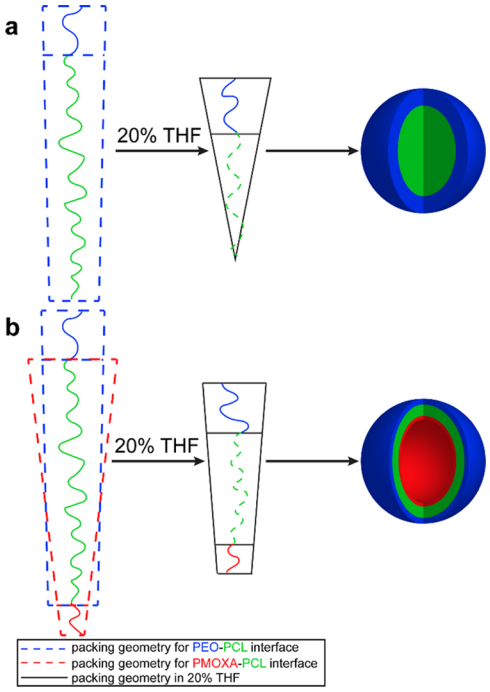

among very few ones able to dissolve our triblock copolymers. The change of the cosolvent led to the formation of completely different aggregates, which were not observed when THF was used as a cosolvent (Figure 6 and Figure S5). On the other hand, the assemblies obtained in the presence of DMF, ACN, or acetone possessed quite similar structures with three-dimensionality. These observations can be explained by only partial solubility of PCL block in these solvents, whereas THF dissolves PCL completely,[42] suggesting its unique role in the self-assembly behavior of PEO-*b*-PCL-*b*-PMOXA polymers.

Equilibrium or Kinetically Frozen Morphologies? Formation of diverse structures by PEO-*b*-PCL-*b*-PMOXA in different self-assembly methods suggests that one or all methods result in morphologies that are under kinetic control. Thermodynamically controlled structures should be insensitive to details in preparation procedure, whereas kinetically controlled morphologies are highly path dependent.[6,7] Therefore, to gain a better understanding about self-assembly equilibrium, we studied how change of details in film rehydration, solvent evaporation, and cosolvent methods influences self-assembly. For the latter purpose, we chose polymers $E_{45}C_{110}M_4$, $E_{45}C_{135}M_4$, and $E_{45}C_{135}M_{20}$ as they have different PCL and PMOXA lengths and self-assemble into different microscale structures. In film rehydration method, stirring rate (300−800 rpm), duration of self-assembly (6−48 h), and conditions of polymer film formation did not influence the self-assembled morphology of the selected polymers. Employment of different heating and cooling conditions for self-assembly also did not affect the type and size of the structures (Figure 7, Figure S6). These findings suggest that the structures formed in film rehydration method are energetically favorable and the system is on the way to approach thermodynamic equilibrium. The diameter values of polymersomes possessed high deviation (~40%) from the mean diameter value (Table 1). This deviation can be partially attributed to the dispersity of the polymers and the presence of ~15% high molecular weight impurities.[16] We assume, however, that the main reason for this high deviation, as well as for the coexistence of multiple morphologies (Table S1, Figure S2), is the fact that the system does not fully achieve global equilibrium on the experimental time scale (24 h), which is associated with hindered structural evolution due to slow kinetics of high molecular weight polymers.[7,43] Longer experimental times (>24 h) are problematic because of high temperature (62 °C): water evaporates from the solution containing self-assembled structures and condenses on the walls of the flask above the solution. Further in the text, we refer to the structures formed in film rehydration method as pseudoequilibrium morphologies, because the system might be on the way to achieving global equilibrium in this method.

As has been shown for most of AB[8,44−46] and ABC[30] systems in A-selective solvent, the type of morphology usually changes in the order polymersomes to elongated micelles to spherical micelles with the increase of *f*. Assemblies formed by PEO-*b*-PCL[32] and PEO-*b*-PCL-*b*-PMOXA are exceptions to this rule. These polymers do not form elongated micelles in film rehydration method and self-assemble into microscale structures, whereas most of the systems result in nanoscale assemblies. These observations are associated with the semicrystalline nature of the PCL block and can be possibly attributed to the formation of PCL spherulites in the bulk phase,[47] which might affect formation of the core of the self-assembled structures.

The type of the resulting morphology in the case of solvent evaporation method is strongly influenced by self-assembly conditions, such as stirring speed and position of a magnetic stir bar. For example, while forming mostly 3D networks under standard solvent evaporation conditions (350 rpm), $E_{45}C_{135}M_{20}$ assembled mostly into spherical and some elongated particles at 500 rpm, whereas 100 rpm did not result in self-assembly, but the polymer aggregated into one big piece. Also, when the vial

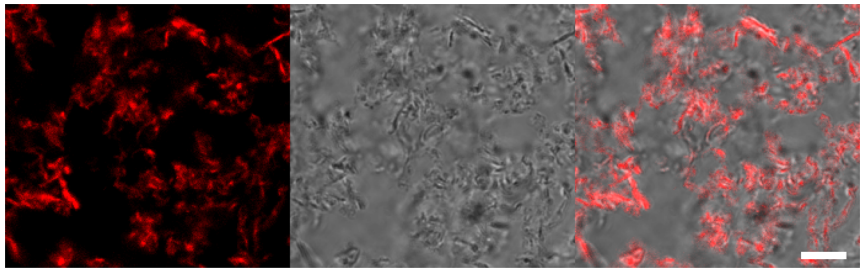

Figure 6. From left to right, LSM, bright field, and their overlay image of the aggregates formed by $E_{45}C_{153}M_4$ obtained using acetone as a cosolvent. Structure was stained with Bodipy 630/650. Scale bar is 10 μm.

DOI: 10.1021/acs.macromol.7b01498
Macromolecules 2017, 50, 7155−7168

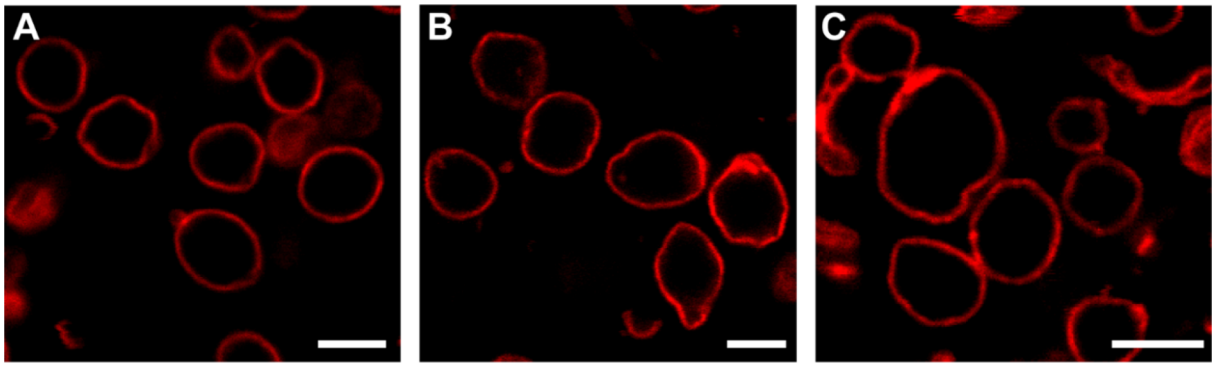

Figure 7. LSM images of the polymersomes formed by $E_{45}C_{110}M_4$ obtained using film rehydration method under different cooling/heating conditions: (A) standard procedure; (B) slow heating; (C) slow cooling. Structures were stained with Bodipy 630/650. Scale bars are 5 μm.

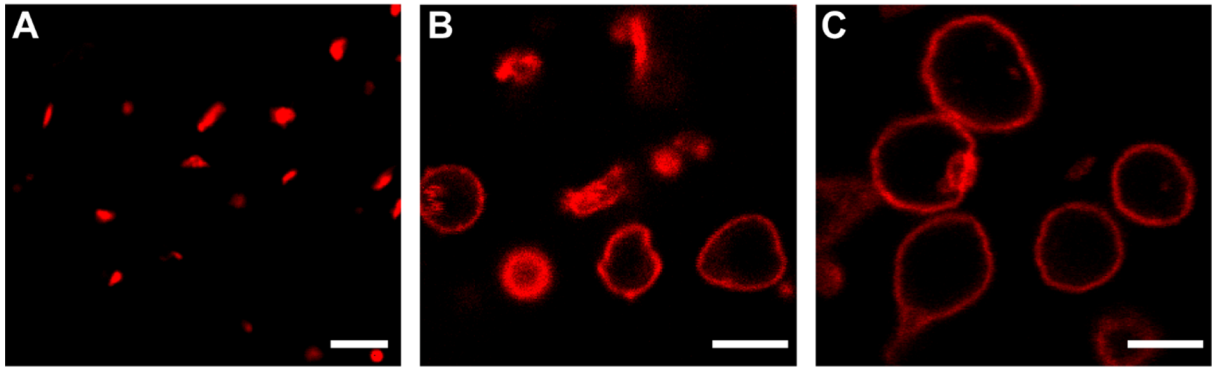

Figure 8. LSM images of the self-assembled structures formed by $E_{45}C_{110}M_4$ in different self-assembly methods: (A) solvent evaporation; (B) solvent evaporation followed by incubation at 62 °C for 24 h; (C) film rehydration. Structures were stained with Bodipy 630/650. Scale bars are 5 μm.

was placed on the side of a stirring plate, and therefore the magnetic stir bar inside located at the side of the vial, 3D networks appeared to be much longer and more branched compared when the vial was at the central position. Some other polymers ($E_{45}C_{110}M_4$, $E_{45}C_{135}M_{10}$, and $E_{45}C_{135}M_{25}$) also formed extended parts of networks under such conditions. Thus, the data indicate that the structures formed in solvent evaporation method are under kinetic control.

In cosolvent method, the type of the resulting morphology is sensitive to the preparation procedure. For instance, when THF solution of $E_{45}C_{153}M_4$ was added more slowly (~40 μL·min^{-1}) into the aqueous stirring solution, the polymer self-assembled into spherical particles but not into polymersomes as under standard conditions (~200 μL·min^{-1}). On the basis of these observations, we concluded that the structures obtained in cosolvent method are under kinetic control.

Transition from Kinetically Frozen to Pseudoequilibrium Morphologies. Kinetically controlled morphologies may undergo transition toward equilibrium structures, for example, as has been demonstrated for poly(acrylic acid)-*block*-polystyrene (PAA-*b*-PS) system in organic solvent−water mixtures by Eisenberg and co-workers.[48,49] In the case of PEO-*b*-PCL-*b*-PMOXA polymers, the transition from kinetically trapped morphologies obtained in solvent evaporation technique to pseudoequilibrium structures observed in film rehydration method is highly unlikely to happen under ambient temperatures due to the semicrystalline nature of the PCL block: the structures obtained in solvent evaporation method were stable for at least 6 months at room temperature. Therefore, to test such transformation, we incubated at 62 °C for 24 h the structures formed by $E_{45}C_{110}M_4$, $E_{45}C_{135}M_4$, and $E_{45}C_{135}M_{20}$ in solvent evaporation method after their self-assembly. After incubation at 62 °C, the assemblies formed by these polymers partially transferred to the ones formed in film rehydration method (Figure 8, Figure S7). These findings confirm that (i) the morphologies formed in solvent evaporation method are under kinetic control and (ii) the transition from kinetically trapped to pseudoequilibrium structures is possible above the melting temperature of the PCL block, which allows for its structural rearrangements.

In solvent evaporation method, elongated structures are the result of the formation of ABC loops at the CH_2Cl_2−H_2O interface and their further aggregation in aqueous solution upon evaporation of CH_2Cl_2 (Scheme 4). Such structures might be not energetically favorable due to a tension at the bending site of the PCL loop and repulsive forces between PEO and PMOXA corona. This could explain why above T_m of PCL, structures obtained in solvent evaporation method transform into structures observed in film rehydration method, which are energetically more favorable. Solvent evaporation method performed at 62 °C should also lead to pseudoequilibrium morphologies, but fast evaporation of the organic solvent (CH_2Cl_2 or $CHCl_3$) led to the formation of the polymer layer on top of the aqueous solution preventing it from self-assembly.

In cosolvent method, THF is present during self-assembly and modifies packing geometry of the polymer molecules compared to film rehydration method (Scheme 5). The latter suggests that THF is involved in stabilization of the assembled morphologies. Nevertheless, polymersomes formed by $E_{45}C_{153}M_{11}$ in cosolvent method were stable after a week of dialysis against water (Figure 5C, inset). However, after a year of storage at room temperature, these polymersomes collapsed

DOI: 10.1021/acs.macromol.7b01498
Macromolecules 2017, 50, 7155−7168

into spherical particles. Such transition was possible presumably due to the presence of residual THF trapped in the hydrophobic core that enabled structural rearrangements of the PCL block. In contrast to cosolvent method, structures formed in film rehydration method, where organic solvent was removed before self-assembly, were stable for at least a year of storage at room temperature. The true equilibrium morphologies for cosolvent method cannot be determined due to the uncertain amount of THF present in the system during storage.

CONCLUSIONS

We reported new aqueous self-assembled structures of micrometer size for amphiphilic triblock copolymers in the example of PEO-*b*-PCL-*b*-PMOXA: cloud-like aggregates and 3D networks.

Morphology trends of diblock copolymers PEO-*b*-PCL are maintained globally the same for all used self-assembly methods: polymersomes to spherical particles with increasing *f*. In contrast, morphology trends of triblock copolymers PEO-*b*-PCL-*b*-PMOXA depend on the self-assembly method and how *f* is varied, through PCL or PMOXA block.

In film rehydration method, the system is on the way to achieving global equilibrium, and we refer to the structures formed in this method as pseudoequilibrium morphologies. Solvent evaporation and cosolvent techniques led to kinetically controlled structures. The kinetically controlled morphologies formed in solvent evaporation method can be transformed, at least partially, to the pseudoequilibrium morphologies above T_m of PCL. In cosolvent method, the type of morphology strongly depended on the cosolvent nature.

The presented family of PEO-*b*-PCL-*b*-PMOXA polymers and their self-assembled structures can be relevant for biomedical applications due to the biocompatible and protein-repellent nature of PEO[50] and PMOXA[51] corona and biodegradability of PCL core.[52,53] Elongated structures and 3D networks formed by PEO-*b*-PCL-*b*-PMOXA are uniquely accessible via solvent evaporation technique. These structures are promising candidates for drug delivery purposes, since anisotropic morphologies possess longer blood circulation time compared to the spherical analogues,[54] and 3D networks based on biodegradable polymers are of special interest for tissue engineering purposes.[55,56] In addition, self-assembled structures formed by PEO-*b*-PCL-*b*-PMOXA possess enormous stability due to the semicrystalline nature of the PCL block: the assemblies formed in film rehydration and solvent evaporation methods were stable after at least 6 months of storage at room temperature, and the structures stayed intact after shaking and centrifugation at 13000*g* for 1−2 h.

Polymersomes formed by ABC triblock copolymers with immiscible A and C blocks should be thermodynamically stable due to different curvature at A−B and C−B interfaces. To definitely prove this, one needs to investigate additionally formation of polymersomes by other narrowly dispersed ABC polymers with amorphous B block with low glass transition temperature (<20 °C).

The conclusions drawn from self-assembly of PEO-*b*-PCL-*b*-PMOXA may not necessarily fully apply to other ABC systems in (A, C)-selective solvent. The semicrystalline nature of the PCL block is responsible for micrometer sizes of the obtained structures and may dictate the trends in the self-assembly of the tested polymers. Therefore, to establish general rules for ABC self-assembly in (A, C)-selective solvents, similar studies should be performed for other ABC systems where B is an amorphous block and the self-assembled structures possess nanometer sizes. In addition, to acquire the full advantage of the complex composition of self-assembled morphologies of PEO-*b*-PCL-*b*-PMOXA, presence of patches or Janus corona due to the phase separation of PEO and PMOXA blocks[34,35] should be investigated.

ASSOCIATED CONTENT

Supporting Information

The Supporting Information is available free of charge on the ACS Publications website at DOI: 10.1021/acs.macromol.7b01498.

Additional experimental details, DSC of polymers $E_{45}C_{110}M_4$, $E_{45}C_{135}M_{20}$, and $E_{45}C_{153}M_4$, LSM images of the self-assembled structures obtained using film rehydration method and solvent evaporation method, characterization of polymers and their microscale self-assembled structures, representative TEM images of negatively stained particles, equations for estimation of lengths and diameters, LSM and bright field images of $E_{45}C_{153}M_4$ obtained using different cosolvents, and $E_{45}C_{153}M_4$ and $E_{45}C_{135}M_{20}$ using different cooling and heating conditions, and *z*-projection of *z*-stack CLSM and LSM images of the self-assembled structures (PDF)

AUTHOR INFORMATION

Corresponding Authors

*E-mail: ev.konishcheva@gmail.com.
*E-mail: wolfgang.meier@unibas.ch.

ORCID

Evgeniia V. Konishcheva: 0000-0003-2995-6279
Wolfgang Meier: 0000-0002-7551-8272

Notes

The authors declare no competing financial interest.

ACKNOWLEDGMENTS

SNSF, NCCR Molecular Systems Engineering, and the University of Basel are acknowledged for financial support. We thank Carola Alampi (C−CINA, University of Basel) for cryoTEM, Samuel Lörcher (University of Basel) for TEM, and Dr. Alexia Loynton-Ferrand (IMCF, University of Basel) for help with *z*-stack CLSM experiments. E.K. acknowledges Dr. Alina Sekretaryova and Dr. Onur Parlak (Stanford University) for fruitful discussions and useful comments.

REFERENCES

(1) Ball, P., H2O. A Biography of Water. *Phoenix*; Orion Books Ltd., London, 2000.
(2) Discher, D. E.; Ahmed, F. POLYMERSOMES. *Annu. Rev. Biomed. Eng.* **2006**, *8* (1), 323−341.
(3) Penczek, S.; Cypryk, M.; Duda, A.; Kubisa, P.; Słomkowski, S. Living ring-opening polymerizations of heterocyclic monomers. *Prog. Polym. Sci.* **2007**, *32* (2), 247−282.
(4) Sedlacek, O.; Monnery, B. D.; Filippov, S. K.; Hoogenboom, R.; Hruby, M. Poly(2-Oxazoline)s − Are They More Advantageous for Biomedical Applications Than Other Polymers? *Macromol. Rapid Commun.* **2012**, *33* (19), 1648−1662.
(5) Braunecker, W. A.; Matyjaszewski, K. Controlled/living radical polymerization: Features, developments, and perspectives. *Prog. Polym. Sci.* **2007**, *32* (1), 93−146.
(6) Mai, Y.; Eisenberg, A. Self-assembly of block copolymers. *Chem. Soc. Rev.* **2012**, *41* (18), 5969−5985.

DOI: 10.1021/acs.macromol.7b01498
Macromolecules 2017, 50, 7155−7168

(7) Jain, S.; Bates, F. S. Consequences of Nonergodicity in Aqueous Binary PEO−PB Micellar Dispersions. *Macromolecules* **2004**, *37* (4), 1511−1523.
(8) Jain, S.; Bates, F. S. On the Origins of Morphological Complexity in Block Copolymer Surfactants. *Science* **2003**, *300* (5618), 460−464.
(9) Zhang, L.; Eisenberg, A. Multiple Morphologies of "Crew-Cut" Aggregates of Polystyrene-*b*-poly(acrylic acid) Block Copolymers. *Science* **1995**, *268* (5218), 1728−1731.
(10) Zhang, L.; Eisenberg, A. Formation of crew-cut aggregates of various morphologies from amphiphilic block copolymers in solution. *Polym. Adv. Technol.* **1998**, *9* (10−11), 677−699.
(11) Dionzou, M.; Morere, A.; Roux, C.; Lonetti, B.; Marty, J. D.; Mingotaud, C.; Joseph, P.; Goudouneche, D.; Payre, B.; Leonetti, M.; Mingotaud, A. F. Comparison of methods for the fabrication and the characterization of polymer self-assemblies: what are the important parameters? *Soft Matter* **2016**, *12* (7), 2166−2176.
(12) Terreau, O.; Bartels, C.; Eisenberg, A. Effect of Poly(acrylic acid) Block Length Distribution on Polystyrene-b-poly(acrylic acid) Block Copolymer Aggregates in Solution. 2. A Partial Phase Diagram. *Langmuir* **2004**, *20* (3), 637−645.
(13) Braun, J.; Bruns, N.; Pfohl, T.; Meier, W. Phase Behavior of Vesicle-Forming Block Copolymers in Aqueous Solutions. *Macromol. Chem. Phys.* **2011**, *212* (12), 1245−1254.
(14) Walther, A.; Millard, P.-E.; Goldmann, A. S.; Lovestead, T. M.; Schacher, F.; Barner-Kowollik, C.; Müller, A. H. E. Bis-Hydrophilic Block Terpolymers via RAFT Polymerization: Toward Dynamic Micelles with Tunable Corona Properties. *Macromolecules* **2008**, *41* (22), 8608−8619.
(15) Zhu, W.; Li, Y.; Liu, L.; Zhang, W.; Chen, Y.; Xi, F. Biamphiphilic triblock copolymer micelles as a multifunctional platform for anticancer drug delivery. *J. Biomed. Mater. Res., Part A* **2011**, *96A* (2), 330−340.
(16) Konishcheva, E. V.; Zhumaev, U. E.; Meier, W. P. PEO-b-PCL-b-PMOXA Triblock Copolymers: From Synthesis to Microscale Polymersomes with Asymmetric Membrane. *Macromolecules* **2017**, *50* (4), 1512−1520.
(17) Stoenescu, R.; Meier, W. Vesicles with asymmetric membranes from amphiphilic ABC triblock copolymers. *Chem. Commun. (Cambridge, U. K.)* **2002**, *24*, 3016−7.
(18) Liu, F.; Eisenberg, A. Preparation and pH Triggered Inversion of Vesicles from Poly(acrylic Acid)-block-Polystyrene-block-Poly(4-vinyl Pyridine). *J. Am. Chem. Soc.* **2003**, *125* (49), 15059−15064.
(19) Mason, A. F.; Thordarson, P. Polymersomes with Asymmetric Membranes Based on Readily Accessible Di- and Triblock Copolymers Synthesized via SET-LRP. *ACS Macro Lett.* **2016**, *5* (10), 1172−1175.
(20) Wittemann, A.; Azzam, T.; Eisenberg, A. Biocompatible Polymer Vesicles from Biamphiphilic Triblock Copolymers and Their Interaction with Bovine Serum Albumin. *Langmuir* **2007**, *23* (4), 2224−2230.
(21) Liu, Q.; Chen, J.; Du, J. Asymmetrical Polymer Vesicles with a "Stealthy" Outer Corona and an Endosomal-Escape-Accelerating Inner Corona for Efficient Intracellular Anticancer Drug Delivery. *Biomacromolecules* **2014**, *15* (8), 3072−3082.
(22) Stoenescu, R.; Graff, A.; Meier, W. Asymmetric ABC-triblock copolymer membranes induce a directed insertion of membrane proteins. *Macromol. Biosci.* **2004**, *4* (10), 930−5.
(23) Stoenescu, R.; Meier, W. Asymmetric Membranes from Amphiphilic ABC Triblock Copolymers. *Mol. Cryst. Liq. Cryst.* **2004**, *417* (1), 185−191.
(24) Liu, G.; Ma, S.; Li, S.; Cheng, R.; Meng, F.; Liu, H.; Zhong, Z. The highly efficient delivery of exogenous proteins into cells mediated by biodegradable chimaeric polymersomes. *Biomaterials* **2010**, *31* (29), 7575−7585.
(25) Schmalz, H.; Schmelz, J.; Drechsler, M.; Yuan, J.; Walther, A.; Schweimer, K.; Mihut, A. M. Thermo-Reversible Formation of Wormlike Micelles with a Microphase-Separated Corona from a Semicrystalline Triblock Terpolymer. *Macromolecules* **2008**, *41* (9), 3235−3242.
(26) Walther, A.; Barner-Kowollik, C.; Müller, A. H. E. Mixed, Multicompartment, or Janus Micelles? A Systematic Study of Thermoresponsive Bis-Hydrophilic Block Terpolymers. *Langmuir* **2010**, *26* (14), 12237−12246.
(27) Dag, A.; Zhao, J.; Stenzel, M. H. Origami with ABC Triblock Terpolymers Based on Glycopolymers: Creation of Virus-Like Morphologies. *ACS Macro Lett.* **2015**, *4* (5), 579−583.
(28) Barthel, M. J.; Schacher, F. H.; Schubert, U. S. Poly(ethylene oxide) (PEO)-based ABC triblock terpolymers - synthetic complexity vs. application benefits. *Polym. Chem.* **2014**, *5* (8), 2647−2662.
(29) Gröschel, A. H.; Schacher, F. H.; Schmalz, H.; Borisov, O. V.; Zhulina, E. B.; Walther, A.; Müller, A. H. E. Precise hierarchical self-assembly of multicompartment micelles. *Nat. Commun.* **2012**, *3*, 710.
(30) Löbling, T. I.; Borisov, O.; Haataja, J. S.; Ikkala, O.; Gröschel, A. H.; Müller, A. H. E. Rational design of ABC triblock terpolymer solution nanostructures with controlled patch morphology. *Nat. Commun.* **2016**, *7*, 12097.
(31) Konishcheva, E.; Häussinger, D.; Lörcher, S.; Meier, W. Key aspects to yield low dispersity of PEO-b-PCL diblock copolymers and their mesoscale self-assembly. *Eur. Polym. J.* **2016**, *83*, 300−310.
(32) Qi, W.; Ghoroghchian, P. P.; Li, G.; Hammer, D. A.; Therien, M. J. Aqueous self-assembly of poly(ethylene oxide)-block-poly(?-caprolactone) (PEO-b-PCL) copolymers: disparate diblock copolymer compositions give rise to nano- and meso-scale bilayered vesicles. *Nanoscale* **2013**, *5* (22), 10908−10915.
(33) Israelachvili, J. N. *Intermolecular and surface forces*; Academic press: 2011.
(34) Taubert, A.; Furrer, E.; Meier, W. Water-in-water mesophases for templating inorganics. *Chem. Commun.* **2004**, *19*, 2170−2171.
(35) Casse, O.; Shkilnyy, A.; Linders, J.; Mayer, C.; Häussinger, D.; Völkel, A.; Thünemann, A. F.; Dimova, R.; Cölfen, H.; Meier, W.; Schlaad, H.; Taubert, A. Solution Behavior of Double-Hydrophilic Block Copolymers in Dilute Aqueous Solution. *Macromolecules* **2012**, *45* (11), 4772−4777.
(36) Student. The probable error of a mean. *Biometrika* **1908**, *6*, 1−25.
(37) Smart, T. P.; Mykhaylyk, O. O.; Ryan, A. J.; Battaglia, G. Polymersomes hydrophilic brush scaling relations. *Soft Matter* **2009**, *5* (19), 3607−3610.
(38) Rajagopal, K.; Mahmud, A.; Christian, D. A.; Pajerowski, J. D.; Brown, A. E. X.; Loverde, S. M.; Discher, D. E. Curvature-Coupled Hydration of Semicrystalline Polymer Amphiphiles Yields flexible Worm Micelles but Favors Rigid Vesicles: Polycaprolactone-Based Block Copolymers. *Macromolecules* **2010**, *43* (23), 9736−9746.
(39) Cameron, N. S.; Corbierre, M. K.; Eisenberg, A. 1998 EWR Steacie Award Lecture Asymmetric amphiphilic block copolymers in solution: a morphological wonderland. *Can. J. Chem.* **1999**, *77* (8), 1311−1326.
(40) Yu, Y.; Zhang, L.; Eisenberg, A. Morphogenic Effect of Solvent on Crew-Cut Aggregates of Apmphiphilic Diblock Copolymers. *Macromolecules* **1998**, *31* (4), 1144−1154.
(41) Bhargava, P.; Zheng, J. X.; Li, P.; Quirk, R. P.; Harris, F. W.; Cheng, S. Z. D. Self-Assembled Polystyrene-block-poly(ethylene oxide) Micelle Morphologies in Solution. *Macromolecules* **2006**, *39* (14), 4880−4888.
(42) Bordes, C.; Fréville, V.; Ruffin, E.; Marote, P.; Gauvrit, J. Y.; Briançon, S.; Lantéri, P. Determination of poly(ε-caprolactone) solubility parameters: Application to solvent substitution in a microencapsulation process. *Int. J. Pharm.* **2010**, *383* (1−2), 236−243.
(43) Won, Y.-Y.; Brannan, A. K.; Davis, H. T.; Bates, F. S. Cryogenic Transmission Electron Microscopy (Cryo-TEM) of Micelles and Vesicles Formed in Water by Poly(ethylene oxide)-Based Block Copolymers. *J. Phys. Chem. B* **2002**, *106* (13), 3354−3364.
(44) Zupancich, J. A.; Bates, F. S.; Hillmyer, M. A. Aqueous Dispersions of Poly(ethylene oxide)-b-poly(γ-methyl-ε-caprolactone) Block Copolymers. *Macromolecules* **2006**, *39* (13), 4286−4288.
(45) Adams, D. J.; Butler, M. F.; Weaver, A. C. Effect of Block Length, Polydispersity, and Salt Concentration on PEO−PDEAMA

DOI: 10.1021/acs.macromol.7b01498
Macromolecules 2017, 50, 7155−7168

Block Copolymer Structures in Dilute Solution. *Langmuir* **2006**, *22* (10), 4534−4540.
(46) Wu, D.; Spulber, M.; Itel, F.; Chami, M.; Pfohl, T.; Palivan, C. G.; Meier, W. Effect of Molecular Parameters on the Architecture and Membrane Properties of 3D Assemblies of Amphiphilic Copolymers. *Macromolecules* **2014**, *47* (15), 5060−5069.
(47) He, C.; Sun, J.; Deng, C.; Zhao, T.; Deng, M.; Chen, X.; Jing, X. Study of the Synthesis, Crystallization, and Morphology of Poly(ethylene glycol)−Poly(ε-caprolactone) Diblock Copolymers. *Biomacromolecules* **2004**, *5* (5), 2042−2047.
(48) Shen, H.; Eisenberg, A. Morphological Phase Diagram for a Ternary System of Block Copolymer PS310-b-PAA52/Dioxane/H2O. *J. Phys. Chem. B* **1999**, *103* (44), 9473−9487.
(49) Zhang, L.; Eisenberg, A. Thermodynamic vs Kinetic Aspects in the Formation and Morphological Transitions of Crew-Cut Aggregates Produced by Self-Assembly of Polystyrene-b-poly(acrylic acid) Block Copolymers in Dilute Solution. *Macromolecules* **1999**, *32* (7), 2239−2249.
(50) Knop, K.; Hoogenboom, R.; Fischer, D.; Schubert, U. S. Poly(ethylene glycol) in Drug Delivery: Pros and Cons as Well as Potential Alternatives. *Angew. Chem., Int. Ed.* **2010**, *49* (36), 6288−6308.
(51) Hoogenboom, R. Poly(2-oxazoline)s: A Polymer Class with Numerous Potential Applications. *Angew. Chem., Int. Ed.* **2009**, *48* (43), 7978−7994.
(52) Goldberg, D. A review of the biodegradability and utility of poly(caprolactone). *J. Environ. Polym. Degrad.* **1995**, 3 (2), 61−67.
(53) Tokiwa, Y.; Calabia, B. P. Biodegradability and Biodegradation of Polyesters. *J. Polym. Environ.* **2007**, *15* (4), 259−267.
(54) Geng, Y.; Dalhaimer, P.; Cai, S.; Tsai, R.; Tewari, M.; Minko, T.; Discher, D. E. Shape effects of filaments versus spherical particles in flow and drug delivery. *Nat. Nanotechnol.* **2007**, *2* (4), 249−255.
(55) Place, E. S.; George, J. H.; Williams, C. K.; Stevens, M. M. Synthetic polymer scaffolds for tissue engineering. *Chem. Soc. Rev.* **2009**, *38* (4), 1139−1151.
(56) Kweon, H.; Yoo, M. K.; Park, I. K.; Kim, T. H.; Lee, H. C.; Lee, H.-S.; Oh, J.-S.; Akaike, T.; Cho, C.-S. A novel degradable polycaprolactone networks for tissue engineering. *Biomaterials* **2003**, *24* (5), 801−808.

DOI: 10.1021/acs.macromol.7b01498
Macromolecules 2017, 50, 7155−7168

Supporting Information

Complex self-assembly behavior of bis-hydrophilic PEO-*b*-PCL-*b*-PMOXA triblock copolymers in aqueous solution

Evgeniia V. Konishcheva[†*], *Ulmas E. Zhumaev*[‡], *Maximilian Kratt*[†], *Valentin Oehri*[†], *Wolfgang Meier*[†*]

[†]Department of Chemistry, University of Basel, Klingelbergstrasse 80, 4056 Basel, Switzerland

[‡]Molecular Spectroscopy Department, Max Planck Institute for Polymer Research, Ackermannweg 10, 55128 Mainz, Germany

*Corresponding authors: ev.konishcheva@gmail.com (Evgeniia V. Konishcheva), wolfgang.meier@unibas.ch (Wolfgang Meier)

Experimental part

Materials. All chemicals were obtained from Sigma-Aldrich and used as received unless otherwise mentioned. Milli-Q water with the resistivity of 15 MΩ·cm was used from a Purelab Option-R 7/15 system (ELGA). Polyethylene oxide monomethyl ether (PEO, 2000 $g \cdot mol^{-1}$) was dissolved in water, lyophilized, and stored under reduced pressure (~0.01 mbar) until further use. ε-Caprolactone (ε-CL) was dried over CaH_2 for 12 h and distilled under reduced pressure (~0.1 mbar). Toluene was dried over CaH_2 and distilled under argon atmosphere prior to use. Tin(II) 2-ethylhexanoate ($SnOct_2$) was distilled under reduced pressure (~0.01 mbar). 2-Methyl-2-oxazoline (MOXA) was purchased from Acros Organics, dried under argon atmosphere over CaH_2 for 12 h and distilled prior to use. Sulfolane was dried over CaH_2 for 24 h under reduced pressure (~0.01 mbar) at 35 °C, distilled, and stored under argon atmosphere. Bodipy 630/650 NHS ester was purchased from Thermo Fisher Scientific Inc.

Nuclear magnetic resonance spectroscopy (NMR). ^1H NMR spectra were recorded in $CDCl_3$ (0.05 % tetramethylsilane) on a Bruker Avance III NMR spectrometer (400.13 MHz). Chemical shifts are reported in ppm. Spectra were processed with MestReNova software.

Gel permeation chromatography (GPC). GPC traces were recorded in WinGPC (v 8.20 build 4815, PSS systems) software. The samples were measured on DMF (20 mM LiBr) GPC system at 60 °C with a flow rate of 1 $ml \cdot min^{-1}$. The samples were passed through 3 PSS GRAM columns (one 30 Å, two 1000 Å, each 30 cm long, 10 μm particles, 0.8 cm diameter). The signals were recorded on Viscotek TDA 305 detector system equipped with a refractive index (RI), a triple UV-Vis operating at different wavelengths (189-506 nm), a 90° light scattering (670 nm), and viscometer detectors. The system was calibrated against narrowly distributed poly(methyl methacrylate) (PMMA) standards.

Differential scanning calorimetry (DSC). DSC measurements were performed on Perkin Elmer DSC 6. The samples (~10 mg) were hermetically sealed in aluminum pans. The scans were recorded with a speed of 10 $ºC \cdot min^{-1}$ in the Pyris Manager software.

Transmission electron microscopy (TEM). 5 μl of polymer assemblies (0.2 $mg \cdot ml^{-1}$) was adsorbed on a glow discharged copper grid (formvar coated, 200 mesh) and blotted off after 1 minute. The sample was washed two times with 5 μl of H_2O and one time with 2% uranyl acetate. 5 μl of 2% uranyl acetate was applied the second time and blotted off after 10 seconds. In the case of cloud-like aggregates, the staining with 2% uranyl acetate was omitted to obtain

better visualization of the structure of these aggregates. The prepared grids were dried in air for at least 10 minutes before imaging. TEM micrographs were recorded on a Philips CM100 transmission electron microscope at an acceleration voltage of 80 kV.

Cryogenic transmission electron microscopy (cryoTEM). 4 µl of aqueous solution of polymer assemblies (2 $mg \cdot ml^{-1}$) was deposited on a glow-discharged lacey carbon grid and incubated for 1 min. The sample was blotted off before plunge freezing in liquid ethane. Imaging was performed on FEI Talos TEM at an acceleration voltage of 200 kV.

Synthesis of PEO-*b*-PCL and PEO-*b*-PCL-*b*-PMOXA. PEO-*b*-PCL were synthesized via kinetically controlled coordination-insertion ring opening polymerization of ε-CL catalyzed by $SnOct_2$.[1] Briefly, PEO was mixed with ε-CL in dry toluene, and then freshly distilled $SnOct_2$ was added. The polymerization was carried out at 110 °C. PEO-*b*-PCL-*b*-PMOXA triblock copolymers were synthesized via cationic ring opening polymerization of MOXA by microwave-assisted synthesis using PEO-*b*-PCL-OTs as macroinitiator.[2] PEO-*b*-PCL-OTs was mixed with MOXA and sulfolane in the glove box, and the polymerization was carried out at 100 °C under microwave irradiation. ^{1}H NMR **PEO-*b*-PCL** (400.13 MHz, δ, $CDCl_3$): 1.38 ppm (m, (O)C-CH_2-CH_2-CH_2-CH_2-CH_2-O-), 1.65 ppm (m, (O)C-CH_2-CH_2-CH_2-CH_2-CH_2-O-), 2.31 ppm (t, J = 7.1 Hz, (O)C-CH_2-CH_2-CH_2-CH_2-CH_2-O-), 3.38 ppm (s, CH_3-O-), 3.65 ppm (s, -O-CH_2-CH_2-O-), 4.06 ppm (t, J = 6.5 Hz, (O)C-CH_2-CH_2-CH_2-CH_2-CH_2-O-). ^{1}H NMR **PEO-*b*-PCL-*b*-PMOXA** (400.13 MHz, δ, $CDCl_3$): 1.38 ppm (m, (O)C-CH_2-CH_2-CH_2-CH_2-CH_2-O-), 1.65 ppm (m, (O)C-CH_2-CH_2-CH_2-CH_2-CH_2-O-), 2.12 ppm (m, (-N(C(O)CH_3)-), 2.31 ppm (t, J = 7.1 Hz, (O)C-CH_2-CH_2-CH_2-CH_2-CH_2-O-), 3.38 ppm (s, CH_3-O-), 3.46 ppm (m, -N(C(O)CH_3)-CH_2-CH_2-), 3.65 ppm (s, -O-CH_2-CH_2-O-), 4.06 ppm (t, J = 6.5 Hz, (O)C-CH_2-CH_2-CH_2-CH_2-CH_2-O-).

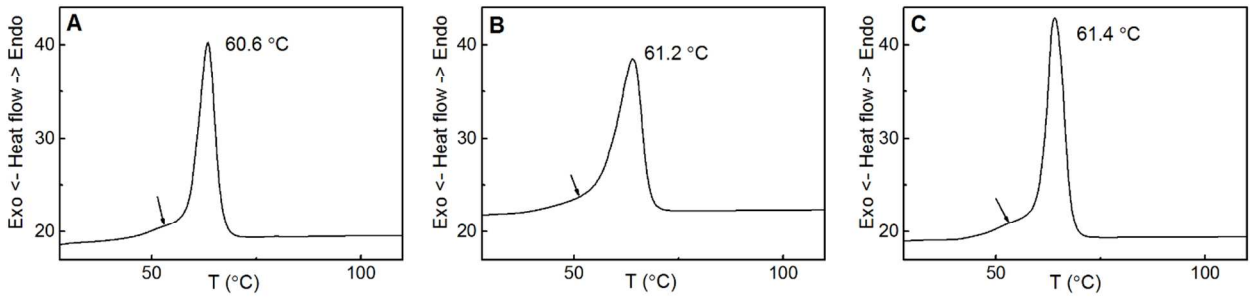

Figure S1. DSC of polymers (A) $E_{45}C_{110}M_4$, (B) $E_{45}C_{135}M_{20}$, and (C) $E_{45}C_{153}M_4$. Scan rate is 10 ºC·min^{-1}. The samples (~10 mg) were measured in hermetically sealed aluminum pans. Small shoulders pointed out by arrows most likely corresponds to the melting of PEO.[3]

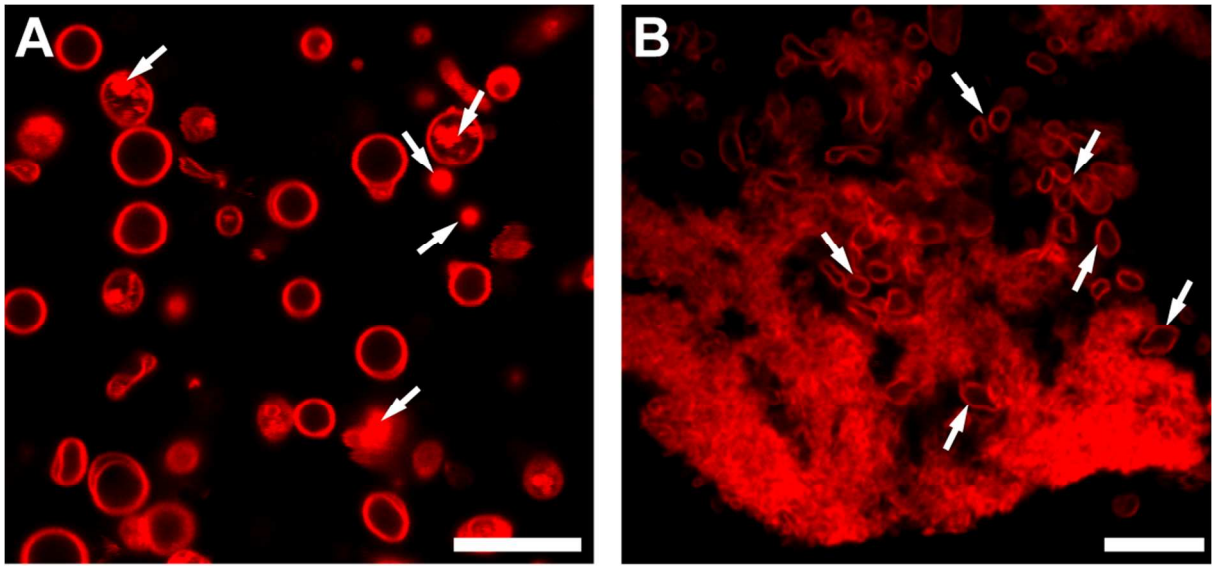

Figure S2. LSM images of the self-assembled structures obtained using film rehydration method formed by: (A) $E_{45}C_{135}M_4$; (B) $E_{45}C_{135}M_{20}$. The arrows point out the presence of the minor coexisting morphology. Structures were stained with Bodipy 630/650. Scale bars are 10 μm.

Table S1. Characterization of PEO-*b*-PCL and PEO-*b*-PCL-*b*-PMOXA polymers and their microscale self-assembled structures.

Polymer[a]	Abbreviation	$Đ_M$[b]	f^c, %	Morphology (film rehydration method)	Morphology (solvent evaporation method)	Morphology (co-solvent method)
PEO(2.0K)-*b*-PCL(5.5K)	$E_{45}C_{48}$	1.19	27	S, D	S	n.t.[d]
PEO(2.0K)-*b*-PCL(5.5K)-*b*-PMOXA(0.2K)	$E_{45}C_{48}M_3$	1.16	29	S, D	S, E	n.t.
PEO(2.0K)-*b*-PCL(5.5K)-*b*-PMOXA(0.6K)	$E_{45}C_{48}M_7$	1.21	32	S, D	S, E	n.t.
PEO(2.0K)-*b*-PCL(7.5K)	$E_{45}C_{66}$	1.15	21	S	S	n.t.
PEO(2.0K)-*b*-PCL(7.5K)-*b*-PMOXA(0.4K)	$E_{45}C_{66}M_5$	1.11	24	P, S	S, E, I	n.t.
PEO(2.0K)-*b*-PCL(11.7K)	$E_{45}C_{103}$	1.05	15	S	S	n.t.
PEO(2.0K)-*b*-PCL(11.7K)-*b*-PMOXA(0.3K)	$E_{45}C_{103}M_4$	1.14	16	P, S	S, E	n.t.
PEO(2.0K)-*b*-PCL(11.7K)-*b*-PMOXA(1.0K)	$E_{45}C_{103}M_{12}$	1.12	20	P, S, C	E, S	n.t.
PEO(2.0K)-*b*-PCL(11.7K)-*b*-PMOXA(1.4K)	$E_{45}C_{103}M_{16}$	1.13	23	C	E, S	n.t.
PEO(2.0K)-*b*-PCL(12.5K)	$E_{45}C_{110}$	1.06	14	S	S	D, S
PEO(2.0K)-*b*-PCL(12.5K)-*b*-PMOXA(0.3K)	$E_{45}C_{110}M_4$	1.12	16	P	S, E	D
PEO(2.0K)-*b*-PCL(15.4K)	$E_{45}C_{135}$	1.15	11	S	S	S, D
PEO(2.0K)-*b*-PCL(15.4K)-*b*-PMOXA(0.3K)	$E_{45}C_{135}M_4$	1.22	13	P, S	E, E_Y, I, S	S, E
PEO(2.0K)-*b*-PCL(15.4K)-*b*-PMOXA(0.8K)	$E_{45}C_{135}M_{10}$	1.22	15	P, C	E_Y, N	S, P, E
PEO(2.0K)-*b*-PCL(15.4K)-*b*-PMOXA(1.7K)	$E_{45}C_{135}M_{20}$	1.23	19	C, P, S	N, S	S
PEO(2.0K)-*b*-PCL(15.4K)-*b*-PMOXA(2.1K)	$E_{45}C_{135}M_{25}$	1.24	21	C, P, S	E_Y, N, S	S
PEO(2.0K)-*b*-PCL(16.8K)	$E_{45}C_{147}$	1.09	11	S, P	S	S, D
PEO(2.0K)-*b*-PCL(16.8K)-*b*-PMOXA(0.3K)	$E_{45}C_{147}M_4$	1.10	12	I, P, S	I, S, E	P, S
PEO(2.0K)-*b*-PCL(16.8K)-*b*-PMOXA(0.8K)	$E_{45}C_{147}M_{10}$	1.12	14	I, S, P	I, E	S, P
PEO(2.0K)-*b*-PCL(16.8K)-*b*-PMOXA(1.5K)	$E_{45}C_{147}M_{18}$	1.11	17	I, S, P	I, E	S, E
PEO(2.0K)-*b*-PCL(17.4K)	$E_{45}C_{153}$	1.08	10	P	S, P	S, D
PEO(2.0K)-*b*-PCL(17.4K)-*b*-PMOXA(0.3K)	$E_{45}C_{153}M_4$	1.13	12	I, S, P	I	P, S
PEO(2.0K)-*b*-PCL(17.4K)-*b*-PMOXA(0.9K)	$E_{45}C_{153}M_{11}$	1.15	14	I, S	I	P, S

[a]Number-average molecular weight of copolymers was determined by ^{1}H NMR spectroscopy.

[b]Dispersity was determined from RI data of samples analyzed by DMF GPC using PMMA calibration.

[c]Hydrophilic weight fraction of PEO (diblocks) and PEO+PMOXA (triblocks) was calculated from ^{1}H NMR data.

[d]not tested

S – spherical particles, P – polymersomes, I – irregularly shaped particles (including precipitate), E – elongated structures, E_Y – elongated structures with Y-junctions, C – cloud-like aggregates, N – 3D networks of elongated structures, D – (partial) dissolution.

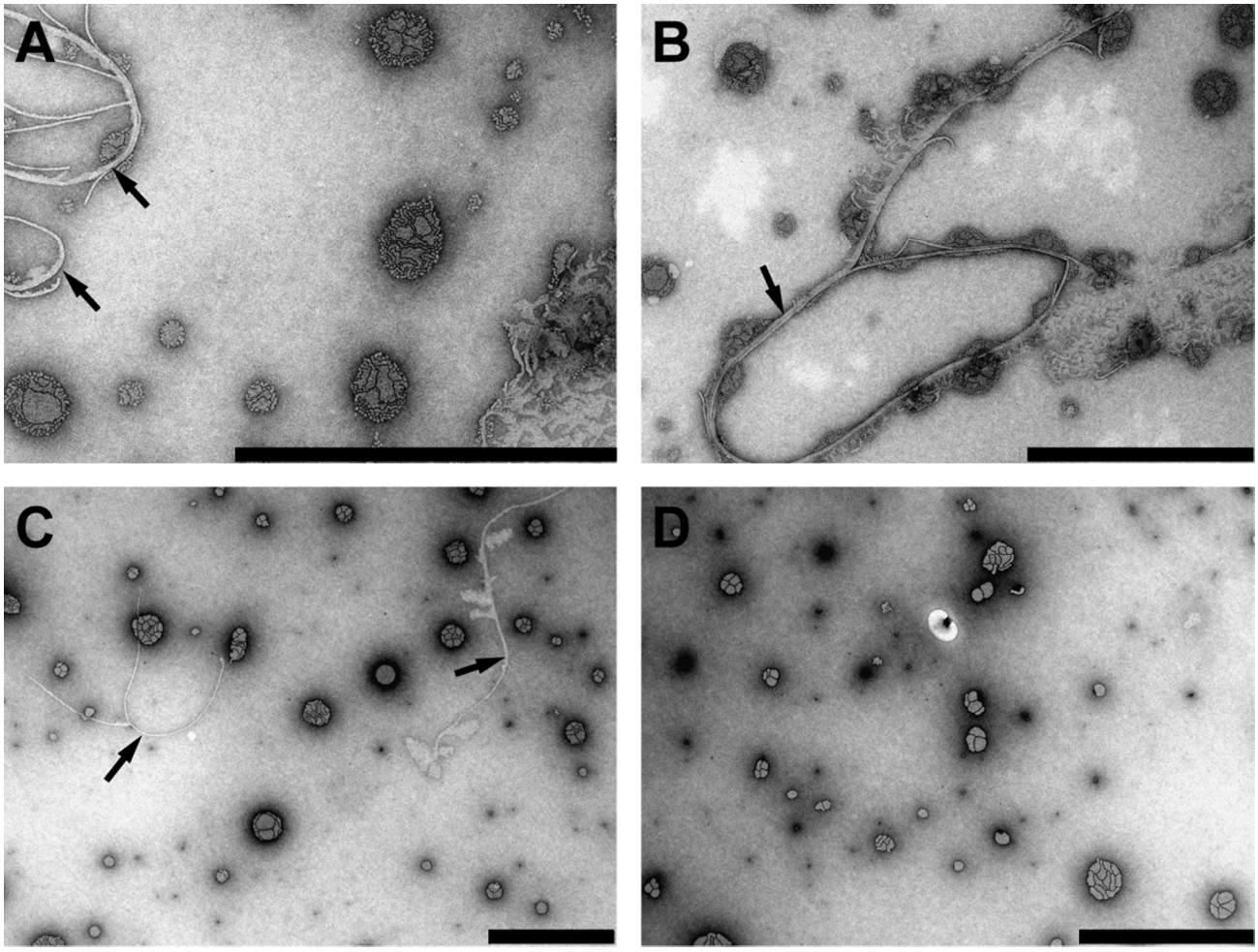

Figure S3. Representative TEM images of negatively stained spherical particles indicating their domain composition. (A, B) $E_{45}C_{103}$, (C, D) $E_{45}C_{147}$. Arrows indicate rods which presumably form during sample preparation. Scale bars are 2 μm.

Estimation of PEO and PMOXA counter lengths:

$$l_{PEO} = 45 \cdot \left(l_{C-C} \cdot \cos\left(\frac{\angle OCC}{2}\right) + 2 \cdot l_{C-O} \cdot \cos\left(\frac{\angle COC}{2}\right)\right) = 45 \cdot \left(1.54 \cdot \cos\left(\frac{109.5°}{2}\right) + 2 \cdot 1.43 \cdot \cos\left(\frac{109.5°}{2}\right)\right) = 162 \text{ Å}$$

$$l_{PMOXA} = n_{PMOXA} \cdot \left(l_{C-C} \cdot \cos\left(\frac{\angle NCC}{2}\right) + 2 \cdot l_{C-N} \cdot \cos\left(\frac{\angle CNC}{2}\right)\right) = n_{PMOXA} \cdot \left(1.54 \cdot \cos\left(\frac{109.5°}{2}\right) + 2 \cdot 1.47 \cdot \cos\left(\frac{109.5°}{2}\right)\right) = n_{PMOXA} \cdot 3.66 \text{ Å}$$

Estimation of PEO and PMOXA diameters:

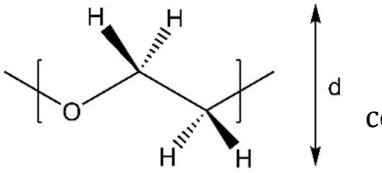

$$d_{PEO} = 2 \cdot l_{C-H} \cdot \cos\left(\frac{\angle HCH}{2}\right) + l_{C-C} \cdot \cos\left(\frac{\angle CCC}{2}\right) = 2 \cdot 1.09 \cdot \cos\left(\frac{109.5°}{2}\right) + 1.54 \cdot \cos\left(\frac{109.5°}{2}\right) = 2.1 \text{ Å}$$

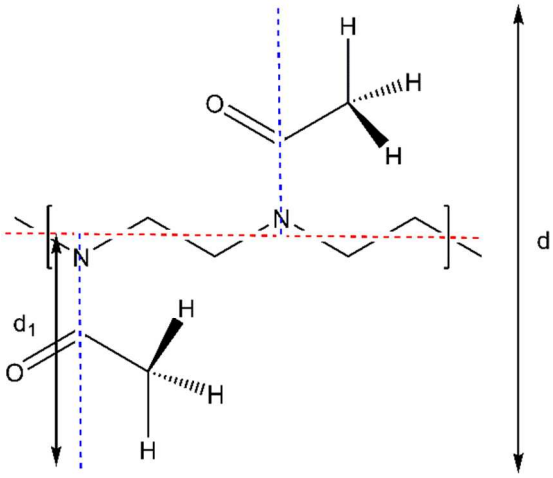

$$d_1 = \frac{1}{2} \cdot l_{N-C} \cdot \cos\left(\frac{\angle CNC}{2}\right) + l_{N-C(O)} + l_{C-C} \cdot \cos\left(\frac{\angle OCC}{2}\right) + l_{C-H} \cdot \cos(90° - (109.5° - 30°)) = \frac{1}{2} \cdot 1.47 \cdot \cos\left(\frac{120°}{2}\right) + 1.32 + 1.54 \cdot \cos\left(\frac{120°}{2}\right) + 1.09 \cdot \cos(10.5°) = 3.53 \text{ Å}$$

$$d_{PMOXA} = 2 \cdot d_1 = 7.1 \text{ Å}$$

Estimation of $E_{45}C_{135}M_{20}$ counter length:

$$l_{I-shape} = 45 \cdot \left(l_{C-C} \cdot \cos\left(\frac{\angle OCC}{2}\right) + 2 \cdot l_{C-O} \cdot \cos\left(\frac{\angle COC}{2}\right)\right) + 135 \cdot \left(5 \cdot l_{C-C} \cdot \cos\left(\frac{\angle OCC}{2}\right) + 2 \cdot l_{C-O} \cdot \cos\left(\frac{\angle COC}{2}\right)\right) + 20 \cdot \left(l_{C-C} \cdot \cos\left(\frac{\angle NCC}{2}\right) + 2 \cdot l_{C-N} \cdot \cos\left(\frac{\angle CNC}{2}\right)\right) = 45 \cdot \left(1.54 \cdot \cos\left(\frac{109.5°}{2}\right) + 2 \cdot 1.43 \cdot \cos\left(\frac{109.5°}{2}\right)\right) + 135 \cdot \left(5 \cdot 1.54 \cdot \cos\left(\frac{109.5°}{2}\right) + 2 \cdot 1.43 \cdot \cos\left(\frac{109.5°}{2}\right)\right) + 20 \cdot \left(1.54 \cdot \cos\left(\frac{109.5°}{2}\right) + 2 \cdot 1.47 \cdot \cos\left(\frac{109.5°}{2}\right)\right) = 1402 \text{ Å} = 140\ nm$$

$$l_{U-shape} \approx \frac{1}{2} \cdot l_{I-shape} = 70\ nm$$

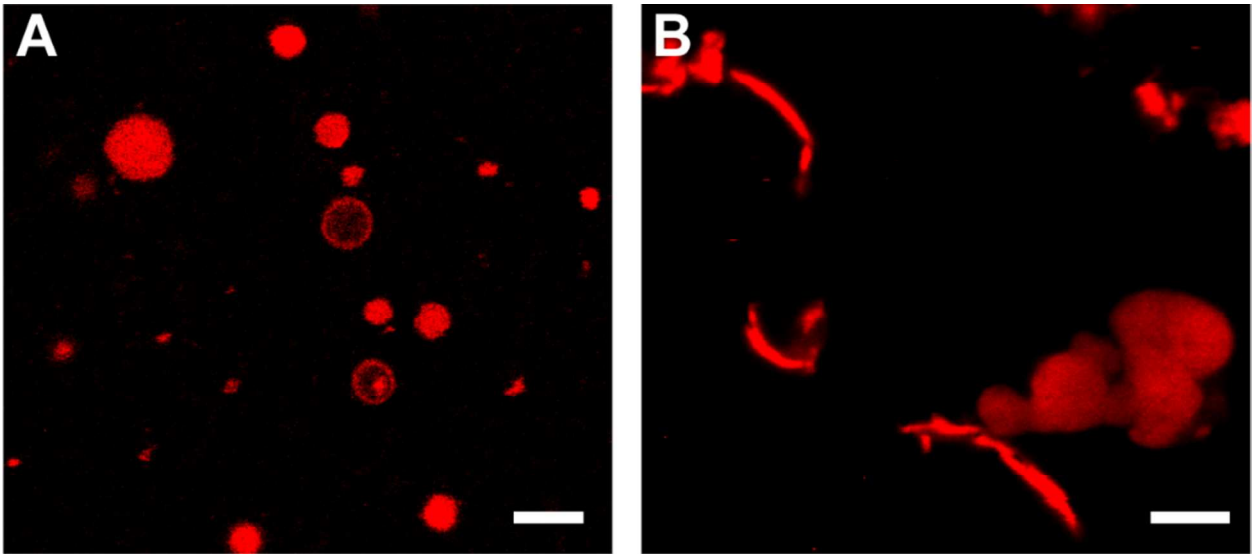

Figure S4. LSM images of the self-assembled structures obtained using solvent evaporation method formed by: (A) $E_{45}C_{153}$ (PEO(2.0K)-*b*-PCL(17.4K), $Đ_M$ = 1.08); (B) PEO(2.0K)-*b*-PCL(16.0K) ($Đ_M$ = 1.23) containing 26% of PEO-*b*-PCL-*b*-PEO.[1] The images indicate that the presence of triblock copolymer PEO-*b*-PCL-*b*-PEO influences dramatically self-assembly in SE method. Structures were stained with Bodipy 630/650. Scale bars are 5 μm.

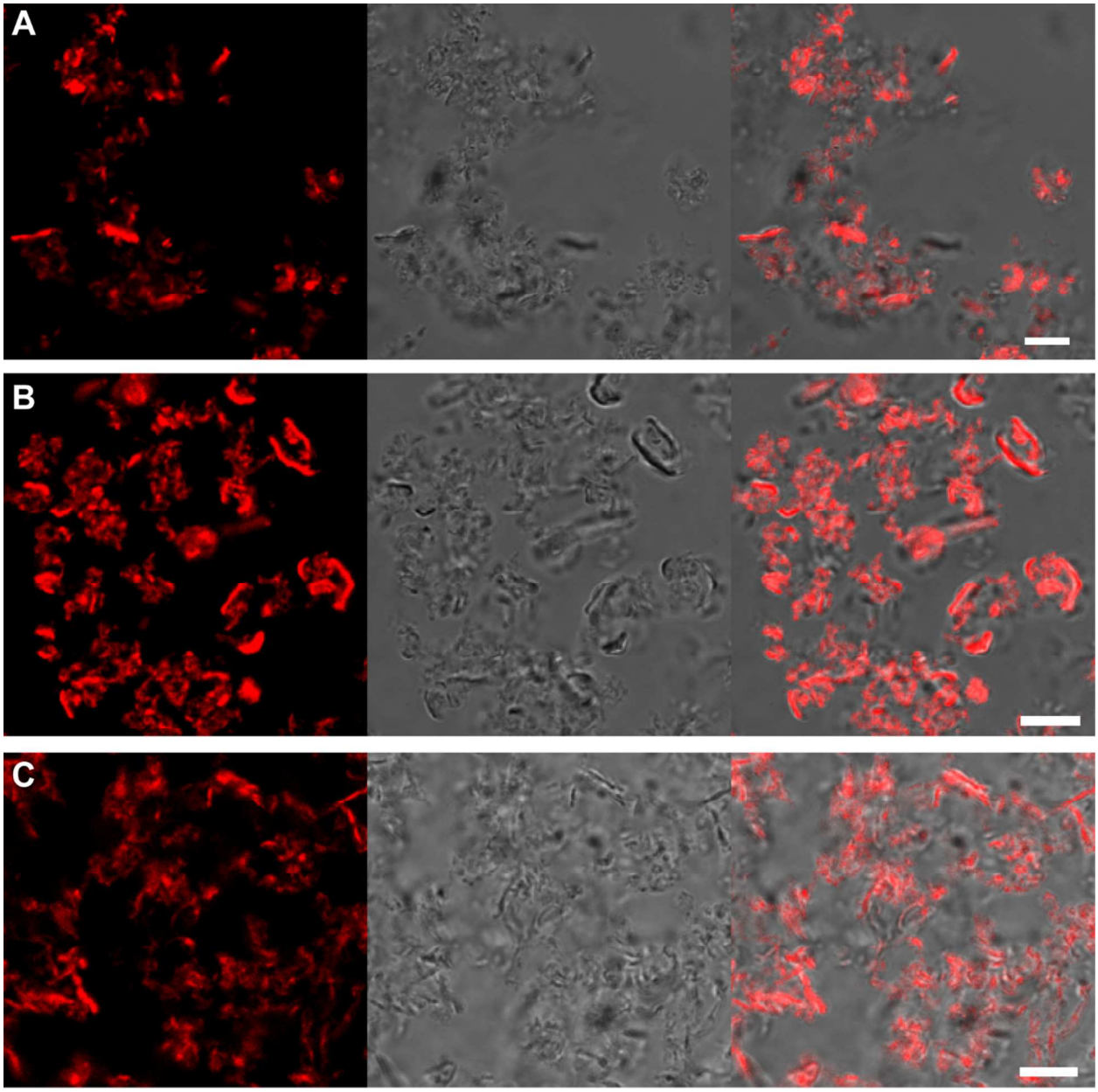

Figure S5. LSM, bright field, and their overlay images of the self-assembled structures formed by $E_{45}C_{153}M_4$ obtained using as a co-solvent: (A) DMF; (B) ACN; (C) acetone. The images indicate that DMF, ACN, and acetone result in similar self-assembled structures. Structures were stained with Bodipy 630/650. Scale bars are 10 μm.

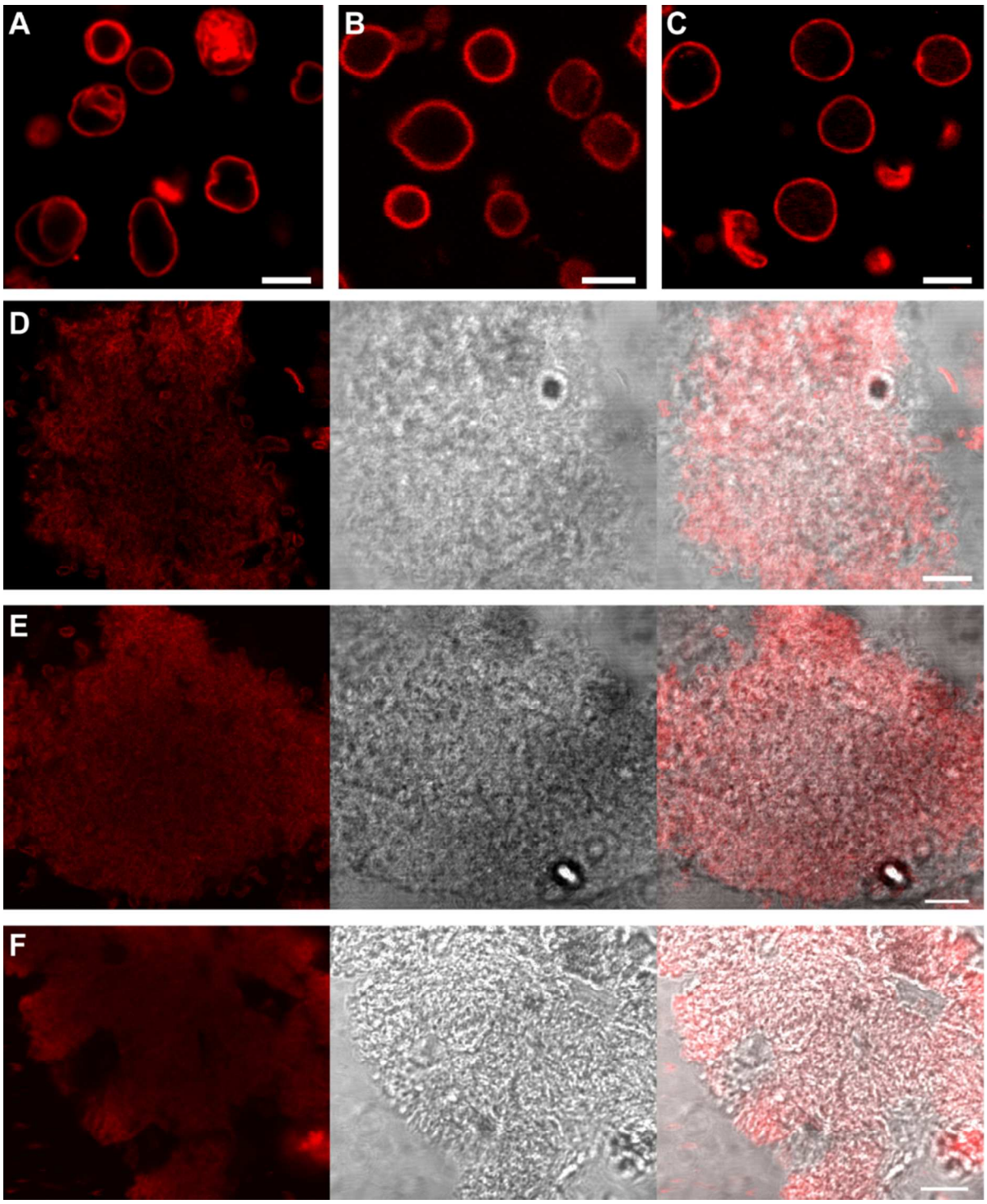

Figure S6. LSM (A-C) and LSM, bright field, and their overlay (D-F) images of the self-assembled structures obtained using film rehydration method formed by copolymers $E_{45}C_{135}M_4$ (A-C) and $E_{45}C_{135}M_{20}$ (D-F) under different cooling/heating conditions: (A, D) standard procedure; (B, E) slow heating; (C, F) slow cooling. Structures were stained with Bodipy 630/650. Scale bars are 5 μm (A-C) and 10 μm (D-F).

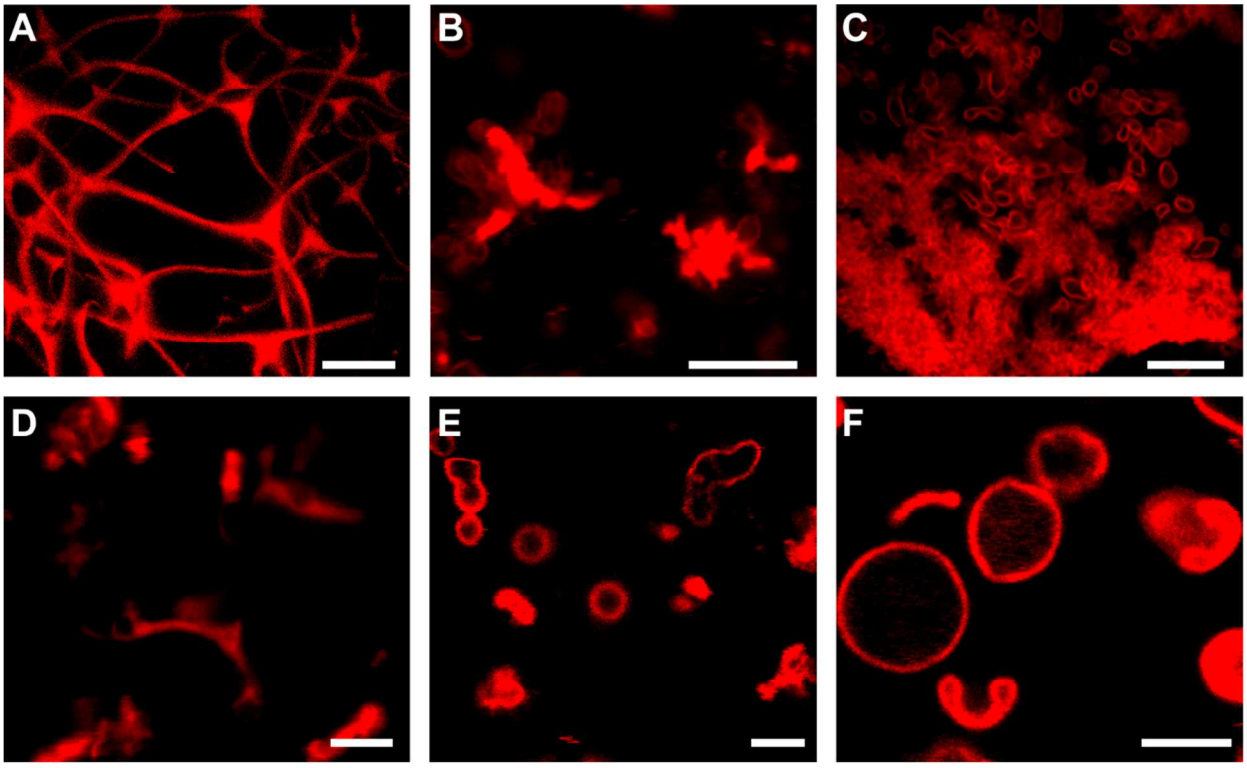

Figure S7. z-Projection of z-stack CLSM (A) and LSM (B-F) images of the self-assembled structures formed by $E_{45}C_{135}M_{20}$ (A-C) and $E_{45}C_{135}M_4$ (D-F) obtained using different methods: (A, D) solvent evaporation; (B, E) solvent evaporation followed by incubation at 62 °C for 24 h; (C, F) film rehydration. Structures were stained with Bodipy 630/650. Scale bars are 10 μm (A-C) and 5 μm (D-F).

References:

1. Konishcheva, E.; Häussinger, D.; Lörcher, S.; Meier, W., Key aspects to yield low dispersity of PEO-b-PCL diblock copolymers and their mesoscale self-assembly. *European Polymer Journal* **2016,** *83*, 300-310.
2. Konishcheva, E. V.; Zhumaev, U. E.; Meier, W. P., PEO-b-PCL-b-PMOXA Triblock Copolymers: From Synthesis to Microscale Polymersomes with Asymmetric Membrane. *Macromolecules* **2017,** *50* (4), 1512-1520.
3. Ghoroghchian, P. P.; Li, G.; Levine, D. H.; Davis, K. P.; Bates, F. S.; Hammer, D. A.; Therien, M. J., Bioresorbable Vesicles Formed through Spontaneous Self-Assembly of Amphiphilic Poly(ethylene oxide)-block-polycaprolactone. *Macromolecules* **2006,** *39* (5), 1673-1675.

4. Effect of the hydrophobicity on self-assembly: the case of linear ABC copolymers

Self-assembly of amphiphilic block copolymers was investigated under various conditions, like polymer concentration, water content, nature of the co-solvent, etc., which has been discussed in details in the section 2. The self-assembly process is driven by hydrophobic interactions, and therefore depends on the chemical nature of a copolymer, i.e. on the balance between the interfacial tension between the hydrophobic core and the solvent outside the core, the repulsive forces between hydrophilic chains in the corona, and the degree of stretching of the hydrophobic chains in the core.[1] This balance can be tuned by changing hydrophilicity/hydrophobicity of the corresponding blocks. However, to the best of our knowledge, the consequences of such change on self-assembly process have never been investigated. The goal of this study is to explore the effect of hydrophobicity on self-assembly of amphiphilic block copolymers. As a model system, bis-hydrophilic poly(ethylene oxide)-*block*-poly(γ-R-ε-caprolactone)-*block*-poly(*N*,*N*-dimethylaminoethyl methacrylate) (PEO-*b*-P(R)CL-*b*-PDMAEMA) copolymers were chosen. Hydrophobicity of P(R)CL was modified by changing R from methyl to phenyl group (Scheme 6). The polymers were synthesized by combining coordination LROP of γ-substituted ε-caprolactones (MCL or PhCL) and ATRP of DMAEMA. These polymers are promising for drug and gene delivery applications due to their unique composition. The hydrophilic parts are biocompatible protein-repellent PEO and cationic pH-responsive PDMAEMA which can complex negatively charged nucleic acids. The hydrophobic blocks, PRCLs, are biodegradable amorphous polyesters. Amorphous hydrophobic block is very advantageous for self-assembly process, because self-assembly in this case can proceed at ambient temperatures, unlike in case of semicrystalline PCL-based polymers. In the latter case self-assembly requires high temperatures above T_m of PCL (~60 °C) or presence of organic solvent.

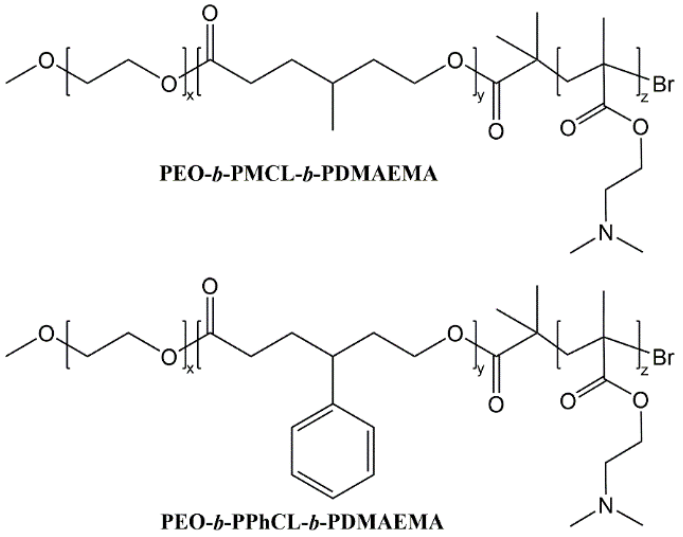

Scheme 6. Structures of PEO-*b*-PMCL-*b*-PDMAEMA and PEO-*b*-PPhCL-*b*-PDMAEMA.

The γ-substituted ε-caprolactones were synthesized via Baeyer-Villiger oxidation according to the previously published procedures.[2-4] However, when following the published purification protocols, the ^{1}H NMR spectrum of MCL exhibited aromatic impurities even after vacuum distillation over CaH_2 (Fig. 2). These impurities affected polymerization of MCL on PEO macroinitiator: the ^{1}H NMR spectra of the resulting PEO-*b*-PMCL copolymers contained the expected peaks, but GPC analysis showed a big fraction of impurities with the molecular weight lower than that of PEO, which are presumably PMCL homopolymer (Fig. 3A). The aromatic impurities could be either 3-chloroperbenzoic acid which was used in excess for synthesis of MCL, or 3-chlorobenzoic acid byproduct formed during the synthesis of MCL. The latter, however, supposedly should be extracted completely by saturated aqueous solution of $NaHCO_3$ (see *Experimental Part*). Therefore, this impurity should be 3-chloroperbenzoic acid which is poorly soluble in aqueous phase. To remove it, the CH_2Cl_2 solution containing MCL was washed with 1 M aqueous $Na_2S_2O_3$. Indeed, after the first extraction the aqueous phase turned cloudy and yellow suggesting the formation of colloidal sulfur. After such extraction, the aromatic peaks disappeared (Fig. 2 inset), and polymerization of MCL on PEO macroinitiator proceeded without formation of PMCL homopolymer (Fig. 3B).

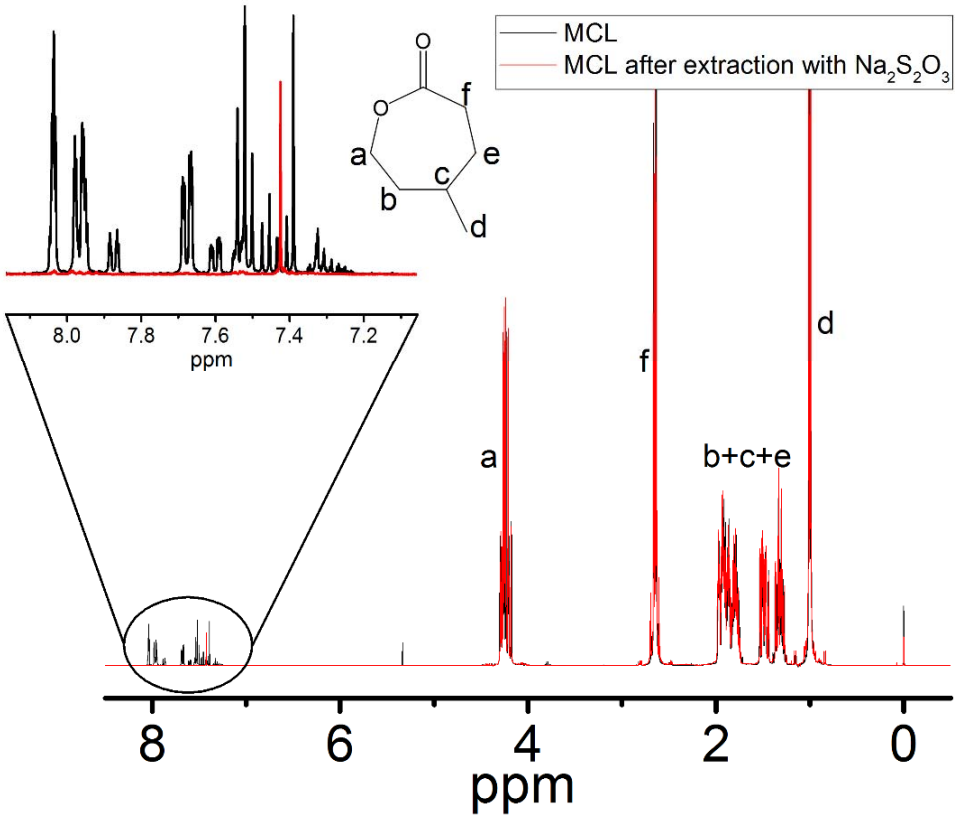

Figure 2. ^{1}H NMR ($CDCl_3$) of MCL before and after washing with 1 M $Na_2S_2O_3$.

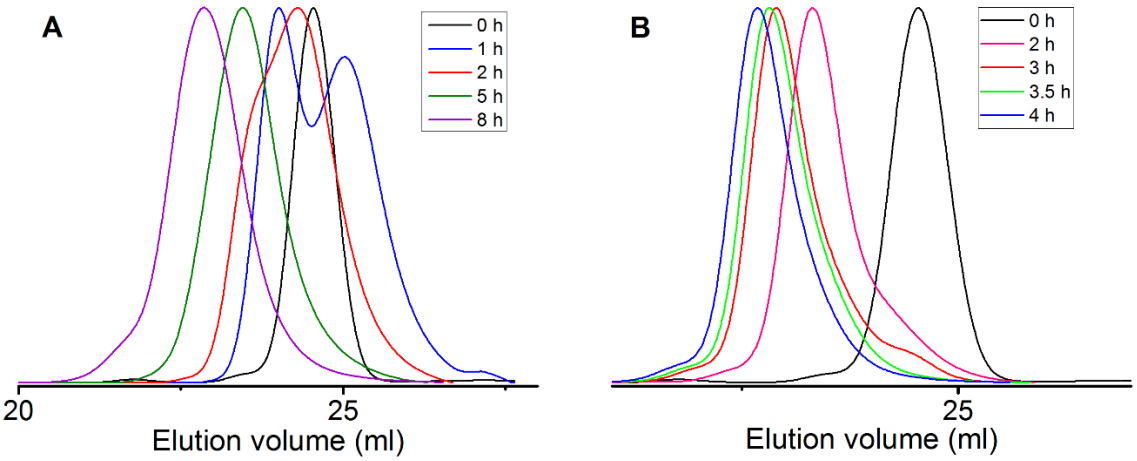

Figure 3. GPC (THF) traces of PEO-*b*-PMCL copolymers obtained using unwashed MCL (A) and washed MCL (B) with 1 M $Na_2S_2O_3$. The polymerizations were conducted in toluene in the presence of 1 eq (with respect to PEO) of freshly distilled $SnOct_2$.

The synthesis of PEO-*b*-PMCL and PEO-*b*-PPhCL was conducted in bulk in the presence of $SnOct_2$ as a catalyst according to the procedure[3] until full monomer conversion. Utilization of $AlEt_3$ catalyst followed by quenching the polymerization with HCl described in the procedure[2] led to the degradation of polyester backbone. The modification with BIBB and further ATRP polymerization was done according to the published procedure,[2] and the polymers were purified via dialysis. Two polymers used in this study contain the same PEO, similar lengths of the hydrophobic blocks and PDMAEMA: PEO(2.0K)-*b*-PMCL(12.8K)-*b*-PDMAEMA(5.8K) (100 units of PMCL, $Đ_M$ = 1.62) and PEO(2.0K)-*b*-PPhCL(20.9K)-*b*-PDMAEMA(5.5K) (100 units of PPhCL, $Đ_M$ = 1.87) (Fig. 4).

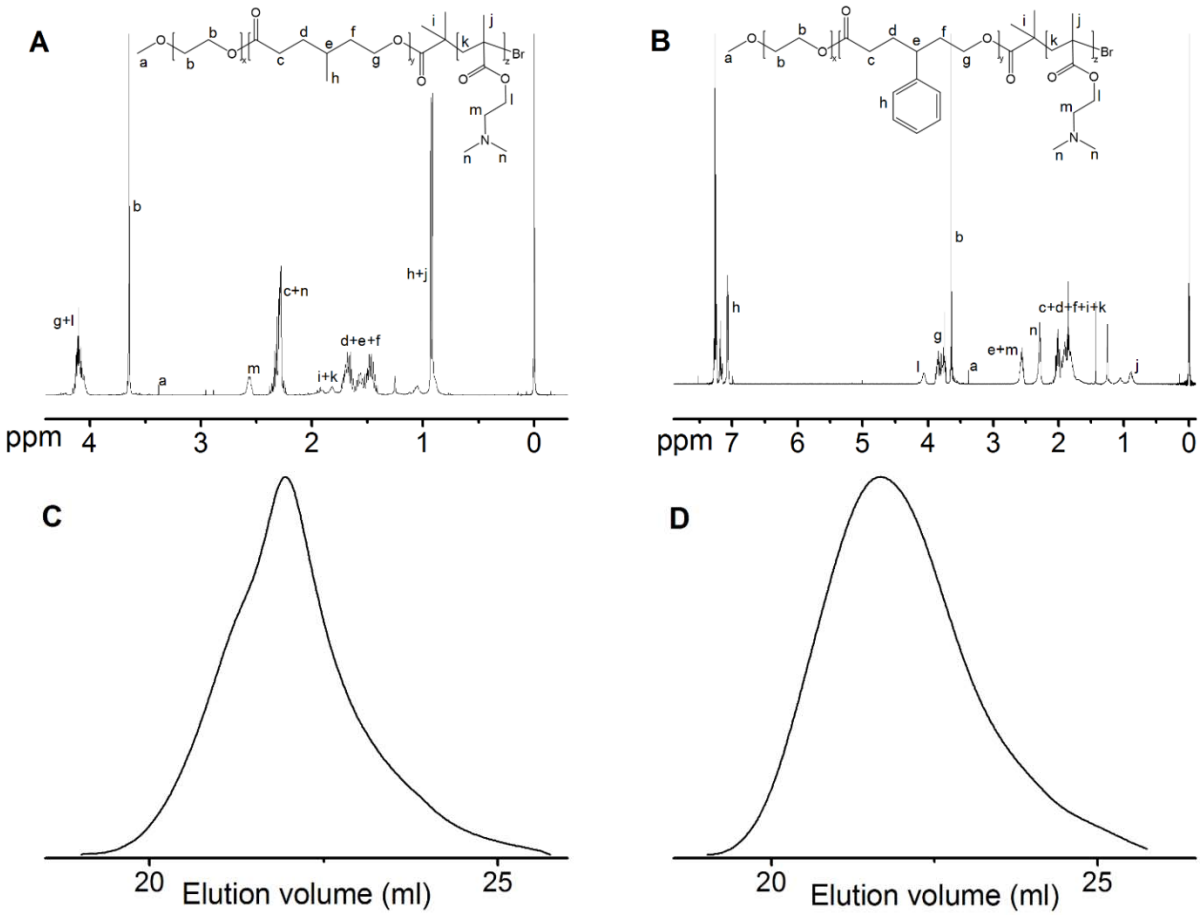

Figure 4. ^1H NMR ($CDCl_3$) (A, B) and GPC ($CHCl_3$) traces (C, D) of PEO(2.0K)-*b*-PMCL(12.8K)-*b*-PDMAEMA(5.8K) (A, C; $Đ_M$ = 1.62) and PEO(2.0K)-*b*-PPhCL(20.9K)-*b*-PDMAEMA(5.5K) (B, D; $Đ_M$ = 1.87).

The polymers were tested for their ability to self-assemble in PBS solution using film rehydration method. After extrusion the size of the particles was characterized by DLS, and their

morphology was observed by TEM and cryoTEM. Both polymers formed spherical aggregates (Fig. 5), which might be micelles assembled from U-shaped polymer chains with both hydrophilic tails (PEO and PDMAEMA) facing the aqueous environment. PMCL-containing polymer formed particles with a hydrodynamic diameter $D_h = 52 \pm 5$ nm, and PPhCL-containing polymer self-assembled into aggregates with $D_h = 87 \pm 3$ nm.

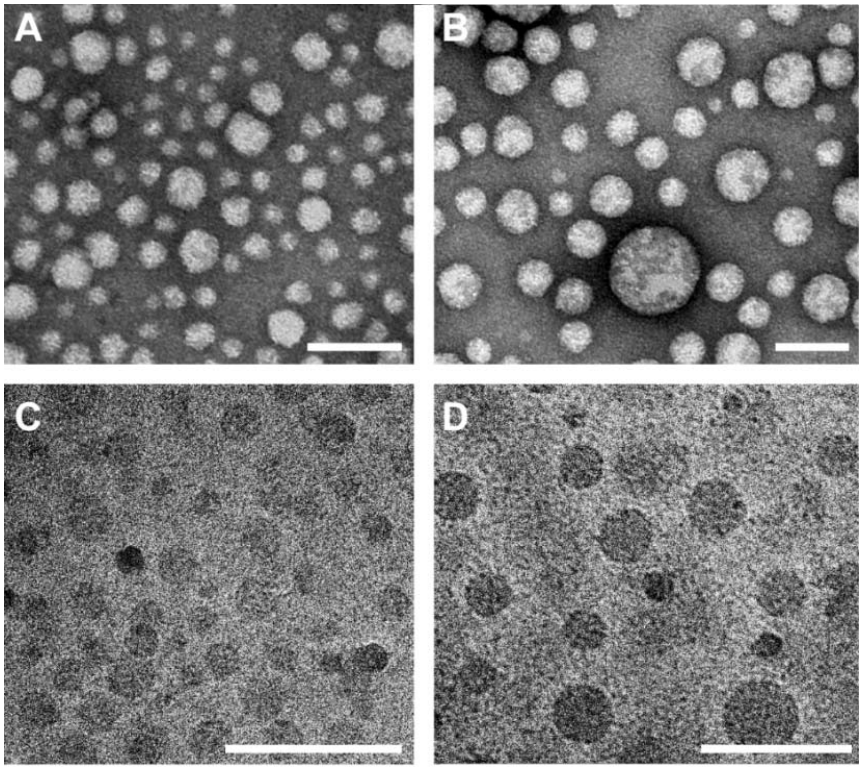

Figure 5. TEM (A, B) and cryoTEM (C, D) images of the assemblies formed by PEO(2.0K)-*b*-PMCL(12.8K)-*b*-PDMAEMA(5.8K) (A, C) and PEO(2.0K)-*b*-PPhCL(20.9K)-*b*-PDMAEMA(5.5K) (B, D). Scale bars are 100 nm.

The size difference can be attributed mainly to the different hydrophobicity of the middle PRCL blocks. Perhaps π-π interactions in the latter case force more polymer chains to aggregate in order to form dense core shielded from water by hydrophilic corona. This fact can be partly confirmed by ^{1}H NMR of the assemblies in D_2O (Fig. 6). The aggregates still possess peaks corresponding to the hydrophilic blocks, PEO and PDMAEMA, but the peaks from hydrophobic blocks become broader and less intense (PMCL) or disappear completely (PPhCL). This fact can be associated with hindered mobility of the hydrophobic chains within the assemblies, which becomes more pronounced for PPhCL due to stronger hydrophobic and π-π interactions.

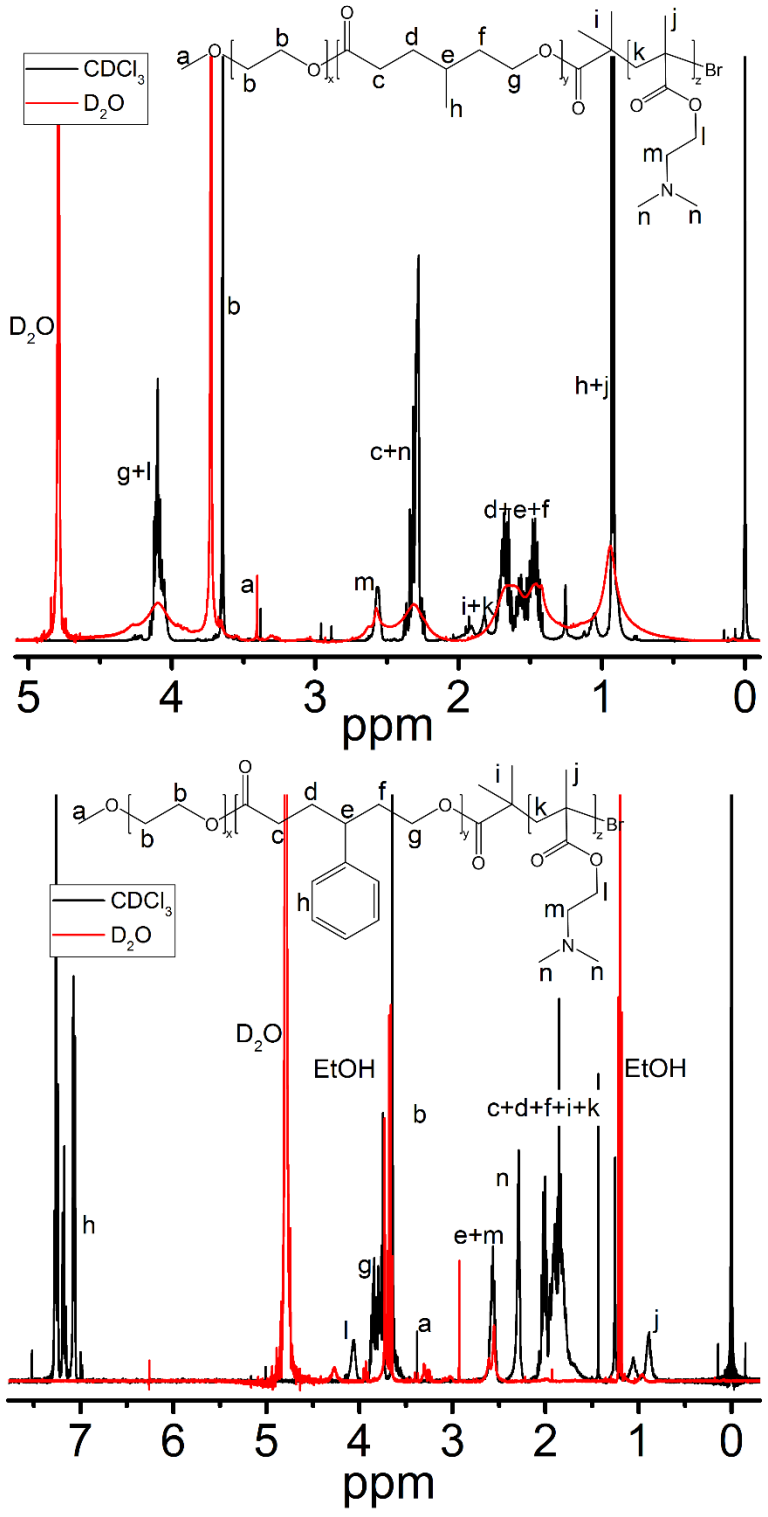

Figure 6. ^{1}H NMR of polymers ($CDCl_3$) and their self-assembled particles (D_2O): upper: PEO(2.0K)-*b*-PMCL(12.8K)-*b*-PDMAEMA(5.8K); lower: PEO(2.0K)-*b*-PPhCL(20.9K)-*b*-PDMAEMA(5.5K).

PEO-*b*-PRCL-*b*-PDMAEMA copolymers have potential application for gene therapy, since cationic PDMAEMA block should be able to complex nucleic acids via electrostatic interactions. Therefore, to determine potential side effects which might be caused by these polymers, the cytotoxicity of the self-assembled structures was investigated on HeLa cells using MTS assay (Fig. 7). Toxicity of the assemblies is induced by the cationic block, PDMAEMA, which interacts with a negatively charged cell membrane leading to its rupture.[5] This effect can be lowered when the length of PDMAEMA is decreased. As can be seen from Fig. 7, the polymer with a shorter PDMAEMA (18 units) possess significantly lower cytotoxicity compared to the polymer with a longer PDMAEMA (~35 units), which also correlates with positive ζ-potential values. The cytotoxic effect of such polymers can be decreased by converting tertiary amine to quarternized group shielded by a bulky residual, as has been shown in literature.[6]

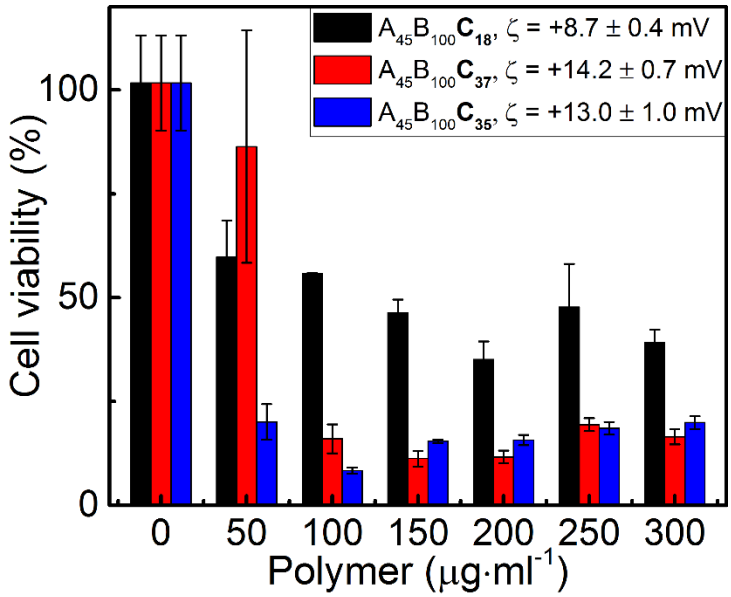

Figure 7. Cell toxicity studies of particles formed by PEO-*b*-PRCL-*b*-PDMAEMA copolymers: PEO(2.0K)-*b*-PMCL(12.8K)-*b*-PDMAEMA(2.8K) (black, ζ = +8.7 ± 0.4 mV), PEO(2.0K)-*b*-PMCL(12.8K)-*b*-PDMAEMA(5.8K) (red, ζ = +14.2 ± 0.7 mV), PEO(2.0K)-*b*-PPhCL(20.9K)-*b*-PDMAEMA(5.5K) (blue, ζ = +13.0 ± 1.0 mV).

In conclusion, PEO-*b*-PRCL-*b*-PDMAEMA copolymers were synthesized via a combination of coordination LROP of γ-substituted ε-caprolactones and ATRP of DMAEMA. The copolymers assembled into spherical nanoparticles. Increase of hydrophobicity led to the formation of larger particles in case of more hydrophobic PPhCL block (D_h = 52 ± 5 nm for PMCL vs. D_h = 87 ± 3 nm for PPhCL), whereas the morphology of the assemblies did not

change. The self-assembled structures exhibited moderate cytotoxicity which can be decreased by using a shorter cationic PDMAEMA block.

Experimental part

Materials. All chemicals were purchased from Sigma-Aldrich and used as received.

Nuclear Magnetic Resonance Spectroscopy (NMR). ^{1}H NMR spectra were recorded in $CDCl_3$ (0.05 % tetramethylsilane) on a Bruker Avance III NMR spectrometer (400.13 MHz). Spectra were processed with MestReNova software, and chemical shifts are reported in ppm.

Gel permeation chromatography (GPC). Both $CHCl_3$ and THF GPC traces were analyzed and recorded in WinGPC (v 8.20 build 4815, PSS systems) and equipped with 3 PLgel MIXED-C columns (30 cm long, 0.8 cm diameter, 5 μm particles) and a refractive index (RI) detectors ran at 1 ml·min^{-1}at 35 °C ($CHCl_3$) or 40 °C (THF). The systems were calibrated against narrow distributed polystyrene standards.

Dynamic light scattering (DLS). DLS and zeta potential measurements were performed on a Zetasizer nano ZSP (Malvern Instruments) equipped with a 633 nm 10 mW He–Ne laser (detection angle 173°). The measurements were performed at 25.0 ± 0.1 °C. The final polymer concentration was 1 mg·ml^{-1}, and each measurement was repeated at least three times with an equilibration time of 2 minutes before starting the measurements. The correlation functions were analyzed using the CONTIN algorithm.

Transmission electron microscopy (TEM). TEM micrographs were recorded on a Philips CM100 transmission electron microscope at an acceleration voltage of 80 kV. 5 μl of a sample was adsorbed on a glow discharged copper grid (formvar coated, 200 mesh) and blotted off after 1 minute. The sample was washed two times with 5 μl of H_2O and one time with 2% uranyl acetate. 5 μl of 2% uranyl acetate was applied the second time and blotted off after 10 seconds. The prepared grids were dried in air for at least 10 minutes before imaging.

Cryogenic transmission electron microscopy (cryoTEM). 4 μl of aqueous solution of polymer assemblies (2 mg·ml^{-1}) were deposited on glow-discharged lacey carbon grid and incubated for 1 min. The sample was blotted off before plunge freezing in liquid ethane. Imaging was performed on FEI Talos TEM at an acceleration voltage of 200 kV.

MTS assay. HeLa cells (5000 cells per well) were seeded in a 96-well Lab-Tek^{TM} plate (Nalge Nunc International, USA), and incubated at 37 °C, 5% CO_2 for 24 h in DMEM

containing 10% fetal calf serum and 1% penicillin/streptomycin. After 24 hours, 10 µl of polymer assemblies suspended in PBS were added to wells containing 90 µl of media. Final polymer concentration varied from 50 to 300 $mg \cdot ml^{-1}$. The solution were incubated for 24 h. Cell growth inhibition was measured using the MTS assay: 20 µl of MTS assay solution was added to each well and incubated for 3 h at 37 °C. Cell viability was determined by the absorbance at 490 nm measured on a microplate reader (SpectraMax M5^e, Molecular Devices, USA) and calculated as a percent of live cells compared to a PBS control (100% cell viability). All samples were corrected against controls containing only media and PBS.

Synthesis of MCL. In a typical experiment, 45 g (1.4 eq.) of 3-chloroperbenzoic acid was dissolved in 660 ml of CH_2Cl_2 in 1 L flask, and then 23.1 ml (1 eq.) of 4-methylcyclohexanone was added dropwise. The solution was stirred for 24 h at 25 ºC. The solution turned milky due to the precipitation of 3-chlorobenzoic acid byproduct. The solution was filtered, and the filtrate was left for ~1 h in dry ice/acetone mixture for efficient precipitation of the byproduct. To remove residual 3-chlorobenzoic acid, the solution was washed with saturated aqueous $NaHCO_3$ (3 × 300 ml). To remove residual 3-chloroperbenzoic acid, the solution was washed with 1 M aqueous $Na_2S_2O_3$ (2 × 300 ml). The 1 M $Na_2S_2O_3$ aqueous phase after the first wash turned milky-yellow due to the formation of colloidal sulfur, whereas the phase after the second wash stayed transparent. Finally, the CH_2Cl_2 phase was washed with saturated NaCl (3 × 300 ml) and left with $MgSO_4$ overnight. Then the solution was filtered and CH_2Cl_2 was removed by rotary evaporation. MCL was dried over CaH_2 for at least 12 h and distilled under reduced pressure prior to use. ^{1}H NMR (400.13 MHz, δ, $CDCl_3$): 1.00 ppm (d, J = 6.7 Hz, 3H, -CH_2-CH(CH_3)-CH_2-), 1.32 ppm (dddd, J = 14, 11, 9.4, 4.5 Hz, 1H, -CH_2-CH(CH_3)-CH_2-), 1.49 ppm (dddd, J = 14, 11, 9.4, 4.5 Hz, 1H, -CH_2-CH(CH_3)-CH_2-CH_2-C(O)-), 1.88 ppm (m, 3H, -CH_2-CH(CH_3)-CH_2-CH_2-C(O)-), 2.65 ppm (m, 2H, -CH_2-C(O)-), 4.24 ppm (m, 2H, -CH_2-O-).

Synthesis of PhCL. PhCL was synthesized in a similar manner as MCL. In a typical experiment, 14 g (1.4 eq.) of 3-chloroperbenzoic acid was dissolved in 250 ml of CH_2Cl_2 in 500 ml flask, and then 10.2 g (1 eq.) of 4-phenylcyclohexanone was added. The solution was stirred for 24 h at 25 ºC. The solution turned milky due to the precipitation of 3-chlorobenzoic acid byproduct. The solution was filtered several times until no white precipitate of the byproduct was observed. To remove residual 3-chlorobenzoic acid, the solution was washed with

saturated aqueous $NaHCO_3$ (3 × 200 ml). To remove residual 3-chloroperbenzoic acid, the solution was washed with 1 M aqueous $Na_2S_2O_3$ (2 × 200 ml). The 1 M $Na_2S_2O_3$ aqueous phase after the first wash turned milky-yellow due to the formation of colloidal sulfur, whereas the second phase stayed transparent. Finally, the CH_2Cl_2 phase was washed with saturated NaCl (3 × 200 ml) and left with $MgSO_4$ overnight. Then the solution was filtered, and CH_2Cl_2 was removed by rotary evaporation. PhCL was recrystallized from dry ethylacetate. ^{1}H NMR (400.13 MHz, δ, $CDCl_3$): 1.86 ppm (m, 1H, -CH_2-CH(Ph)-C*H*$_2$-CH_2-C(O)-), 2.06 ppm (m, 3H, -C*H*$_2$-CH(Ph)-C*H*$_2$-CH_2-C(O)-), 2.81 ppm (m, 3H, -CH_2-C*H*(Ph)-C*H*$_2$-C*H*$_2$-C(O)-), 4.37 ppm (m, 2H, -C*H*$_2$-O-), 7.16-7.36 ppm (m, 5H, Ph).

Synthesis of PEO-*b*-PRCL-*b*-PDMAEMA. Prior to polymerization PEO was dried under vacuum at 100 ºC for 1-2 h to remove water traces. In a typical experiment, to the 0.45 g (1 eq.) of dried PEO 100 eq. of a monomer (MCL or PhCL) was added. Then few drops of the catalyst, $SnOct_2$, was added and the mixture was stirred under Ar atmosphere at 110 ºC until the solution become very viscous that the stir bar inside the flask could not move (typically 3 h for MCL and 24 h for PhCL). The polymerization mixture was cooled down to room temperature and dissolved in THF. The THF solution was precipitated twice into ice-cold hexanes to remove residual monomer and catalyst. The ATRP macroinitiators, PEO-*b*-PRCL-Br, were synthesized using 2-bromoisobutyryl bromide (BIBB). 2.5 g (1 eq.) of a polymer was dissolved in 10 ml of anhydrous THF and then 5 eq of TEA was added. The mixture was cooled down by ice bath, and then 10 ml of THF solution containing 5 eq. of BIBB was added dropwise. The solution was let to warm up to room temperature and stirred overnight. The mixture was filtered to remove TEA salts and precipitated twice in ice-cold hexanes to remove residual BIBB. Then the ATRP macroinitiator (2.3 g, 1 eq.) was dissolved in anhydrous 20 ml THF/MeOH (1:1) mixture, followed by addition of 100 eq. of the monomer (DMAEMA), which was passed through basic alumina to remove inhibitor. In the meantime, the ATRP catalyst (1 eq. of CuBr and 1 eq. of PMDETA) was prepared in a small volume of anhydrous DMF. The catalyst and the solution with polymer were bubbled with Ar for at least 20 min, and then the catalyst was added while Ar was still bubbling. The polymerization was carried out at 50 ºC for 3 h, which corresponds to ~30% of conversion. The polymerization was quenched by exposing mixture to air. The final polymers were dialyzed first against THF/H_2O (8:2) for 2 days, and then against pure THF for one day (solution was exchanged 9 times).

PEO-*b*-PMCL-*b*-PDMAEMA: ^{1}H NMR (400.13 MHz, δ, $CDCl_3$): 0.92 ppm (d, J = 6.4 Hz, -(O)C-CH_2-CH_2-CH(CH_3)-CH_2-CH_2-O-C(O)-C(CH_3)$_2$-CH_2-C(CH_3)-), 1.57 ppm (m, -(O)C-CH_2-CH_2-CH(CH_3)-CH_2-CH_2-O-C(O)-C(CH_3)$_2$-CH_2-C(CH_3)-), 2.30 ppm (m, -(O)C-CH_2-CH_2-CH(CH_3)-CH_2-CH_2-O-C(O)-C(CH_3)$_2$-CH_2-(CH_3)C(C(O)-O-CH_2-CH_2-N(CH_3)$_2$)-), 2.56 ppm (m, -C(O)-O-CH_2-CH_2-N(CH_3)$_2$)-), 3.38 ppm (s, CH_3-O-CH_2-CH_2-O-), 3.64 ppm (s, CH_3-O-CH_2-CH_2-O-), 4.10 ppm (m, -(O)C-CH_2-CH_2-CH(CH_3)-CH_2-CH_2-O-C(O)-C(CH_3)$_2$-CH_2-(CH_3)C(C(O)-O-CH_2-CH_2-N(CH_3)$_2$)-).

PEO-*b*-PPhCL-*b*-PDMAEMA: ^{1}H NMR (400.13 MHz, δ, $CDCl_3$): 0.88 ppm (m, -C(CH_3)$_2$-CH_2-C(CH_3)-), 1.92 ppm (m, -(O)C-CH_2-CH_2-CH(Ph)-CH_2-CH_2-O-C(O)-C(CH_3)$_2$-CH_2-C(CH_3)-), 2.29 ppm (s, -C(C(O)-O-CH_2-CH_2-N(CH_3)$_2$)-), 2.56 ppm (m, -(O)C-CH_2-CH_2-CH(Ph)-CH_2-CH_2-O-C(O)-C(CH_3)$_2$-CH_2-(CH_3)C(C(O)-O-CH_2-CH_2-N(CH_3)$_2$)-), 3.38 ppm (s, CH_3-O-CH_2-CH_2-O-), 3.64 ppm (s, CH_3-O-CH_2-CH_2-O-), 3.82 ppm (m, -(O)C-CH_2-CH_2-CH(Ph)-CH_2-CH_2-O-), 4.06 ppm (m, -C(C(O)-O-CH_2-CH_2-N(CH_3)$_2$)-), 7.16-7.36 ppm (m, Ph).

Self-assembly. Self-assembled structures were prepared using film rehydration method. 10 mg of a polymer dissolved in 1 ml of CH_2Cl_2 were placed into a 5 ml round-bottom flask. The solvent was removed by rotary evaporation. To a dry polymer film 1 ml of PBS was added and the mixture was stirred overnight at room temperature. The assemblies were extruded using 200 nm pore size membrane and characterized by DLS, TEM, and cryoTEM.

References

1. Mai, Y.; Eisenberg, A., Self-assembly of block copolymers. *Chemical Society Reviews* **2012,** *41* (18), 5969-5985.
2. Matter, Y.; Enea, R.; Casse, O.; Lee, C. C.; Baryza, J.; Meier, W., Amphiphilic PEG-b-PMCL-b-PDMAEMA Triblock Copolymers: From Synthesis to Physico-Chemistry of Self-Assembled Structures. *Macromolecular Chemistry and Physics* **2011,** *212* (9), 937-949.
3. Petersen, M. A.; Yin, L.; Kokkoli, E.; Hillmyer, M. A., Synthesis and characterization of reactive PEO-PMCL polymersomes. *Polymer Chemistry* **2010,** *1* (8), 1281-1290.
4. Zupancich, J. A.; Bates, F. S.; Hillmyer, M. A., Aqueous Dispersions of Poly(ethylene oxide)-b-poly(γ-methyl-ε-caprolactone) Block Copolymers. *Macromolecules* **2006,** *39* (13), 4286-4288.
5. Lv, H.; Zhang, S.; Wang, B.; Cui, S.; Yan, J., Toxicity of cationic lipids and cationic polymers in gene delivery. *Journal of Controlled Release* **2006,** *114* (1), 100-109.
6. Dinu, I. A.; Duskey, J. T.; Car, A.; Palivan, C. G.; Meier, W., Engineered non-toxic cationic nanocarriers with photo-triggered slow-release properties. *Polymer Chemistry* **2016,** *7* (20), 3451-3464.
7. Isenberg, B. C.; Williams, C.; Tranquillo, R. T., Small-Diameter Artificial Arteries Engineered In Vitro. *Circulation Research* **2006,** *98* (1), 25-35.

Conclusions and Outlook

In this thesis, detailed synthetic procedure for bis-hydrophilic ABC triblock copolymers (PEO-*b*-PCL-*b*-PMOXA and PEO-*b*-PRCL-*b*-PDMAEMA) was presented. Comprehensive investigation of their aqueous self-assembly was carried out under different conditions and studied by means of LSM, TEM, and cryoTEM.

The main principles which were established for self-assembly of PEO-*b*-PCL-*b*-PMOXA should be verified on other ABC systems, especially where B is an amorphous block, and polymers form nanoscale structures.

As has been discussed in the section 2.3., bis-hydrophilic ABC copolymers should result in patchy assemblies with spatially separated domains in the corona. It would be interesting to investigate if PEO-*b*-PCL-*b*-PMOXA and PEO-*b*-PRCL-*b*-PDMAEMA form structures with patchy corona.

PEO-*b*-PCL-*b*-PMOXA copolymers are of a potential interest for biomedical applications due to its non-toxic nature and biodegradability of the PCL block. Particularly, microscale 3D networks may find applications as a scaffold for tissue engineering. Their highly branched structure would be advantageous for growing the small-diameter blood vessels.[7]

PEO-*b*-PRCL-*b*-PDMAEMA copolymers offer a synthetic platform for gene delivery applications. In this regard, complexation and release of nucleic acids should be tested. The toxicity of these polymers can be reduced by shielding the positive charges of PDMAEMA block. This could be achieved by increasing the PEO length, which should “wrap” the surface of the assemblies.

Acknowledgments

I acknowledge all the people without whom I would not be able to accomplish this thesis.

First of all, I would like to thank Prof. Wolfgang Meier for providing me a great opportunity to do my PhD in his group and all the freedom which he gave me. I would like to acknowledge both Prof. Wolfgang Meier and Prof. Cornelia Palivan, who actively took part in supervising me at the beginning of my PhD, for motivating me to work independently.

I am very grateful that Prof. Richard Hoogenboom has agreed to be my co-referee. I am also very thankful for his numerous works published about polyoxazoline synthesis which helped me to develop the synthesis of the polymers used in this thesis.

I want to thank my husband, Dr. Ulmas Zhumaev (MPIP, Mainz), who, apart from being very supportive, was a very helpful supervisor. Even though he is a specialist in electrochemistry, he was constantly discussing with me my projects, gave me ideas and advice, and taught me how to write a paper. Without him I would most probably not be able to accomplish my PhD.

I would like to thank my dearest colleague and great friend, "soon-to-be-doctor" Samuel Lörcher, for his help in the lab, fruitful discussions, and critical comments.

Dr. Daniel Häussinger is acknowledged for the help with various NMR experiments and his patience while explaining the results to me.

I thank Carola Alampi and Andrej Bieri for cryoTEM experiments and Dr. Alexia Loynton-Ferrand for consulting me with LSM.

I am very thankful to my former colleague Dr. Jason Duskey for doing the cell toxicity experiments, useful comments, and correcting my English.

I thank Pascal Richard and Dr. Dalin Wu for their great experience in organic synthesis which they have shared with me. I am thankful to our lab technician, Sven Kasper, for the nice organization in the chemistry labs. I also have to mention here the microwave reactor from Biotage, which made the synthesis of PEO-*b*-PCL-*b*-PMOXA, and thus this thesis, possible.

I would like to thank the Chemistry students, Maximilian Kratt and Valentin Oehri, whose results obtained during their block course has inspired me for the third publication.

I am very grateful for the support from my senior colleagues, Dr. Gesine Gunkel-Grabole, Dr. Viktoriia Postupalenko, and Dr. Mariana Spulber.

I thank my amazing officemates and colleagues, Serena Rigo, Dr. Justina Kowal, Sagana Thamboo, Myrto Kyropoulou, Davy “Tiger” Daubian, Dr. Fabian Itel, Dr. “Dj” Severin Sigg, Dr. Juan Liu, Dr. Adrian Najer, Dr. Martin Rother, for creating a great atmosphere and making the tough moments easier to handle.

I also want to thank Dr. Corey Rice, collaboration with whom led to the tasting of a lot of good and fancy wine. I will never forget his unique loud laugh inside the Physical Chemistry building.

SNSF, NCCR Molecular Systems Engineering, and the University of Basel are acknowledged for financial support.

Before starting my PhD at the University of Basel, I was very lucky to work with Dr. Oleg Voronin at the Lomonosov Moscow State University. Although this is not directly related to the work which has been carried out in this group, I believe the knowledge which he has shared with me was very important and helpful.

I would like to thank my first Chemistry teacher, Mrs. Elza Kozhanova. Her tough teaching methods made me love Chemistry.

I am very grateful that two of my best friends, Dr. Alena Istrate and Dr. Andrei Istrate, shared with me the joy of discovering wonderful nature of Switzerland, the most beautiful country I have ever seen in my life.

Finally, I want to thank my parents, Nataliia and Vyacheslav Konishchevi, for bringing myself to this world and being always very supportive and understanding.